UNIVERSITY OF BIRMINGHAM

EXPLORING THE IMMUNE MICROENVIRONMENT OF PRIMARY AND METASTATIC COLORECTAL CANCER

---

by

GHALEB GOUSSOUS

A thesis submitted to the University of Birmingham for the degree of

DOCTOR OF MEDICINE

Institute of Immunology and Immunotherapy

College of Medical and Dental Sciences

University of Birmingham

October 2020

Dedication

I dedicate this thesis to my wife Rose and my children, Makram, Ruby and Jude. Without their unconditional love and unwavering support, I wouldn't have been able to complete this work.

Acknowledgements

Firstly, I would like to thank my supervisor, Professor Benjamin Willcox. His support and expert guidance were key in the success of this work. I have never met a person more enthusiastic about immunology! I will be eternally grateful for being given the opportunity to work with his group and to have access to his lab, equipment and consumables. I also would like to thank my co-supervisor, Professor Gary Middleton. His expert knowledge and astute advice were invaluable in helping me navigate through a field I had little knowledge of when I first started. Also, I am extremely grateful to my other co-supervisor, Mr Tariq Ismail for all the support, kindness and encouragement he'd shown me were throughout my time in post.

In addition, I am very grateful to all the following people: Dr Carrie Willcox for helping get my project off the ground and for all the assistance with the lab work, I wouldn't have been able to even start without her help. To Mr Neeraj Lal for introducing me to cancer immunology and for his help and advice with digital pathology. To Mr Christopher Bagnall for his efforts and expertise in immunohistochemistry staining, optimisation and automated staining. To Dr Andrew Beggs and his group for their help with the DNA and RNA work. To Dr Martin Davey for his help with flow cytometry, Dr Mahboob Salim, Dr Fiyaz Mohammed and Mr Alfie Baker for their help and guidance in the lab especially with the bacterial work. To Dr Maha Ibrahim for teaching me how to do manual staining and for helping make sense of histopathology. To Dr Heather Long and Dr Jianmin Zuo for giving me cell lines to help validate MHC Class I and II antibodies.

From the clinical side, I am very grateful for all the help I received from the Heart of England Trust histopathology department, namely, Dr Gerald Langman for his help in obtaining the samples for the project. His expertise was also crucial in reviewing IHC slides and validating multiplex immunofluorescence staining. I am grateful to Miss Hollie Bancroft for her efforts in finding, sectioning and delivering the samples. I also would like to thank Mr Babu Naidu for putting me in the directing of the first project and for sharing the original database of patients.

I also am grateful to the UHB charities for funding some of my consumables and for supporting my study leave costs.

Finally, I would like to thank my family and friends for all their support throughout the whole process.

Abstract

This thesis explores the immune microenvironment of primary and metastatic colorectal cancer.

In the first workstream, I examined the immune profile of colorectal pulmonary metastases and compared it to that of the primary in 34 matched primary-metastasis paired samples. I used whole-slide digital pathology scoring algorithms to characterise and quantify main immune cell infiltrates and ascertain their lineage and orientation. I also assessed expression levels of two key immune checkpoint blockade targets, PD-1 and PD-L1 as well as expression of MHC class I and II molecules. My results suggest that the microenvironment of pulmonary colorectal metastases is more immunologically active than that of the primary tumour with clear type 1 immunity signatures. This immunity however is supressed by overexpression of checkpoint blockade proteins.

The second workstream explored the microenvironment of a particular subgroup of mismatch repair proficient, microsatellite stable colorectal cancer which is characterised by upregulated coordinated immune response cluster (CIRC). This exploited a seven-plex immunofluorescence panel to stain for key immune markers and a digital pathology platform to phenotype and quantify them. The immune microenvironment of this group was then compared to those of mismatch repair deficient and proficient controls. The results revealed that this subgroup of tumours have comparable immune signatures to those of *bona fide* mismatch repair deficient tumours, suggestive of a heightened type 1 immunity.

Collectively, these findings highlight substantial intra and inter-patient heterogeneity in intra-tumoural immunity in colorectal cancer and have implications for development of targeted immunotherapies in the advanced cancer setting.

Table of Contents

List of Figures

List of Tables

List of Abbreviations

5-FU	5-fluorouracil
ACT	Adoptive Cell Transfer
ADCC	Antibody-Dependent Cell-mediated Cytotoxicity
ADCP	Antibody-Dependent Cellular Phagocytosis
ALL	Acute Lymphoblastic Leukemia
CEA	Carcinoembryonic Antigen
APC	Adenomatous Polyposis Coli
APC	Allophycocyanin
APC	Antigen Presenting Cell
BCG	Bacillus Calmette–Guérin
BRAF	v-Raf murine sarcoma viral oncogene homolog B
CAR-T	Chimeric Antigen Receptor T-cell
CD	Cluster of Differentiation
CDC	Complement-Dependent Cytotoxicity
CE	Conformité Européene
CHO	Chinese Hamster Ovary
CIITA	(MHC) Class II Transactivator
CIMP	CpG island methylator phenotype
CIN	Chromosomal Instability
CIRC	Coordinated Immune Response Cluster
CMS	Consensus Molecular Subtypes
CO_2	Carbon Dioxide
COX	Cyclooxygenase
CPB	Checkpoint Blockade/Blocker
CpG	Cytosine-phosphate-Guanine
CRC	Colorectal cancer
CRISPR	Clustered Regularly Interspaced Short Palindromic Repeats
CST	Cell Signaling Technology® (company)
CTLA-4	T-lymphocyte-Associated Protein 4
DAB	3,3’-diaminobenzidine
DAPI	4′,6-diamidino-2-phenylindole
DC	Dendritic Cell
DC-LAMP	Dendritic Cell Lysosomal Associated Membrane Glycoprotein
DCC	Deleted in Colorectal Carcinoma
DMEM	Dulbecco's Modified Eagle's Medium
dMMR	Deficient Mismatch Repair
DNA	Deoxyribonucleic acid
EDTA	Ethylenediaminetetraacetic Acid
EGFR	Epidermal Growth Factor Receptor
EMT	epithelial – mesenchymal transition

EpCAM	Epithelial Cell Adhesion Molecule
ESMO	European Society for Medical Oncology
FACS	Fluorescence-Activated Cell Sorting
FAP	Familial Adenomatous Polyposis
FCS	Foetal Calf Serum
FDA	Food and Drug Administration
FFPE	Formalin Fixed Parafin Embedded
FOXP3	Forkhead Box P3 protein
GFP	Green Fluorescent Protein
GI	Gastrointestinal
GM-CSF	Granulocyte-Macrophage Colony-Stimulating Factor
GUCY2C	Guanylate Cyclase 2C
HBRC	Human Biomaterials Resource Centre
HLA	Human Leukocyte Antigen
HPV	Human Papilloma Virus
HRAS	Harvey Rat Sarcoma Viral Oncogene Homolog
HRP	Horse Radish Peroxidase
ICI	Immune Checkpoint Inhibitors
IF	Immune fluorescence
IFN	Interferon
IHC	Immunohistochemistry
IL	Interleukin
IMS	Industrial Methylated Spirit
IQR	Interquartile Range
IRAS	Integrated Research Application System
IVD	In-Vitro Diagnostic (medical use)
KBF1	p50 NF- κB homodimer
KOC1	KH Domain Containing Protein Overexpressed in Cancer 1 (gene)
KRAS	Kirsten Rat Sarcoma Viral Oncogene Homolog
LAG-3	Lymphocyte-Activation Gene 3
LB	Lysogeny Broth
LVI	Lympho-vascular invasion
MACS	Magnetic-Activated Cell Sorting
mCRC	Metastatic Colorectal Cancer
MEK/ERK	Mitogen-activated protein kinase/ extracellular signal-regulated kinase
MHC	Major Histocompatibility Complex
MLH-1	mutL homolog 1 gene
MMR	Mismatch Repair
MSH	MutS Homolog gene
MSI	Microsatellite Instability

MSI	Multi-spectral Image
MSS	Microsatellite Stable
MWT	Microwave Treatment
NEB	New England BioLabs
NF-κB	Nuclear Factor kappa-light-chain-enhancer of activated B cells
NHS	National Health Service
NK	Natural Killer (cell)
NRAS	Neuroblastoma Rat Sarcoma viral oncogene homolog
ORF	Open Reading Frame
OS	Overall Survival
PADRE	Pan DR Epitope
PBST	Phosphate Buffered Saline
PCR	Polymerase Chain Reaction
PD-1	Programmed Death Protein - 1
PD-L1	Programmed Death Protein Ligand - 1
PE	Phycoerythrin (Flourophore)
PEI	Polyethylenimine
PET	Positron Emission Tomography
PFA	paraformaldehyde
PFS	Progression-Free Survival
pMMR	Proficient Mismatch Repair
PMS	PMS1 Homolog 2, Mismatch Repair System Component
POLD1	Polymerase δ (delta)
POLE	Polymerase ε (epsilon)
R&D	Research and Development
RAS	Rat Sarcoma Viral Oncogene Homolog
RNA	Ribonucleic Acid
RNF43	Ring Finger 43 (gene)
ROI	Region of Interest
RORγ	Retinoic Acid Receptor - Related Orphan Receptor gamma
RPMI	Roswell Park Memorial Institute
SOC	Standard of Care
SOC	Super Optimal Broth
SSI	Site-Specific Information
TAA	Tumour Associated Antigen
TBET	T-box Expressed in T cells/T-box Transcription Factor TBX21
T_C	T Cytotoxic lymphocyte
TCB	T Cell Bispecific antibody
TCGA	The Cancer Genome Atlas
TCR	T-Cell Receptor
T_H	T Helper lymphocyte

TIGIT	T cell immunoreceptor with Ig and ITIM (immunoreceptor tyrosine-based inhibition motif)
TIL	Tumour Infiltrating Lymphocytes
TMA	Tissue Microarray
TNF	Tumour Necrosis Factor
TNM	Tumour, Node, Metastasis
TOMM34	Translocase of Outer Mitochondrial Membrane 34 (gene)
TP53/P53	Transformation-related Protein 53
TREG	Regulatory T-Cell
TSA	Tyramide Signal Amplification
UK	United Kingdom
US	United States
VEGF	Vascular Endothelial Growth Factor
WNT	Wnt Signaling (Wingless-related integration site)

1. Chapter One: Introduction

1.1. Colorectal Cancer

1.1.1. Statistics

Colorectal cancer (CRC) is defined as cancer that afflicts the colon or the rectum. It is the third commonest cancer of adults worldwide accounting for over 1.8 million new cases in 2018, which is a tenth of all newly diagnosed cancers (Bray et al., 2018).

In the UK, over 42,000 new cases of CRC were diagnosed in 2017 and CRC now stands as the second commonest cause of cancer-related mortality superseded only by lung cancer. CRC has a slight predilection to the male sex in a 5:4 ratio. The incidence of CRC starts rising significantly after the sixth decade of life and peaks in the eighth decade of life (Cancer Research UK).

1.1.2. Pathogenesis

The overwhelming majority of CRCs are classified as adenocarcinomas accounting for around 90% of all tumours (Bosman et al., 2010). Other rarer types include sarcomas, neuroendocrine tumours, lymphomas and melanomas. The focus of this work is on adenocarcinomas and therefore all further references to CRC will be related to adenocarcinomas.

1.1.2.1. The Adenoma-Carcinoma sequence

CRC tumorigenesis is one of the most extensively studied topics in cancer biology. The morphological progression of CRC from a benign adenomatous polyp to a *bona fida* invasive cancer has been observed and reported since the 1950s (Grinnell and Lane, 1958). The concept was detailed and cemented by St Mark's Hospital

histopathologist Dr Basil Morson in 1974. Through studying specimens of resected CRC with contiguous benign adenomas, Morson established a temporal model where early adenomas progress into intermediate then advanced adenomas ultimately transforming into invasive carcinomas. He also recognised that the size of the polyp is the most important risk factor in the polyp's potential to transform into a cancer, with polyps over 20mm in size having an almost 50:50 chance of malignant transformation (Morson, 1974).

1.1.2.2. The genetic basis of CRC development

Like most cancers, the evolution of CRC is a multi-step process where mutations in key oncogenes and tumour-suppressor genes sequentially accumulate leading to the development of invasive malignancy (Weinberg, 1989).

The genetic bases for the development of CRC were studied by Bret Vogelstein and Eric Fearon through comparing the frequency of genetic alterations present at different stages of the adenoma-carcinoma sequence (Vogelstein et al., 1988). They then published their landmark paper in 1990 describing the genetic model for the development of CRC. This model is characterised by the clonal expansion of cells that acquire a survival advantage through the accumulation of mutations in key genes that either activate oncogenes or –more importantly – inactivate key tumour suppressor genes in a step-wise fashion (Fearon and Vogelstein, 1990). This model is illustrated in figure 1.1.

The earliest genetic alteration in adenoma-carcinoma sequence is the inactivation of the Adenomatous Polyposis Coli (*APC*) tumour-suppressor gene on the long arm of chromosome 5 (Powell et al., 1992, Polakis, 1997). Germline transmission of a

mutated *APC* gene is responsible for developing a condition called Familial Adenomatous Polyposis (FAP). In this condition, hundreds or even thousands of adenomatous polyps develop in the colon and rectum leading in an inevitable development of CRC in the fourth and fifth decades of life (Nieuwenhuis and Vasen, 2007). The product of the APC gene is important for a number of cellular functions such as proliferation and differentiation. It is a key component of the WNT signalling pathway and forms part of the destruction complex responsible for degrading β-catenin in the cytoplasm. When mutated, β-catenin accumulates within cells and leads to unchecked and disorganised proliferation of intestinal cells giving rise to adenomas (Minde et al., 2011).

The next step in the sequence of genetic alterations is the acquisition of mutations in genes encoding key proteins in MEK/ERK cell signalling pathway such as the Rat Sarcoma Viral Oncogene Homolog (*RAS)* gene family (KRAS, NRAS or HRAS). Mutation of the *RAS* oncogene ushers the transformation of an early adenoma into an intermediate adenoma. Nearly half of larger adenomas (>10mm) and invasive carcinomas process this alteration in comparison to only 10% of smaller adenomas (Bos et al., 1987, Vogelstein et al., 1988). This is then followed by a mutation in the Deleted in Colorectal Carcinoma (*DCC*) gene which heralds the development of late or significant adenomas. This gene is mapped to the long arm of chromosome 18 and losses on this chromosome are found in 70% of CRCs and 50% of late adenomas (Fearon et al., 1990). The final transformation into invasive malignancy occurs with the mutation on the Transformation-related Protein 53 (*TP53*) gene. Deletions on the short arm of chromosome 17 in the region mapped to harbour the *TP53* gene has been

observed in almost three quarters of CRC but seldom in adenomas (Fearon and Vogelstein, 1990, Vogelstein et al., 1988).

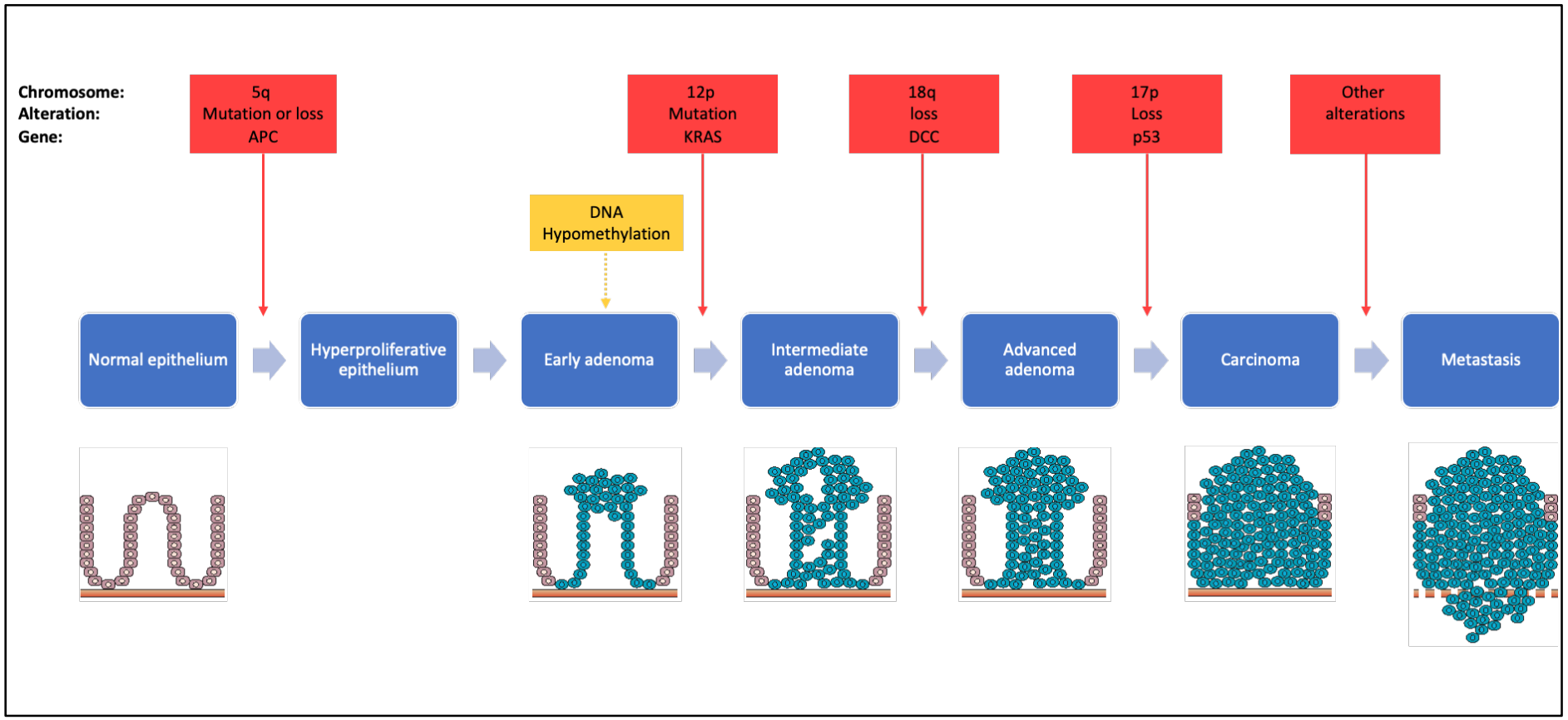

Figure 1.1: A schematic depicting the adenoma to carcinoma sequence as described by Fearon and Vogelstein (Fearon and Vogelstein, 1990). The illustrations below the schematic are adapted from Walther et al. (Walther et al., 2009).

1.1.2.3. Pathways to the development of CRC

As most genes implicated in the development of CRC are tumour-suppressor genes, for a phenotypic effect to occur, both copies of the gene have to be inactivated as postulated by Knudson's two-hit theory (Knudson, 1971). As the rate of naturally occurring mutations in healthy cells is not sufficient to accomplish the required number of genetic alterations for malignant transformation in the lifetime of the cell, a degree of genetic instability is required. This instability increases the rate of mutations well above the baseline for normal cells creating a so-called "mutator phenotype" which accelerates the accumulation of mutations including driver mutations that ultimately lead to the development of cancer (Loeb et al., 2003, Vogelstein et al., 2013). In CRC there are three main mechanisms to acquire this genomic instability; chromosomal instability (CIN), Mismatch repair deficiency (dMMR) and CpG island methylator phenotype (CIMP) (Nguyen and Duong, 2018).

1.1.2.3.1 Chromosomal Instability (CIN)

Around 85% of CRC development can be attributed to a phenomenon called chromosomal instability where large parts of specific chromosomes are either lost or gained through the process of the cell cycle. This is a result of a number of defects in the cell cycle regulatory mechanisms such as defects in the chromosome segregation, telomere dysfunction and deficiencies in the DNA damage response mechanisms. The phenotypic features that result from this pathway are characterised by aneuploidy, loss of heterozygosity and chromosomal amplifications (Pino and Chung, 2010). Evidence of genomic imbalance is present in various stages of the adenoma to carcinoma pathway and affects key chromosomes implicated in the development of CRC (Shih et al., 2001).

1.1.2.3.2 Mismatch repair deficiency

Around 12 - 15% of CRCs are a result of a deficiency in the DNA mismatch repair mechanisms (dMMR) (The Cancer Genome Atlas, 2012). Mismatch repair proteins are responsible for maintaining the fidelity of the base-base pairing during DNA replication. A mutation in one or more of the four DNA mismatch repair genes (*MLH-1, MSH-2, MHS-6* or *PMS-2*) results in a phenomenon called micro-satellite instability (MSI) where short DNA sequence repeats (micro-satellites) accumulate all through the genome. As a result, MSI tumours tend to have a disproportionately higher number of mutations than micro-satellite stable (MSS) tumours (Bhattacharyya et al., 1994, Eshleman et al., 1995, Vogelstein et al., 2013). Those tumours also tend to evoke a stronger immune response probably as a result of a higher number of neo antigens (Drescher et al., 2010)

Mutations in MMR genes can be either transmitted as a germline mutation in one or more of the four genes (e.g. Lynch syndrome) or more commonly acquired as a result of epigenetic silencing (through hyper-methylation) of the *MLH-1* gene (Kawakami et al., 2015).

Microsatellite instability can be diagnosed either by immunohistochemically staining for MMR proteins (Lindor et al., 2002) or using a polymerase chain reaction (PCR) - based assay for specific markers (Buhard et al., 2006). Newer technology uses next generation sequencing to detect microsatellite areas in the genome (Middha et al., 2017, Kautto et al., 2017, Haraldsdottir, 2017). Based on the testing results, tumours can be segregated into three categories: High micro-satellite instability (MSI-hi) if two or more markers are positive, low micro-satellite instability (MSI-lo) if only one marker

is positive and micro-satellite stable tumours (MSS) if all markers tested are negative (Boland et al., 1998).

Tumours that result from micro-satellite instability tend to have distinct histopathological phenotypes characterised by predilection to proximal colon, poor differentiation, mucinous phenotype and florid lymphocytic infiltrates (Boland and Goel, 2010).

Clinically, it is important to establish the microsatellite status of CRC as this information is key to determining the prognosis of the disease and in informing the treatment decision-making process. These tumours traditionally carry better prognoses than similarly staged tumours with a MSS phenotype (Gryfe et al., 2000, Samowitz et al., 2001, Popat et al., 2005). MSI-hi tumours also tend to have a lesser propensity to metastasise with only 5% of metastatic CRC having an MSI-hi phenotype as compared to 15% in earlier stages (Malesci et al., 2007, Venderbosch et al., 2014). When those tumours metastasise however, they generally tend to have a poorer prognosis than MSS tumours with an average overall survival of 13.6 months in comparison to 16.8 months for patients with MSS tumours (Goldstein et al., 2014, Venderbosch et al., 2014, Guinney et al., 2015). MSI-hi tumours have also been found to be less responsive to 5-flurouracil based chemotherapy, a first line chemotherapeutic agent in CRC (Kawakami et al., 2015, Copija et al., 2017).

1.1.2.3.3. CpG Island Methylator Phenotype

This pathway of CRC development emphasises the role of epigenetic genomic alteration in carcinogenesis. Essentially, CpG (Cytosine – phosphate – Guanine) islands are regions in the genome that are enriched in CG dinucleotide sequences.

Those regions are found most abundantly in gene promoter areas (Illingworth et al., 2010). The age-related methylation of cytosine in those regions has an impact on the expression of the corresponding genes with hyper-methylation resulting in stable silencing of the corresponding gene (Bird, 2002, Deaton and Bird, 2011). In CRC, hyper-methylation of the promoter regions of certain tumour suppressor genes results in epigenetic silencing of those genes and ultimately resulting in the development cancer (Toyota et al., 1999, Lao and Grady, 2011). Epigenetic silencing of the *MLH1* gene has been implicated in the development of sporadic microsatellite unstable (MSI) cancers (Weisenberger et al., 2006, Boland and Goel, 2010).

Study of methylation of CpG islands methylation was shown to be significantly higher in CRC when compared to normal mucosa and benign adenoma (Beggs et al., 2013). The degree of methylation of specific markers gives rise to three biologically distinct subgroups: CIMP-high, CIMP-low and CIMP-negative, the latter group essentially conforming to the classical chromosomal instability pathway (Ogino et al., 2006, Ogino et al., 2007, Nosho et al., 2008).

CIMP has been implicated in the serrated pathway of CRC pathogenesis. The serrated pathway is an alternative, albeit analogous model to the adenoma-carcinoma CRC tumorigenesis in which traditional adenomatous polyps are replaced by serrated lesions as the precursor to colorectal adenocarcinomas (Jass, 2003). This pathway accounts for around 10% of colorectal adenocarcinomas. Those tumours are characterised by predominance of microsatellite instability, abundance of BRAF mutations and predilection to the proximal colon (Rosenberg et al., 2007, Mäkinen, 2007, Yamane et al., 2014).

1.1.2.3.4. POLE/POLD1 mutations

A rare subset of microsatellite stable (MSS) colorectal tumours with a hyper-mutated phenotype is a result of either germline or somatic mutations afflicting the exonuclease domain of DNA polymerase-ε (POLE) or DNA polymerase-δ (POLD1). These mutations result in proofreading errors during DNA replication culminating in missense and nonsense mutations (The Cancer Genome Atlas, 2012, Palles et al., 2013, Briggs and Tomlinson, 2013, Valle et al., 2014, Jansen et al., 2016). The incidence of these mutations in colorectal cancer is in the region of 2 – 8% (Mur et al., 2020). The hyper-mutated phenotype of these tumours makes them suitable targets for immunotherapy (Bourdais et al., 2017).

1.1.2.4. Molecular subtypes

CRC is a heterogeneous disease. This is a result of different pathogenesis pathways, the interplay of genetic, epigenetic and environmental influences. This heterogeneity gives rise to differences in tumour phenotype, clinical behaviour, prognosis and response to various treatment modalities. In an attempt to classify different subtypes, several different systems were proposed, mainly based on the molecular biology of the tumours (Schlicker et al., 2012, Marisa et al., 2013, Sadanandam et al., 2013, Budinska et al., 2013, De Sousa et al., 2013, Roepman et al., 2014).

In order to come up with a robust classification system, an international consortium of expert groups was formed to standardise the different classifications and draw them into one ‘gold standard’ classification. In 2015 the Consensus Molecular Subtypes of CRC (CMS) was introduced. This system draws on the strengths of six previous molecular classifications and encompasses data from different data sets. It explores the key biological features of different subtypes in addition to transcriptomic, genomic

and proteomic features. It also attempts to explore the relationship between the subtype and the clinical outcome. In this classification, the tumours are sub-categorised into 4 subgroups with a small proportion of tumours not conforming to a single subgroup and thought to be a transitional group (Guinney et al., 2015). This classification is based on primary tumours and does not categorise metastatic disease. The four groups are:

CMS1 (14%): This subgroup essentially represents the micro-satellite unstable tumours. This includes both the germline dMMR group as well as the epigenetically silenced group (CIMP-high). The tumours in this subcategory were enriched in BRAF mutations and characteristically displayed an inflamed phenotype with upregulation of immune markers (Guinney et al., 2015).

CMS2 (37%): This subgroup represents tumours derived via the canonical chromosomal instability pathway. This group demonstrated prominent aneuploidy and loss of heterozygosity as well as stigmata of activation of the WNT pathway (Guinney et al., 2015).

CMS3 (13%): This subgroup was characterised by metabolic dysregulation. This group had a mixture of MSI and MSS tumours and was enriched with CIMP-low tumours and with prevalence of KRAS mutations (Guinney et al., 2015).

CMS4 (23%): This subgroup was characterised by upregulation of genes involved in the epithelial – mesenchymal transition (EMT) and increased transforming growth factor –β expression. This group had a higher stromal component with increased angiogenesis markers. This group had the worst clinical outcomes in terms of disease-free and overall survival (Guinney et al., 2015).

1.1.3. Staging of CRC

The prognosis of CRC is heavily influenced by the stage of the disease at diagnosis which is traditionally assessed using the gold standard TNM (Tumour, (Lymph) Node, Metastasis) system. Table 1.1 demonstrates the colorectal TNM classification in more detail as detailed in the 8th edition of the TNM manual (Brierley et al., 2016).

On the basis of the TNM system, tumours can be staged into 4 stages denoting the extent (how advanced) of the disease and therefore influencing the choice of treatment. Those stages are delineated in Table 1.2.

T (Tumour)	**TX** Primary tumour cannot be assessed	
	T0 No evidence of primary tumour	
	Tis Carcinoma in situ: invasion of lamina propria	
	T1 Tumour invades submucosa	
	T2 Tumour invades muscularis propria	
	T3 Tumour invades subserosa or into non-peritonealised peri-colic or perirectal tissues	
	T4 Tumour directly invades other organs or structures and/or perforates visceral peritoneum	**T4a** Tumour perforates visceral peritoneum
		T4b Tumour directly invades other organs or structures
N (Node)	**NX** Regional lymph nodes cannot be assessed	
	N0 No regional lymph node metastasis	
	N1 Metastasis in 1 to 3 regional lymph nodes	**N1a** Metastasis in 1 regional lymph node
		N1b Metastasis in 2 to 3 regional lymph nodes
		N1c Tumour deposit(s), i.e. satellites in the subserosa, or in non-peritonealised pericolic or perirectal soft tissue without regional lymph node metastasis
	N2 Metastasis in 4 or more regional lymph nodes	**N2a** Metastasis in 4–6 regional lymph nodes
		N2b Metastasis in 7 or more regional lymph nodes
M (Metastasis)	**M0** No distant metastasis	
	M1 Distant metastasis	**M1a** Metastasis confined to one organ (liver, lung, ovary, non-regional lymph node(s)) without peritoneal metastases
		M1b Metastasis in more than one organ

Table 1.1: TNM classification of colorectal cancer – 8th edition (Brierley et al., 2016).
Tumour: this denotes the extent of invasion through the layers of the bowel wall.
Node: describes the number of nodes involved and their distance from the tumour.
Metastasis: this denotes whether the distant spread is present or not.

Stage	Sub-stage	T (Tumour)	N (Node)	M (Metastasis)
Stage 0		Tis	N0	M0
Stage I		T1, T2	N0	M0
Stage II	IIA	T3	N0	M0
	IIB	T4a	N0	M0
	IIC	T4b	N0	M0
Stage III	IIIA	T1, T2	N1	M0
		T1	N2a	M0
	IIIB	T1, T2	N2b	M0
		T2, T3	N2a	M0
		T3, T4a	N1	M0
	IIIC	T3, T4a	N2b	M0
		T4a	N2a	M0
		T4b	N1, N2	M0
Stage IV	IVA	Any T	Any N	M1a
	IVB	Any T	Any N	M1b
	IVC	Any T	Any N	M1c

Table 1.2: Colorectal cancer stages based on the TNM scores – 8th edition (Brierley et al., 2016)

1.1.4. Management of early disease (Stage I-III)

The mainstay curative treatment of non-metastatic CRC is surgical resection. This is sometimes preceded by pre-operative neo-adjuvant treatment in the form of radiotherapy with or without chemotherapy in rectal cancer or chemotherapy alone in colon cancer. This treatment is designed to render the tumour more amenable to a curative resection. In stage III disease and selected patients with a high-risk stage II disease, adjuvant chemotherapy is recommended to enhance the chances of achieving a lasting cure.

1.1.5. Advanced CRC (Stage IV)

Advanced disease is generally a term used to denote either disease that cannot be treated surgically (even after neo-adjuvant treatment) due to loco-regional or metastatic spread that renders curative resection impossible, or recurrent disease either local or metastatic that presents after the primary tumour has been treated. In spite of advances in screening, about a quarter of all new diagnoses of CRC are detected at an advanced stage and up to half of patients detected at an early stage will go on to develop advanced disease at a later stage after seemingly initial curative treatment (Cancer Research UK, Siegel et al., 2018). After the liver, the lung is the commonest site of metastatic spread and account for 10% of metastatic CRC (Mitry et al., 2010). The metastatic process is a complex one and it is not entirely clear if the metastatic potential is driven by the tumorous cells themselves (cell autonomous) or by the tumour micro-environment which is analogous to the seed and the soil paradigm. Modern thinking suggests that it is likely to a combination of the two (Liu et al., 2017).

The management of metastatic disease remains an area of debate and innovation. Whilst some metastatic disease is still amenable to surgical treatment with a curative intent (Weiser et al., 2013), for the majority with metastatic disease this spells a grave outlook with less than a fifth surviving for 5 years (The Office of National Statistics, 2019). The advent of modern targeted agents such as anti-vascular endothelial growth factor VEGF, anti-epithelium growth factor monoclonal antibodies and immunotherapies ushered in an era of promise for patients with un-resectable disease. The survival of patients with advanced disease has almost doubled in the past two decades with a median of 30 months from diagnosis (Van Cutsem et al., 2016). Later in this chapter, I will explore the various immunotherapies in advanced CRC and the biomarkers employed in their utilisation.

Due to the theme of this thesis, the majority of the work will be focused on advanced colorectal.

1.2. A brief overview of cancer immunology

1.2.1. Immune surveillance and Immunoediting

The interplay between the immune system and malignancy is not a new concept. In addition to its role in fending against infections, the role if the immune system in preventing the development of cancers is now well established. The ability of the immune system to specifically recognised and efficiently eliminate deviant antigens, put it at the heart of the body's defence against nascent tumours that have developed mutations and as result, displayed new non-self-antigens (Burnet, 1970, Thomas, 1982). The last three decades have seen a dramatic expansion in the field of cancer immunobiology which has resulted in better understanding of the pivotal role of the

immune system in moulding the tumour microenvironment, moving away from the notion that tumorigenesis is a purely cell-autonomous phenomenon. The concept of immunoediting in the pathogenesis of cancer is now well-established (Dunn et al., 2004, Kim et al., 2007, Schreiber et al., 2011). The cycle of immunoediting involves three phases (the three *Es*): *Elimination*, *Equilibrium* and *Escape*.

1.2.2. Elimination

One of the key roles of the immune system is the identification and elimination of tumour cells, this is also known as immunosurveillance. Although this function is carried out by all components of the host's immune system, the adaptive immune system plays the central role. As tumour cells develop, they start presenting abhorrent neoantigens that are recognised by the immune system as non-self. Those antigens trigger an anti-tumour immune response leading to elimination of the abnormal cells before they develop into a fully-fledged cancer. Generally speaking, antigens presented by tumour fall into two broad categories: tumour specific antigens (TSA) and tumour associated antigens (TAA). The former is a type of antigen that is only expressed on tumour cells and not on normal cell. Examples of such antigens are products of onco-viral infections (e.g., human papilloma virus), mutations in key oncogenes such as p53 and cancer germline genes. As those antigens are not normally expressed on normal cells, they tend to be immunogenic and effective in triggering an immune response. TAAs on the other hand are antigens that can be expressed on normal cells, albeit at a low level. Such antigens result from overexpression of non-mutated genes or expression of differentiation antigens that are normally expressed by normal cells of a specific tissue type (Coulie et al., 2014, Vigneron, 2015).

1.2.3. Equilibrium

In this phase, the tumour cells undergo a Darwinian-type selection to outsmart the immune system. Selection pressures exerted by the cells of the immune system favour development of less immunogenic cancer cell clones. This phase of immunoediting is perhaps the longest of the three phases as it involves constant cycles of tumour growth and elimination until a non-immunogenic phenotype is selected or the immune system is supressed preventing attack of tumour cells (Kim et al., 2007).

1.2.4. Escape

In this phase, cells that selectively learned how to evade the attack of the immune system begin to grow into a *bona fide* cancer. Tumours employ numerous strategies to avoid the immune system and those mechanisms generally fall into two broad categories: actively supressing the immune response or by "laying low" and avoiding recognition by the immune system. The former mechanism can be mediated by inhibitory immune cells (such as regulatory T lymphocytes) and cytokines or by over expression of immune checkpoint molecules (such as programmed death proteins and their ligands). The latter employs mechanisms of rendering the tumour cell unrecognisable by the immune system by ways such as down regulation of Major Histocompatibility Molecules (MHC).

1.2.5. Tumour Infiltrating Lymphocytes (TILs)

These cells are mononuclear cells of the adaptive immune system (T and B lymphocytes) that can be seen infiltrating the surroundings of the tumour on histological analysis. These infiltrates are a surrogate marker of the tumour's immunogenicity and are a hallmark of an adaptive immune attack. The density of those infiltrates in the tumour micro-environment have been consistently shown to carry a

favourable prognosis in several different cancer types (Shankaran et al., 2001, Sato et al., 2005, Lee et al., 2008).

1.2.6. The Cancer-Immunity Cycle

To summarise the interplay between cancers and the immune system, Chen and Mellman introduced the concept of the Cancer-Immunity Cycle (Chen and Mellman, 2013). This cycle depicts the key steps in the development of an anti-tumour immune response and the mechanisms employed by tumours to escape this response. More importantly, it highlights the opportunities to harness the might of the immune system in developing novel anti-cancer immunotherapies.

The cycle is broadly composed of a sequence of seven steps implicated in mounting an effective immune response that grows stronger with each revolution of the cycle [Figure 1.2]. The release of tumour neoantigens kickstarts the cycle. In the presence of pro-inflammatory signals (chemokines and cytokines), those antigens are taken up by professional antigen presenting cells (APCs) such as dendritic cells (DCs) that then migrate to central lymph glands where they present those antigens to T-lymphocytes. Those T-lymphocytes are primed and activated and differentiate into either effector or regulatory T-lymphocytes which determines the nature of the immune response. The activated effector cells travel from the lymph glandes to the tumours in the blood stream and leave the blood vessels adjacent to the tumour. Those cells then infiltrate the tumour bed and bind to tumour cells bearing those specific neoantigens with their T-Cell Receptors (TCR). The final step in the cycle is when those effector cells exert their cytotoxic properties resulting in the killing of cancer cells and the release of more tumour neoantigens (Chen and Mellman, 2013).

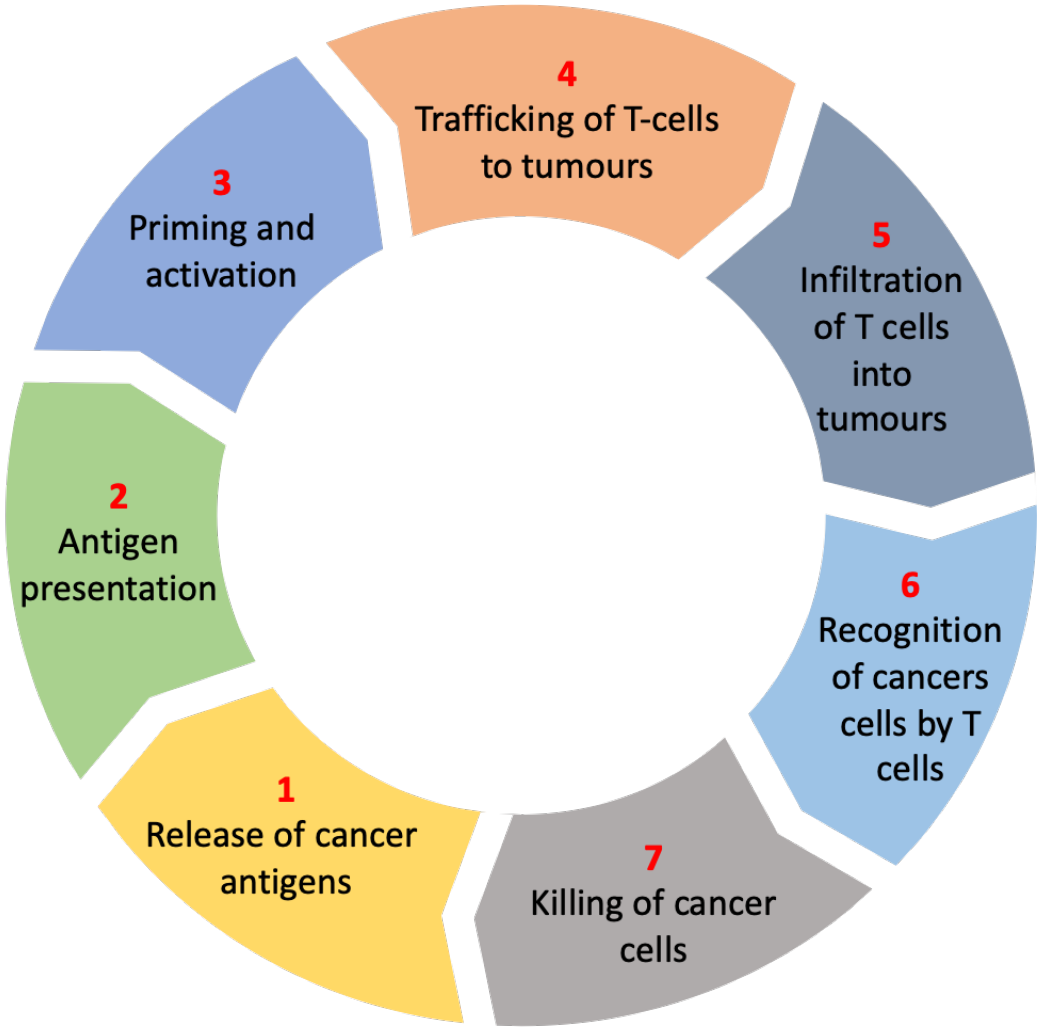

Figure 1.2: A schematic depicting the Cancer-Immunity Cycle as described by Chen and Mellman (Chen and Mellman, 2013)

1.3. Colorectal Cancer Immunology

1.3.1. Role of TILs

CRC is no exception, and several authors have demonstrated that TILs have favourable prognostic connotations (Ropponen et al., 1997, Baier et al., 1998, Naito et al., 1998, Diederichsen et al., 2003). In their landmark paper Jérôme Galon and his colleagues demonstrated that the density of T lymphocytes in the tumour centre and at the invasive margin has a profound prognostic impact especially in stages I – III (Galon et al., 2006). They demonstrated that tumours with high TIL infiltrates had significantly better prognoses than ones with poor infiltrates regardless of the pathological (TNM) stage. The weight of evidence supporting the impact of immune infiltrates on the prognosis of CRC provided the impetus to refine the traditional TNM staging system by including information about the immune response. This has given rise to a global task force calling for the introduction of the Immunoscore® as an adjunct to the TNM system (Galon et al., 2012). The value of the Immunoscore® as a prognostic tool was confirmed in a number of studies showing a strong association between high scores and improved disease-free and overall survival (Mlecnik et al., 2016a, Mlecnik et al., 2016b, Angell and Galon, 2013). An international consortium later validated the Immunoscore® as a reliable prognostic tool in Stage I-III CRC calling for it to become an adjunct to the TNM staging system (Pagès et al., 2018). The favourable outcomes from large phase III trials paved the way to the introduction TNM-Immune (TNM-I), a new classification integrating the Immunoscore® (Pagès et al., 2020). The prognostic and predictive value of the Immunoscore® has also been demonstrated in colorectal metastases (Mlecnik et al., 2020, Van den Eynde et al., 2018, Mlecnik et al., 2018).

1.3.2. Roles of different immune subtypes

Due to the complexity of the immune system and the multifaceted nature of tumorigenesis it has been demonstrated that different immune subsets have different – and at times contrasting prognostic effects – in different cancer types. In CRC, it has been demonstrated that infiltration with cytotoxic T lymphocytes, helper T lymphocytes with a T_H1 polarity, memory T lymphocytes ($CD45RO^+$) and Regulatory T cells have positive prognostic impacts (Fridman et al., 2012, Ling et al., 2016, Ladoire et al., 2011). On the other end of the spectrum T_H17 lymphocytes were found to have a negative prognostic influence on prognosis probably due to their role in fostering chronic inflammation (Tosolini et al., 2011, De Simone et al., 2013). It is however well known that there is great variability in the immune response in CRC. The factors that govern the magnitude of this response remain unclear. It is likely that tumour-intrinsic factors such as the neo-antigen load have an impact on the immune response. This is clearly demonstrated in tumours with high micro-satellite instability (MSI-hi) which have a high mutational burden and therefore generate more neo-antigens and subsequently a more florid immune response (Phillips et al., 2004, Ionov et al., 1993). In an attempt to probe the role of tumour genotype in determining the immune response Lal *et al.* bio-informatically interrogated CRC transcriptomic data from The Cancer Genome Atlas (TCGA). Through two-dimensional hierarchal clustering they found four distinct subgroups on the basis of the expression of a T_H1-centric cluster of genes termed the coordinated immune response cluster (CIRC). They found that the group with the highest expression of CIRC was enriched in MSI-hi tumours and tumours harbouring a POL mutation. Intriguingly, Lal's work also demonstrated that about 30% of micro-satellite stable (MSS) tumours also invoked a high immune response manifested in a

high CIRC signature (Lal et al., 2015). The reasons for this are not entirely clear. In the second workstream of this thesis I will be exploring the immune microenvironment of this subgroup of patients through multiplexed immunofluorescence staining and digital pathology quantification.

It is also conceivable that factors extrinsic to the tumour such as the colonic microbita play a role in shaping the immune response (Dejea et al., 2014). To add to the complexity, the emerging role of intra-tumoural heterogeneity is now recognised as a characteristic feature of cancer (Tabassum and Polyak, 2015). This has profound implications for the interpretation of immunological tumour microenvironment data and on the search for biomarkers and therapeutic targets.

The immune signature of CRC is not only prognostic but also predictive of a response to both traditional and immunological adjuvant and neoadjuvant therapies. It is now known that a functioning immune system is vital for the cytotoxic and cytostatic action of several chemotherapeutic agents (Zitvogel et al., 2013) as well as immunotherapies (Tumeh et al., 2014). It is however difficult to completely dissect out the purely prognostic effect of immunity from that of the chemotherapy. In a murine spontaneous mammary cancer model, Jonkers and his colleagues highlighted that the role of adaptive immunity on the tumour response to chemotherapy might not be as crucial as previously postulated (Ciampricotti et al., 2012).

1.3.3. Immunology in metastatic CRC

Although intra-tumoural immunity in CRC has been proven to be both prognostic and predictive, most of the studies have been focused on primary tumour site. There is a dearth of literature studying the immunobiological microenvironment at distant

metastatic loci. Information about the immunobiology at metastatic sites is of vital importance in understanding immunoevasion mechanisms that result in metastasis. It is also important to clarify whether the immune signatures of the primary tumour can be viewed as a surrogate for the secondary. This information has important implications in planning potential targeted treatment with immunotherapies.

In the first workstream of this project, my aim is to compare the immune signatures of primary and pulmonary secondary CRC in samples obtained from the same patient. Using paired samples theoretically eliminates inter-patient confounding factors. Pulmonary metastases were chosen to be studied on the basis of the assumption that; unlike the liver the lungs are perfused solely by systemic blood which would theoretically protect them from the immune-modulating effects of perfusion by portal blood. The liver is frequently regarded as a *bona fide* lymphoid organ, it is constantly exposed to antigens derived from food and bowel flora and has rich resident innate and adaptive immune cells (Crispe, 2009). It is likely that the liver possesses mechanisms that allow for immunological tolerance of those antigens which might also impact the immune response to liver metastases (Knolle and Gerken, 2000). It has also been shown in a mouse model that the hepatic CD4 T-cells are functionally skewed towards a TH2 polarity and produced higher levels if IL-4, 5 and 10 when activated than their splenic counterparts (Katz et al., 2005).

To inform my choice of markers for staining, I used data from literature exploring immune signatures of primary and secondary CRC. Before commencing my research project, I was able to locate one paper that addressed that topic directly. In this study Remark and his colleagues compared the densities of cytotoxic lymphocytes ($CD8^+$), mature dendritic cells (DC-$LAMP^+$) and natural killer cells ($NKp46^+$) in primary CRC

and pulmonary secondaries. They found that the density of $CD8^+$ in the primary site correlated negatively with the density at the metastasis site. There was no significant difference in the two other markers. They also found that higher $CD8^+$ and DC-$LAMP^+$ cell densities at the metastatic site correlated with improved Overall Survival (OS) (Remark et al., 2013).

Due to the paucity of literature on immune signatures in CRC lung metastases, I reviewed studies exploring the immune signatures in CRC liver metastases. In a study from Memorial Sloan-Kettering Cancer Center, Katz *et al*. studied the correlation between densities of different T-cell markers (CD3, CD4, CD8, CD45RO) and overall survival in patients with CRC liver metastases. They stratified their sample of patients into those that survived ≤2 years and those that survived ≥10 years and stained Tissue Micro Arrays (TMA) with the corresponding markers. The authors found a significant correlation between high densities of CD3 and CD8 in the group of patients who survived ≥10 years. Paradoxically, they found that the density of $CD4^+$ cells was higher in the group that survived ≤2 years. The strongest prognostic correlation was found in the combination of CD4 and CD8 densities, showing that patients with high CD8 and low CD4 counts have the best prognosis. This interesting finding can be explained by the fact that the CD4 population could have been predominantly a regulatory subtype ($FOXP3^+$) or skewed to a T_H2 polarity (Katz et al., 2009). In another study, Wagner and colleagues performed flow cytometry studies on TILs from 16 CRC liver metastases looking at cytotoxic and helper T-cell populations and their activation markers. They found that the numbers of $CD8^+$ cells were higher in the normal liver parenchyma adjacent to the liver metastases than the metastases themselves. They however found that the proportion of activated ($CD25^+$ and $CD69^+$) and cytotoxically active ($CD107a^+$)

CD8 cells in the metastases was significantly higher. Conversely, they found that the numbers of helper T-cells ($CD4^+$) cells in the metastases were higher than adjacent normal parenchyma and that the numbers of activated ($CD25^+$) CD4 T-cells positively correlated with the numbers of activated $CD8^+$ T cells pointing to their role in activating cytotoxicity of CD8 T-cells (Wagner et al., 2008). In a study from the same research group the authors investigated the correlation between TILs density in metastatic (liver) CRC and response to chemotherapy. They improvised a scoring system of IHC stained sections using densities of CD3, CD8 and Granzyme B in either the primary tumour or the liver metastasis. They demonstrated that the densities of those markers correlated positively with response to chemotherapy and time to progression. In the main cohort, there were 10 primary/secondary pairs; in this sub-cohort the authors did not find any concordance between the densities of the same marker in the primary and the metastatic site (Halama et al., 2009). The same group then went on to validate their predictive scoring system in a larger cohort of CRC liver metastases (n=101). They used the same markers (CD3, CD8 and Granzyme B) and an improved weighted scoring system (double impact for CD3 density and single impact for both CD8 and Granzyme B). The authors demonstrated that increased infiltrates at the invasive margin of the metastatic deposit was predictive of response to chemotherapy. They also found a statistically significant correlation between a high score and progression-free survival (Halama et al., 2011).

Since the completion of my research work, a number of research papers studied the impact of the immune microenvironment in colorectal metastases. Mlecnik *et al.* performed a comprehensive immune profiling of 441 resected colorectal metastases from 153 patients. The vast majority (98.4%) of the metastases included in the study

were liver metastases. They recorded the Immunoscore® and the T and B cell score on all the samples. The authors found that the immune cell infiltrates were significantly higher in the invasive margins of the metastases than in the tumour cores except for FOXP3 expressing cells. They also demonstrated that there is a great degree of heterogeneity between patients and between different metastases in the same patients. Most importantly they showed that high scores correlated with improved disease-free survival, overall survival and response to chemotherapy (Mlecnik et al., 2018, Mlecnik et al., 2020). In another study from the same research group, Van den Eynde *et al.* examined the TIL infiltrates, immune scores and mutations in 603 resected metastases from 222 patients (96.6% liver metastases). Their results showed great degree of heterogeneity between the primary tumour and the metastasis in terms of adaptive cell infiltrates, mutations and Immunoscore®. The authors also reported significant intra and inter-metastatic heterogeneity. They reported significantly higher immune cell infiltrates in the invasive margins of tumours than the tumour cores. Also, they found that immune cell infiltrates were higher in the metastasis than the matched primary. The authors also demonstrated improved relapse-free survival and overall survival in patients with high a Immunoscore® (Van den Eynde et al., 2018). In another publication from the same group, Angelova *et al.* conducted an in-depth examination (histological, genomic and transcriptomic) on 31 samples of colorectal metastases from two patients who survived multiple metastatectomies with prolonged survival. This examination allowed the authors to glean insight into the temporal evolution of those metastases and their microenvironment. They reported significant inter-metastatic heterogeneity in terms of the mutations load, routes to metastasis and immune cell infiltrates. They also correlated the density of the immune infiltrates with immune

escape mechanisms finding that tumours with a high Immunoscore® were more prone to undergo immunoediting as an escape mechanism with resultant neoantigen depletion. This immunoediting correlated strongly with a T_H1-type anti-tumoural immunity (Angelova et al., 2018). In the most recent paper from Jérôme Galon's group, Baldin *et al.* assessed the impact of the immune score, histopathological features and RAS mutation status on the prognosis of colorectal liver metastases in a sample of 582 resections from 221 patients. The authors found that adverse histopathological features, RAS mutation and a low Immunoscore® lead to a shorter time to relapse after surgery but only the Immunoscore® had a significant impact on overall survival (Baldin et al., 2020).

Taken collectively, it is obvious that cells of the adaptive immune system play a key part in the prognosis of CRC and its metastases.

1.4. Immunotherapy in CRC

Immunotherapy is a form of biological targeted cancer treatment that utilises the functions of the body's immune system to recognise, control and eliminate neoplastic cells. This can be achieved either by sensitising the immune system against cancer cells, reversing the inhibitory pathways that supress the immune system (i.e., removing the brakes), boosting the immune system by enhancing co-stimulatory pathways or by engineered immune cells designed to target certain tumour associated antigens. Several of those methods have shown promise in CRC. Below, I will give an overview of some immunotherapeutic methods used in metastatic CRC:

1.4.1. Checkpoint blockade

Immune responses are governed by a myriad of stimulatory and inhibitory pathways and molecules called immune checkpoints. Those molecules and their ligands are expressed on both immune and non-immune cells and are important in keeping the immune system in check to ensure an adequate but proportional response is mounted against a non-self-antigen such as a tumour associated antigens. Both co-stimulatory and co-inhibitory molecules have been exploited in cancer immunotherapy but thus far mainly blockade of co-inhibitory molecules has shown the most promise. Therefore, references to checkpoint blockade (CPB) or immune checkpoint inhibition (ICI) generally means suppression of the co-inhibitory pathways. This strategy employs the use of monoclonal antibodies to block inhibitory receptors on tumour cells and TILs to essentially take the brake off an effective anti-tumour immune response.

Several clinically relevant CPB targets emerged over the last couple of decades. The two most eminent and perhaps most relevant in CRC are cytotoxic T-lymphocyte-associated protein 4 (CTLA-4) and programmed death protein-1 (PD-1) and its two ligands PD-L1 and L2).

CTLA-4 is a protein that is homologous to CD28 on the surface of T-lymphocytes. Due to this homology, CTLA-4 competes with CD28 for binding B7-family stimulatory ligands on antigen presenting cells (APC) such as CD80 (B7-1) and CD86 (B7-2). For T-cell activation several stimulatory signals have to take place in addition to the T-cell receptor (TCR) – antigen – MHC interaction. One of those stimulatory pathways is set in train by the interaction of CD28 with B7-family proteins. When CTLA-4 binds B7-family proteins it produces inhibitory signals that suppress T-cell activation and maturation (Krummel and Allison, 1995). The competitive binding to the B-7 ligands

also reduces their availability to bind CD28, hence suppressing stimulatory signals. This process occurs in the lymph nodes and happens early in the immune response at the priming stage of T-cell activation; therefore, it is thought of as a “central” checkpoint. The inhibitory effect of CTLA-4 is also thought to be, in part, due its constitutive expression on T-cells (T_{REG}) that have an important role in promoting immune tolerance by interaction with activated T-cells (Buchbinder and Desai, 2016, Syn et al., 2017).

PD-1 is another member of the CD28 superfamily and is expressed on the surface of T-cells, B-cells and myeloid-derived suppressor cells (MDSCs). PD-1 acts as an inhibitor of TCR activation signals which in turn suppresses T-cells’ effector functions. PD-1 also suppresses T-cells’ ability to secrete effector chemokines and cytokines such as interferon-γ (IFN-γ), tumour necrosis factor α (TNF-α) and interleukin-2 (IL-2). This loss of effector functions despite TCR engagement is called T-cell exhaustion (Wherry, 2011). PD-1 has two known ligands; the PD-L1 is the more ubiquitously expressed of the two. It is expressed by dendritic cells, activated T and B lymphocytes as well as some tumour cells. PD-L2 is usually more restricted to dendritic cells (Freeman et al., 2000, Latchman et al., 2001). The inhibitory role of the PD-1/PD-L1/PD-L2 access takes place later in the immune response at the effector phase of T-cell activity therefore it is thought of as a “peripheral” checkpoint (Buchbinder and Desai, 2016).

Clinical trials using CPB demonstrated great promise in achieving durable tumour control in a number of advanced solid tumours, namely melanoma and lung cancer (Brahmer et al., 2012, Topalian et al., 2012). The mutational burden of those tumours emerged as a biomarker for response to immunotherapy probably due to its direct link

to the intensity of the immune microenvironment (Rizvi et al., 2015, Samstein et al., 2019, Chan et al., 2019). This heightened tumour mutational burden results in the generation of a large number of neo-antigens that in turn result in a more florid immune response as those neo-antigens get presented on major histocompatibility complexes (Schumacher and Schreiber, 2015, Linnemann et al., 2015).

Probably due to the heterogeneity of CRC and the paucity of clear biomarkers, the results of immunotherapy have not been as promising in the early trials (Chung et al., 2010, Topalian et al., 2012, Brahmer et al., 2012). This paradigm changed when the results of the phase I KEYNOTE-016 trial showed that patients with deficient mismatch repair mechanisms (MSI-hi) had a significantly better response to Pembrolizumab, a PD-1 blocker, when compared to those with proficient mismatch repair mechanisms (Le et al., 2015). In this trial, the response rate and the progression-free survival rate were 40% and 78% respectively in dMMR-MSI-Hi metastatic CRC cohort (*n*= 10) as opposed to 0% and 11% in the pMMR-MSS cohort (*n*= 18). The median progression-free survival (PFS) and overall survival (OS) were not reached in the MSI group and were 2.2 month and 5 months in the pMMR-MSS cohort. Similar favourable results were seen in the smaller dMMR-MSI-Hi non-CRC cohort (*n*= 7) (Le et al., 2015).

This favourable response seen in the trials is likely to be due to the inflamed phenotype of this tumour subset secondary to an increased tumour mutation burden and the subsequent increase in neoantigens (Giannakis et al., 2016, Chalmers et al., 2017, Le et al., 2017). This inflamed tumour microenvironment, as well as being rich in pro-inflammatory cells and mediators is also enriched in checkpoint blockade proteins and this is important in mitigating the risk of an unchecked immune response that would be harmful to the host (Llosa et al., 2015). This fact was corroborated by Lal and

colleagues in a transcriptomic analysis of the TCGA database which found that CRC tumours with a high immune signatures (a group enriched in dMMR-MSI-Hi tumours) also had evidence of over-expression of certain CPB molecules such as CTLA-4, PD-1, PD-L1 and LAG-3 (Lal et al., 2015).

Those promising findings in earlier trials and the identification of the hyper-mutated phenotype as a biomarker sparked a series of important trials exploring the utility of CPB in hyper-mutated CRC subsets. Checkmate-142 was an open-label, multicentre, phase 2 trial that assessed the effectiveness of Nivolumab – a PD-1 blocker – as a single agent or in combination with Ipilimumab – a CTLA-4 blocker – in the treatment of chemo-refractory mCRC. In the monotherapy cohort, 74 patients with dMMR-MSI-Hi mCRC received Nivolumab. Over half (54%) of the patients in this cohort had previously been on three or more lines of treatment. The authors showed that 31.1% of the cohort had an objective response to treatment and that 69% had disease control for at least 12 weeks. At a median follow-up of a year, the median duration of response was not reached and all patients who showed an objective response were alive at the time of data analysis. The authors demonstrated a durable response to treatment with a 12-month progression-free rate of 50%, a 12-month overall survival of 73% and a median progression-free survival of 14.3 months (Overman et al., 2017). The second cohort of the Checkmate-142 trial had 119 patients with dMMR-MSI-Hi mCRC cancers treated with a combination of Nivolumab and Ipilimumab. In this cohort, greater than three quarters (76%) of patients received at least two prior treatment lines. The results revealed a 55% objective response rate and an 80% disease control rate for 12 weeks or more. In this cohort too, the median duration of response was not reached at a median 13.4 month follow. The 12-month progression-free rate was 71% and the 12-

months overall survival rate of 85% (Overman et al., 2018b). The added benefit was at the cost of a modest increase in the occurrence of grade 3 and 4 treatment-related side effects at 20% for the single agent cohort and 32% in the combination cohort (Overman et al., 2017, Overman et al., 2018b, Morse et al., 2019b). In light of the encouraging results of those trials, expedited US Food and Drugs Administration (FDA) approval was granted for the use of Pembrolizumab, Nivolumab and a combination of Nivolumab and Ipilimumab in adult and paediatric dMMR-MSI-Hi mCRC refractory to first line therapy in May 2017, July 2017 and July 2018 respectively. (Overman et al., 2018a, Morse et al., 2019a, Cohen et al., 2019, Kreidieh et al., 2020). The latest trial results to be published were the ones from the phase II, open-label, multicentre KEYNOTE-164 trial where Le *et al* used Pembrolizumab in the treatment 124 patients with dMMR-MSI-Hi mCRC tumours that progressed on ≥1 conventional treatment line (cohort A, *n*= 61) or ≥2 treatment line (Cohort B, *n*= 61). At a median follow up of 31.3 months for cohort A and 24.2 months for cohort B, the results demonstrated an objective response in 33% of the patients in both cohorts. The responses were sustained with median duration of response not reached in either cohort. Cohort A patients fared better than cohort B with median progression free survival of 2.3 months and 4.1 months respectively. Whilst overall median survival of 31.4 months in cohort A, it was not reached in cohort B. The safety profile of the treatment was favourable with only 16% and 13% of patients in cohorts A and B respectively suffering significant (grade 3 and 4) treatment-related adverse effects (Le et al., 2020).

The encouraging results in the context of second- and third-line treatment of dMMR-MSI-Hi mCRC sparked interest in exploring the effectiveness CPB as a first line treatment in this group of advanced tumours. KEYNOTE-177 is a phase III open label

randomised trial that explored the benefit of Pembrolizumab monotherapy as a first-line treatment of dMMR-MSI-Hi mCRC in comparison to standard of care (SOC) therapies with chemotherapeutic and/or biological treatments. The recently published results showed a statistically significant superior progression-free survival in the Pembrolizumab group (16.5 months vs 8.2 months). It also showed a significantly improved overall response in the Pembrolizumab group (43.8% vs 33.1%) and at 24 months 83% of responding patients in the Pembrolizumab group had ongoing responses as opposed to 35% in the SOC group. Interestingly, the patients in the Pembrolizumab arm of the study suffered far less grade 3 & 4 treatment-related side effects (22% vs 66%) (André et al., 2020) (NCT02563002).

The utility of CPB in also currently being explored in the context of adjuvant therapy for stage III dMMR-MSI-Hi CRC after initial curative intent resection. ATOMIC (NCT02912559) is a randomised open-label phase III trial currently actively recruiting 700 patients who had a curative resection for stage III cancer into receiving conventional chemotherapy either with or without a Atezolizumab, a PD-L1 blocker. The primary aims of this trial is to compare disease-free survival up to 5 years after receiving treatment. The secondary outcome measures are overall survival and occurrence of treatment-related adverse events (NCT02912559).

The use of CPB as a neoadjuvant in early colon cancer was explored in the single-centre randomised open-label phase II NICHE Trial. This trial recruited 40 patients with both dMMR (20 patients) and pMMR (20 patients) early colon cancers. The dMMR cohort was treated with a combination of Nivolumab and Ipilimumab for 6 weeks prior to surgery. The pMMR cohort is split in half; one half received Nivolumab and Ipilimumab in a similar regime as the dMMR cohort and the other half received the

same combination in addition to Celecoxib, a cyclooxygenase-2 inhibitor (COX-2). The primary outcome of the trial was to assess the safety of the combination in the context of neoadjuvant treatment (NCT03026140). The authors reported that all 20 patients in the dMMR cohort experienced a pathological response to the treatment with 19 having a major pathological response where 10% or less residual tumour is visible. Strikingly, 12 patients had a complete response. More interestingly, 27% of the pMMR cohort demonstrated a pathological response. The authors reported that pMMR tumours infiltrated by $CD8^{+}$/$PD\text{-}1^{+}$ lymphocytes were predictive of a response (Chalabi et al., 2020). For early rectal cancer, the same Dutch group are due to start recruiting patients to the TARZAN trial which will assess the effectiveness of Atezolizumab (in addition to Bevacizumab, a vascular endothelial growth factor VEGF inhibitor) following radiotherapy in achieving a complete (or near complete) response in resectable rectal cancer (NCT04017455).

Although most of the previously presented trial focused on dMMR-MSI-Hi tumours, there has been evidence of CPB treatment success in other hyper-mutated MSS mCRC subtypes, namely, tumours with mutated DNA polymerase-ε (*POLE*). A case report of an 81-year-old patient with a POLE mutated metastatic tumour showed clinical response after treatment with Pembrolizumab (Gong et al., 2017).

This demonstrated the importance of careful patient selection and bio-marker identification to tailor individualised targeted therapies that avoid unnecessary toxicity in patients who may not benefit from the treatment. Those findings have proven a great promise for immunotherapy in CRC, it is however clear that there is a prerequisite for the presence of a demonstrable immune response. Other immunotherapy strategies

that demonstrated benefit in other tumour types such as adoptive T-cell transfers and cancer vaccines may prove beneficial in tackling this.

Unfortunately, around 95% of metastatic CRC falls in the MSS subtype which doesn't lend itself as readily to treatment with CPB as the tumours are generally more immunologically inert. The conundrum of how to render MSS tumours more susceptible to immunotherapy has been an area of heated research in the past few years; with the aim to find a strategy to immune-sensitise MSS tumours by combination therapies (either with conventional chemotherapy, other CPB agents or other biological therapies such as vascular endothelial growth factor inhibitors), tumour vaccines, adaptive cell transfers and bi-specific T-cell engaging antibody therapy (Kreidieh et al., 2020).

1.4.2. Bispecific antibodies (BsAb)

Bispecific antibodies are bio-engineered fusion proteins that possess two or more antibody variable binding sites that are able to bind two different antigens simultaneously in an MHC-unrestricted manner. One of the binding sites is traditionally specific to a tumour-associated antigen (TAA) and the other binding site is usually specific to an immune cell such as a T-cell (e.g., CD3). This results in the ability to physically approximate the two cells (the target and the effector) to essentially create an immunological synapse that facilitates activation of the T-cell to mediate its effector functions. As some bispecific antibodies also possess an Fc domain (fragment crystallisable) they can interact with Fc receptors and exert effector functions on accessory cells (e.g., natural killer cells and macrophages) and complement proteins namely antibody-dependent cell mediated cytotoxicity (ADCC), complement-dependent cytotoxicity (CDC), and antibody-dependent cellular phagocytosis (ADCP).

Some of those antibodies are designed to also simultaneously block key oncological receptors (such as epidermal growth factor receptor (EGFR)) (Yu et al., 2017).

Bispecific antibodies showed promise in the treatment of haematological malignancies such as acute lymphoblastic leukaemia (ALL) (Wu et al., 2015). Their utility in the treatment of solid tumours however remains under investigation. In CRC, bispecific antibodies targeting TAAs such carcinoembryonic antigen (CEA) or epithelial cell adhesion molecule (EpCAM) were developed and tested in pre-clinical and early clinical trials (Yu et al., 2017). Herrmann et al. demonstrated that bispecific antibodies with EpCAM and CD3 binding domains successfully eliminated CRC cells lines (HT-29) and imparted a significant anti-tumoural activity on mice injected with 5000-fold the tumorigenic dose of CRC initiating stem cells (Herrmann et al., 2010). Lutterbuese et al. showed that bispecific antibodies designed to bind EGFR on tumour cells and CD3 on T-lymphocytes resulted in elimination of colorectal tumour cell lines even in the presence of a RAS or BRAF mutations' which would normally confer resistance to anti-EGFR agents (Lutterbuese et al., 2010). In a phase 1 trial, Catumaxomab, a bispecific antibody designed to bind EpCAM of tumours and CD3 on T-lymphocytes, was administered to 16 patients with disseminated epithelial solid tumours of which 13 were mCRC. Although the aim of the trial was to assess the drug's safety profile and establish its safe doses, the investigators reported stable disease in only two patients and progression in the rest (Mau-Sorensen et al., 2015). MEDI-565 is a bispecific antibody with CEA and CD3 binding sites. It showed specificity in engaging CEA expressing cell and halted the growth of colorectal tumour cells in murine models (Lutterbuese et al., 2009). In a phase 1 trial, 39 patients with advanced gastrointestinal cancers (72% of them colorectal) received escalating doses of MEDI-565. Although

the aim of the trial was to assess the safety profile of the drug, the authors reported stable disease in 28% of the patients and a median overall survival of 5.5 months (Pishvaian et al., 2016). MEDI-565 cytotoxicity was enhanced by the addition of PD-1/PD-L1 blockade in an in vitro study on CEA-expressing cell lines (Osada et al., 2015). Perhaps the bispecific antibody with the most promise is RO6958688 which is a new T-cell bispecific antibody (TCB) with CEA/CD3 binding specificity. It has shown *in vitro* cytotoxic activity in CEA-expressing cells regardless of any co-existing genetic mutations in relevant oncogenes and tumour-suppressor genes. The cytotoxicity was proportional to the level of CEA expression. It also showed *in vivo* effect on causing tumour regression in a murine xenograft model. More interestingly, RO6958688 converted immunologically naïve tumours into inflamed ones with increased expression of checkpoint blockade targets (Bacac et al., 2016a, Bacac et al., 2016b). RO6958688 entered phase 1 trials in advanced CEA-expressing solid tumours as a single agent or in combination with a PD-L1 blocker (NCT02324257, NCT02650713). Preliminary results from these trials were presented in the European Society of Medical Oncology (ESMO) and the American Society of Clinical Oncology (ASCO) meetings in 2017. In 45 patients with mCRC (31 in the single agent arm and 14 in in the combination arm), there was radiological evidence of a tumour inflammatory response within two days after the initiation of therapy. Metabolic partial response (on positron emission tomography PET) was experienced in 29% and 50% of patients at 4-6 weeks in the single agent and the combination cohorts respectively. The treatment-associated adverse effects were tolerable and comparable between the two cohorts (Argilés et al., 2017, Tabernero et al., 2017). Interestingly, the majority of mCRC patients in both cohorts were MSS.

Bispecific antibodies are amongst the most promising immunotherapies for MSS tumours. The majority of mCRC patients enrolled in the previously mentioned trials were MSS patients. This is likely to be due to that fact that bispecific antibodies enhance the immune cell infiltration of tumour beds rendering the microenvironment more 'inflamed'. It has also been shown that those newly inflamed microenvironments are enriched in T_H1 polarising cytokines (Goere et al., 2013, Fossati et al., 2015).

1.4.3. Tumour vaccines

Vaccinations have been effectively employed for centuries to artificially expose the immune system to pathogen-associated antigens to generate lasting immune responses, both humoral and cellular. Preventative vaccinations to cancer-associated pathogens such as hepatitis B and human papilloma virus (HPV) have shown great potential in preventing hepatocellular carcinoma and cervical cancer, respectively (Kim et al., 2011, Roden and Stern, 2018). The utility of tumour vaccinations has more recently been explored in the context of therapeutic immunotherapy against established cancers. The targets for such vaccines have traditionally been tumour-associated antigens (TAA). Those antigens are considered self-antigens but in the context of cancer they are usually either mutated or over expressed on tumour cells. As a result the immune system's affinity to those antigens is reduced as part of the natural immune tolerance mechanisms during development (Hollingsworth and Jansen, 2019). In CRC the most commonly used TAAs are CEA, EGFR, p53, βhCG, 5T4 and gastrin (Merika et al., 2010). To enhance the immune response to the vaccine, adjuvants are used to stimulate the initial aspects of the sensitisation process such as enhancing recruitment and stimulation of antigen presenting cells (APC) to engulf the introduced antigens and effectively present them to effector cells of the immune

system. Examples of commonly used adjuvants are Bacillus Calmette–Guérin (BCG) and granulocyte-macrophage colony-stimulating factor (GM-CSF) (Jiang et al., 2019).

Tumour vaccines generally fall into several categories depending of the type of antigen, administration vector and the adjuvants used to augment the immune response to vaccine (Hollingsworth and Jansen, 2019, Kreidieh et al., 2020). Broadly speaking there are four categories:

Cell-based vaccines: those vaccines use lysates of whole cells, either autologous from cells derived from the actual tumour or allogeneic derived from several tumour cell lines. This technique is advantageous in the fact that it does not require prior identification of antigens and can generate responses to a large number of antigens (Le et al., 2010). This approach was trialled in a phase III randomised controlled study in the adjuvant setting in CRC (stage II and III) where 98 patients were randomised into having a resection followed by an autologous cell - BCG vaccine or resection alone. Although the researchers did not demonstrate any statistical advantage to using the vaccine in the whole cohort, they showed a statistically improved overall and disease-free survival in the colon cancer cohort (Hoover Jr et al., 1993). In another randomised controlled trial of node-negative CRC (stage I and II). Vermorken et al. randomised 256 patients into receiving an autologous, radiation-attenuated whole tumour cells with BCG following complete surgical resection. The group demonstrated that the vaccinated group had significantly less recurrences and longer recurrence-free survival. This advantageous effect was however only observed in stage II tumours (Vermorken et al., 1999). The positive results from the previous two trials were not replicated in another phase III randomised trial with a larger number of stage II and III colon cancer patients (n=412). The authors did not report any survival advantage in

the vaccine cohort over the observation-only cohort (Harris et al., 2000). In another phase III randomised controlled trial of an autologous tumour cell vaccine infected with the Ulster non-lytic strain of the Newcastle virus, researchers randomised 51 patients to receive the vaccine or a placebo following surgical resection of CRC liver metastases. The researchers did not demonstrate any significant survival or recurrence advantage between the groups. On subgroup analysis however, a significant overall survival and recurrence-free survival advantage was found in colon cancer patients but not rectal cancer patients (Schulze et al., 2009).

Dendritic cell vaccine: this methodology uses the body's professional APC to present TAAs to the immune system. In this approach, autologous immature DCs are collected by leukapheresis, transfected with genes encoding the TAAs and matured *ex-vivo* then re-injected into the patient where they deliver their immune priming functions. This approach is beneficial in the fact that is bypasses the host's APC dysfunction and malignancy induced inertia (Drake et al., 2014, Palucka and Banchereau, 2012). In the context of mCRC, an early phase I trial of a DC vaccine pulsed with a CEA derived peptide epitope called CAP-1 was tested for safety in 21 patients with advanced, CEA-producing malignancies (11 were mCRC). The authors highlighted the safety of the vaccine but did not elude to any disease-specific outcomes (Morse et al., 1999). In a phase II randomised controlled trial of 52 patients (28 experimental and 24 placebo) with chemo-refractory mCRC, DCs were pulsed with an autologous whole-cell tumour lysate and injected back into the patients. The trial was terminated due to futility and the authors failed to demonstrate any tangible disease-related outcomes between the groups. They however demonstrated improved T_H1 immunity in responders (Caballero-Banos et al., 2016).

Peptide-based vaccines: these vaccines use specific peptide sequences from TAAs as opposed to whole-cell vaccines that contain numerous peptides. As a result, these vaccines tend to be more specific and depending on the length of the peptides they differentially activate CD4 and CD8 cells. Although short sequence peptides enter cells more readily, they only succeed in activation of CD8 T lymphocytes as they are only expressed in the context of MHC I, the lack of CD4 activation hampers their utility. Whilst long sequence peptides are more difficult to uptake, they present the peptides in both MHC I and MHC II resulting in activation of both CD4 and CD8 lymphocytes (Zhang et al., 2009). To circumvent the difficulties with peptide vaccines, it is possible to use DNA or RNA instead where it incorporates into the transcription machinery of DCs and produces the required epitopes to evoke an immune response (Hollingsworth and Jansen, 2019). FXV was a phase II trial of a polyvalent peptide vaccine containing 5 HLA-A*2402-restricted peptides derived from 3 oncogenes (RNF43, TOMM34, KOC1) and two from vascular endothelial growth factor (VEGF). Ninety-six patients with advanced chemotherapy naïve CRC were enrolled (50 were HLA-A*2402 matches and 46 were unmatched) to receive standard oxaliplatin-based chemotherapy along with the vaccine. The researchers failed to demonstrate any significant differences between the two groups in terms of response rate, progression-free survival or overall survival (Hazama et al., 2014).

Virus-based vaccines: those vaccines utilise the viruses as vectors to deliver genetic sequences encoding tumour associated antigenic peptides that are combined into the viral genetic backbone and use the viral machinery to transcribe those sequences into peptide. This methodology benefits from the immunogenicity of the virus itself to enhance the immune response. Viruses used for this purpose have a high safety profile

and low pathogenicity to the host such as poxviruses, adenoviruses and alphaviruses (Larocca and Schlom, 2011, Hollingsworth and Jansen, 2019). In a phase I study of an adenovirus (Ad5) delivered cancer peptide (GUCY2C-PADRE), 10 patients with early-stage CRC (stage I or II) were recruited to receive the vaccine after resection of their cancer. The aim of the study was to assess the safety of the vaccine and determine its immunological properties. The authors reported minimal treatment-related adverse effects and showed that the vaccine generated split immunity with activation of CD8 T-lymphocytes but not CD4 T-lymphocytes (Snook et al., 2019). As most TAAs serve as weak antigens to stimulate T-cell responses, combining the antigen with a co-stimulatory molecule arose as an attractive method to enhance the response. Combining CEA with B7.1 (CD80) in a non-replicating Canarypox virus vaccine was proven safe in phase I trials (Hörig et al., 2000, von Mehren et al., 2000). This was followed by a phase II trial of that vaccine where 118 patients with mCRC were vaccinated before or concurrently with their conventional chemotherapy. The authors reported no additional benefit from the vaccine over chemotherapy alone in terms of disease control. The authors however reported evidence of anti-CEA cellular immunity with a type 1 orientation (Kaufman et al., 2008).

1.4.4. Cellular Immunotherapy

This relatively young field of 'living' immunotherapy involves using the patient's own ex vivo-activated and expanded -and sometime bioengineered- anti-tumour immune cells to fight cancer (Ruella and Kalos, 2014, Rosenberg and Restifo, 2015). This modality is an umbrella term that encompasses several subcategories such as adoptive cell transfer (ACT) which is also known as tumour infiltrating lymphocyte (TIL) therapy with or without TCR engineering and chimeric antigen receptor T cell (CAR-T) therapy

(Ruella and Kalos, 2014, Johnson and June, 2017). The former essentially involves harvesting the patient's lymphocytes and selectively expanding those with an anti-tumour affinity. The expanded cells are then infused back into the patient after the patient had undergone lymphodepletion (Rosenberg and Restifo, 2015). As most native anti-tumour T-cells generally have a low affinity to the specific TAA, re-engineering the T-cell receptor (TCR) could mitigate this shortcoming. Because TCRs work in an MHC-restricted manner, CAR-T therapy utilises the antibodies' ability to bind antigens without the need for MHC presentation to bypass this hurdle. In CAR-T cells, the extracellular TCR domain is replaced with an antibody TAA-specific variable light and heavy chains attached to the normal TCR signalling mechanisms (Wrona and Potemski, 2019, Johnson and June, 2017).

Cellular immunotherapy has demonstrated effectiveness in the treatment of haematological malignancies and melanoma (Ruella and Kalos, 2014, Rosenberg and Restifo, 2015). Anti-CD19 CAR-T therapy has been FDA approved for the treatment of refractory B-cell acute lymphoblastic leukaemia (ALL) (Wrona and Potemski, 2019). Their use in solid tumours –other than melanoma- is still emerging and remains mostly in the pre-clinical or early clinical phases of research (Johnson and June, 2017). In CRC, in vitro studies demonstrated that peripheral blood Natural Killer (NK) calls harvested from healthy individuals and activated with IL-2 and IL-15 were capable of lysing five CRC tumour cell lines treated with the anti-EGFR monoclonal antibody Cetuximab. This cytotoxic effect was mediated by antibody dependent cellular cytotoxicity (ADCC) and was unaffected by mutations of the EGFR downstream signalling molecules such as RAS and BRAF (Veluchamy et al., 2016). The same group then confirmed the cytotoxic effects of NK adoptive cell transfer in vivo in a

murine mCRC model. They also demonstrated that peripheral blood NK cells from mCRC patients (n= 10) had significantly impaired cytotoxicity compared to NK cells from healthy volunteers (n= 10) (Veluchamy et al., 2017). Turin and colleagues demonstrated the ability of NK cells to lyse autologous mCRC cells grown ex vivo. They observed that although the native NK cells had an impaired cytotoxic function, this function recovered when the cells were activated with IL-2 and IL-15. The cytotoxic potential was further augmented by incubating the cells with Cetuximab (Turin et al., 2018).

A CEA-specific TCR engineered ATC showed effectiveness in an early study of 3 chemo-refractory mCRC patients. In those patients, peripheral blood T-lymphocytes were harvested and retrovirus-transfected with a murine-engineered TCR with a high affinity to CEA in an HLA-A*2021 MHC molecule. All three patients developed severe colitis which limited the utility of this approach (Parkhurst et al., 2011). CAR-T cell therapy is also finding its place in the treatment of chemo-refractory mCRC. In a phase I trial of a CEA-specific CAR-T cells, 6 patients with extensive hepatic metastasis from CEA positive GI tumours (5 mCRC and 1 metastatic pancreaticobiliary adenocarcinoma) were injected autologous CAR-T cells with or without concomitant IL-2 infusion. The authors reported no significant treatment related side effects. They observed successful trafficking of CAR-cells into the metastases (5 out of 6 patients) as well as a significant reduction in serum CEA levels in patients who received IL-2. Five out of the six patients died of disease progression and one patient had prolonged disease control and was alive at 23 months of follow up (Katz et al., 2015). In a phase 1 trial, 10 patients with mCRC received intravenous infusions of anti-CEA CAR-T cells. The authors reported minimal treatment-associated adverse effects. Seven of the ten

patients had stable disease on therapy with two showing a sustained response at 30-week follow up (Zhang et al., 2017a). GUCY2C-specific CAR-T cells also showed anti-CRC cytotoxicity in pre-clinical cell line and murine models (Magee et al., 2018).

1.5. Thesis hypotheses

In the first section of this thesis, I hypothesise that the response to colorectal cancer defers at the metastatic site to that at the primary site. I hypothesise that the immune response in the lung would be stronger than in the bowel perhaps owing to a less immune suppressed microenvironment.

In the second section of the thesis, I hypothesise that there is a unique subset of MSS colorectal tumours that evokes an immune response as strong as that evoked by *bona fide* MSI-hi tumours.

1.6. Thesis aims

In the first section, I will be focusing on understanding the differences in the immune cell infiltrates and the expression of immune-related molecules such as checkpoint blockade markers and major histocompatibility complexes.

In the second section, I will be exploring the immune microenvironments of primary CRC with MSI-hi and MSS biology. I will be specifically focusing on comparing a specific category of MSS tumours with a heightened immune response and comparing that to tumours with MSI-hi biology.

2. Chapter Two: Patients, Materials and Methods

2.1. Ethical approval

For this work, I used an existing ethical approval that was granted to Professor Wilcox's research group by the Research Ethics Committee to study the immunobiology of solid tumours (Reference: 13/WM/0339). To tailor it to my study, I made minor amendments to the methodology (mainly the marker staining panel) and updated the patient information leaflets. Those amendments were submitted and approved by The Integrated Research Application System (IRAS). I then applied to the participating hospitals' Research and Development (R&D) departments using the IRAS Site-Specific Information (SSI) form to obtain samples. The coordination of sample collection between participating sites was facilitated by a dedicated research nurse (Miss Hollie Bancroft).

2.2. Patients

2.2.1. Primary vs Secondary (Results in Chapter Four)

In order to compare the immune signatures between primary and secondary tumours, I obtained a list of consecutive patients who had lung metastasectomies following bowel resections for primary CRC. The primary operations for bowel cancer were perform by a network of hospitals in the West Midlands region (and the pulmonary metastasectomies were performed exclusively at Heartlands Hospital (Heart of England NHS Foundation Trust now part of University Hospitals Birmingham NHS Foundation Trust) which is the regional centre for thoracic oncological surgery. The formalin-fixed paraffin embedded (PPFE) blocks of the primary tumour were requested from the pathology departments of the corresponding network hospitals and the blocks

for the metastasectomies were requested from the pathology department at Heartlands hospital. 4μm histological sections were taken from the blocks prior to commencement of staining. After sectioning the slides were stored in a dark and dry storage cupboard and stained at the soonest opportunity. The stained slides were digitally scanned immediately after completion of staining.

2.2.2. MSS vs MSS-hi vs MSI (Results in Chapter Five)

Three cohorts of samples were obtained for this study. All samples were in the form of FFPE 4μm histological sections.

The study cohort consisted of 10 samples from MSS colorectal tumours that were found to have a high MHC Class II expression (IHC) which is central to the coordinated immune response cluster. Those samples were selected from a cohort of MSS colorectal tumours (n=106) and 10% of the samples with the highest MHC Class II expression were chosen (n=10). A power calculation was not possible due to the limited number of study samples, difficulty to predict the size of the difference and the exploratory nature of this study. Those sections were donated by a colleague who was investigating the CIRC in CRC (Dr N. Lal).

For comparison, two control cohorts were obtained. The first cohort consisted of 10 consecutive samples of mismatch repair deficient (dMMR) CRC. The mismatch repair status was ascertained by loss of expression of one or more of the mismatch repair proteins (MLH1, MSH2, MSH6 and PMS2) on immunohistochemistry (IHC) (Lindor et al., 2002). The second control cohort consisted of 10 consecutive samples of mismatch repair proficient (pMMR) CRC. Those tumours were identified by positively staining for all MMR proteins on IHC. Both control cohorts were obtained from Heart of England

NHS Foundation Trust (now part of University Hospitals Birmingham Foundation Trust) and selected by an experienced consultant histopathologist (Dr Gerald Langman).

The slides were stored and processed in a similar fashion to that described in the previous section.

Due to prior anonymisation of the study cohort, it was not possible to obtain patient and disease information, therefore matching patients (for patient and tumour characteristics) was not possible.

2.3. Antibody choice

The antibody market is saturated with different companies that offer antibodies to stain virtually any marker. The sensitivity and specificity of some antibodies is questionable though (Bordeaux et al., 2010). There are different levels of validation; the highest of those levels is conformity to the European CE (Conformité Européene) standards and license for in-vitro diagnostic medical use (IVD-CE). However, there is a plethora of antibodies that are intended for research use only. The levels of validation in this group vary widely, ranging from robustly validated antibodies using gene knock out or knock down, use of blocking peptides and employing series of positive and negative controls. On the other end of the spectrum there are antibodies with limited data on validation processes.

For the studies in this thesis, I used the IVD-CE antibodies where available. Alternatively, I used antibodies that were supplied with robust validation data. For those antibodies that do not fall into either of the two categories I decided to validate them myself as detailed further down on this chapter [Table 2.1].

I elected to strike a pragmatic balance between cost and time efficiency and elected to validate the antibodies by transfecting cell lines with plasmids containing the gene of interest. I then confirmed successful transfection by flow cytometry and then assessed immunoreactivity on FFPE sections using standard IHC methods.

Antibody	Manufacturer	Validation
CD3	Leica	IVD-CE
CD4	Leica	IVD-CE
CD8	Leica	IVD-CE
PD-1	Cell Marque	IV-DCE
T-BET	Cell Signalling Technology	Robust validation – Blocking peptide
PD-L1	Cell Signalling Technology	Robust validation – Blocking peptide
FOXP3	Abcam	Minimal validation information
MHC Class I	Abcam	Minimal validation information
MHC Class II	Abcam	Minimal validation information
RORγt	Merck	Minimal validation information

Table 2.1: List of the antibodies used in this project and their level of validation

2.4. Validation of antibodies

2.4.1. Validation process

I elected to validate the antibodies by transfecting cell lines with expression plasmids containing the gene of interest. I then ascertained the success of transfection by flow cytometry using negative and positive controls. To simulate staining on FFPE sections, I pelleted the transfected cells, fixed them in formalin and embedded them in paraffin. I then 4μm histological sections and immunohistochemically stained them with the

antibody being validated. Positive and negative controls were also processed in a similar fashion. I carried out both manual and automated staining of these sections. Advice on interpretation of staining was sought from an experienced histopathologist (Dr Maha Ibrahim).

2.4.2. Cell line selection

In order to choose the most appropriate cell line to perform the transfection I chose lines that natively did not expressed or had very low levels of expression of the protein I am intending to validate. This was achieved by reviewing expression databases for mRNA (such as the Cancer Cell Line Encyclopaedia (Barretina et al., 2012) or by locating publications advising on expression levels of those proteins. The ease of handling, transfection efficacy and availability were also factors that were taken into consideration for cell line choice.

2.4.2.1. MHC Class II

To validate the MHC class II mAb I obtained a stably CIITA (Class II major histocompatibility complex transactivator) lentiviral transduced HEK293 cell line from Dr Heather Long. I used both K562 and parental HEK293 as negative control.

2.4.2.2. FOXP3 and RORγt

To validate the FOXP3 and RORγt antibodies I used the HEK 293T cell line. The HEK293 cell line is a human embryonic kidney cell line and the HEK293T variant which contains SV40 large T-antigen. This cell line was chosen because it does not express FOXP3 or RORγt innately and because this cell line is easy to handle and transfect. I used the parental HEK293T as a negative control.

2.4.2.3. MHC Class I

To validate MHC Class I I chose the K562 cell line. The K562 is a human chronic myelogenous leukaemia cell line that does not express MHC class I or class II due to its lack of expression of KBF1 and NF-κB (Blanchet et al., 1992). I also attempted to work with CHO (Chinese Hamster Ovarian) cells under the presumption that the native hamster MHC Class I will not cross-react with the anti-human HLA class I molecules. I used parental K562 cells as a negative control and HEK293T as a positive control.

2.4.3. Cell Culture

2.4.3.1. K562

K562 suspension cells were maintained in Roswell Park Memorial Institute (RPMI) 1640 medium with 10% Foetal Calf Serum (FCS) at 37°C in 5% CO2. The cells were passaged twice a week at a ratio 1:10 depending on the density of the suspension.

2.4.3.2. HEK293/HEK293T

HEK293/HEK293T cells were maintained in Dulbecco's Modified Eagle's (DMEM) medium with 10% FCS at 37°C in 5% CO2. The cells were passaged at 1:10 ratio when 85 – 90% confluent.

2.4.3.3. CHO

CHO cells were maintained in Nut Mix medium with 10% FCS at 37°C in 5% CO2. The cells were split at 1:10 ratio when 85 – 90% confluent.

2.4.4. Plasmids (Figure 2.1)

2.4.4.1. MHC Class I

Those plasmids were donated by Dr Heather Long.

pcDNA 3.1 with HLA-A*0301

pcDNA 3.1 with HLA-B*40.01

pcDNA 3.1 with HLA-Cw07.02

2.4.4.2. FOXP3 and RORγt

Those plasmids were purchased from Sino Biological (Sino Biological Inc, Beijing, China).

Human FOXP3 ORF mammalian expression plasmid, C-GFPSpark tag

Human RORγt ORF cDNA clone expression plasmid, C-GFPSpark tag

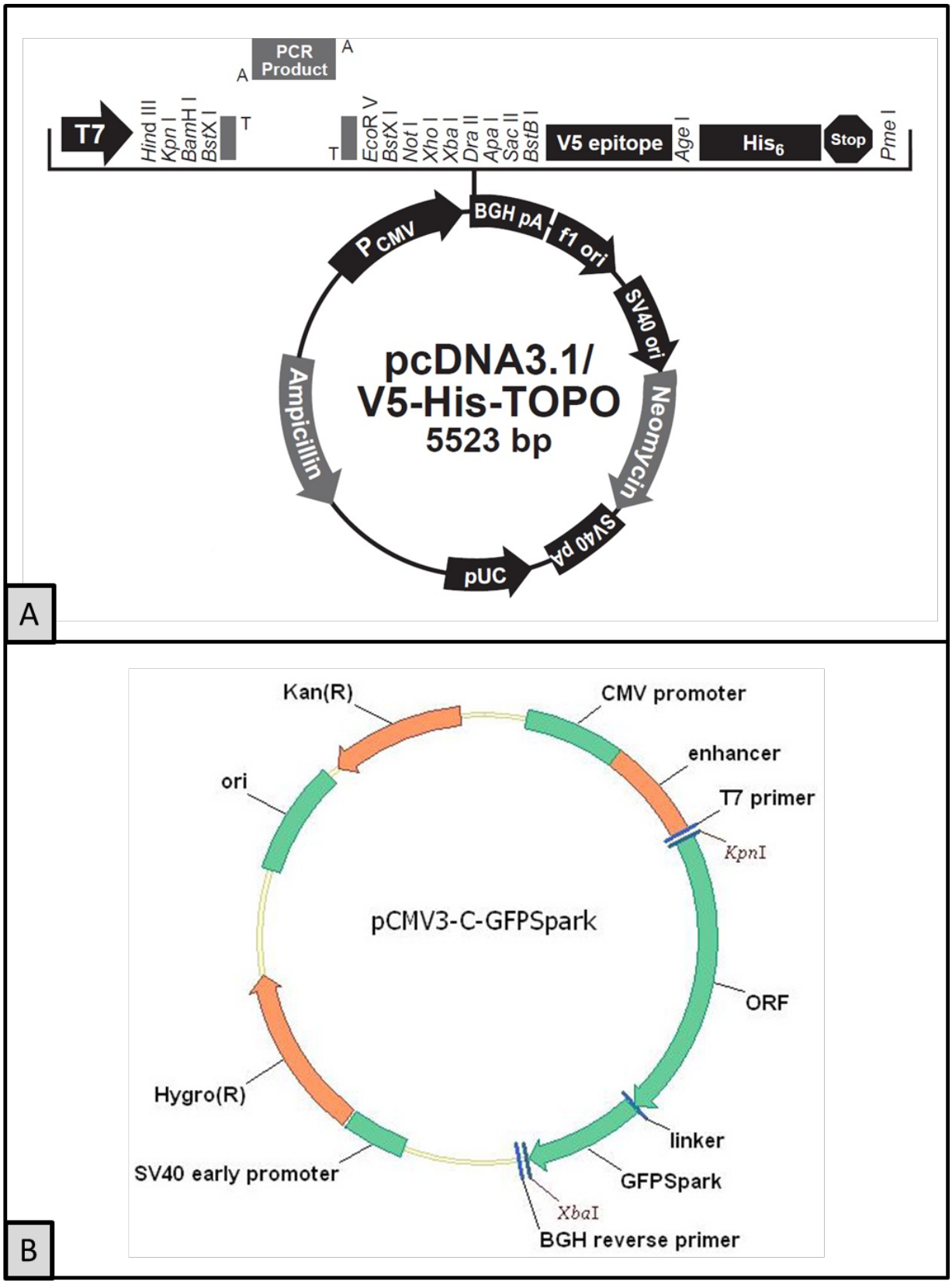

Figure 2.1: Schematic diagram of the pcDNA 3.1/V5-His-TOPO plasmid (A) used in MHC class I validation and pCMV3-C-GFPSpark plasmid (B) used in FOXP3 and RORγt validation.

2.4.5. Plasmid cloning

Producing plasmids for transfection: in order to bulk up the quantity of plasmids purchased I performed bacterial transformation and mini-prep.

2.4.5.1. Bacterial transformation

The plasmid solution and NEB 5-alpha competent E.Coli (New England BioLabs, Ipswich, MA, USA) were slowly thawed on ice. Then 100ngs of plasmid was added to the bacterial tube and incubated on ice for 30 min. The suspension was then placed in a water bath at 42°C for 30 seconds and then cooled on ice for 25min. 950µl SOC (Super Optimal Broth) was added to the tube and incubated at 37°C for 60min. 50µl of the suspension was then plated onto an antibiotic selection plate and incubated overnight at 37°C. Representative colonies were then selected and inoculated into antibiotic/Lysogeny Broth (LB) solution and incubated overnight. Bacteria were then pelleted ready for mini-prep.

2.4.5.2. Plasmid DNA isolation (mini-prep) - BioLine ISOLATE II Plasmid Mini Kit

Bacterial pellets were re-suspended in 250µls Buffer P1 and 250µls of P2 lysis buffer was then added, mixed and incubated for 5min before adding 300µls of P3 neutralisation buffer. The lysate was then centrifuged for 5 min at 11,000 x g. The plasmid DNA was then bound by centrifuging the supernatant through a spin column. The silica membrane was then washed sequentially with 500uls wash buffer 1 and then 650uls wash buffer 2. The membrane was then dried by centrifugation. Plasmid DNA was then eluted using 50µls of Elution Buffer P. The concentration of plasmid DNA was quantified using spectrophotometry. Plasmids were then sequenced to confirm presence of correct gene.

2.4.5.3. Transfection

2.4.5.3.1. Polyethylenimine (PEI) transfection – This protocol was used for HEK293T cells

Appropriate number of cells was seeded onto a tissue culture plate with DMEM + 10% FCS and incubated overnight and then current media was exchanged for fresh media. Transfection master mix consisted of plasmid DNA added to a 1:10 mixture of PEI and Opti-MEM. The transfection mix was added in a dropwise manner and incubated for 2 days. Transfection efficacy was examined by flow cytometry.

2.4.5.3.2. Lipofectamin 2000 – Used to transfect CHO cells

Appropriate number of cells was seeded onto a tissue culture plate with Nut Mix + 10% FCS and incubated overnight and then current media was exchanged for fresh media. Transfection master mix consisted of plasmid DNA added to a 1:20 mixture of Lipofectamin 2000 and Opti-MEM. The mixture was incubated for 20 min and then added in a dropwise manner. The plate was then incubated for 2 days. Transfection efficacy was examined by flow cytometry.

2.4.5.3.3. Electroporation – used to transfect K562 cells (Delgado-Canedo et al., 2006)

Cell suspension at 1 x 10^7 cells/ml concentration was prepared in serum-free RPMI 1640. 300µls were added to a sterile Bio-Rad electroporation cuvette. 11.25µg of plasmid DNA was added and incubated for 15min at room temperature. The solution was then pulsed at 875V/cm electrical field, 500µF capacitance and infinite resistance. The suspension was then centrifuged (13,000rpm for 30sec) and stood for 20min. The supernatant was discarded,

and the cells were re-suspended in 3mls of RPMI 1640 + 10% FCS and incubated at 37°C in 5% CO2.

N.B. All cells were incubated in antibiotic selection media titrated to a concentration derived from a killing curve.

2.4.6. Flow cytometry

Cells in the cell suspension were counted and the volume containing 1 x 10^5 cells transferred to a 96-well plate. Cells were then pelleted by centrifugation and then re-suspended in MACS buffer containing the primary antibody conjugated to a fluorophore (at the recommended concentration). Further two wells were used for isotype control and negative control (MACS buffer). The cells were incubated with the antibody for 30 minutes at 4°C. They were then washed with MACS buffer and fixed in 2% paraformaldehyde (PFA). Flow cytometry was performed on BD LSR II Flow Cytometer running the BD FACSDiva™ software (BD Biosciences, Franklin Lakes, NJ, USA).

2.4.7. Pelleting and embedding cells

Cells were pelleted by centrifugation (1000rpm for 5 min) and fixed in 10% Formaldehyde. The pellets were then embedded into paraffin blocks and cut into 4µm sections and mounted onto glass slides.

2.5. Immunohistochemistry (IHC) Staining

2.5.1. Manual staining

Formalin-fixed paraffin-embedded sections were deparaffinised by sequential immersion in Xylene three times for 10 minutes each. They were then dehydrated in graded ethanol concentrations (100%, 95% and 70%) for 3 minutes in each tub. Endogenous tissue peroxidase was quenched by immersion in 0.3% hydrogen peroxide for 15 minutes. Antigen retrieval was achieved by serial boiling steps in citrate buffer adjusted to a pH of 6. Casein was used as a blocking serum for 10min at room temperature. The primary antibody (at the recommended concentration) was applied and incubated over night at 4°C and then washed with Phosphate Buffered Saline + 0.1% Tween 20 (PBST) three times for 5 minutes each. ImmPRESS™ Horse Radish Peroxidase (HRP) Universal Antibody (Vector Laboratories, Burlingame, CA, USA) was used as the secondary antibody and was incubated for 30 minutes at room temperature and then washed off with PBST. ImmPACT™ 3,3'-diaminobenzidine (DAB) Peroxidase (HRP) Substrate (Vector Laboratories, Burlingame, CA, USA) was applied to the pellet for about 1min until the desired staining intensity was achieved. The slides were then washed under running water for 5 minutes. The sections were then counterstained using Mayer's Haematoxylin Solution (Sigma-Aldrich Co. St. Louis, Missouri, USA) for 3 minutes. The sections were then dehydrated by immersion in escalating concentrations of Industrial Methylated Spirit (IMS) (75%, 95% AND 100%) for 3 minutes in each tub. The sections were then immersed in two tubs of Hiso-Clear® (National Diagnostics, Atlanta, Georgia, USA) for 5 minutes in each tub. The slides were then dried and a drop of DPX Mountant (Sigma-Aldrich Co. St. Louis, MO, USA) was applied to the pellet and covered with a coverslip.

2.5.2. Automated staining

Automated staining was carried out on the Leica BOND-RX Immunohistochemistry Stainer (Leica Biosystems, Wetzlar, Germany) by Mr Christopher Bagnall, biomedical scientist at the Human Biomaterials Resource Centre (HBRC) in Birmingham, UK.

2.5.3. IHC staining conditions optimisation

In order to achieve optimal staining resolution and chromatic contrast, serial primary antibody concentrations were used above and below the vendor's recommended concentration. Optimisation was performed on surplus human tonsillar tissue obtained from the HBRC. Optimisation was carried out only for antibodies that were not used before in the institute. For commonly used antibodies (e.g., CD8), previously agreed staining conditions were used.

2.5.4. Automated staining conditions

The final automated staining conditions are listed in Table 2.2:

Ab	Vendor	Clone	Host	Dilution	pH	Buffer	Temp
CD3	Leica	LN10	Mouse	1:100	9	EDTA*	100°C
CD4	Leica	4B12	Mouse	1:50	9	EDTA*	100°C
CD8	Leica	4B11	Mouse	1:400	9	EDTA*	100°C
FOXP3	Abcam	236A/E7	Mouse	1:400	9	EDTA*	100°C
TBET	CST	D6N8B	Rabbit	1:400	9	EDTA*	100°C
RORγt	Merck	6F3.1	Mouse	1:4000	9	EDTA*	100°C
PD1	Cell Marque	NAT105	Mouse	1:50	9	EDTA*	100°C
PDL1	CST	E1L3N	Rabbit	1:200	9	EDTA*	100°C
HLA Class I	Abcam	EMR8-5	Mouse	1:400	9	EDTA*	100°C
HLA Class II	Abcam	CR3/43	Mouse	1:200	9	EDTA*	100°C

Table 2.2: List of primary antibodies used for the IHC and immunofluorescence. The staining conditions are outlined for automated staining. * Leica Epitope Retrieval Solution 2 (Leica Biosystems, Wetzlar, Germany) which is an EDTA based solution with a pH of 9

2.6. Multiplex Immunofluorescence (IF)

Multispectral immunofluorescence immunohistochemistry staining is a technology that allows sequentially staining of formalin fixed paraffin embedded (FFPE) tissue for multiple markers. This allows the analysis of those markers without loss of the information about the spatial geography of those markers within that tissue (Parra et al., 2017).

For the purposes of my project, I used Perkin Elmer's Opal 7-Color Automation IHC Kit (Perkin Elmer, Waltham, MA, USA). This kit is designed to stain for six different markers in addition to a nuclear counter stain (DAPI).

The Opal technology workflow involves sequential steps of immunohistochemical staining analogous to the one described in the classical IHC section. What is different however is the fluorescent Tyramide Signal Amplification (TSA) step that permanently deposits a fluorophore marker in the tissue that will not be affected by subsequent microwave stripping treatment. The cycle of staining is repeated for subsequent markers with different fluorophores until all the markers are stained. The nuclei are then counterstained with DAPI (4′,6-diamidino-2-phenylindole) and the slide is covered [Figure 2.2].

After the staining process has been completed the sides could be viewed using a fluorescence or a confocal microscope that uses light at different wave lengths to excite the different fluorophores that in turn emit light at a specific wavelength that can be captured using emission filters. The specific excitation and emission wave lengths of the fluorophores used in this study are listed in Table 2.3.

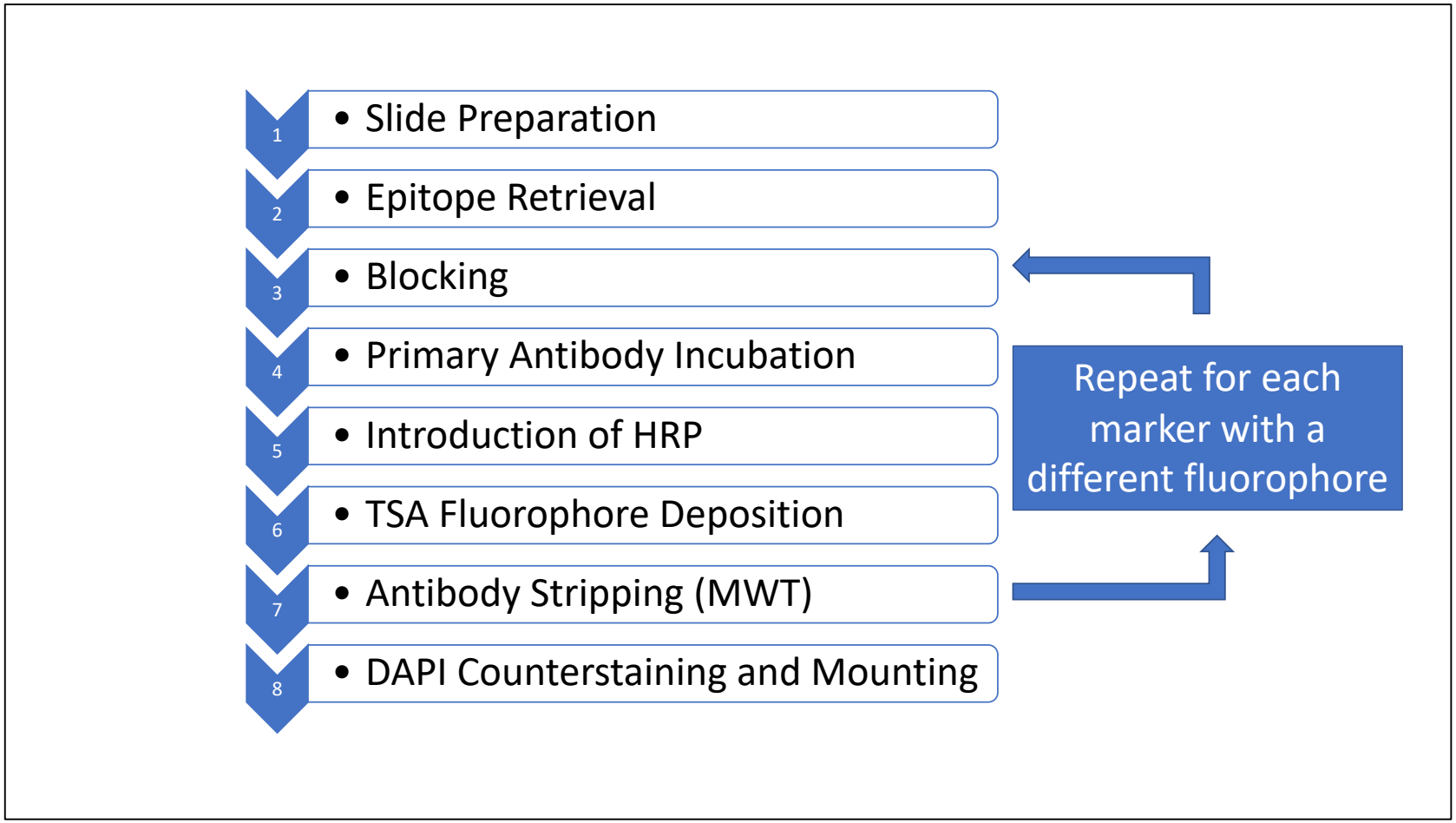

Figure 2.2: A schematic showing the Opal multiplex staining process (adapted from the Opal Multiplex IHC Assay Development Guide, Perkin Elmer 2014). HRP= Horseradish Peroxidase, MWT= Microwave treatment.

Fluorophore	Wavelength		Colour
	Excitation	Emission	
DAPI	358nm	461nm	Blue
Opal 520	494nm	525nm	Green
Opal 540	523nm	536nm	Yellow
Opal 570	550nm	570nm	Red
Opal 620	588nm	616nm	Amber
Opal 650	627nm	650nm	Orange
Opal 690	676nm	694nm	Clear

Table 2.3: Table showing the excitation and emission properties of the fluorophores used in this study (adapted from the Opal™ Immunology Discovery Kit user manual, Perkin Elmer)

2.6.1. Panel development - T-cell panel

Multiplex immunofluorescence was used to study the differential expression of different immune markers in mismatch proficient and deficient CRC (Results in Chapter 5).

To achieve this, a seven-plex panel was optimised encompassing a cohort of immune markers. The panel was designed to be T-cell-centric and included traditional cell surface markers (CD4 and CD8) as well as specific transcription factors (FOXP3, TBET and RORγt). The combination of different surface markers and transcription factors were used as indicators of lineage as detailed in Table 2.4. MHC Class II was added in view of its importance in the CIRC signature.

Phenotype	Marker
CD4	CD4 stain only
T_{REG}	CD4 (Membrane) + FOXP3 (Nuclear)
T_H1	CD4 (Membrane) + T-Bet (Nuclear)
T_H17	CD4 (Membrane) + RORγt (Nuclear)
CD8	CD8 stain only
T_C1	CD8 (Membrane) + T-Bet (Nuclear)
MHC class II	Class II stain only
Other	No membrane or nuclear stain – DAPI only

Table 2.4: Table showing the different phenotypes explored with the T-cell multiplex panel.

2.6.2. Optimisation of the multiplex panel

Manufacturer's recommended dilutions were used on each antibody with a two-fold increase and decrease in dilution used to find optimal condition with DAB staining. The optimal dilution for antibody was then paired with each of the Opal dyes (Opal 520, Opal 540, Opal 570, Opal 620, Opal 650 and Opal 690) to ascertain compatibility. Single antibody/fluorophore combination was used for the creation of a spectral library. After best combination of antibody and fluorophore was ascertained order of staining was optimised by switching order of sequential marker staining. Optimal panel combination was achieved when the multiplex image was comparable to that of the single IHC staining for each of the markers. The final marker-fluorophore combination is detailed in Table 2.5.

Marker seq.	Marker	Concentration	Fluorophore	Fluorophore concentration
1	CD4	1:50	Opal 520	1:400
2	CD8	1:400	Opal 540	1:400
3	FOX-P3	1:400	Opal 570	1:400
4	T-BET	1:400	Opal 620	1:200
5	RORγt	1:4000	Opal 650	1:400
6	MHC Class II	1:200	Opal 690	1:200
7	Nuclear counterstain	N/a	DAPI	Pre-diluted

Table 2.5: Final marker fluorophore pairing shown with final primary antibody and fluorophore concentrations and sequence of staining.

Following the optimisation step, the staining for this study was completed on the Leica Bond-RX Automated Research Stainer (Leica Microsystems, Milton Keynes, UK).

2.6.3. Multiplex IF Slide analysis

2.6.3.1. Image capture and analysis

For the purposes of this study the slides were viewed and scanned using the Vectra 3.0 Automated Quantitative Pathology Imaging System (Pekin Elmer, Waltham, MA, USA). Cell phenotyping and scoring of various immune cell subsets was carried out using the inForm® 2.2.0 – Tissue Finder Advanced Image Analysis Software (Perkin Elmer, MA, USA) as detailed in the scoring section (2.6) below. This software allows accurate quantification and scoring of different markers in different tissue compartments using machine learning algorithms.

2.6.3.2. Creation of a spectral library and immunofluorescent scanning

Due to the overlapping emission wavelengths of the different fluorophores, it is important to optimise the detection of the specific emission signal and reduce the bleed over. This process is known as spectral un-mixing. To achieve this a “spectral library” of the different fluorophores is created.

To create a spectral library, Vectra 3.0 Automated Quantitative Pathology Imaging System (Perkin Elmer, MA, USA) platform was used to scan singly stained slides with individual fluorophores as well as an unstained slide to subtract tissue auto-fluorescence at 200X using all the fluorescence filters. The images were then used in the inForm software to establish the spectral library to allow accurate fluorophore separation (spectral un-mixing).

Multi-spectral scanning was carried out on the Vectra 3.0 platform. The whole slide was initially scanned at 100x using all the available filters (DAPI, FITC, CY3, TEXAS RED and CY5) and then Phenochart™ 1.0.4 Whole Slide Contextual Viewer for Annotation & Review (Perkin Elmer, MA, USA) was used to annotate areas of interest which were then scanned at higher resolution (200X or 400X) to create multi-spectral images (MSI’s).

For the purposes of cell type analysis and quantification, six high power fields (400X) were selected at random from the tumour areas of each slide and high-resolution multispectral images were captured for digital quantification.

2.7. Digital Pathology Scoring

2.7.1. Single marker scoring

Digital scoring of IHC single marker slides was undertaken using the Definiens Tissue Studio software (Definiens AG, Munich, Germany).

After completion of automated staining the whole slides were digitally scanned at 400X using the Leica SCN 400 (Leica Microsystems, Wetzlar, Germany).

2.7.1.1. DAB threshold setting and protocol building

To enable the software to analyse and score a specific marker, a custom-built protocol was designed for this individual marker. This starts with setting up DAB thresholds to enable the software to differentiate between stained and unstained cells and with fine tuning to avoid labelling background staining as a false positive.

The threshold setting is undertaken by choosing a training set of stained slides. For each marker two excess tonsillar tissue, two CRC and two lung slides (6 in total) were used as a training set. Those thresholds were manipulated to ensure reproducibility between tissues and different slides. Once the thresholds are set for a marker, the same thresholds were applied to the whole cohort in order to avoid observer bias.

2.7.1.2. Solution (protocol) building

After the DAB thresholds are set, a modular solution is designed to automate the scoring process.

The solution starts with manually annotating the region (or regions) of interest (ROI) on each scanned slide which would include the tumour area/s. This step also involved de-selecting any areas of artefactual staining or damaged tissue to avoid false

interpretation [Figure 2.3]. After the ROI is annotated, 6 to 8 training regions are selected and viewed at 100X. The software then segments the selected areas on the basis of their morphological features [Figure 2.4]. The user then annotates samples of these segments with the different tissue compartments of interest to 'train' software to differentiate between tumour stromal and tumour epithelial areas based on morphology. The software then uses computer-learning algorithms to apply the segmentation to the whole ROI [Figure 2.5].

After the tissue segmentation is completed, a further of 6-8 training regions are selected at 400X to complete the cellular segmentation training. The software uses haematoxylin and a characteristic nuclear size to determine nuclei. Cells are then simulated by defining the average distance of the cell membrane from the nucleus [Figure 2.6]. Once the cellular training is completed, the pre-set DAB thresholds are applied, and the solution is saved to be applied to the cohort [Image 2.7]. Figure 2.8 shows a consolidated flowchart of the whole process of analysis and scoring.

The scoring can be done either on cell number basis or on area (pixel basis). The former is applicable if cells are clearly demarcated and haematoxylin nuclear staining is sharp. The latter is best used if nuclear detection is difficult or if tissue is homogeneous (e.g., connective tissue). For the purposes of his thesis, all the scoring was done on cell basis.

2.7.1.3. Slide processing

To analyse the cohort, the slides are loaded to the software's workspace and the pre-designed solution is uploaded. For each slide quality control steps are undertaken to

ensure fidelity of tissue and cellular segmentation before applying the protocol to the whole ROI.

The output is then converted from text format into a spreadsheet in Microsoft Excel (Microsoft, Redmond, Washington, U.S.A.).

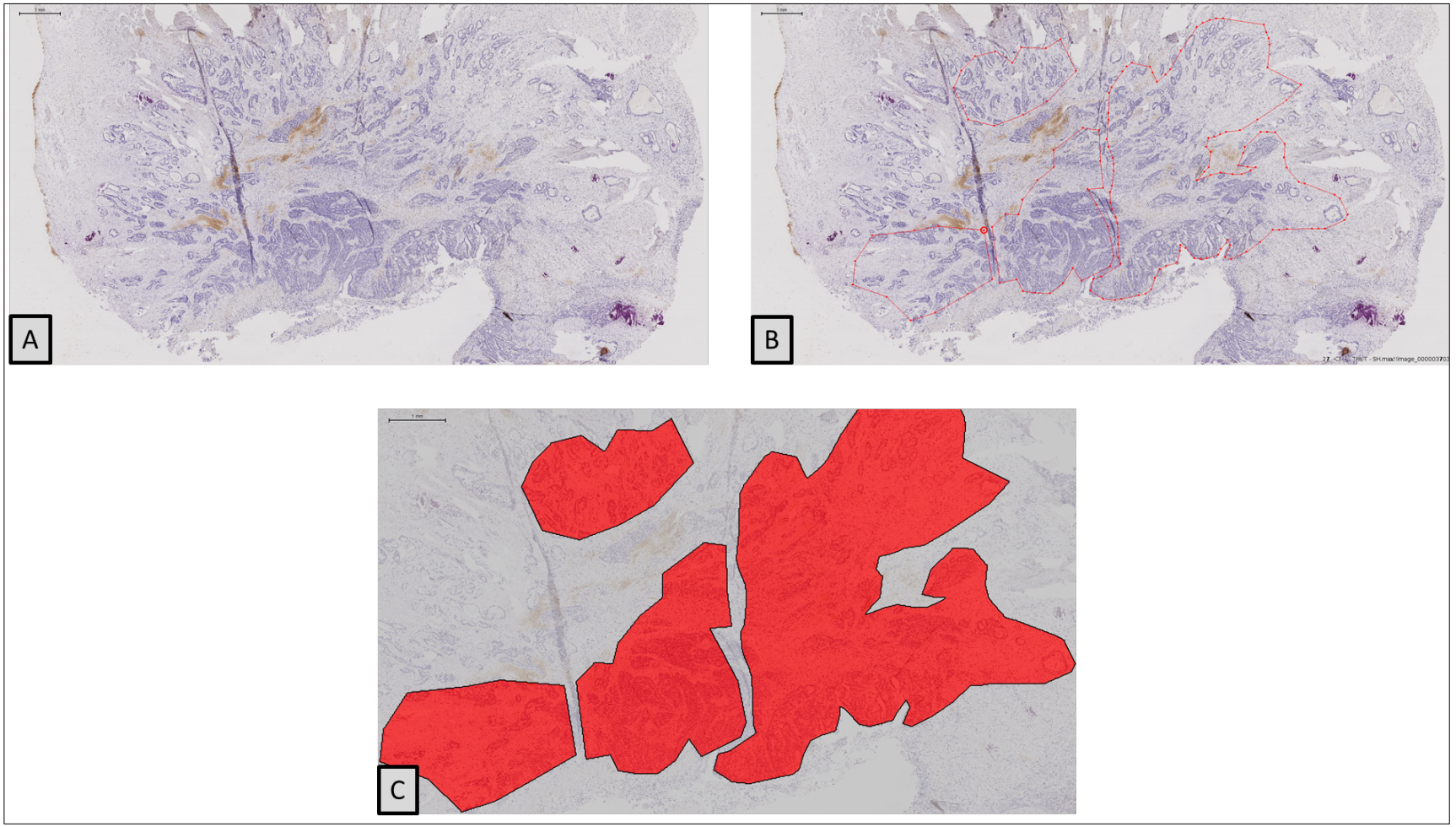

Figure 2.3: Definiens® digital pathology scoring algorithm building Step 1 – Region of interest (ROI) selection. This figure shows the first step in analysing a stained slide which involves manual selection of the area of interest. This process also excludes areas of damage and non-specific staining. Image A is a bright field microscopy snapshot of colorectal cancer section stained for CD4. Image B shows the drawn polygon around the cancer tissue and excluding areas of non-specific staining. Image C shows confirmation of the region of interest highlighted in red. 40X magnification.

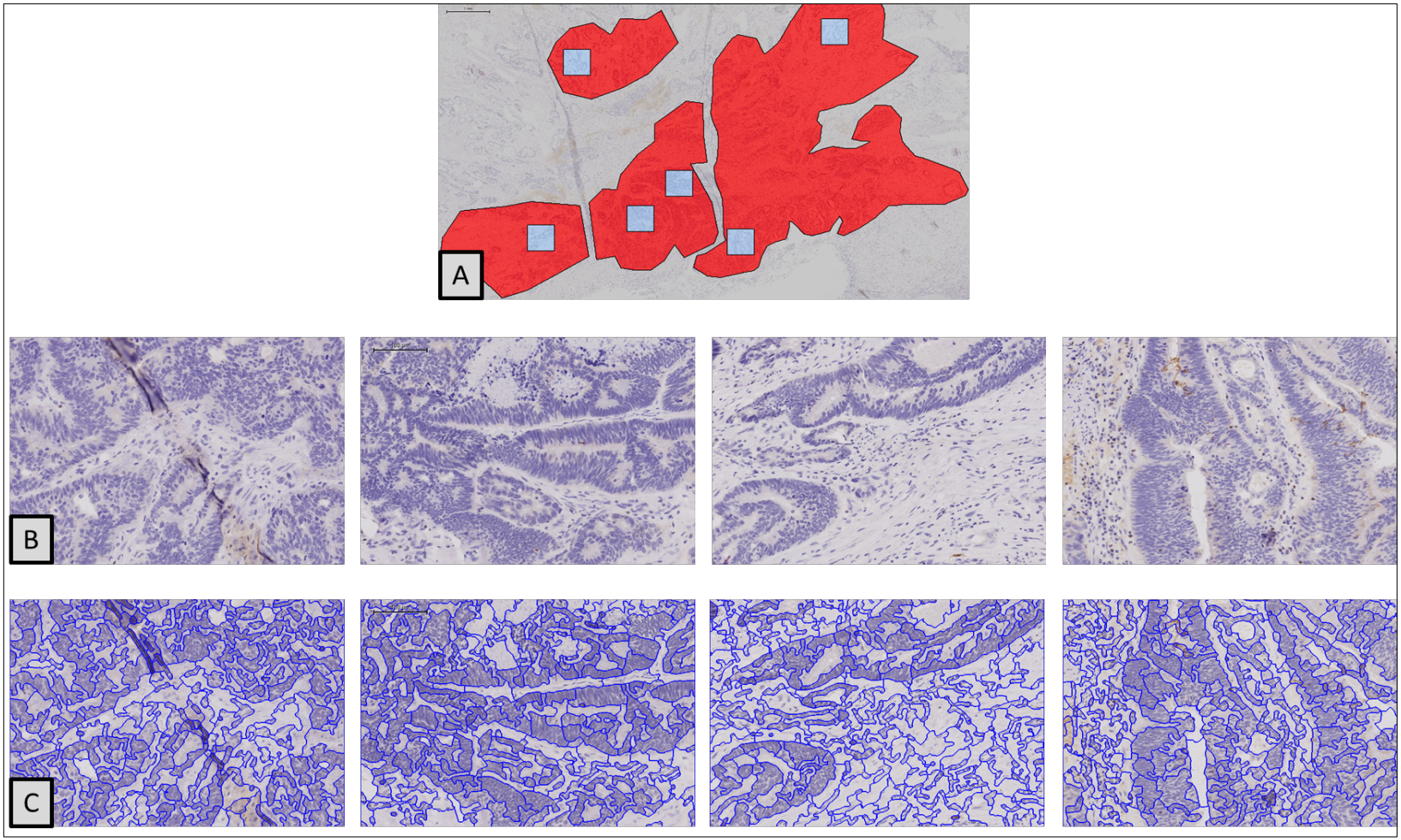

Figure 2.4: Definiens® digital pathology scoring algorithm building Step 2 – Auto-segmentation. This figure shows the software segmenting the tissue into polygons based on morphological features. In the first instance, representative areas of the tissue are selected at random – Figure A. Then those selected areas are magnified to 100X – Figure B and the segmentation is applied – Figure C.

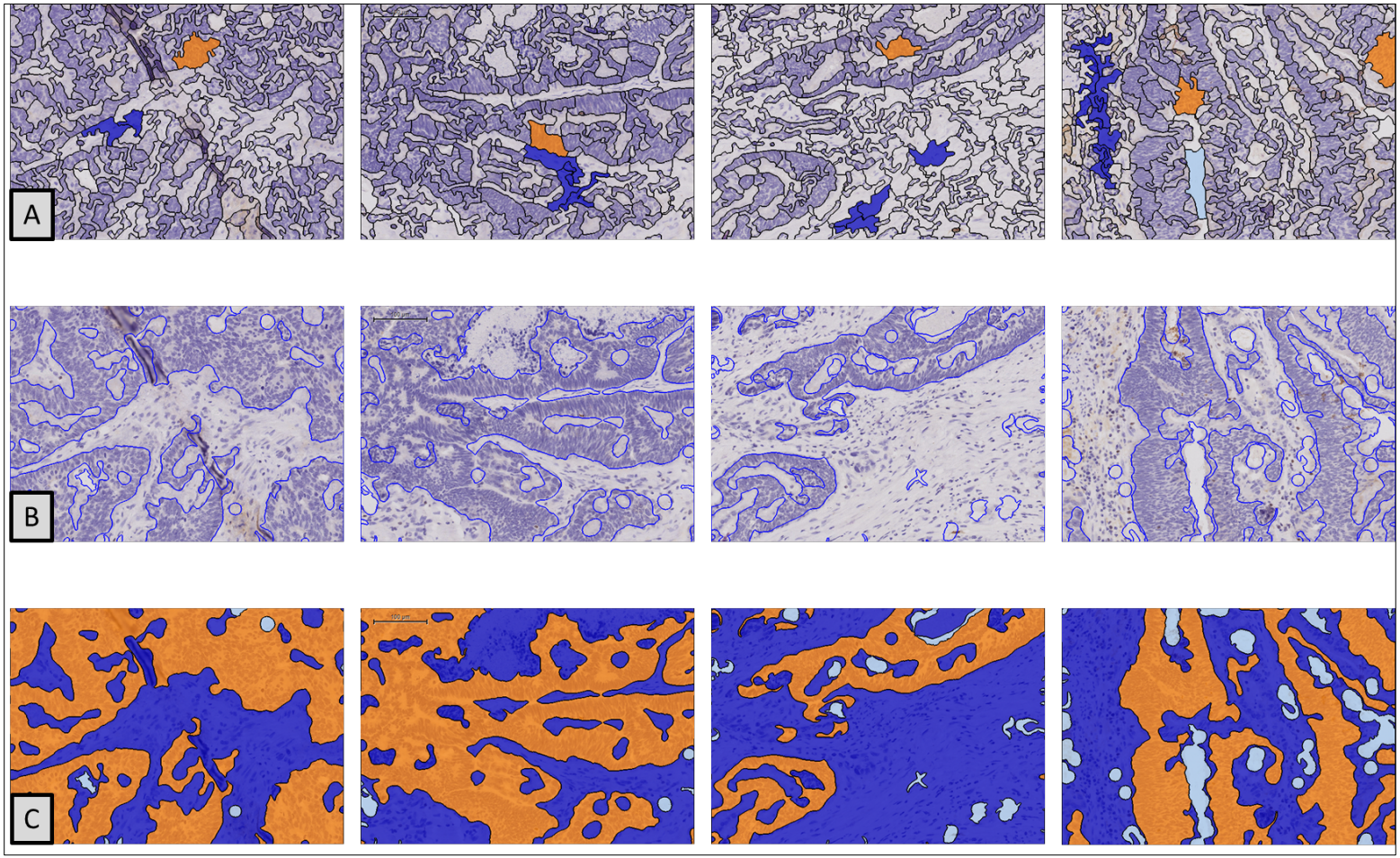

Figure 2.5: Definiens® digital pathology scoring algorithm building Step 3 – Tissue segmentation training. This figure demonstrates the process of training the software to recognise different tissue compartments. The user demonstrates to the software the tissue compartments (in this case: orange for tumour epithelium, blue for tumour stroma and light blue for tissue gaps) – Figure A. The software then applies machine learning algorithms and rolls out the segmentation automatically to the rest of the tissue – Figure B and C. The process of training can be repeated several times as the software 'learns' the variations in tissue morphology which results in more accurate segmentation.

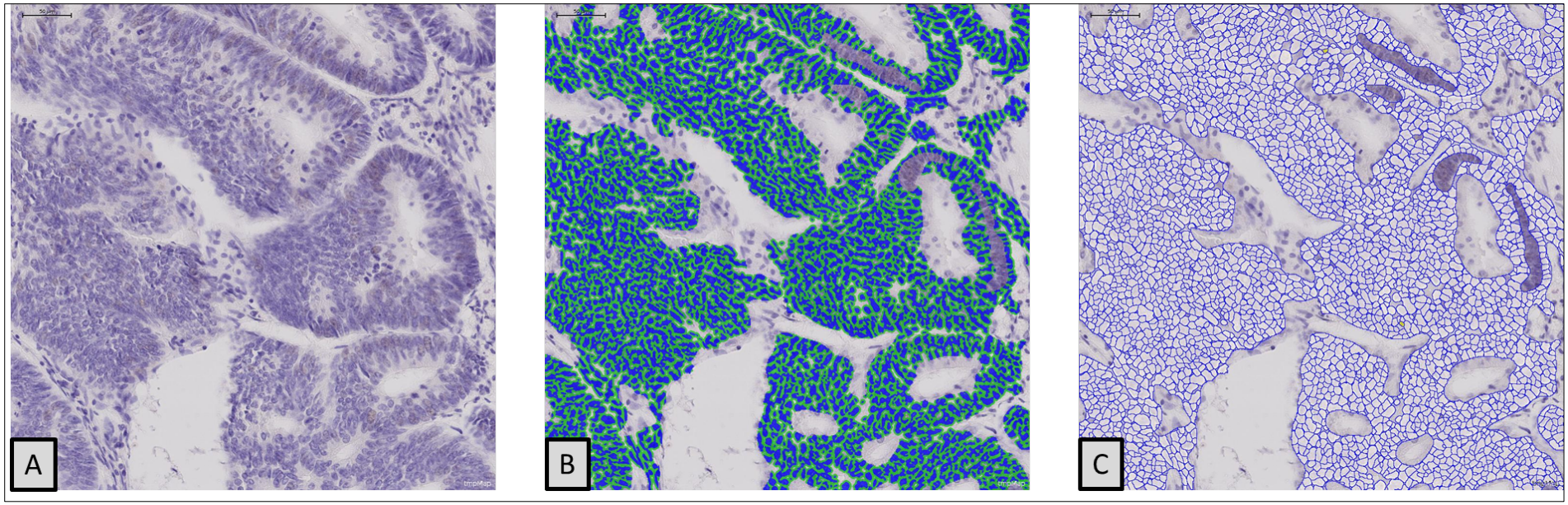

Figure 2.6: Definiens® digital pathology scoring algorithm building Step 4 – Cellular segmentation. This figure demonstrates the software identifying cells based on their nuclei that are stained with haematoxylin. This process also takes into account the typical size of the nucleus and the intensity of haematoxylin staining. The nuclear size and haematoxylin threshold are set by the user depending and adjusted to optimise nuclear pick up rate – Image A. The cells are then digitally recreated based on the growth from the nucleus and the density of nuclei. Image B shows nuclei in blue and cytoplasm in green. Image C shows the final cellular segmentation. 200X magnification.

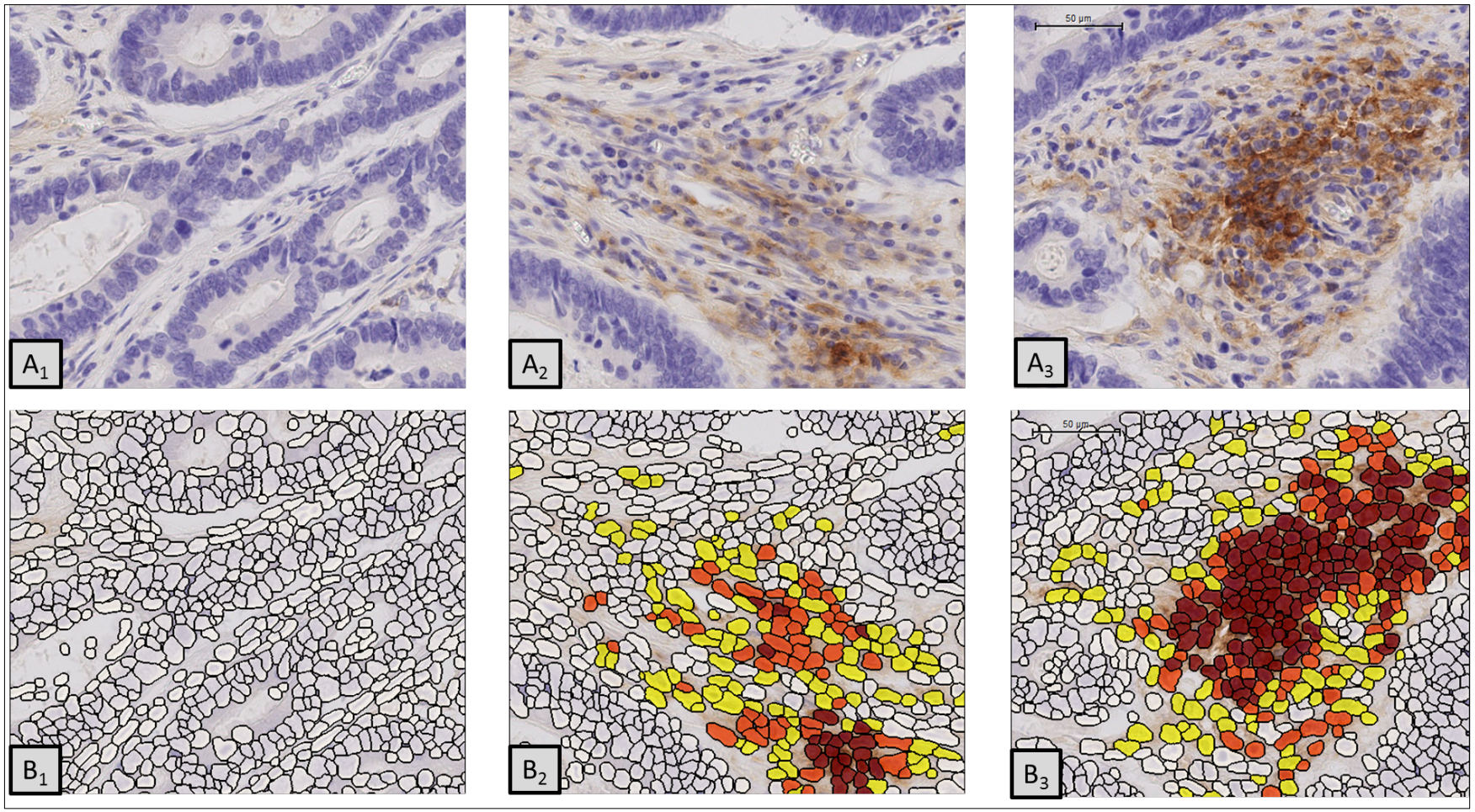

Figure 2.7: Definiens® digital pathology scoring algorithm building Step 5 – Cellular analysis. This figure shows the final step which is the cellular analysis and scoring. In this step, the software detects DAB staining in the context of the cellular segmentation in the previous step. The DAB threshold is set by the user depending on the intensity of staining. In cases where the intensity of staining is relevant (e.g., for calculation of histological scores) the threshold can be set to detect low, medium and high intensity staining (yellow, orange and red consecutively). 400X magnification.

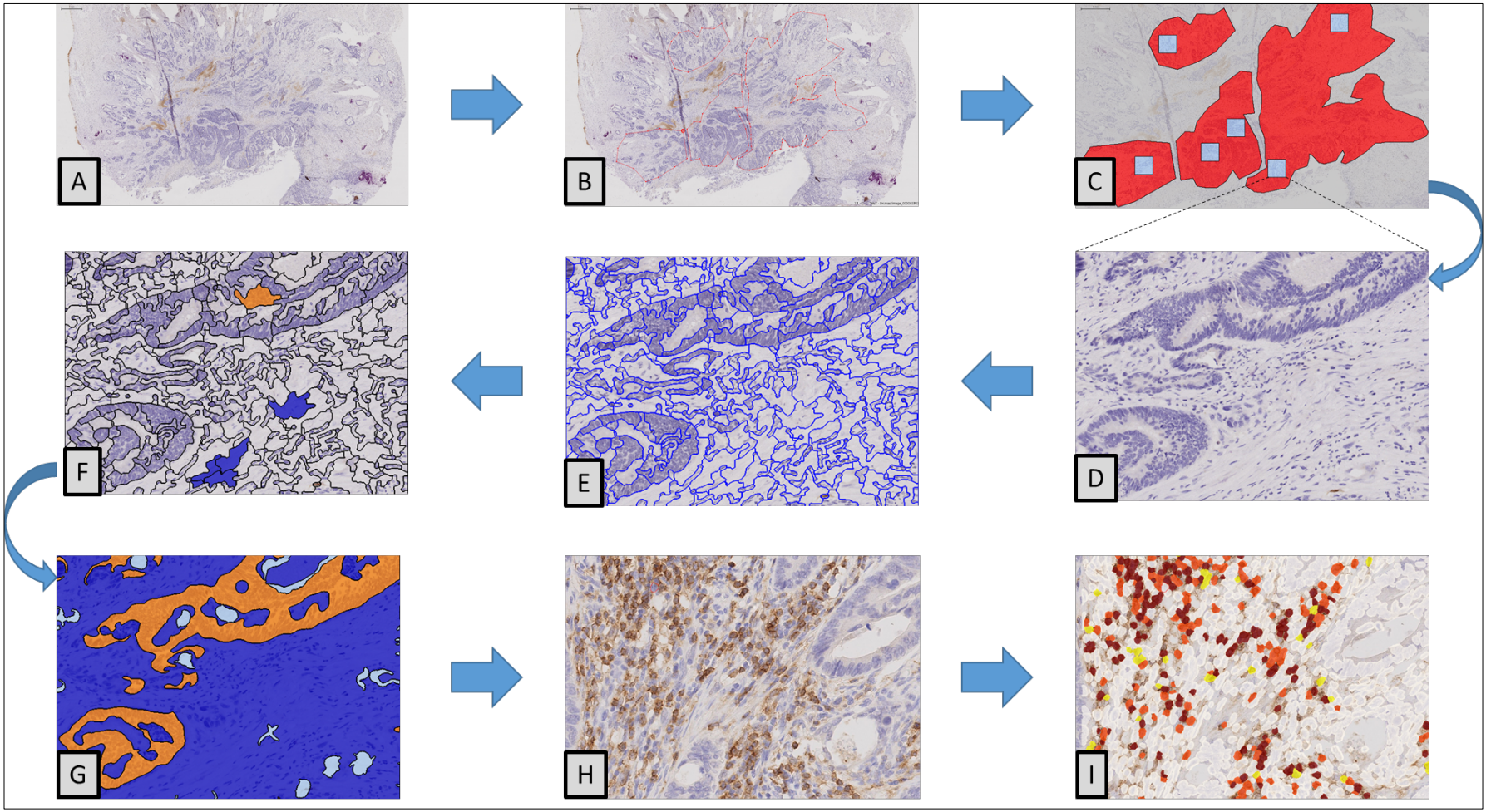

Figure 2.8: A schematic flowchart demonstrating the Definiens® work stream to analyse and score tissue. Figure A is a screen shot of the slide. Figure B is selection of the region of interest (ROI). Figures C and D is selection of representative tissue for segmentation training. Figure E is auto-segmentation followed by user training in figure F. Figure G is the automated roll out of the segmentation across the whole ROI. Figure H is cellular segmentation and analysis.

2.7.2. Multiplex immunofluorescence (IF)

Digital scoring of the multi-spectral images (MSI) was undertaken using the inForm® 2.2.0 – Tissue Finder Advanced Image Analysis Software (Perkin Elmer, MA, USA) software.

2.7.2.1. Protocol building

Analogously to the IHC scoring on Definiens Tissue Studio, the scoring of IF stained slides starts with building an analysis and scoring protocol. The first step involves the creation of a spectral library as described previously. This step is important to enable the inForm software to correctly 'read' the MSIs. The six randomly selected high power filed MSIs are then uploaded for analysis. Tissue segmentation into stromal and epithelial compartments is performed in a semi-automated fashion which involves manual drawing of polygons to refine the segmentation accuracy. The next step is the cellular segmentation where the software detects cells by virtue of detecting the nuclei which are stained with DAPI. The cells are then simulated by outwards growth from the nuclei. After the cellular segmentation is complete, the spectral library is applied and the different fluorophores are un-mixed. The final step is the phenotype labelling where the software is 'educated' to identify the distinct immunofluorescence of each marker or combination of markers. The protocol is then saved and applied to the slides in the cohort after annotating the ROI's. Figure 2.9 shows a brief overview of the process of digital analysis and scoring. Quality control steps were built into the protocol to allow the user to scrutinise the segmentation on each slide before final scoring.

2.7.2.2. Cell phenotyping

The software was trained to score eight different phonotypes on the basis of staining combinations. As a visual aid, a colour can be chosen by the user and assigned to

each phenotype to create a phenotype map of the tissue. Table 2.6 demonstrates those phenotypes and assigned colours.

Phenotype	Marker	Colour assigned
$CD4^+$	CD4 only	Green
T_{REG}	CD4 + FOXP3+	Orange
T_H1	CD4 + T-Bet+	Cyan
T_H17	CD4 + RORγt+	Magenta
$CD8^+$	CD8 only	Yellow
T_C1	CD8 + T-Bet+	Pink
MHC Class II +	Class II only	Red
Other*	Nuclear stain only	White

Table 2.6: Cellular phenotyping used in immunofluorescent slide scoring and colours assigned to each phenotype. * Other denotes cells that have not positively stained for any of the six markers and are only positive for the nuclear counterstain (DAPI).

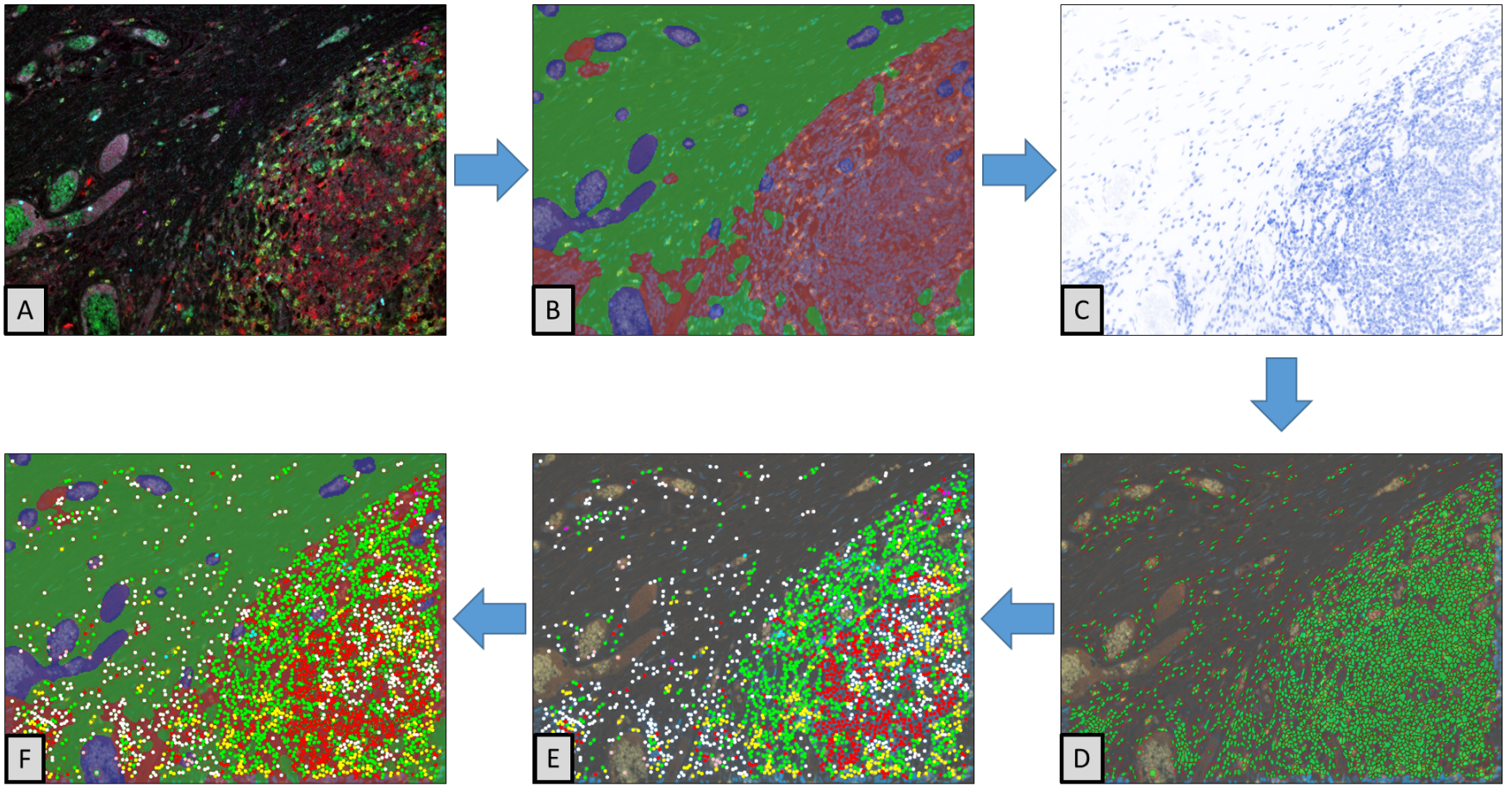

Figure 2.9: InForm® multiplex digital pathology scoring algorithm building. This flowchart shows the work stream involved in building an immunofluorescence multiplex analysis and scoring protocol. Image A is a multispectral image of colorectal cancer stained with the opal 7-plex kit with all filters applied. Image B shows the tissue segmentation step where the tissue compartments are identified (in this case: Red is for tumour epithelium, green is for tumour stroma and blue is for tissue gaps). Image C demonstrates nuclear recognition based on the DAPI stain. Image D is the cellular simulation based on the nuclear detection. Image E show a phenotype map of the different phenotypes detected in the tissue. Image F shows the phenotype map superimposed on the tissue segmentation.

2.8. Statistical analysis

Database maintenance and basic statistical analysis (measures of central tendency) was done using Microsoft Excel. More detailed analysis was performed using GraphPad Prism 7 (GraphPad Software, La Jolla, CA, USA). Data's conformity to the normal Gaussian distribution was assessed using the Kolmogorov–Smirnov test. For data that was found to be normally distributed, parametric tests were used. For data that was not normal distributed non-parametric tests were used.

Due to the fact that the majority of the data did not conform to the normal distribution, non-parametric tests were used almost universally. To compare medians in the primary-secondary pairs (chapter 4), the Wilcoxon signed-rank test was used. To compare non-paired samples (Chapter 5), Mann–Whitney U test was used for non-parametric data and the unpaired student t-test was used for parametric data. For comparison of categorical data, Chi square (χ^2) was used.

Statistical significance was set at a p-value of <0.05 and denoted as an asterisk (*). A p-value of <0.01 was denoted with a double asterisk (**). A p-value of <0.001 was considered highly significant and denoted with a triple asterisk (***).

2.9. Quality Control

Regular quality control steps were undertaken in the process of building an automated algorithm. Random slides were reviewed to ensure the fidelity of tissue segmentation and cellular phenotyping. Expert opinion and advice were sought from two experienced histopathologists, Dr Gerald Langman and Dr Maha Ibrahim.

3. Chapter Three: Validation Results

3.1. Antibody validation results

3.1.1. MHC class II

Flow cytometry of the CIITA transduced HEK293 cells confirmed that 98.3% expressed MHC Class II were stained with an APC (Allophycocyanin)-conjugated anti-human HLA-DR antibody (BioLegend, San Diego, CA, USA) [Figure 3.1A]. The pelleted cells were then stained manually and demonstrated clear membranous reactivity in the transduced cell line when compared to the parental cell line. Automated staining was then carried out on the Leica Bond-RX auto-stainer and showed similar results [Figure 3.1 B & C]. Subjectively, automated staining quality outperformed manual staining and resulted in sharper images.

3.1.2. FOXP3

FOXP3 validation was successful as well. Flow cytometry of transiently transfected HEK293T cells showed 44.7% transfection efficacy two days following the transfection (Green Fluorescent Protein (GFP) tag). To confirm the co-expression of the FOX-P3 gene and the GFP tag, the cells were stained with Alexa Fluor® 647 anti-human FOXP3 antibody (Clone 259D) (BioLegend, San Diego, CA, USA) after pre-treatment with eBioscience transcription factor staining buffer set (ThermoFisher, Waltham, MA, USA) as per manufacturer's instructions. Doubly positive cells (42.2%) were deemed as proof of co-expression [Figure 3.2]. The pelleted cells were then fixed in 10% formalin and embedded in paraffin. The pellets were then stained on the Leica Bond-RX auto-stainer and showed clear nuclear reactivity [Figure 3.3]. The percentage of positively stained cells corresponded with the percentage of cells found positive on flow cytometry.

3.1.3. Retinoic Acid Receptor - Related Orphan Receptor gamma (RORγ)

The RORγ transcription factor is present in two closely related isoforms; the first isoform is ubiquitous and can be found in many tissues such as the liver, the lungs and muscle. The second isoform (RORγt) however is restricted to the thymus and expressed by thymocytes destined to differentiate into IL-17 producing T_H17 cells (He et al., 1998, Ivanov et al., 2006).

Several antibody clones from different vendors were tried and the most reliable staining was produced by using clone 6F3.1 from Merck (Merck, Darmstadt, Germany). This antibody is not isoform-specific and stains both isoforms. Given that this marker was to be used as part of a multiplex panel containing CD4, it was felt the dual positivity (CD4+/RORγ+) cells would be correlate to T_H17 lineage.

Validation was carried out using HEK293T cell lines transiently transfected with both constructs. Transfection efficacies two days after transfection were assesses by expression of the GFP tag on flow cytometry and found to be 33.3% and 28.7% for isoform 1 and 2 consecutively. Similar to the FOX-P3 validation, co-expression of RORγ gene and the GFP tag was assesses by staining the cells with Affymetrix eBioscience anti-human/Mouse RORγt antibody (Clone AFKJS-9) (ThermoFisher Scientific, Waltham, MA, USA) after pre-treatment with eBioscience transcription factor staining buffer set (ThermoFisher Scientific, Waltham, MA, USA) as per manufacturer's instructions. Doubly positive cells (27.4% and 24% for isoforms 1 and 2 consecutively) were deemed as proof of co-expression [Figures 3.4 and 3.5]. The pelleted cells were then embedded in paraffin and stained on the Leica Bond-RX auto-stainer and showed clear nuclear reactivity [Figure 3.6]. The percentage of positively stained cells corresponded with the percentage of cells found positive on flow cytometry for both constructs.

3.1.4. MHC class I

K562 cells were initially transfected with three different alleles of MHC Class 1 (A*03.01, B*40.01 and Cw07.02) using the electroporation protocol outlined in the techniques section. Cells that survived selection in Geneticin (G418)-containing RPMI 1640 medium were assessed for HLA expression using flow cytometry and stained with a PE (Phycoerythrin)-conjugated anti-human HLA-A, B, C antibodies (BD Pharmingen). The flow cytometry did not demonstrate any expression when compared to the parental cell line as a negative control and HEK293 cells as positive control. I then attempted to transfect CHO cells with the same plasmids using the Lipofectamin protocol detailed in the techniques section and this approach yielded negative results on flow cytometry as well.

To exclude the possibility of having mislabelled plasmids I sequenced them and confirmed the presence of the correct genes. At this stage I elected to try a different cell line and after consulting with other groups, I was given a 721.221 cell line (a human B-lymphoblastoid cell line that lacks the expression of HLA-A,B and C due to mutated HLA gene complex (Shimizu and DeMars, 1989) that was stably transfected with HLA-A2 and HLA-Cw1 by Dr Jianmin Zuo. Those cell lines were stained with the same flow cytometry antibodies and again yielded negative results.

Suspecting that the antibody I was using for the flow cytometry might be defective I decided to change my antibody choice and purchased a new PE-tagged anti-human HLA-A, B and C antibody (Biolegend (Clone W6/32)). The staining conditions for this new antibody were optimised using HEK293T cells.

I then obtained a K562 cell line stably transfected with HLA-A2 and HLA-Cw1 Dr Jianmin Zuo. When I stained those new cell lines, I found that 97.6% of the HLA-A2-transfected cells and 84.4% of the HLA-Cw2 were positive on flow cytometry [Figure

3.7]. Interestingly, the same cell lines were stained with the original antibody and the results were negative indicating that the original antibody was defective.

The pelleted, formalin-fixed and paraffin embedded cells were then stained manually and despite a degree of background staining in the parental cell line there was obvious membranous reactivity of the transfected cell lines especially the HLA-Cw1 line. The staining was then repeated on the Leica Bond-RX auto-stainer and the results were comparable [Figure 3.8]. It was however noticed that the staining using the automated method yielded less background stain.

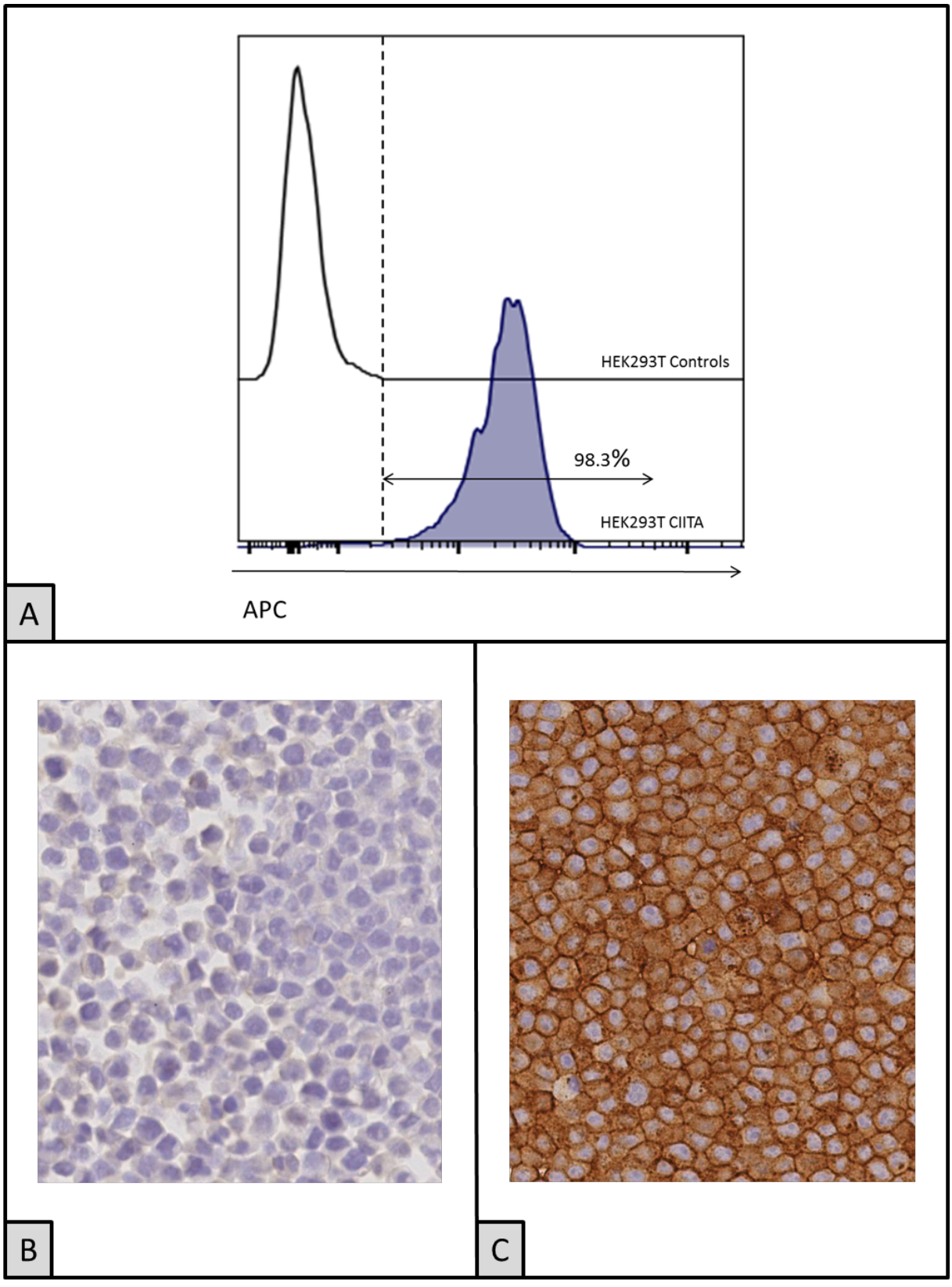

Figure 3.1: MHC class II validation results. Figure A shows the flow cytometry histogram showing the expression of MHC Class II in transfected HEK293 cell lines (filled histogram) compared to parental cell line (unfilled histogram). The two lower images are high power bright field microscopy screenshots of pelleted, formalin fixed and paraffin embedded cells stained with anti-human MHC Class II antibodies where figure B is of the parental cell line and figure C is of the CIITA transfected cell line. 400X magnification

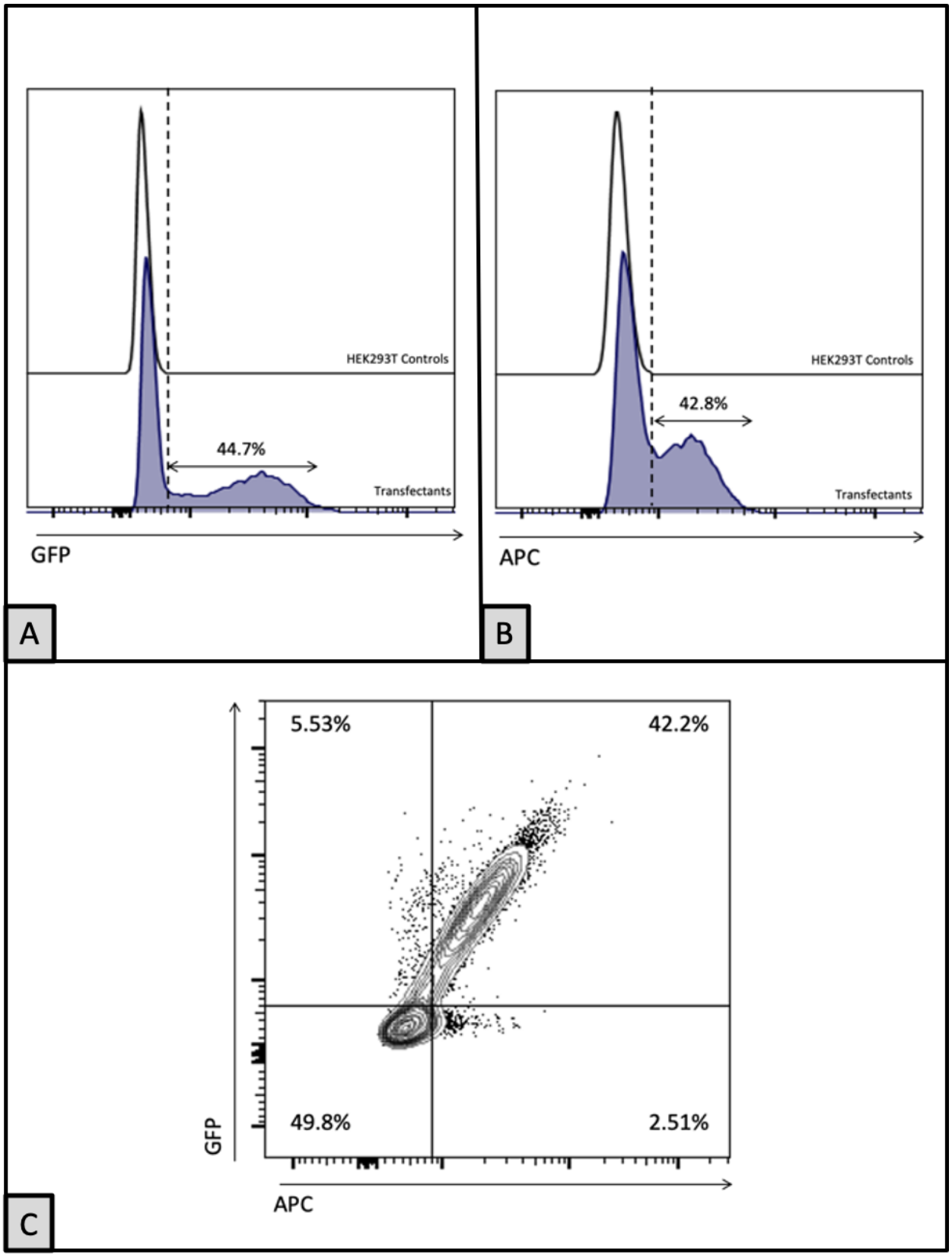

Figure 3.2: Flow cytometry histograms showing the expression of FOXP3 in transiently transfected HEK293T cell lines (filled histogram) compared to parental cell line (unfilled histogram). Figure A shows the expression of GFP which is the marker on the transfected plasmid. Figure B shows the expression of FOXP3 when stained with APC conjugated anti-human FOXP3 antibody. Figure C shows the co-expression of GFP and FOXP3 in the top right compartment confirming successful transfection in 42.2%.

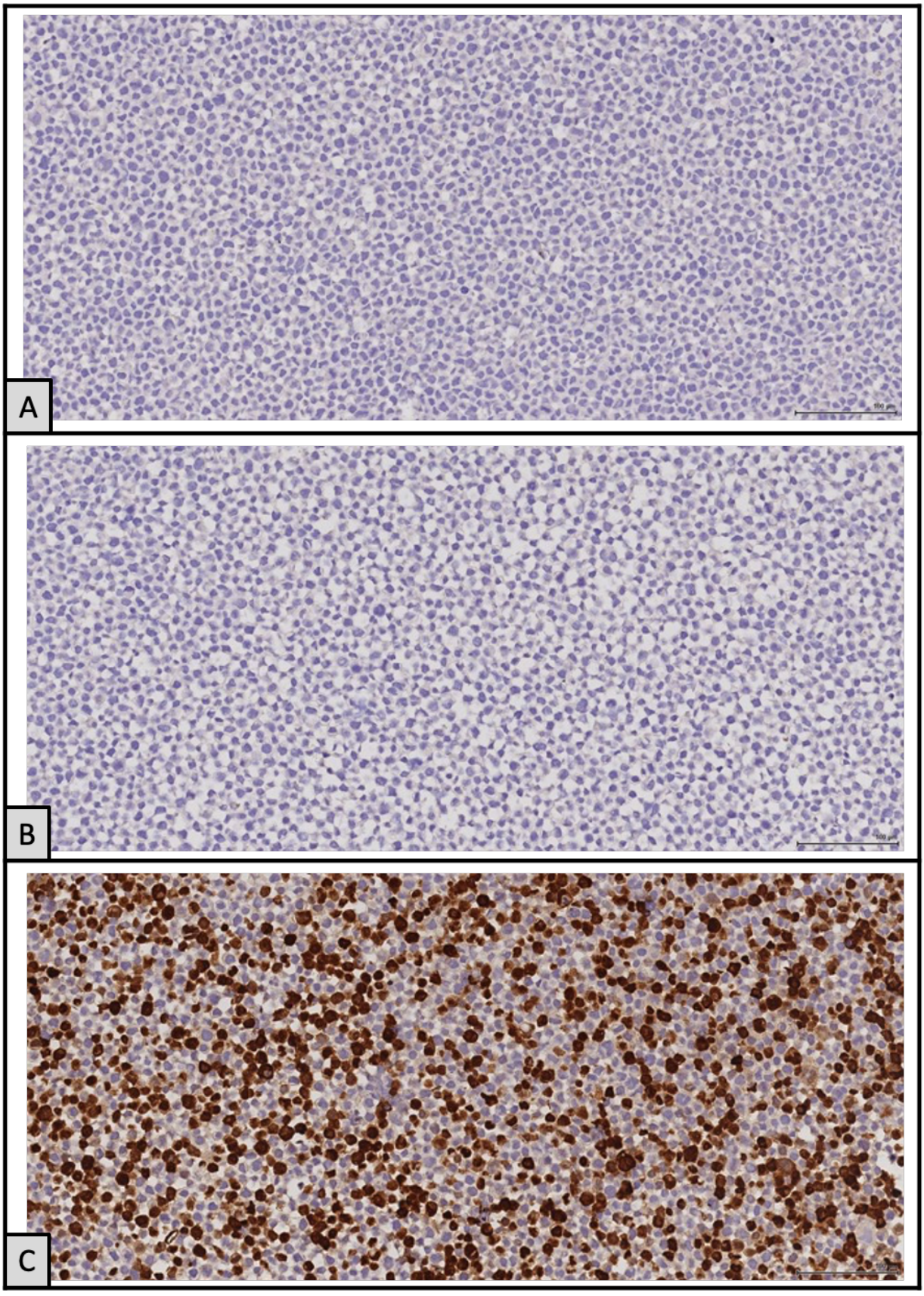

Figure 3.3: Bright field microscopy images of HEK293T cells stained with anti-human FOXP3. The top image (A) is of the parental cell line. The middle image (B) is of mock transfection (C) is of a cell line transfected with FOXP3. 400X Magnification.

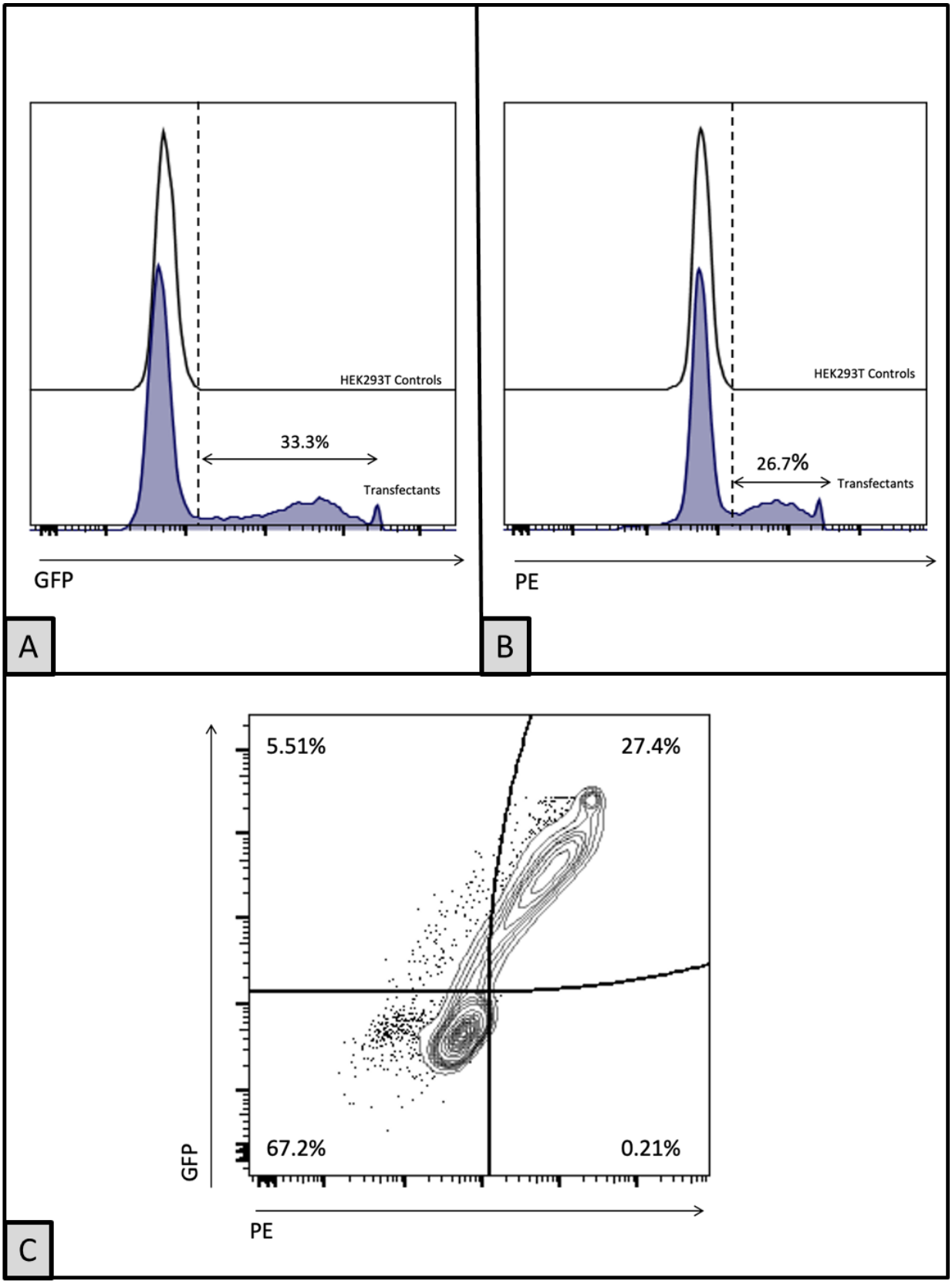

Figure 3.4: Flow cytometry histograms showing the expression of Isoform 1 of RORγt in transiently transfected HEK293T cell lines (filled histogram) compared to parental cell line (unfilled histogram). Figure A shows the expression of GFP which is the marker on the transfected plasmid. Figure B shows the expression of RORγt when stained with PE conjugated anti-human RORγt antibody. Figure C shows the co-expression of GFP and RORγt in the top right compartment confirming successful transfection in 27.4%.

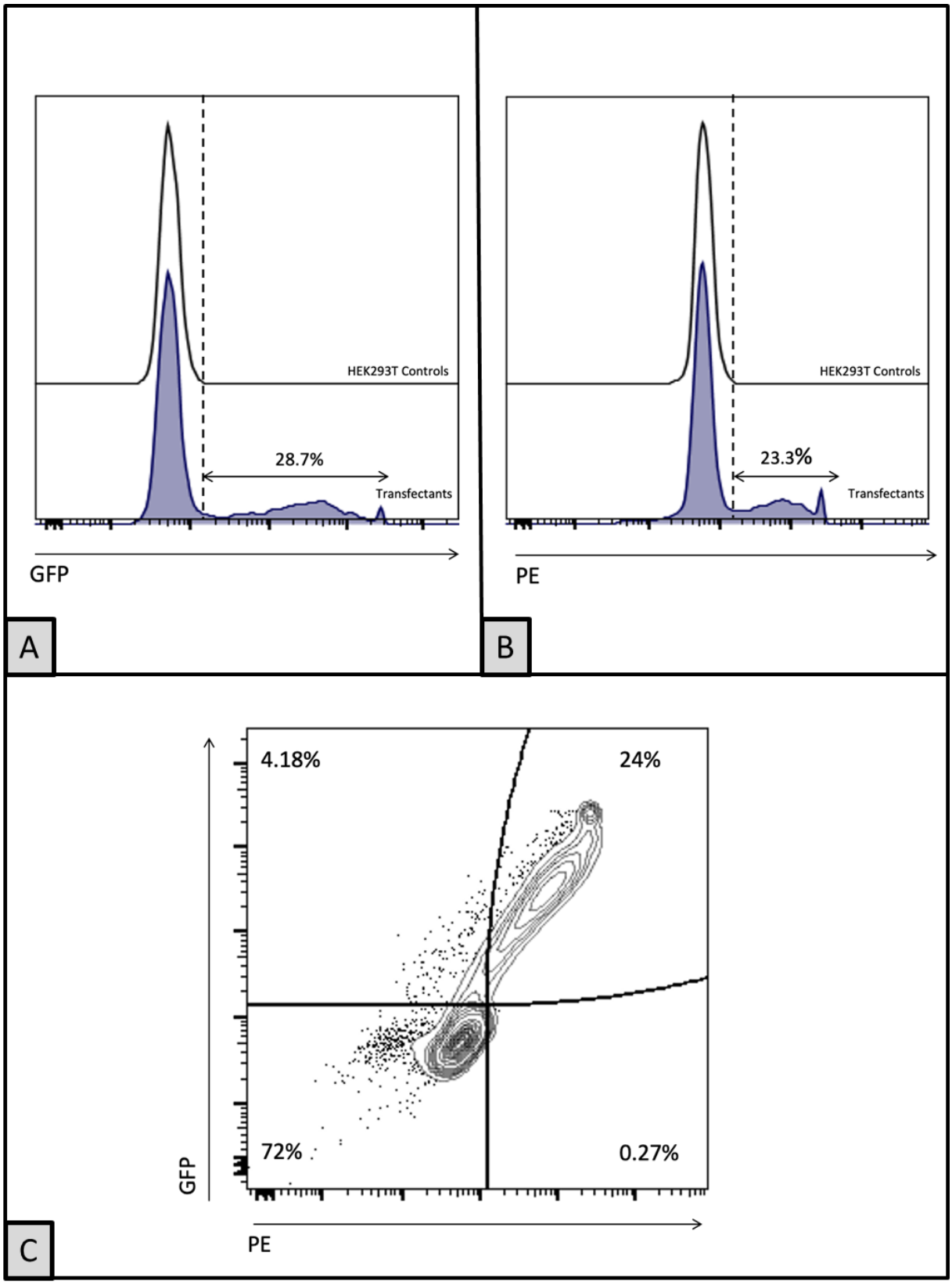

Figure 3.5: Flow cytometry histograms showing the expression of Isoform 2 of RORγt in transiently transfected HEK293T cell lines (filled histogram) compared to parental cell line (unfilled histogram). Figure A shows the expression of GFP which is the marker on the transfected plasmid. Figure B shows the expression of RORγt when stained with PE conjugated anti-human RORγt antibody. Figure C shows the co-expression of GFP and RORγt in the top right compartment confirming successful transfection in 24%.

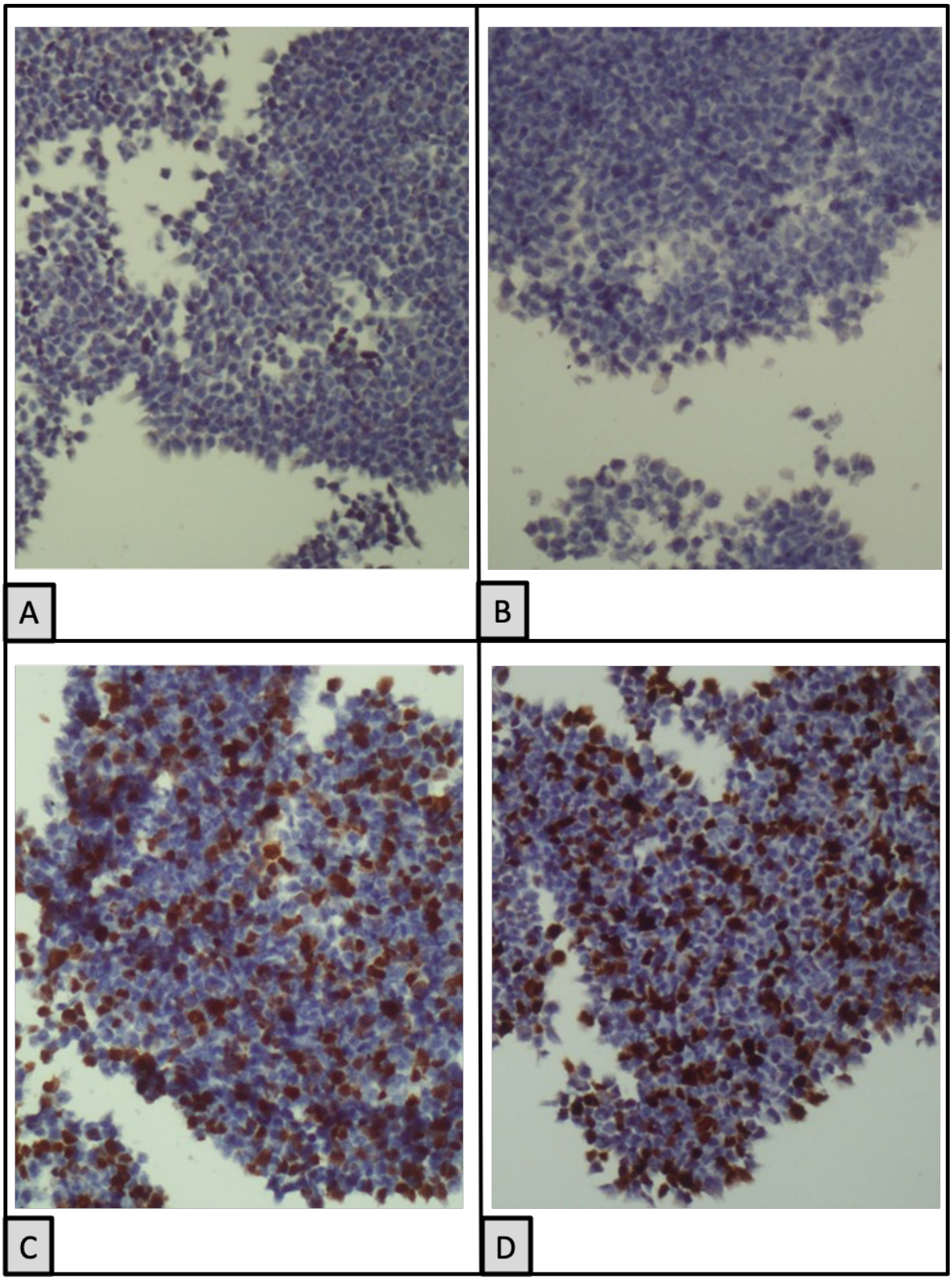

Figure 3.6: Bright field microscopy images of HEK293T cells stained for both isoforms of human RORγt. Image (A) is of the parental cell line. Image (B) is of mock transfection, image (C) is of a cell line transfected with Isoform 1 of RORγt and image (D) is of a cell line transfected with Isoform 2 of RORγt. 400X magnification.

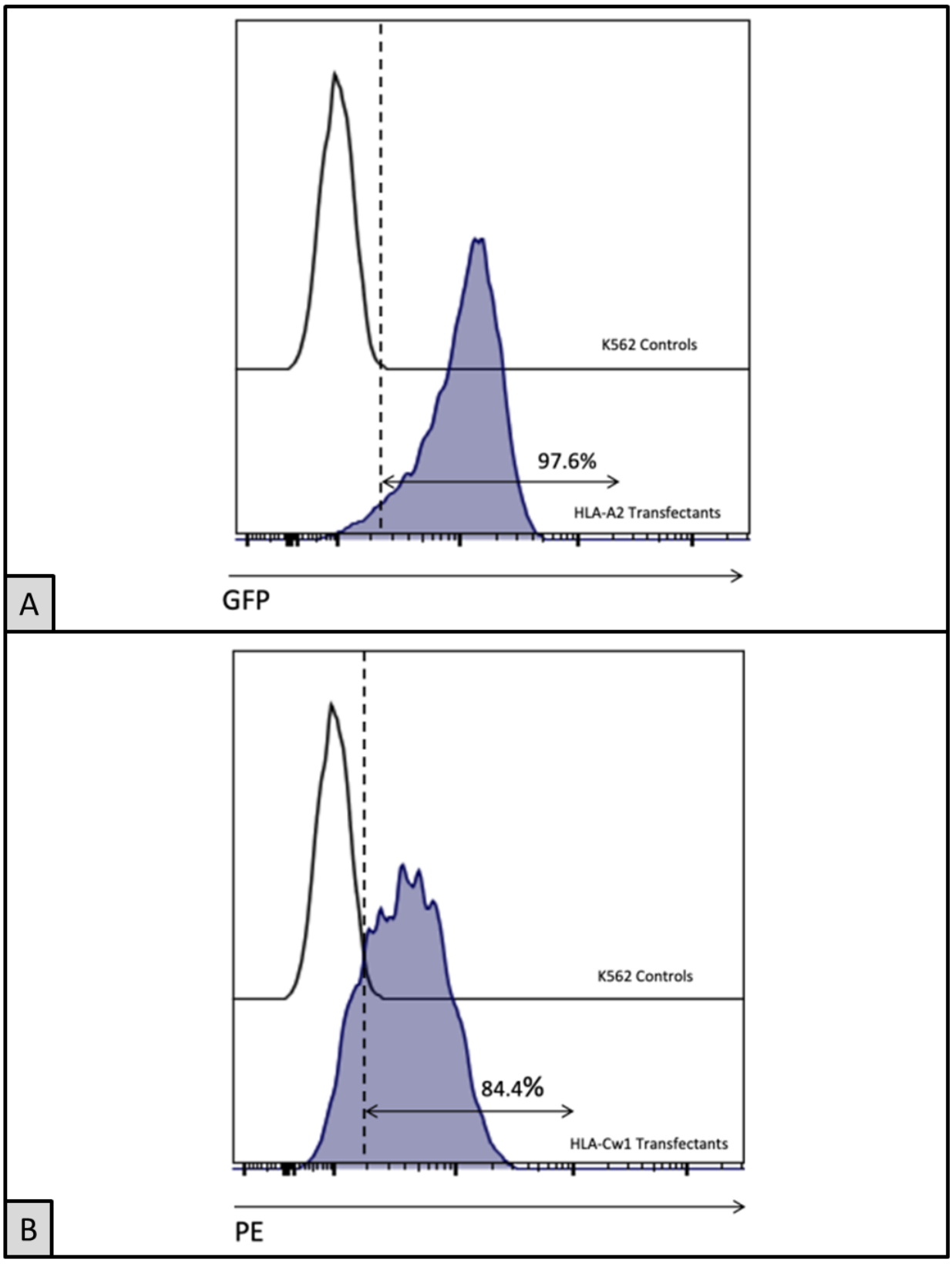

Figure 3.7: Flow cytometry histograms showing the expression of MHC Class I in transfected K562 cell lines (filled histogram) compared to parental cell line (unfilled histogram). The above figure (A) shows expression of HLA-A2 and the below figure (B) shows the expression of HLA-Cw1

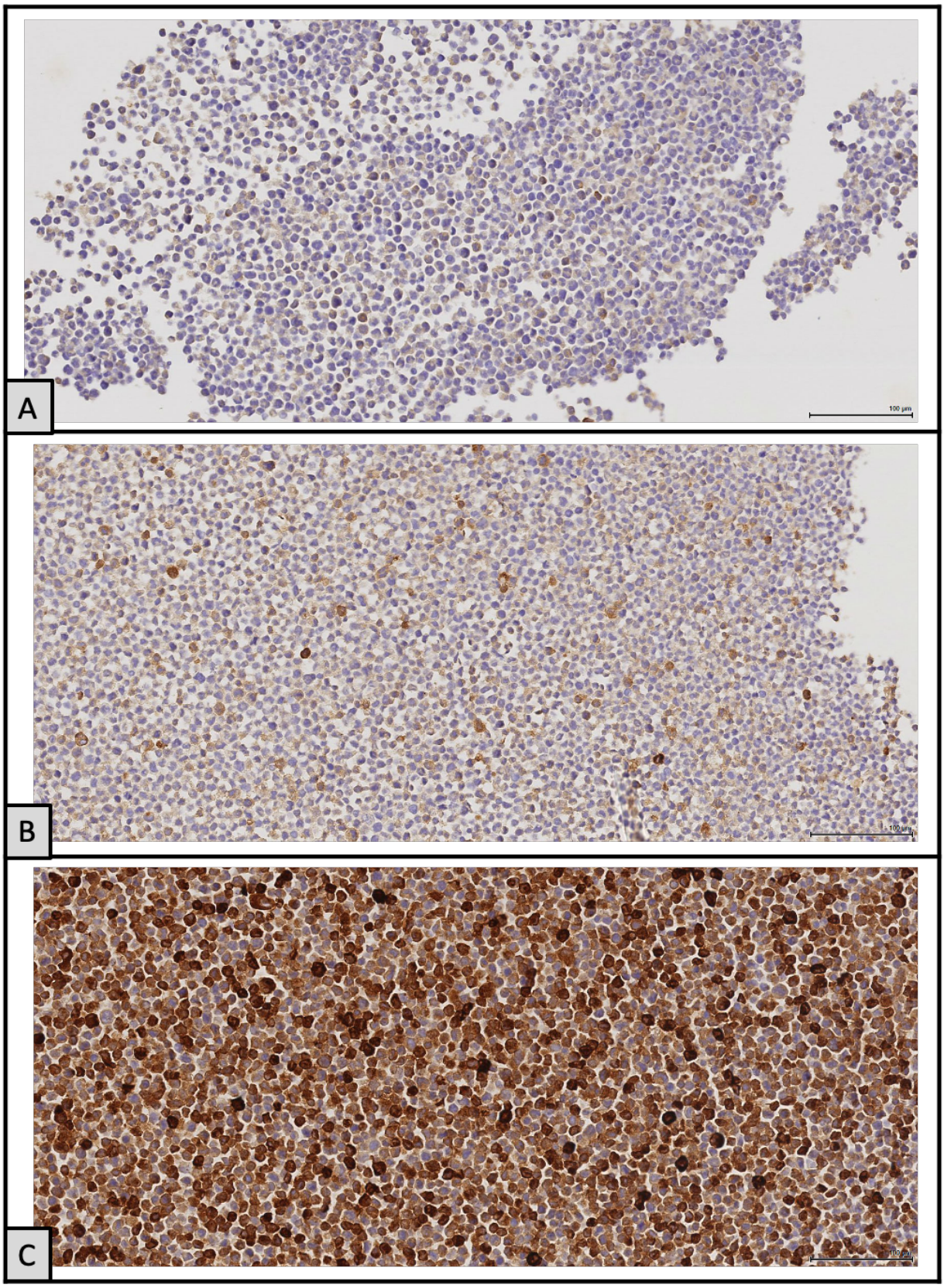

Figure 3.8: Bright field microscopy images of K562 cells stained with anti-human HLA-A, B and C. The top image (A) is of the parental cell line. The middle image (B) is of a cell line transfected with HLA-A2 and the bottom image (C) is of a cell line transfected with HLA-Cw1. Magnification 400x

3.2. Validation of the immunofluorescence multiplex staining

To validate the consistency of staining and ensure comparability with conventional IHC with DAB staining, three training sets of slides were created using excess tonsillar tissue. Each set contained 8 sequential cuts from the same block, the first slide was stained with the full complement of fluorescent dyes and then each subsequent slide was conventionally singly stained (IHC with DAB) with each corresponding marker. The slides were then reviewed and visually compared by an experienced consultant histopathologist (Dr Gerald Langman) [Images 3.9 to 3.15].

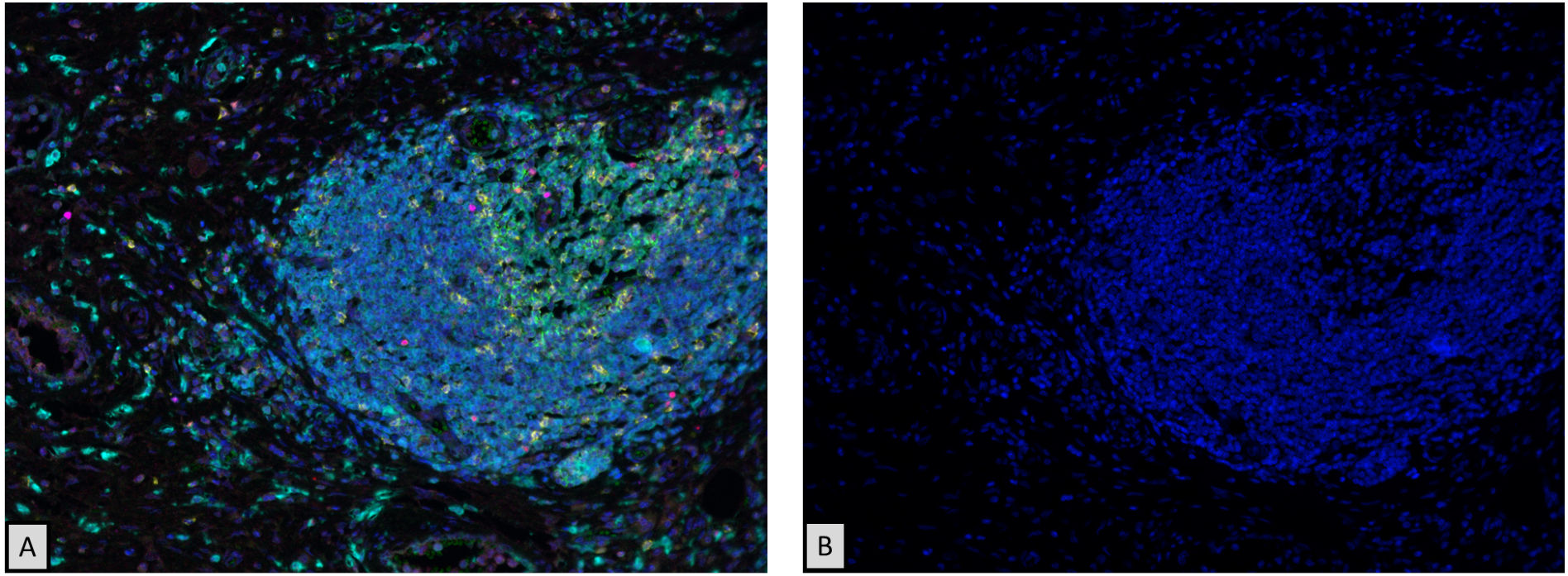

Figure 3.9: Multiplex staining validation. Figure A is a composite multispectral image of a human tonsil stained with the T-cell panel outlines in the text. The image is captures using the Vectra 3 platform using all the filters. Figure B is captures using the DAPI only filter showing the nuclei. 200X magnification.

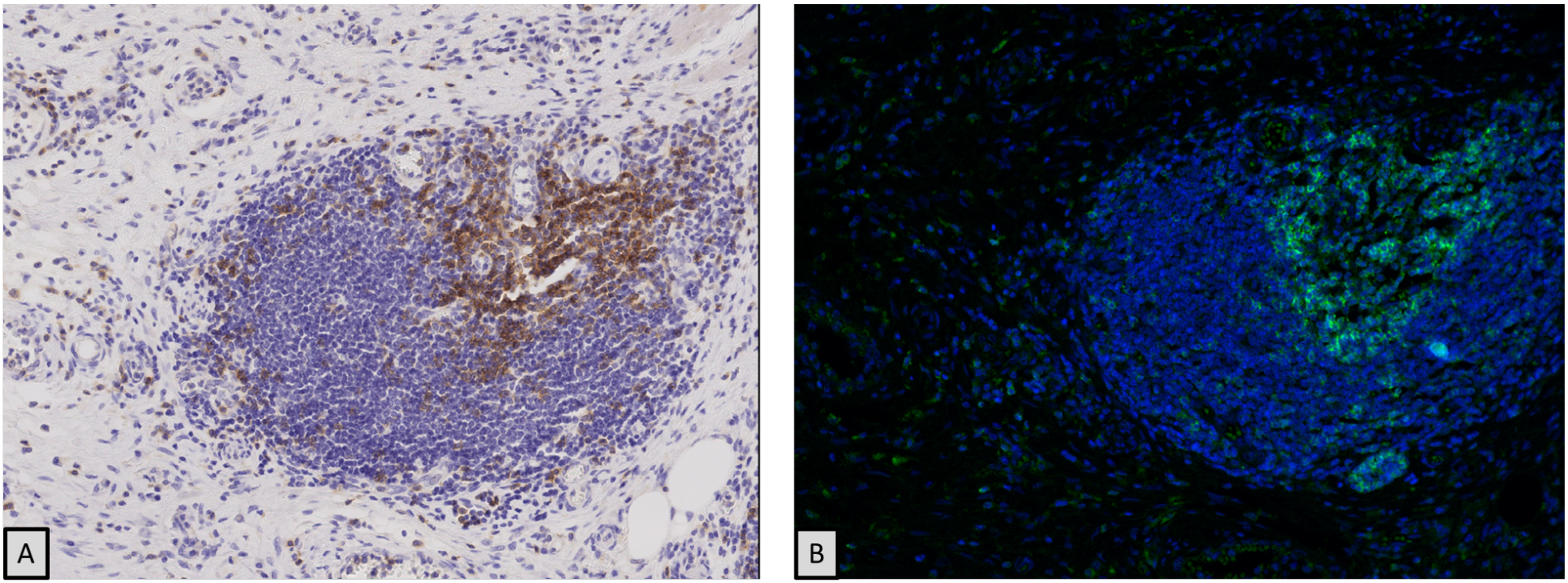

Figure 3.10: Multiplex staining validation. Figure A is a bright field microscopy screenshot of a section of human tonsil stained immunohistochemically (DAB) for CD4. Figure B is fluorescent microscope image captured of a section of the same tonsil stained using the Opal multiplex kit. In this image only the Opal 520 filter is applied which represents the fluorophore used for CD4. 200X magnification.

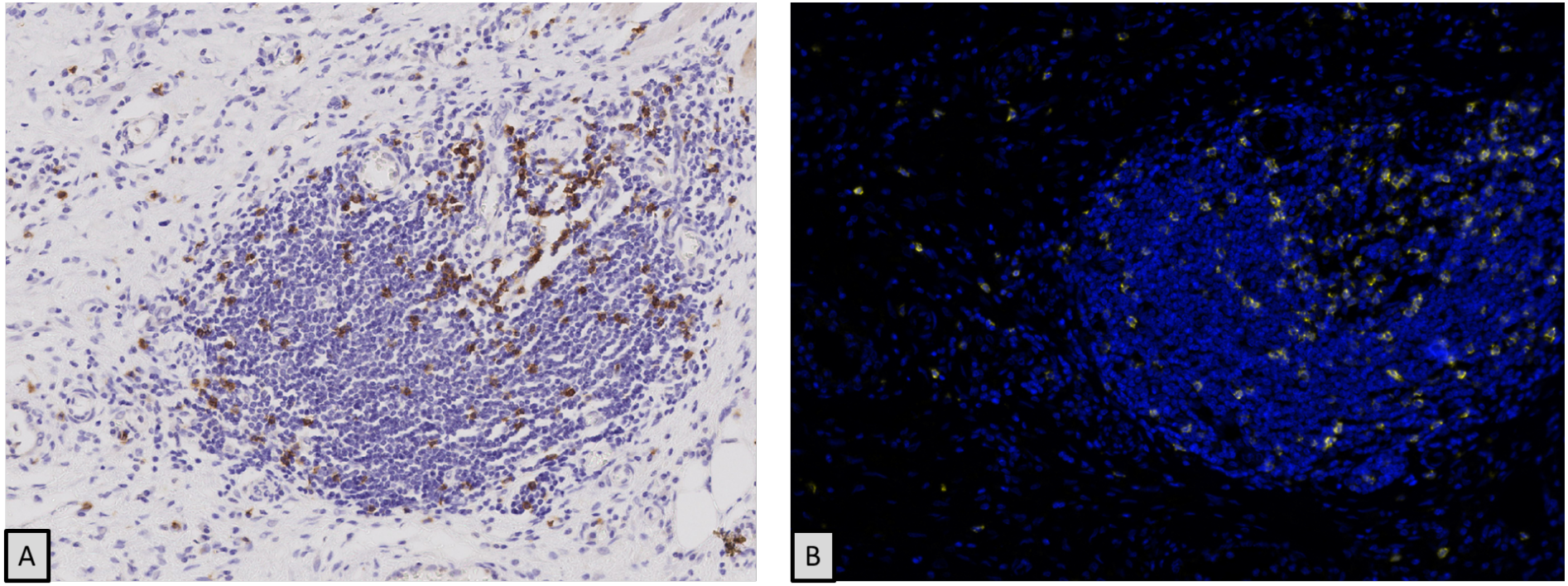

Figure 3.11: Multiplex staining validation. Figure A is a bright field microscopy screenshot of a section of human tonsil stained immunohistochemically (DAB) for CD8. Figure B is fluorescent microscope image captured of a section of the same tonsil stained using the Opal multiplex kit. In this image only the Opal 540 filter is applied which represents the fluorophore used for CD8. 200X magnification.

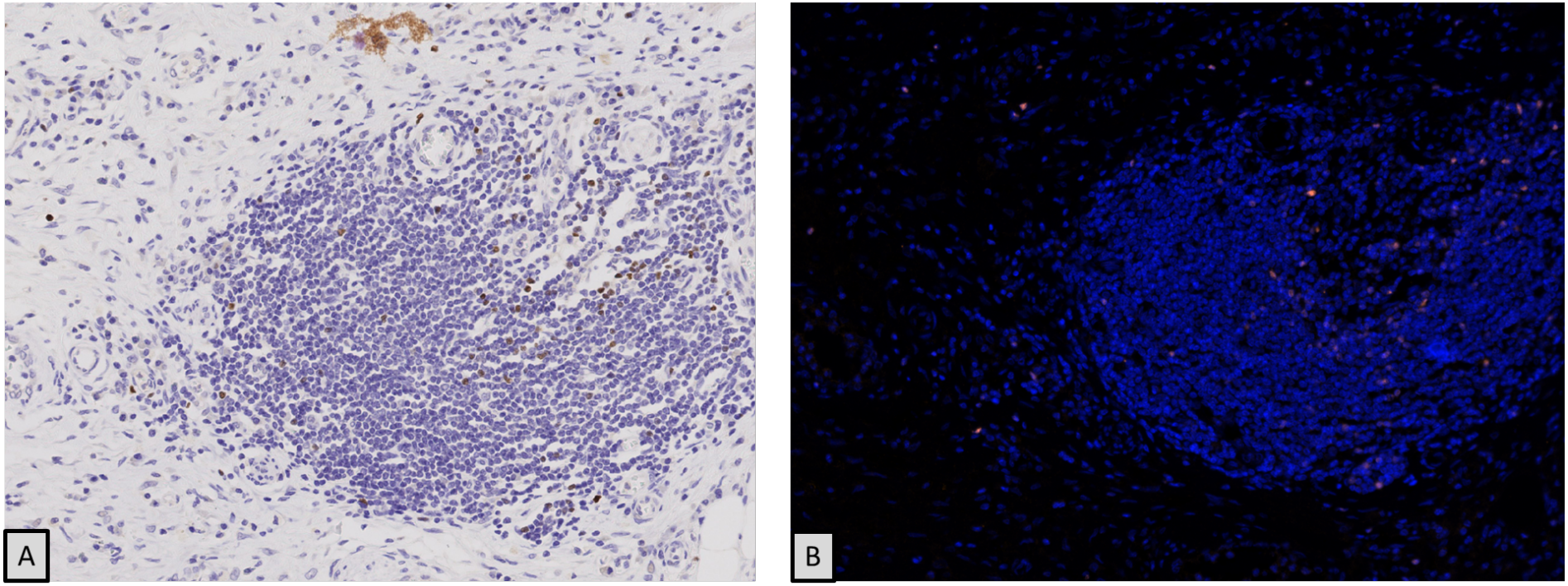

Figure 3.12: Multiplex staining validation. Figure A is a bright field microscopy screenshot of a section of human tonsil stained immunohistochemically (DAB) for FOXP3. Figure B is fluorescent microscope image captured of a section of the same tonsil stained using the Opal multiplex kit. In this image only the Opal 570 filter is applied which represents the fluorophore used for FOXP3. 200X magnification.

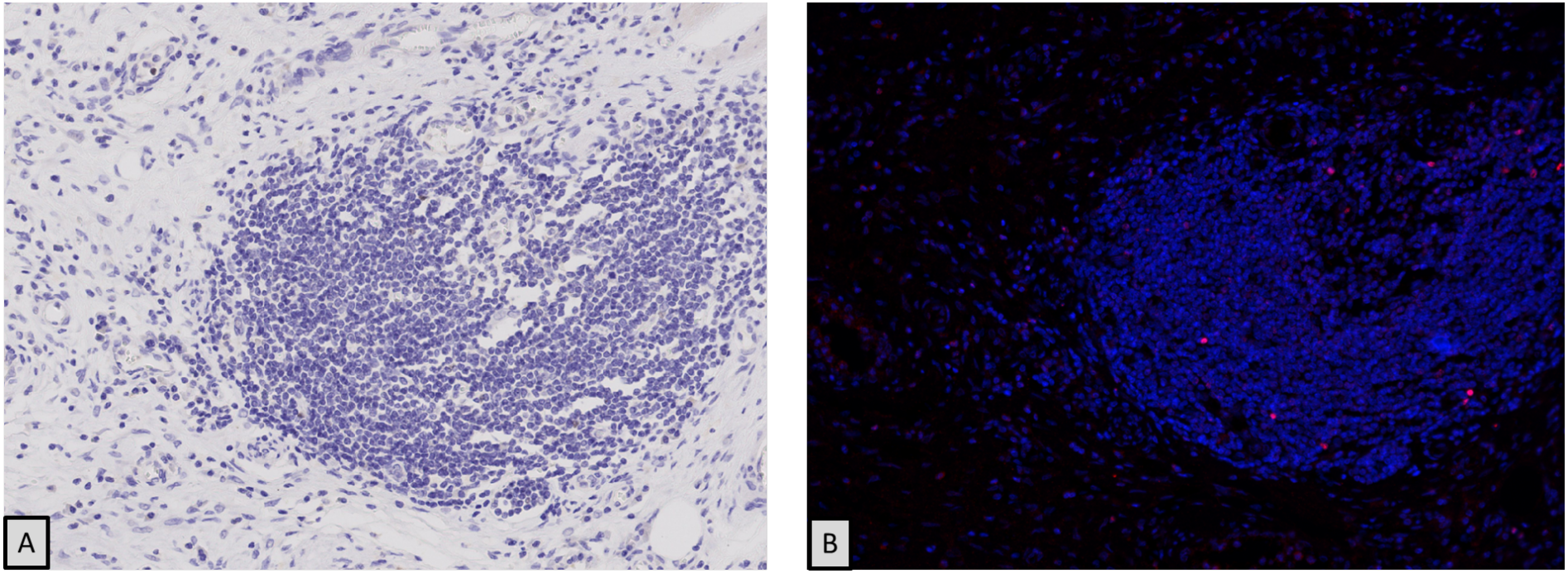

Figure 3.13: Multiplex staining validation. Figure A is a bright field microscopy screenshot of a section of human tonsil stained immunohistochemically (DAB) for T-Bet. Figure B is fluorescent microscope image captured of a section of the same tonsil stained using the Opal multiplex kit. In this image only the Opal 620 filter is applied which represents the fluorophore used for T-Bet. 200X magnification.

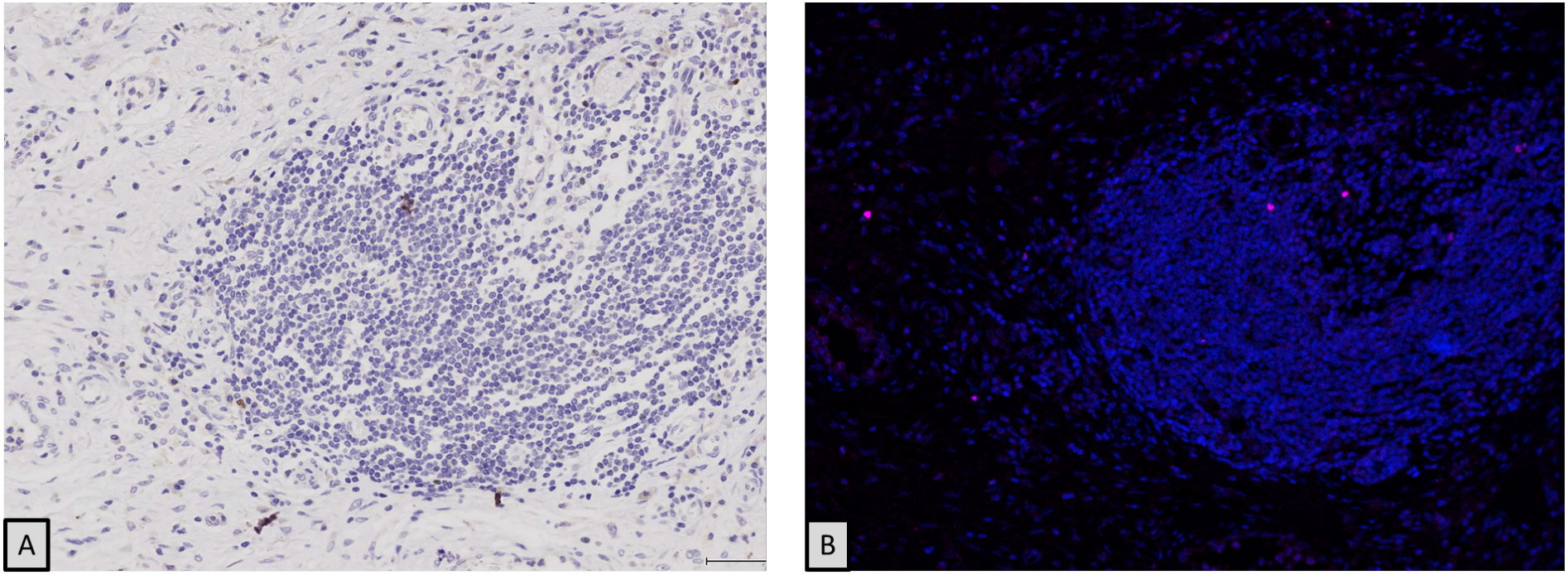

Figure 3.14: Multiplex staining validation. Figure A is a bright field microscopy screenshot of a section of human tonsil stained immunohistochemically (DAB) for RORγt. Figure B is fluorescent microscope image captured of a section of the same tonsil stained using the Opal multiplex kit. In this image only the Opal 650 filter is applied which represents the fluorophore used for RORγt. 200X magnification.

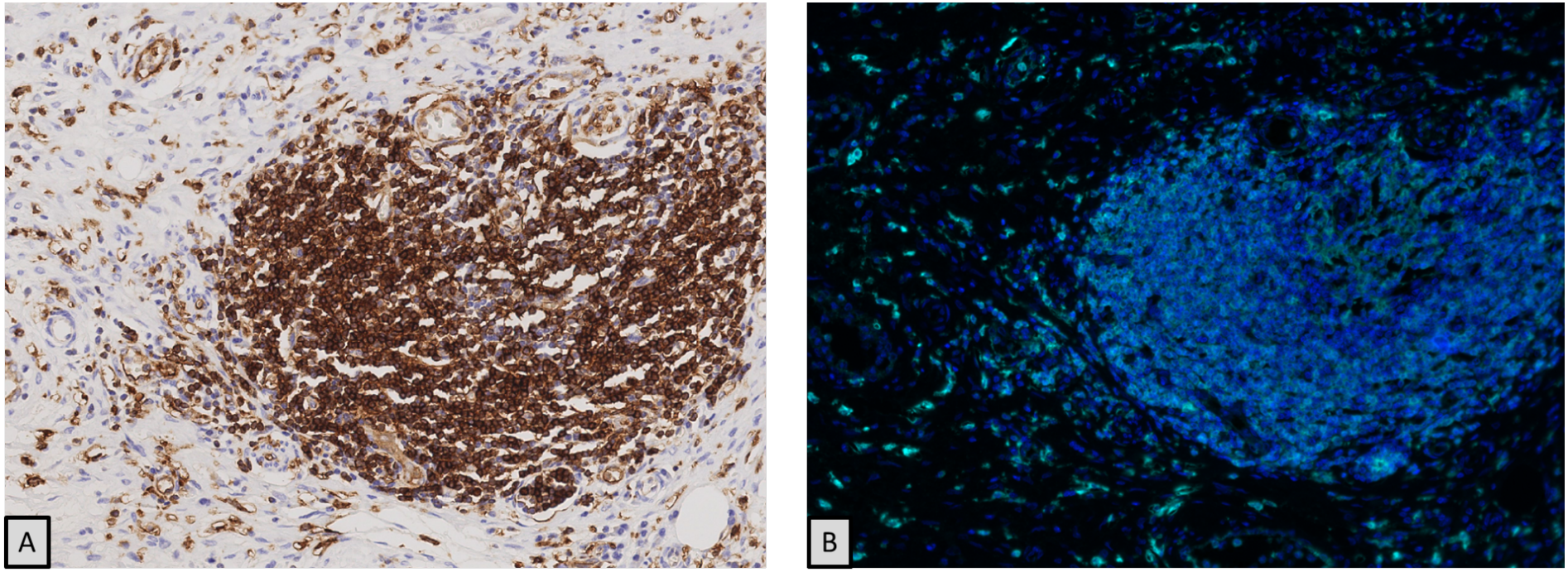

Figure 3.15: Multiplex staining validation. Figure A is a bright field microscopy screenshot of a section of human tonsil stained immunohistochemically (DAB) for MHC Class II. Figure B is fluorescent microscope image captured of a section of the same tonsil stained using the Opal multiplex kit. In this image only the Opal 690 filter is applied which represents the fluorophore used for RORγt. 200X magnification.

4. Chapter Four: Comparing the Immune Microenvironment of Primary Colorectal Cancer and Pulmonary Metastases

4.1. Introduction

As outlined in the introduction, it is now established that the immune microenvironment plays a pivotal role in the prognosis of CRC. The emergence of novel therapies such as Checkpoint Blockade ushered in a new era of targeted therapies.

The majority of contemporary literature is focused on primary disease, but it is a well-known fact that progression to metastatic disease is what usually a transition towards terminal phases of the disease. Therefore, in order to inform optimal development of immunotherapy strategies, it is of vital importance to understand the biology of tumours at the metastatic site and to understand the immunobiology and its relationship to the primary tumour is crucial.

4.2. Chapter hypothesis

I hypothesise that colorectal lung metastases evoke a different immune response to that at the primary site due to differences in the microenvironments between the two sites.

4.3. Chapter aims

The aim of this chapter is to explore the differences in the immune microenvironment in primary CRC and matched pulmonary metastases. This may help understand the impact of different milieux and inform development of immunotherapies.

To gain a broad understanding of the immune microenvironment, the histological sections were stained for cluster of differentiation 3 (CD3), a T-lymphocyte marker to gauge the differences in the density of Tumour Infiltrating Lymphocytes (TILs). To glean further understanding of the type of infiltrating T-lymphocytes, the sections were stained for a T-helper cell marker (CD4) and a T-cytotoxic marker (CD8). The functional orientation of T-cells was assessed by staining for two transcription markers, T-BET and FOXP3, markers of type 1 and regulatory T-lymphocytes respectively.

Differential checkpoint blockade molecules expression was evaluated by staining the sections for two quintessential CPB therapeutic targets; Programmed Cell Death Protein 1 (PD-1) and its ligand PD-L1.

In view of their central role in the adaptive immune response, the differential expression of Major Histocompatibility Complexes (MHC) was studied by staining the sections for MHC I & II.

4.4. Patient and disease characteristics

Thirty-eight patients were identified for this project between December 1994 and September 2016. Paired samples were obtained for 34 patients (89%) which formed the study cohort. Twenty-one (61.7%) were female. The median age at the primary CRC resection was 64.5 years (range: 37 – 77 years). The primary resections were performed between 1994 and 2010. The median age at lung metastasectomy was 68 years (range: 40 – 79 years). Lung metastasectomies took place at a median 24 months (range: 4 – 104 months) from the primary resections. The metastasectomies were performed between 1997 and 2016.

The median time from primary colorectal resection to staining the sections was 169 months (range: 80 – 261 months). The median tome from metastasectomy to staining the section was 131 months (range: 1 – 229 months).

Complete pathological data for the primary tumour were available for 21 patients (61.8%). Incomplete date however was available for 29 patients (85.3%). The reason for the incomplete data set is the fact that some samples were anonymised, and I was not able to trace the samples to the original records. Table 4.1 summarises the pathological data of the primary tumours. All tumours were adenocarcinomas.

Characteristic	Number	Percentage
Tumour location (n=29)		
Right colon	6	20.7%
Left colon	9	31%
Rectum	14	48.3%
Differentiation (n=21)		
Well	1	4.7%
Moderate	17	81%
Poor	3	14.3%
Tumour (n=21)		
T1	0	0%
T2	2	9.5%
T3	12	57.1%
T4	7	33.3%
Lymph Node Status (n=29)		
N0	8	27.6%
N1	13	44.8%
N2	8	36.8%
LVI (n=21)		
Yes	17	78.9%
No	3	15.8%
Suspected	1	5.3%

Table 4.1 Pathological characteristics of the primary tumours in the paired cohort. LVI: Lympho-vascular invasion.

4.5. Results of comparing Tumour Infiltrating Lymphocytes (TILs) in primary colorectal cancer and pulmonary metastases

4.5.1. CD3 expression

To determine the distribution of CD3 expressing cells in the tumour, the densities of CD3 expressing cells were studied in the tumours' stromal and epithelial compartments. The densities were then compared between the primary and the secondary site in corresponding compartments.

Thirty-four paired sections were stained. In the primary tumour cohort, two sections were excluded because no tumour was found, therefore thirty-two sections were included in the primary tumour analysis. In the pulmonary metastases cohort only one section was excluded as it did not contain a tumour. This section contained only small islands of tumour cells probably indicating that the section was taken from the edge of the tumour mass embedded in the FFPE block. Therefore, thirty-three sections were included in the metastases' analysis. Taking the exclusions on both sides into consideration, thirty pairs were included in the paired head-to-head analysis.

To ensure consistency, the densities were calculated in three ways: number of cells per square millimetre (mm^2), Histological score (H-score) and percentage of positive cells. The correlation between the three measures was assessed using the Spearman correlation coefficient and found to highly concordant [Table. 4.2]. For consistency, the results will be presented as density (positive cell/mm^2).

Measures	Spearman rho	P-value
H-score vs.% positive cells	0.992	0.000
H-score vs. positive cells/mm^2	0.960	0.000
% positive cells vs. cells/mm^2	0.959	0.000

Table 4.2 Demonstration of the correlation of three different modes of presenting the density of CD3 cells in stained tissues.

4.5.1.1. CD3$^+$ cell densities in stroma and epithelium

Thirty-two sections of primary CRC were stained for CD3 and analysed using the Definiens platform. The cell densities were significantly higher in the stromal compartment compared to the epithelial compartment (median 303.64 cells/mm^2 vs 61.29 cells/mm^2, Wilcoxon signed rank test p= 0.0015) [Image 4.1A].

Amongst the thirty-three lung metastases sections stained, the distribution of CD3$^+$ cells was similar with significant predilection to the stromal compartment (median 1056.72 cells/mm^2 vs 138.22 cells/mm^2, Wilcoxon signed rank test p <0.0001) [Image 4.1B].

4.5.1.2. Comparison of CD3$^+$ densities between the primary and secondary site

The densities of T-lymphocytes were compared in thirty pairs of samples. The density of CD3$^+$ lymphocytes was found to be significantly higher in the stroma of the pulmonary metastatic site when compared to the stroma of the primary site (median 1060.28 cells/mm^2 vs 303.64 cells/mm^2, Wilcoxon signed rank test p <0.0001) [Image 4.1C]. Although the densities of CD3$^+$ cells in the epithelial compartments did not show

a significant difference it did demonstrate a similar trend (median 136.5 cells/mm^2 vs 61.29 cells/mm^2, Wilcoxon signed rank test p= 0.0957) [Image 4.1D].

CD3 Analysis results

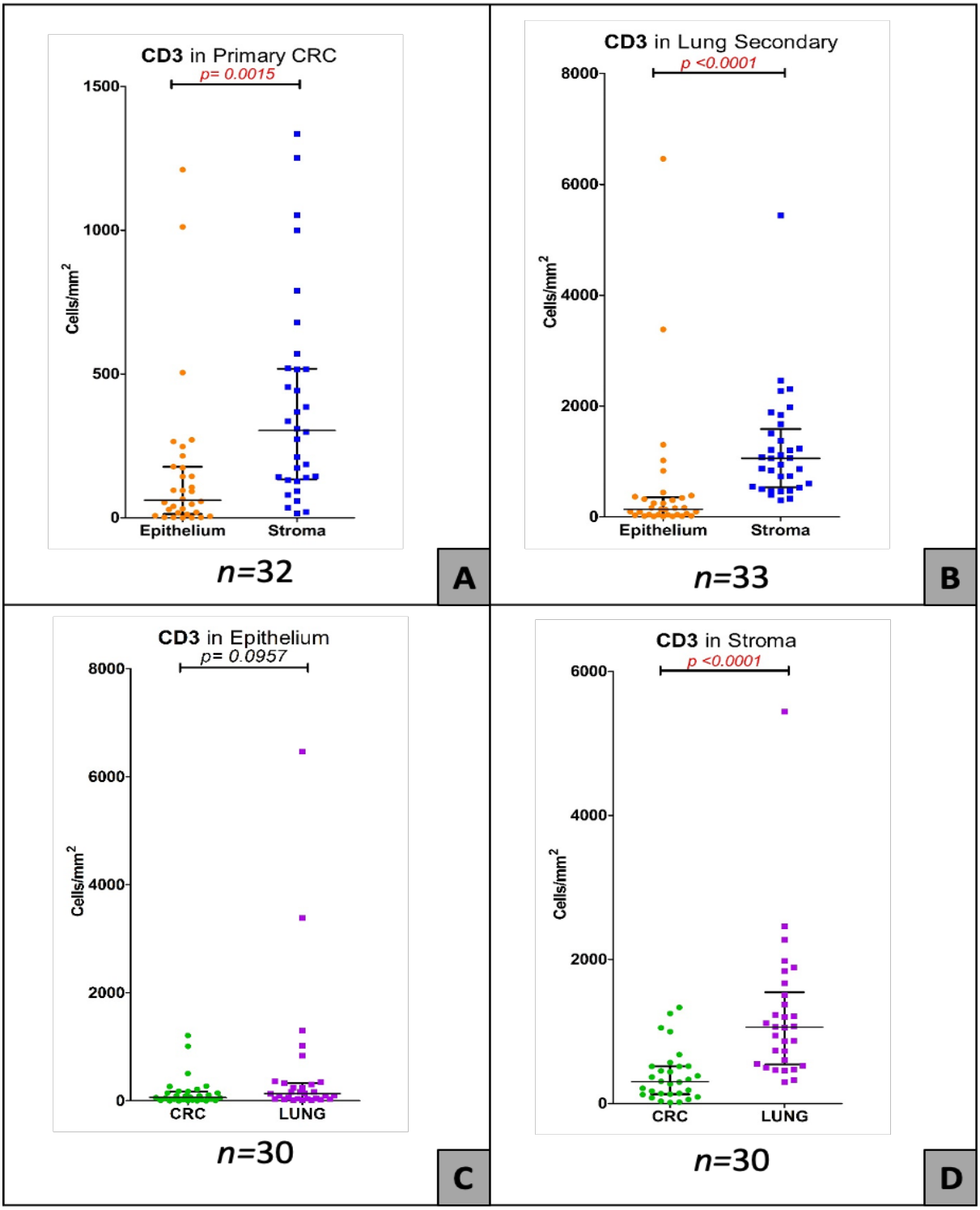

Figure 4.1 CD3 analysis in primary and secondary colorectal cancer pairs
A. Shows the density of $CD3^+$ cells in the epithelial and stromal compartments of the primary tumour. **B.** Shows the density of $CD3^+$ cells in the epithelial and stromal compartments of the lung metastases. **C.** Shows the densities of $CD3^+$ cells in the epithelial compartment of paired colorectal primary and lung metastasis. **D.** Shows the densities of $CD3^+$ cells in the stromal compartment of paired colorectal and lung metastasis.

4.5.2. CD4 expression

In order to determine the density and differential distribution of $CD4^+$ lymphocytes, primary tumour and lung metastasis sections were stained and digitally analysed.

Thirty-four primary tumour sections were stained for CD4 expression. Two sections were excluded due to absence of tumour and a further two sections were excluded as one was damaged by the staining process and the other could not be analysed due to excessive non-specific background staining. The final primary tumour analysis therefore included thirty sections.

Thirty-four lung metastasis sections were stained for CD4 expression. One section was excluded due to absence of tumour, leaving thirty-three sections in the final lung metastases analysis.

Allowing for the aforementioned exclusions, the primary-secondary comparative analysis included twenty-eight paired sections.

4.5.2.1. $CD4^+$ cell densities in stroma and epithelium

The $CD4^+$ cell densities were found to be significantly higher in the stromal compartment of the tumour and the metastasis when compared to the epithelial compartment. In the primary site the median density of the cells was 151.60 cells/mm^2 in the stromal compartment as compared to 70.29 cells/mm^2 in the epithelial (Wilcoxon signed rank test p=0.0237) [Image 4.2A]. In the lung metastasis, the median density of $CD4^+$ cells was 563 cell/mm^2 in the stroma and 78.78 cell/mm^2 in the epithelium (Wilcoxon signed rank test p= 0.0005) [Image 4.2B].

4.5.2.2. *Comparison of $CD4^+$ densities between the primary and secondary site*

Whilst the difference in median $CD4^+$ cell density did not reach statistical significance in the epithelial compartment (69.42 cells/mm^2 in the primary vs. 83.07 cells/mm^2 in the metastatic site, Wilcoxon signed rank test p= 0.25), it was significantly higher in the metastatic site when the stromal compartment was analysed (151.60 cells/mm^2 in the primary vs. 563.3 cells/mm^2 in the metastatic site, Wilcoxon signed rank test p <0.0001) [Image 4.2 C&D].

CD4 Analysis results

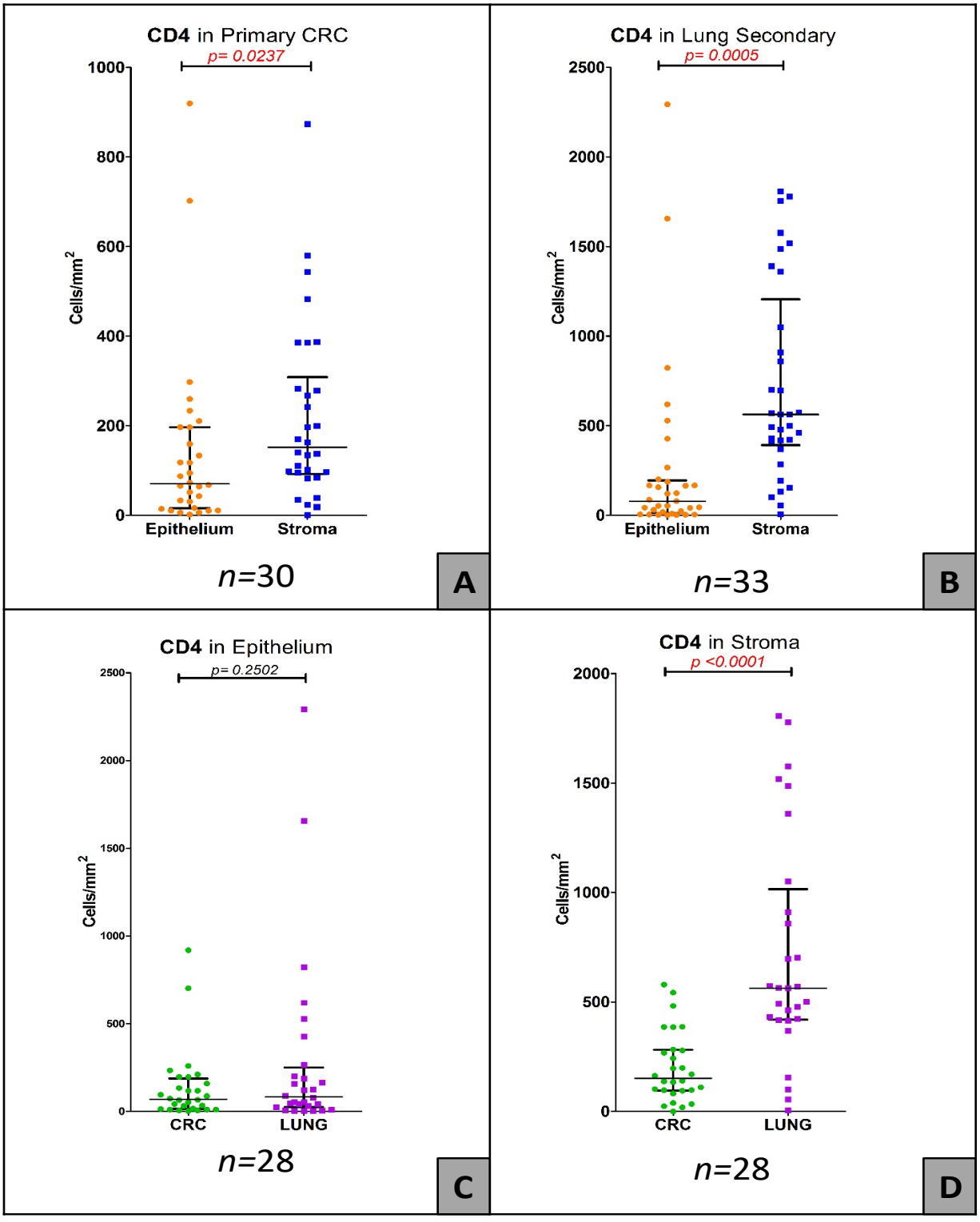

Figure 4.2: CD4 analysis in primary and secondary colorectal cancer pairs
A. Shows the density of $CD4^+$ cells in the epithelial and stromal compartments of the primary tumour. **B.** Shows the density of $CD4^+$ cells in the epithelial and stromal compartments of the lung metastases. **C.** Shows the densities of $CD4^+$ cells in the epithelial compartment of paired colorectal primary and lung metastasis. **D.** Shows the densities of $CD4^+$ cells in the stromal compartment of paired colorectal and lung metastasis.

4.5.3. CD8 expression

To determine the differential distribution of $CD8^+$ cytotoxic lymphocytes the sections were stained and digitally analysed in a manner analogous to the previously described methods.

Thirty-four primary CRC sections were stained for CD8 expression. Two sections were excluded due to absence of tumour and one due to damage sustained in the automated staining process rendering the slide not suitable for meaningful analysis. This left a total of thirty-one slides for analysis.

Out of the thirty-four lung metastasis sections stained for CD8 expression, one section was excluded due to absence of tumour and one contained excessive non-specific staining precluding meaningful analysis. This meant that thirty-two slides were analysed.

After taking out the exclusions on both sides, twenty-nine pairs formed the final head-to-head comparison cohort.

4.5.3.1. CD8 cell densities in stroma and epithelium

Although the density of $CD8^+$ cells was found to be higher in the stromal compartment of the primary tumour and the metastasis, this difference was not found to be statistically significant. In the primary tumour the median density was 84.65 cells/mm^2 in the epithelial compartment as compared to 106.83 cells/mm^2 in the stromal (Wilcoxon signed rank test p=0.2358) [Image 4.3A]. This was analogous to the metastatic site where the median density of $CD8^+$ cells was 282.24 cells/mm^2 in the epithelial compartment as opposed to 377.51 cells/mm^2 in the stromal compartment (Wilcoxon signed rank test p=0.4054) [Image 4.3B].

4.5.3.2. *Comparison of $CD8^+$ cell densities between the primary and secondary site*

When it came to comparing $CD8^+$ cell densities in the primary and metastatic site, statistically significant differences were found in both the stromal and epithelial compartment comparisons with significantly higher densities in the metastatic site. When comparing the epithelial compartments, the density of $CD8^+$ cells at the primary tumour site was 88.07 cells/mm^2 versus 310.01 cells/mm^2 the lung secondary site (Wilcoxon signed rank test p=0.0174) [Image 4.3C]. This was also true for when comparing the epithelial compartments where the density of $CD8^+$ cells was 115 cells/mm^2 at the primary site as opposed to 374.08 cells/mm^2 at the secondary site (Wilcoxon signed rank test p=0.0001) [Image 4.3D].

4.5.4. $CD4^+$ to $CD8^+$ ratio

In this section I explored the ratio of $CD4^+$ lymphocytes to $CD8^+$ lymphocytes in each of the tumour compartments in both the primary and secondary sites.

The proportion of $CD4^+$:$CD8^+$ lymphocytes was relatively constant in the stroma of the primary and the secondary sites at a ratio of 3:2 (χ^2 p=0.41). The ratio of the two subsets was reversed in the epithelium of both the primary and secondary sites with a higher proportion of CD8 lymphocytes. This $CD4^+$:$CD8^+$ ratio rose from 7:8 in the epithelium of the primary colorectal tumour to a 1:4 in the epithelium of the lung metastasis (χ^2 p<0.0001) [Image 4.4].

CD8 Analysis results

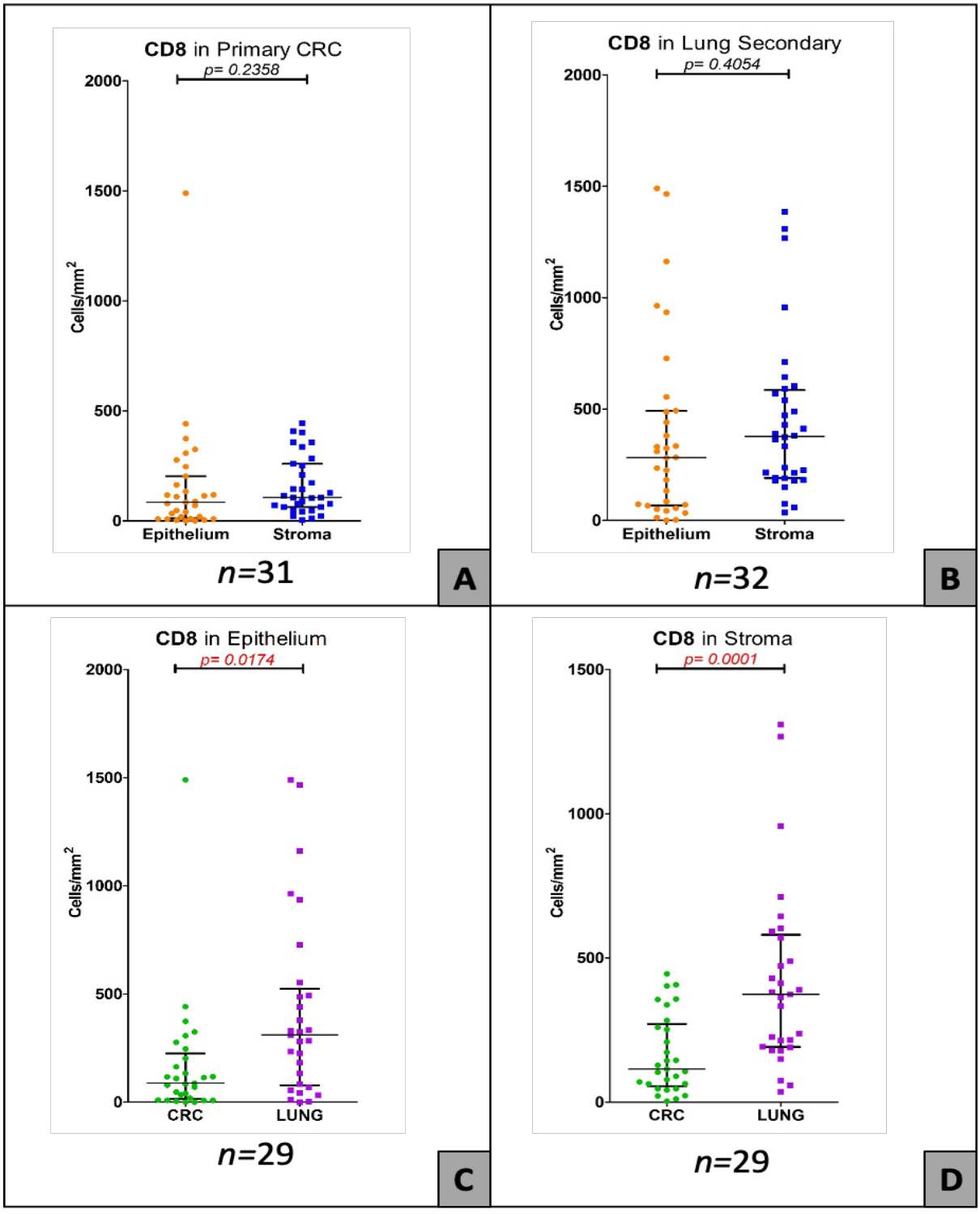

Figure 4.3: CD8 analysis in primary and secondary colorectal cancer pairs
A. Shows the density of $CD8^+$ cells in the epithelial and stromal compartments of the primary tumour. **B.** Shows the density of $CD8^+$ cells in the epithelial and stromal compartments of the lung metastases. **C.** Shows the densities of $CD8^+$ cells in the epithelial compartment of paired colorectal primary and lung metastasis. **D.** Shows the densities of $CD8^+$ cells in the stromal compartment of paired colorectal and lung metastasis.

CD4:CD8 Ratio

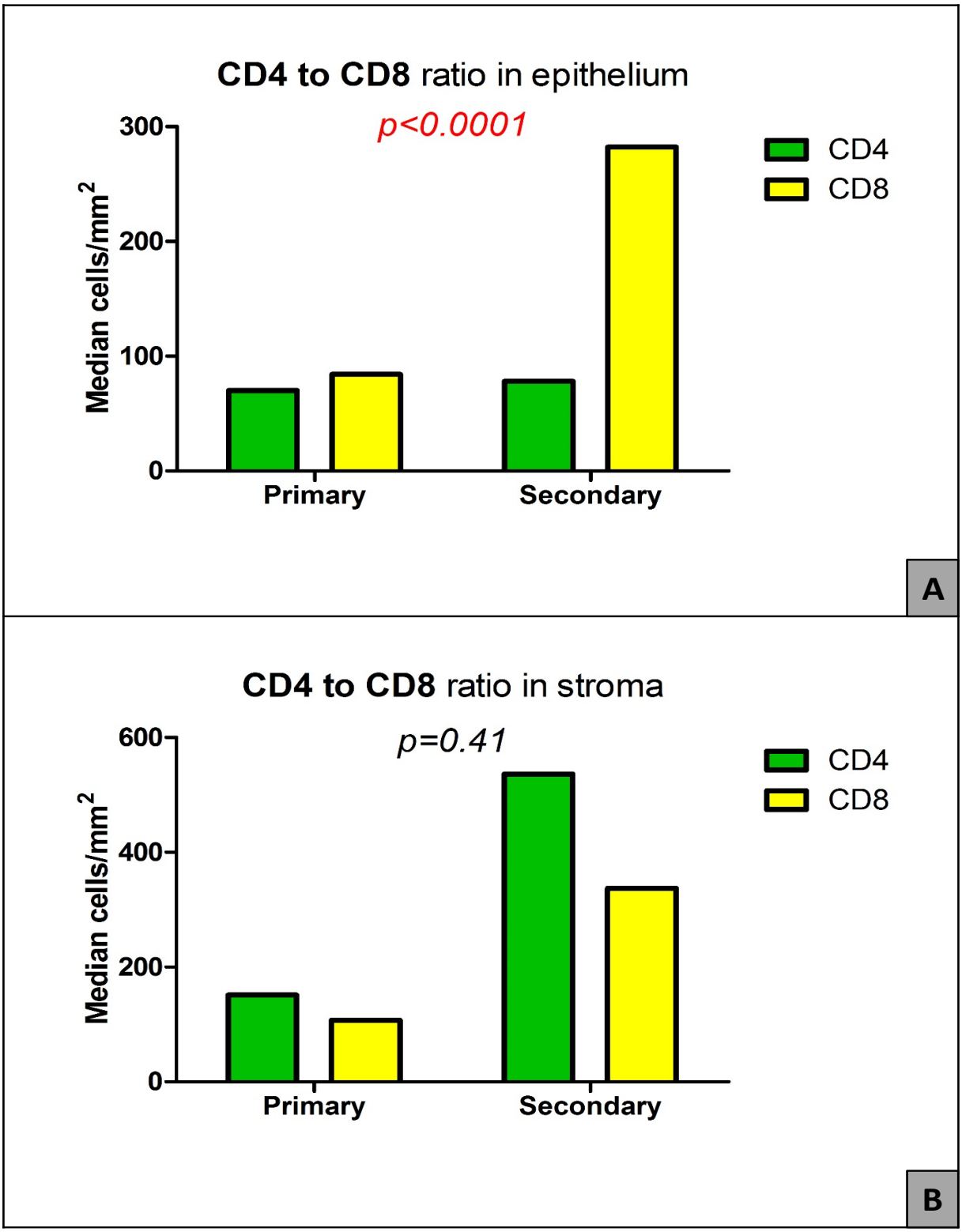

Figure 4.4: $CD4^+$ to $CD8^+$ ratio analysis in matched pairs
A. Shows the proportion of $CD4^+$ to $CD8^+$ lymphocytes in the epithelium of both the primary colorectal and the secondary lung metastatic site. **B.** Shows the proportion of $CD4^+$ to $CD8^+$ lymphocytes in the stroma of both the primary colorectal and the secondary lung metastatic site.

4.6. Results of comparing the functional orientation of TILs in primary colorectal cancer and pulmonary metastases

In order to better understand the role of tumour infiltrating lymphocytes, it was important to determine the functional orientation of those cells. To determine whether those lymphocytes play a role in mediating an anti-tumoural T_H1 response, the sections were stained for the T-box transcription factor 21 (TBET) which is key in driving the expression of interferon-gamma (IFN-γ) and in regulation of T_H1 lineage differentiation (Lazarevic et al., 2013). Conversely, to establish if the infiltrating lymphocytes are of a regulatory nature, the sections were stained for the forkhead box P3 transcription factor (FOXP3) which is the master regulator responsible for polarising lymphocytes to assume a regulatory orientation (T_{Reg}) (Lu et al., 2017).

4.6.1. TBET expression

To study the expression of differential expression of TBET, corresponding primary tumour and lung metastasis sections were stained and digitally analysed.

Out of the thirty-four primary tumour stained sections, six were excluded for the following reasons: four slides did not contain sufficient tumour for analysis, two slides had excessive non-specific background staining that prevented digital quantification. This left twenty-eight slides that formed the final analysis cohort.

Out of the thirty-four metastasis sections, two were excluded from the analysis, one for absence of tumour and the other for having too little tumour for meaningful analysis. Therefor thirty-two slides were left for digital analysis.

Accounting for the exclusions in both cohorts, twenty-six pairs were included in the head-to-head final comparison of primary and secondary tumours.

4.6.1.1. TBET-expressing cell densities in stroma and epithelium

In the primary tumour, the densities of TBET-expressing cells were equivalent in the epithelial and stromal compartments. The median density in the epithelial compartment was 27.09 cells/mm^2 and 24.70 cells/mm^2 in the stromal compartment (Wilcoxon signed rank test p=0.9909) [Image 4.5A]. This was not the case at the metastatic site where significantly higher densities were found in the stromal compartment. The median density was 48.26 cells/mm^2 in the epithelium compared to 180.2 cells/mm^2 in the stroma (Wilcoxon signed rank test p=0.0096) [Image 4.5B].

4.6.1.2. Comparison of TBET-expressing cell densities between the primary and secondary site

Upon comparing the differential expression between corresponding compartments in the primary and the secondary sites, significantly higher densities were found in the secondary site. The median TBET-expressing cells density was 21.97 cells/mm^2 in the epithelial compartment of the primary tumour versus 64.46 cells/mm^2 in the epithelium of the metastasis (Wilcoxon signed rank test p=0.029) [Image 4.5C]. In the stroma of the primary tumour the density was 24.70 cells/mm^2 as opposed to 180.21 cells/mm^2 in the stroma of the metastasis (Wilcoxon signed rank test p=0.0008) [Image 4.5D].

TBET Analysis results

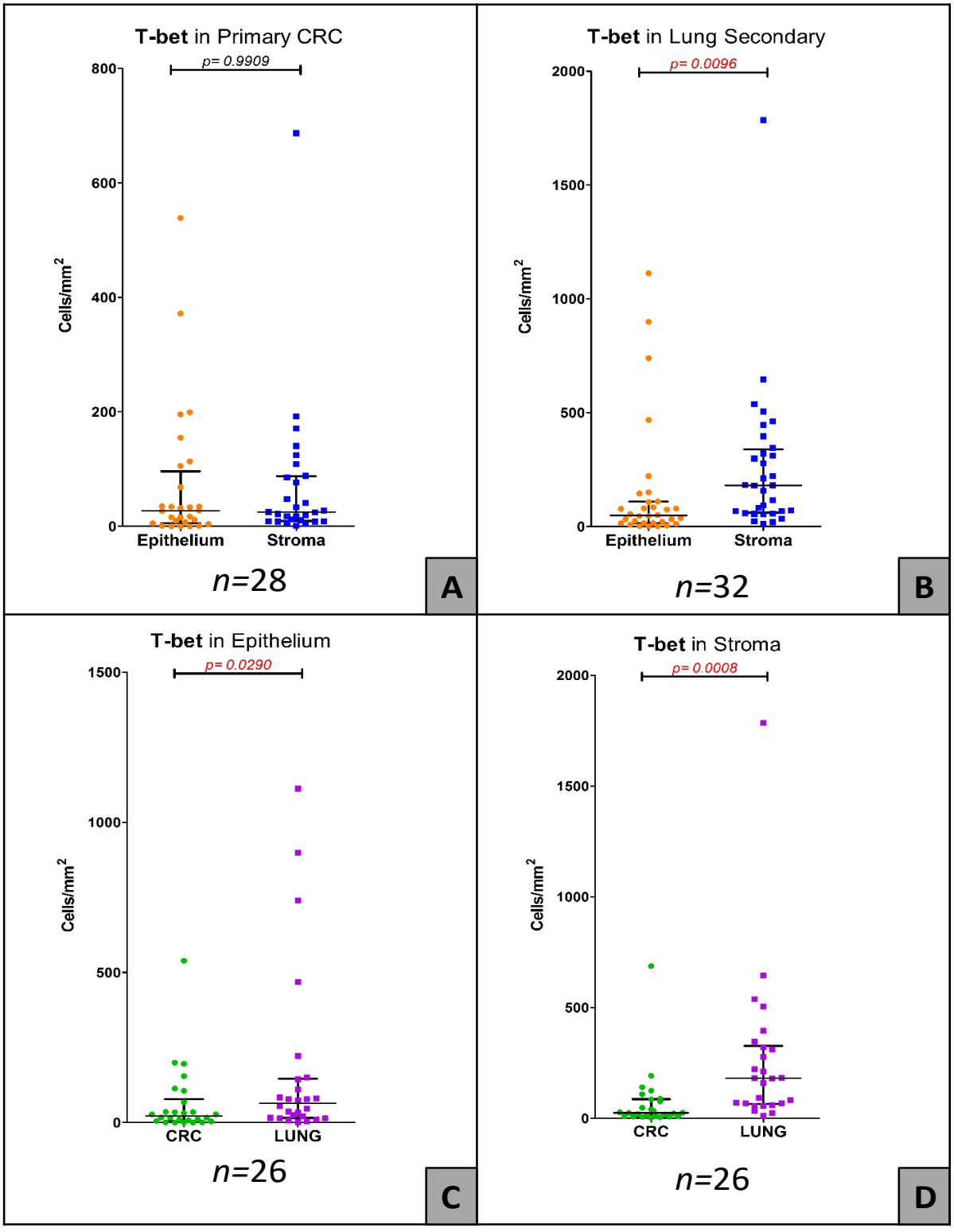

Figure 4.5 TBET expression analysis in primary and secondary colorectal cancer pairs
A. Shows the density of TBET-positive cells in the epithelial and stromal compartments of the primary tumour. **B.** Shows the density of TBET-positive cells in the epithelial and stromal compartments of the lung metastases. **C**. Shows the densities of TBET-positive cells in the epithelial compartment of paired colorectal primary and lung metastasis. **D.** Shows the densities of TBET-positive cells in the stromal compartment of paired colorectal and lung metastasis.

4.6.2. FOXP3 expression

To study the densities of regulatory T-lymphocytes the slides were stained for the expression of nuclear FOXP3 and digitally analysed.

Out of the thirty-four primary tumour slides stained, thirty were analysed to study the expression of FOXP3 in the stromal and epithelial compartments. Three slides were excluded as they did not contain tumour tissue and one slide was excluded due to excessive non-specific staining. Similarly, out of the thirty-four secondary tumour slides stained, thirty-two were included in the analysis as two slides did not contain tumour.

Taking into account the excluded slides in both cohorts, twenty-nine pairs made up the final comparison cohort.

4.6.2.1. FOXP3-expressing cell densities in stroma and epithelium

The density of FOXP3 expressing cells was higher in the stromal compartment of both the primary and lung secondary tumours. This however only reached statistical significance in the secondary site. In the primary tumours, the median density in the epithelium was 52.74 cells/mm^2 as compared to the stroma where the median density was 133.40 cells/mm^2 (Wilcoxon signed rank test p=0.1881) [Image 4.6A]. In the lung metastases, the median density in the epithelium was 56.44 cells/mm^2 versus 216.99 cells/mm^2 in the stroma (Wilcoxon signed rank test p=0.0003) [Image 4.6B].

4.6.2.2. Comparison of FOXP3-expressing cell densities between the primary and secondary site

When the corresponding tumour compartments were compared at the primary and the secondary site, whilst no difference was found in the epithelial compartment a significantly higher density was detected in the stromal compartment. The median

densities of FOXP3-expressing cells in the epithelial compartments were 47.41 cells/mm^2 in the primary tumours and 53.49 cells/mm^2 in the secondary ones (Wilcoxon signed rank test p=0.574) [Image 4.6C]. Whereas the densities in the stromal compartments were 133.7 cells/mm^2 in the primary tumours versus 216.8 cells/mm^2 in the secondary (Wilcoxon signed rank test p=0.0421) [Image 4.6D].

4.6.3. TBET to FOXP3 ratio

Here, I assessed the ratios of TBET expressing cells to FOXP3 expressing cells in both the epithelium and the stroma of the primary tumour and the secondary lung metastasis.

The proportion of TBET to FOXP3 cells in the epithelium narrows from 1:2 the primary site to about 6:7 in the lung metastatic site, this however does not reach statistics significance (χ^2 p=0.09). In the stroma on the other hand, the ratio narrowed considerably in the secondary site, going from a 1:5 ratio in the primary stroma to an 8:9 ratio in the metastatic site stroma (χ^2 p<0.0001) [Image 4.7].

FOXP3 Analysis results

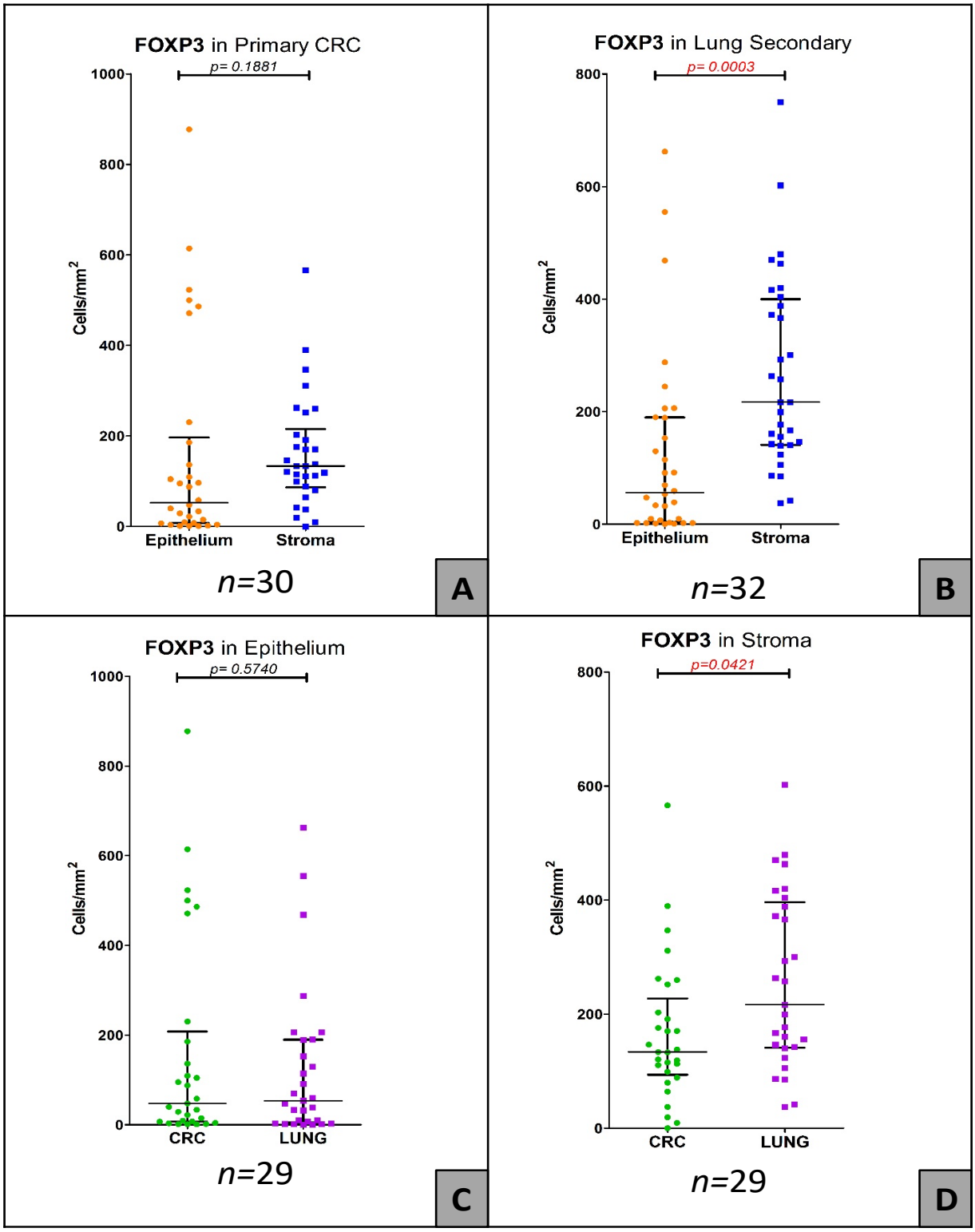

Figure 4.6: FOXP3 expression analysis in primary and secondary colorectal cancer pairs
A. Shows the density of FOXP3-positive cells in the epithelial and stromal compartments of the primary tumour. **B.** Shows the density of FOXP3-positive cells in the epithelial and stromal compartments of the lung metastases. **C.** Shows the densities of FOXP3-positive cells in the epithelial compartment of paired colorectal primary and lung metastasis. **D.** Shows the densities of FOXP3-positive cells in the stromal compartment of paired colorectal and lung metastasis.

TBET:FOXP3 Ratio

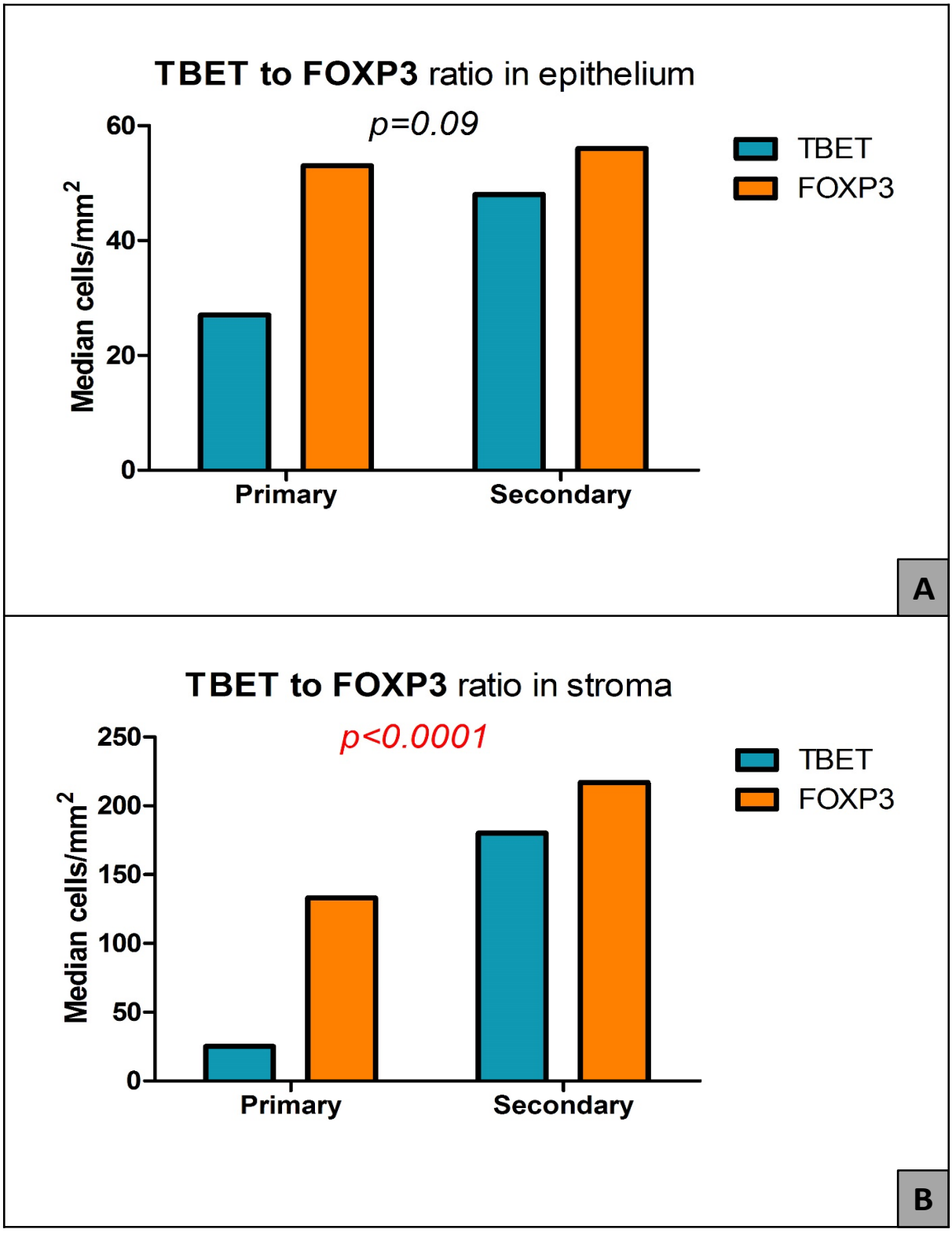

Figure 4.7: TBET to FOXP3 ratio analysis in matched pairs
A. Shows the proportion of TBET to FOXP3 cells in the epithelium of both the primary colorectal and the secondary lung metastatic site. **B.** Shows the proportion of TBET to FOXP3 cells in the stroma of both the primary colorectal and the secondary lung metastatic site.

4.7. Results of comparing the expression of checkpoint blockade molecules in primary colorectal cancer and pulmonary metastases

With the emergence of novel checkpoint blockade therapeutic agents and the demonstration of their effectiveness in controlling advanced disease in various solid tumours, including CRC, it was felt that studying their expression in paired samples would be of both scientific and therapeutic interest. To this end, paired sections were stained for two checkpoint blockade proteins that have been shown to be expressed in CRC and already have therapeutic agents available on the market. The first one was the programmed cell death protein 1 and the second was its ligand PD-L1.

The results for checkpoint blockade molecules expression were presented as percentage of cells positive for the stained protein.

4.7.1. PD-1 expression

To study the expression of PD-1, paired sections were stained for the protein and digitally analysed.

Out of the thirty-four primary section stained, twenty-seven made the final analysis cohort. Four slides were excluded due to lack of tumour on the section, three slides had excessive non-specific staining preventing meaningful analysis. In the lung metastases cohort, twenty-nine sections out of the thirty-four stained were analysed. Two sections were excluded due to lack of tumour on the slide and three were excluded due to non-specific staining.

Taking the exclusions on both sides into account, twenty-five pairs made up the final comparison cohort.

4.7.1.1. PD-1 expression in stroma and epithelium

In both the primary and secondary tumours, the expression of PD-1 was significantly higher in the epithelium than in the stroma. The median density of expression on the primary site was 0.36% of all cells in the epithelium versus 0.19% of all the cells in the stroma (Wilcoxon signed rank test p=0.0192) [Image 4.8A]. Similarly, the median density of PD-1 expression the lung metastases was 0.81% in the epithelium versus 0.45% in the stroma (Wilcoxon signed rank test p=0.0001) [Image 4.8B].

4.7.1.2. Comparison of PD-1 expression between the primary and secondary site

When corresponding tissue compartments were compared, significantly higher densities of PD-1 expressing cells were found in the metastatic site. The density of expression in the epithelial compartment was 0.36% of all cells in the primary as opposed to 0.81% in the secondary (Wilcoxon signed rank test p=0.0123) [Image 4.8C]. The density of expression in the stromal compartment was 0.18% in the primary versus 0.44% in the secondary site (Wilcoxon signed rank test p=0.0166) [Image 4.8D].

PD-1 Analysis results

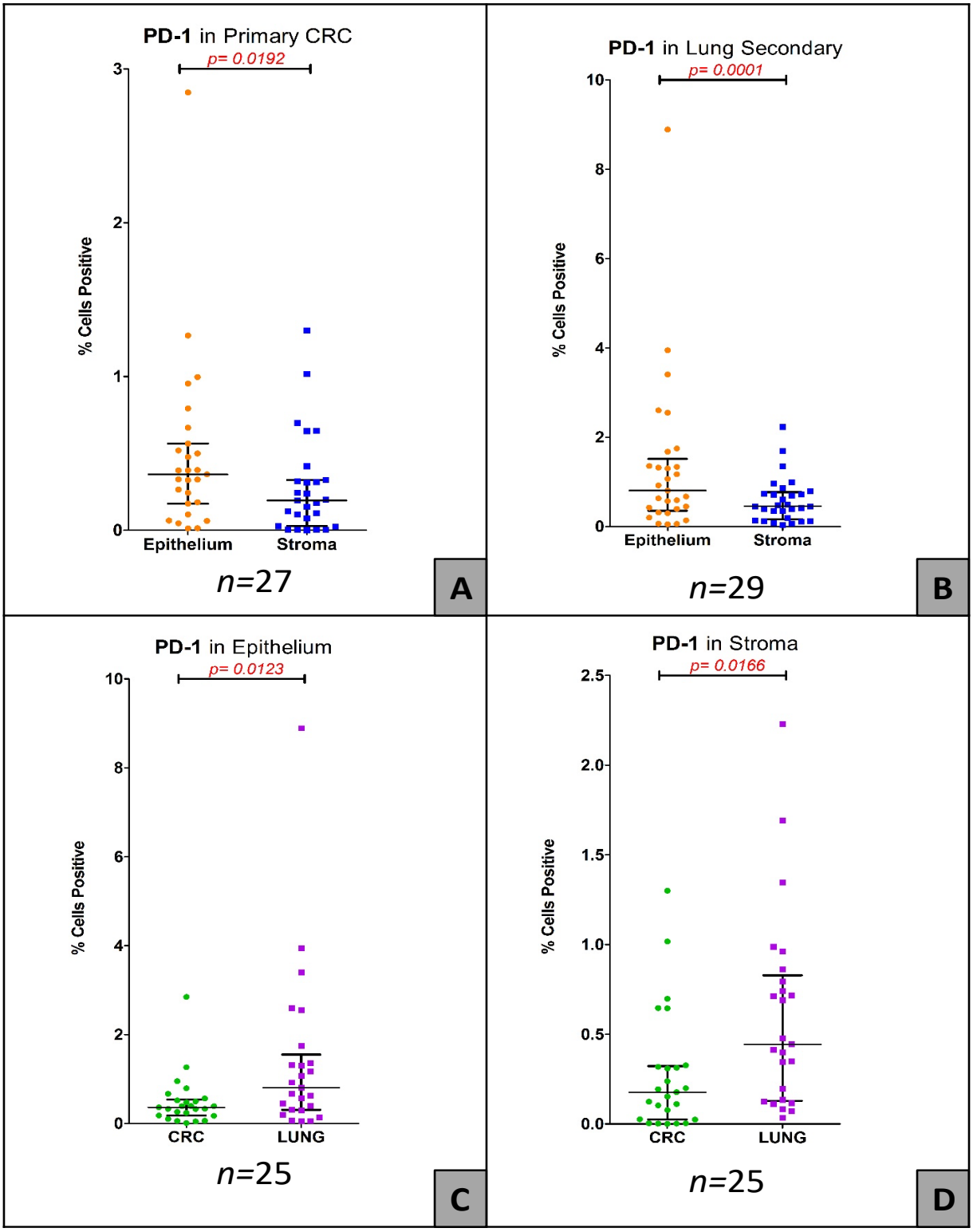

Figure 4.8: PD-1 expression analysis in primary and secondary colorectal cancer pairs
A. Shows the density of PD-1 -positive cells in the epithelial and stromal compartments of the primary tumour. B. Shows the density of PD-1 -positive cells in the epithelial and stromal compartments of the lung metastases. C. Shows the densities of PD-1 -positive cells in the epithelial compartment of paired colorectal primary and lung metastasis. D. Shows the densities of PD-1 -positive cells in the stromal compartment of paired colorectal and lung metastasis.

4.7.2. PD-L1 expression

The analysis if PD-L1 expression was performed in a manner analogous to that of PD-1.

Out of the 34 primary sections stained, twenty-six made the final primary tumour analysis cohort. Four slides have no tumour and one slide had very little tumour to allow analysis. Further two slides contained excessive non-specific staining and the tissue on two slides was fragmented in the staining process. Out of the thirty-four secondary sections stained, thirty-two were analysed. Two slides were excluded because they did not contain tumour.

Allowing for exclusions on both sides, twenty-five slides made the final paired primary-secondary comparison cohort.

4.7.2.1. PD-L1 expression in stroma and epithelium

Reflecting a reverse pattern of expression to the PD-1 molecule, PD-L1 expression was found to be significantly higher in the stromal compartment of both the primary colorectal tumour and the secondary lung metastasis. In the epithelial compartment of the primary tumour the median percentage of positive cells was 0.32% as opposed to the stroma where the median percentage of positive cells was 1.62% (Wilcoxon signed rank test p=0.0003) [Image 4.9A]. In lung metastases, the percentage of positive cells in the epithelium was 2.6% versus 6.1% in the stroma (Wilcoxon signed rank test p=0.003) [Image 4.9B].

4.7.2.2. Comparison of PD-L1 expression between the primary and secondary site

The differential expression of PD-L1 followed a similar trend to that of PD-1 with significantly higher expression in the secondary site in both compartments, the epithelium and the stroma.

In the epithelium, the median percentage of positive cells was 0.31% in the primary colorectal tumour as opposed to 1.38% in the lung metastasis (Wilcoxon signed rank test p=0.0255) [Image 4.9C]. In the stroma, the median percentage of positive cells was 1.45% in the primary colorectal tumour versus 5.31% in the lung metastasis (Wilcoxon signed rank test p=0.0047) [Image 4.9D].

PD-L1 Analysis results

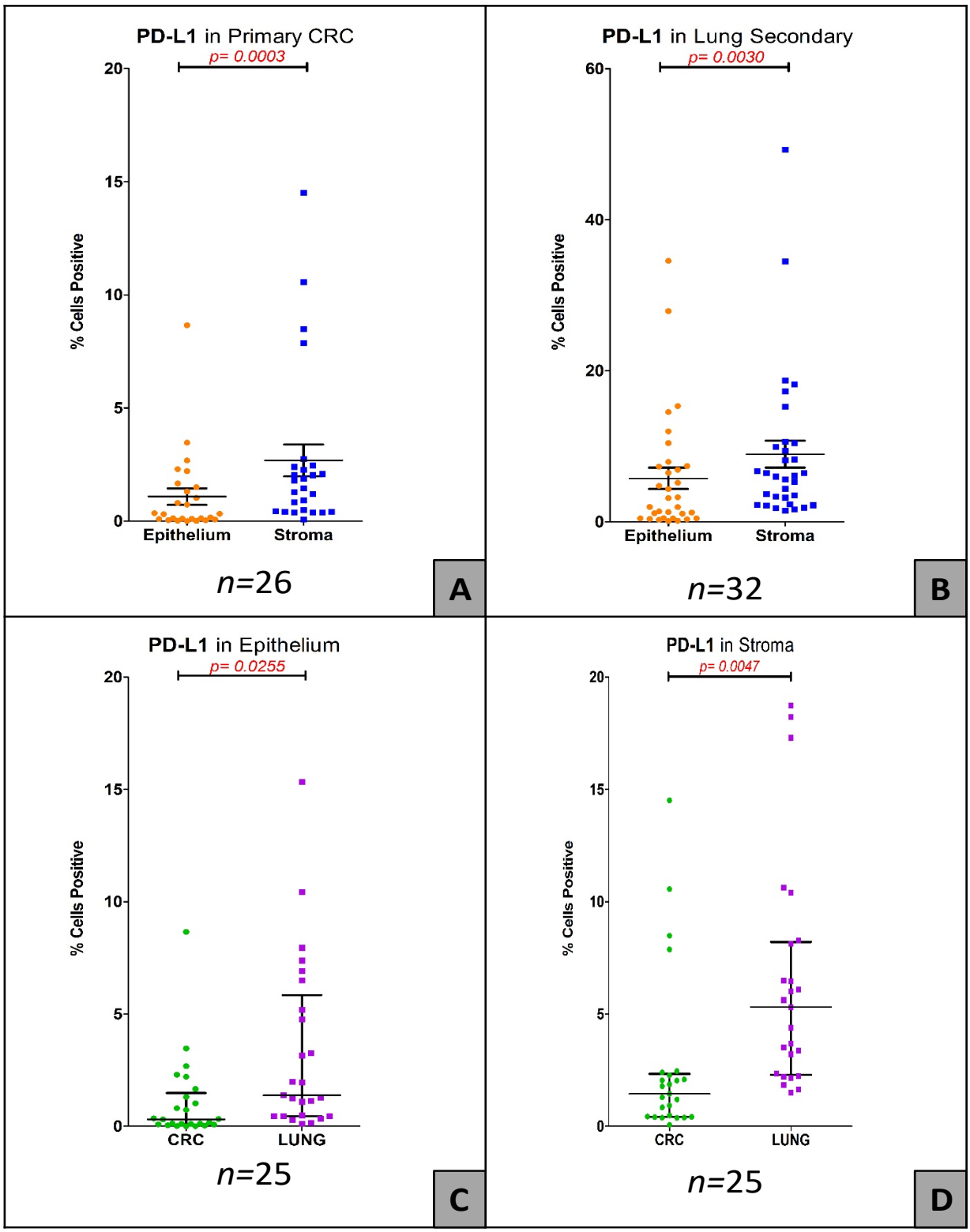

Figure 4.9: PD-L1 expression analysis in primary and secondary colorectal cancer pairs
A. Shows the density of PD-L1 -positive cells in the epithelial and stromal compartments of the primary tumour. **B.** Shows the density of PD-L1 -positive cells in the epithelial and stromal compartments of the lung metastases. **C.** Shows the densities of PD-L1 -positive cells in the epithelial compartment of paired colorectal primary and lung metastasis. **D.** Shows the densities of PD-L1 -positive cells in the stromal compartment of paired colorectal and lung metastasis.

4.8. Results of comparing the expression of Major Histocompatibility Complexes (MHC) in primary colorectal cancer and pulmonary metastases

Major Histocompatibility Complexes (MHC), also known as Human Leukocyte Antigens (HLA) are key players in the immune micro-environment of tumours. It has been shown that downregulation or loss of MHC class I proteins expression is a *bona fida* mechanism of immune evasion and might even have impact on the prognosis of CRC (Watson et al 2006, Zeestraten et al 2014). Similarly, MHC class II molecules expression is vital in mediating anti-tumoural immunity and were found to be central in the coordinated immune response cluster (CIRC) (Lal et al, 2015).

4.8.1. Expression of MHC Class I

The differential expression of classical MHC Class I proteins (HLA-A, B and C) was studied by staining the primary and secondary with a universal anti-HLA-ABC antibody and digitally analysing the sections as previous described.

Out of the thirty-four primary colorectal sections stained, thirty-two were analysed. Two sections were excluded as they did not contain a tumour. Out of the thirty-four lung metastasis sections stained, thirty-two were analysed. Two slides were excluded due to absence of tumour.

Twenty-nine pairs of sections formed the final comparison cohort after exclusions from both sides.

4.8.1.1. MHC Class I expression in stroma and epithelium

In both the primary colorectal site and the lung metastasis, the percentage of MHC Class I positive cells was higher in the epithelial compartment. In the primary site, the medial percentage of MHC Class I positive cells was 93.06% in the epithelium when compared to 60.55% in the stroma (Wilcoxon signed rank test $p<0.0001$) [Image 4.10A]. Similarly, in the secondary site, the median percentage of MHC Class I positive cells was 96.56% in the epithelium versus 84.49% in the stroma (Wilcoxon signed rank test $p=<0.0001$) [Image 4.10B].

4.8.1.2. Comparison of MHC Class I expression between the primary and secondary site

The proportion on MHC Class I expressing cells was significantly lower in the primary colorectal tumour site than the lung secondary in both the epithelial and stromal compartments. In the epithelial compartment, the median percentage of MHC Class I expressing cells was 90.99% in the primary and 96.60% in the secondary (Wilcoxon signed rank test $p=0.0046$) [Image 4.10C]. In the stromal compartment, the median percentage of MHC Class I expressing cells was 59.91% in the primary versus 84.48 in the secondary (Wilcoxon signed rank test $p=0.0002$) [Image 4.10D].

MHC Class I Analysis results

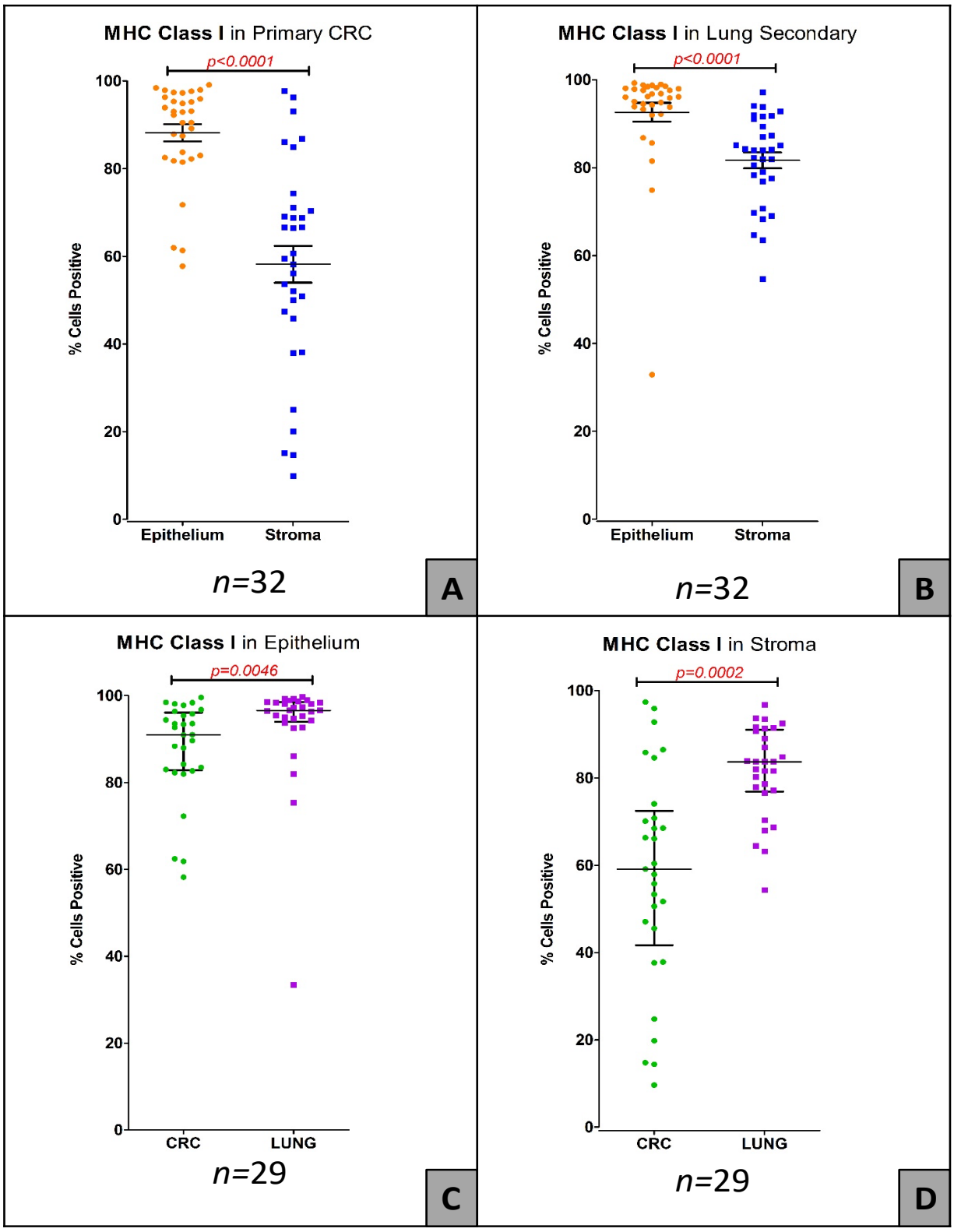

Figure 4.10: MHC Class 1 expression analysis in primary and secondary colorectal cancer pairs
A. Shows the density of MHC-1 -positive cells in the epithelial and stromal compartments of the primary tumour. **B.** Shows the density of MHC-1 -positive cells in the epithelial and stromal compartments of the lung metastases. **C.** Shows the densities of MHC-1 -positive cells in the epithelial compartment of paired colorectal primary and lung metastasis. **D.** Shows the densities of MHC-1 -positive cells in the stromal compartment of paired colorectal and lung metastasis.

4.8.2. Expression of MHC Class II

The differential expression of MHC Class II proteins was studied by staining the paired sections and digitally analysing the captured images.

Out of the thirty-four primary colorectal sections stained, thirty-one were analysed. Three sections were excluded due to absence of tumour. Out of the thirty-four lung metastases sections stained, thirty-two were analysed. Two sections did not contain tumour.

With the exclusions on both sides taken into consideration, twenty-nine pairs of sections formed the final comparison cohort.

4.8.2.1. MHC Class II expression in stroma and epithelium

The expression of MHC Class II proteins was found to be significantly higher in the stromal compartment in both the primary CRC and the lung metastasis. In the primary tumour, the median percentage of MHC Class II positive cells was 0.13% in the epithelium and 18.98% in the stroma (Wilcoxon signed rank test $p<0.0001$) [Image 4.11A]. Similarly, in the lung metastasis, the median percentage of MHC Class II positive cells was 0.17% in the epithelium versus 36.92% in the stroma (Wilcoxon signed rank test $p=0.0002$) [Image 4.11B].

4.8.2.2. Comparison of MHC Class II expression between the primary and secondary site

When paired specimens were compared, it was observed that the concentration of MHC Class II positive cells was higher in the secondary site in both compartments although it only reached statistical significance when stromal compartments were compared. In the epithelial compartment the median percentage of MHC Class II

positive cells was 0.13% in the primary colorectal tumour and 0.15% in the lung metastasis (Wilcoxon signed rank test p=0.2993) [Image 4.11C]. In the stromal compartment, the median percentage of MHC Class II positive cells was 18.98% in the primary colorectal tumour and 38.62% in the lung metastasis (Wilcoxon signed rank test p=0.0001) [Image 4.11D].

MHC Class II Analysis results

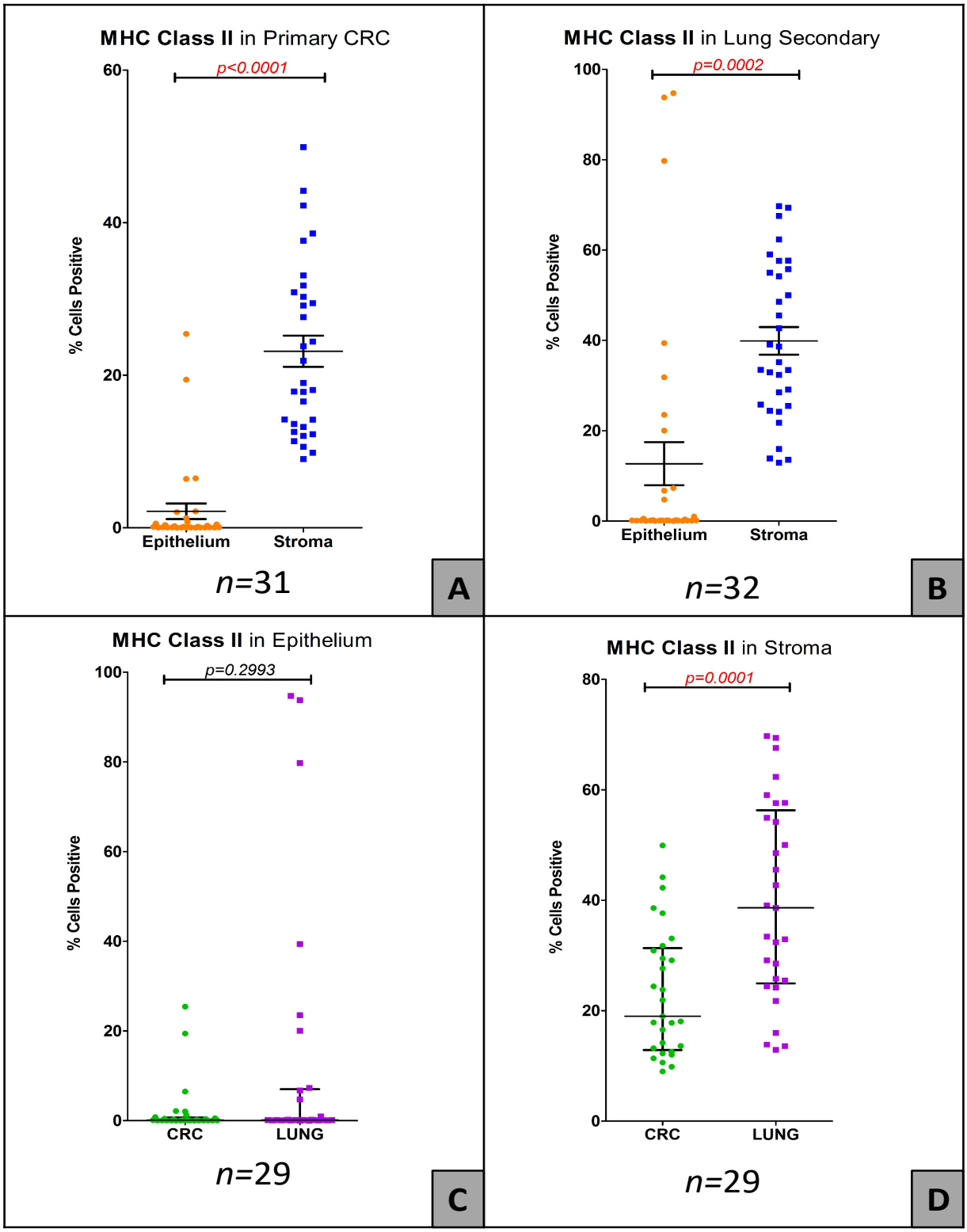

Figure 4.11: MHC Class 2 expression analysis in primary and secondary colorectal cancer pairs
A. Shows the density of MHC-2 -positive cells in the epithelial and stromal compartments of the primary tumour. **B.** Shows the density of MHC-2 -positive cells in the epithelial and stromal compartments of the lung metastases. **C.** Shows the densities of MHC-2-positive cells in the epithelial compartment of paired colorectal primary and lung metastasis. **D.** Shows the densities of MHC-2 -positive cells in the stromal compartment of paired colorectal and lung metastasis.

4.9. Chapter summary and discussion

This study clearly demonstrated that the immune microenvironment of colorectal lung metastases is significantly more inflamed with an obvious T_H1 bias. This immune response however seems to be suppressed by over expression of checkpoint molecules.

In this chapter, I examined the immune microenvironment in paired samples of primary CRC and lung metastases using immunohistochemical staining for specific immune subsets and molecules. The idea behind using paired samples from the same patient, as opposed to unmatched samples, was to minimise the effect of differences in the host's general biology, genetic composition and environmental influences. This approach, at least theoretically, would mean that any differences are more likely to be a result of the particular anatomical site milieu, microenvironment, and changes upon transition to the metastatic phase. As discussed in the introduction, lung metastases were selected (rather than liver metastases) to avoid the immune suppressive T_H2-skewed liver microenvironment and due to the paucity of literature on colorectal lung metastases.

I approached the subject from five directions. Firstly, I assessed the geography of tumour infiltrating lymphocytes (TILs) and determined their location within the tumour stroma and the tumour epithelium. Secondly, I compared the density of TILs in the paired samples and determined the proportion of CD4 and CD8 lymphocytes in primary tumour and the lung metastasis. Thirdly, I examined the functional orientation of those TILs, namely T_H1 and T_{REG}-related transcription factor expression. Fourthly, I assessed the expression of two quintessential checkpoint blockade targets: PD-1 and PD-L1.

Finally, I probed the differential expression of major histocompatibility complexes (MHC) I and II. To the best of my knowledge this is the first study of its kind to approach this topic in paired samples.

To achieve the aims of this study, I utilised a sophisticated digital pathology platform (Definiens™ Tissue studio) to carry out entire-tumour area analysis, involving scoring on whole-slide digitally scanned images (WSI). I then manually devised scoring algorithms for each individual marker to enable the software to accurately score the marker of interest. Using the whole-tumour area rather than microscope-selected high-power fields, allows for deeper analysis of the marker and its differential expression within tissue compartments, resulted in an accurate quantification of the immune subset densities and aided in standardising the data output across the samples (Madabhushi and Lee, 2016). Analysing the entire tumour area also eliminates potential observer bias when selecting 'regions of interest' for examination.

In terms of the geography of TIL distribution, T-lymphocytes in general ($CD3^+$) as well as both main conventional T cell subsets ($CD4^+$ and $CD8^+$) were localised predominantly in the stromal compartment of the tumour. Upon matched-pair comparison, the densities of TILs were found to be higher in the secondary tumour, and this was especially significant in the stromal compartment. Those results are consistent with observations from two recent trials where the investigators found higher density of lymphocytes in the invasive margin of tumours than the core of the tumour (Van den Eynde et al., 2018, Mlecnik et al., 2018). My findings are also consistent with the findings of Van den Eynde *et al.* who found higher immune cell infiltrates in the metastatic sites than the primary tumour. Their cohort however had predominantly liver metastases (96.6%) (Van den Eynde et al., 2018).

Interestingly, whilst the proportion of $CD4^+$ to $CD8^+$ lymphocytes was constant in the stroma of primary and secondary tumours with a $CD4^+$ predominance, this ratio was reversed in the epithelium with $CD8^+$ cells being the predominant subset. This shift was most pronounced in the epithelium of lung metastases. The predominance of $CD8^+$ lymphocytes in the epithelium and $CD4^+$ lymphocytes in the stroma is consistent with previously reported results by Banner and colleagues (Banner et al., 1993). Based on this interesting finding, I speculate that $CD4^+$ T cells preferentially exert regulatory functions in the stroma of the tumour whilst $CD8^+$ lymphocytes preferentially migrate into the tumour epithelium to deliver their cytotoxic functions.

Upon studying the functional orientation of the TILs, it was noted that the expression of both TBET and FOXP3 transcription factors was higher in the stroma than the epithelium of both the primary and the metastatic tumours. This is concordant with the fact that lymphocytes are more abundant in the stroma, especially $CD4^+$ lymphocytes. Similarly, when the expression of transcription factors was compared in matching pairs, the expression of both TBET and FOXP3 was higher in the secondary tumour than the primary tumour. The difference in expression was significant in both the stroma and the epithelium in the case of TBET and only reached significance in the stromal compartment for FOXP3. What is also interesting, is the fact that whilst the proportion of $TBET^+$ to $FOXP3^+$ cells remained stable in the epithelial compartment of both the primary and the metastatic tumours, this ratio narrows significantly in the stroma of the secondary with a significantly bigger increase number of $TBET^+$ cells in the stroma. Those results are intriguing as they suggest a more T_H1-focused stromal response in the metastatic site when compared to the relatively immune suppressed primary site. The significantly higher TBET expression in the epithelium of the metastatic tumour

can be explained by the fact that TBET is likely to be expressed by the more prevalent CD8 cells in the epithelium adding evidence pointing to a strong IFN-γ induced T_C1 effector response in the lung metastatic site.

The notion of a heightened type 1 immune response in the secondary tumour is further strengthened by the finding that both MHC class I and II are significantly increased in expression in the metastatic deposits when compared to the primary tumours. This is likely due to IFN-γ induced stimulation of MHC expression pathways, potentially enhancing antigen presentation (Boehm et al., 1997, Steimle et al., 1994, Zhou, 2009). This finding also builds on the work of Lal et al. who demonstrated that MHC class II expression is central to a T_H1 response in what has been termed the 'coordinated immune response cluster' (CIRC) signature (Lal et al., 2015).

Examination of the expression of PD-1 and its ligand, PD-L1 determined that both molecules are over-expressed in the metastatic tumour in both the stroma and the epithelium. This finding is also consistent with a heightened T_H1 response in the metastatic tumour as both molecules are part of the T_H1-focussed CIRC signature (Lal et al., 2015). Interestingly however, the compartmental distribution of the two molecules was inverse, with PD-L1 abundant in the stroma and PD-1 predominant in the epithelium. This could be explained by the expression of PD-1 on CD8+ cells that are present in higher numbers in the epithelium. It is also plausible that the overexpression of PD-L1 in the stroma leads to apoptosis of PD-1 positive TILs in the stroma resulting in a lower density.

Collectively, these findings strongly point to a more T-cell-rich microenvironment in the stroma of tumours, combined with cytotoxic T cells being more prone to migrate into

the tumour epithelium. It is also apparent that the immune milieu of the lung metastases is more inflamed with a prominence of a type-1 response. This inflamed microenvironment however is supressed by over-expression of checkpoint molecules.

One of the unique strengths of this study lie in the fact that matched samples were used. To the best of the authors knowledge, this is the first study exploring the differences in the immune microenvironment between the primary cancer and lung metastases. The other strength of this study is the use of digital pathology to analyse a whole slide rather than individual high-power fields. This improves the reliability of the results and reduces observed bias. The use of robustly validated antibodies to stain individual markers and employing quality-assured, custom-built algorithms used to score to score them reflect the robustness of the methodology used and lend credibility to the results.

The main weakness of this study is the inability to link the immunological results to actual patient outcomes. This was not possible due to fact that patient information was limited, and long-term outcomes were not available. Due to the limited number of sections, careful consideration was given to which markers to stain for as a priority. Considering this limitation, the markers used in this study were chosen to glean maximal information about the nature of the microenvironment.

Future avenues to explore would be to assess the genomic and transcriptomic differences between the primary and secondary sites to ascertain the differences at tumour level. It would also be interesting to explore the differences in the MMR status between the sites and whether the tumours change CMS grouping when they metastasise. Another interesting avenue to explore is to look at the differences in the

immune microenvironment in metastases at different sites such as the liver. The data from this study is being utilised to explore this aspect. I am working collaboratively with a colleague who is looking at matched liver metastases and a manuscript is currently being prepared for publication.

5. Chapter Five: Exploring the Immune Microenvironment in Mismatch Repair Deficient and Proficient Colorectal Cancer with High and Low Coordinated Immune Response Cluster (CIRC)

5.1. Introduction

It is well established that CRCs that develop through the defective DNA mismatch repair (dMMR) pathway (either through inherited germline mutations or through sporadically acquired somatic mutations) are histologically characterised by dense lymphocyte infiltrates when compared with cancers arising through the canonical pathway with proficient DNA mismatch repair (pMMR) mechanisms. This subset of cancers is also known to have a better stage-adjusted prognosis (Stages I-III). More importantly, information about the status of mismatch repair proficiency forms an important pillar in the decision-making process about adjuvant treatment. This is due to the fact that dMMR tumours tend to be less responsive to 5-fluorouracil (5-FU) chemotherapy and therefore adjuvant therapy is not recommended in stage II cancers (Sinicrope, 2010, Kawakami et al., 2015). More recently, there has been evidence that this subset of tumours is more responsive to checkpoint blockade therapy opening new therapeutic avenues (Le et al., 2017, Overman et al., 2017, Le et al., 2015, Le et al., 2020). There is also evidence of the benefit of anti-inflammatory agents such as Aspirin and Ibuprofen as chemoprotective agents (Burn et al., 2011, Movahedi et al., 2015, Ait Ouakrim et al., 2015, Boland et al., 2018).

It is known that some colorectal tumours with proficient mismatch repair mechanisms exhibit high lymphocyte infiltrates (TILs) analogous to those with deficient repair mechanisms (Lal et al., 2015). Our group showed that those tumours demonstrate an over expression of a cluster of immune genes called coordinated immune response cluster (hi-CIRC). Central to this cluster is the expression of the major histocompatibility molecule type II (MHC Class II) (Lal et al., 2015).

It is of interest to find out whether those pMMR tumours with a high CIRC have similar immune microenvironments to tumours with dMMR. This could have implications on how those tumours might behave and subsequently on their susceptibility to adjuvant chemotherapy.

5.2. Chapter hypothesis

The hypothesis for this chapter is that there is a group of MSS CRC that evoke a strong immune response equivalent to that of a *bona fide* MSI-hi tumours. Those tumours can be defined by a high expression of MHC Class II as a surrogate for the CIRC.

5.3. Chapter aims

Compare the immune microenvironment in three distinct cohorts of CRC: dMMR, pMMR and pMMR hi-CIRC.

5.3. Results

5.3.1. General observations of stained section

On general review of the stained sections, it was apparent that the proportion of immune cells was visibly higher in the dMMR cohort. This was arranged in clusters of MHC Class II positive cells surrounded by mainly $CD4^+$ and some $CD8^+$ lymphocytes.

The general appearance of the pMMR hi-CIRC cohort resembles that of the dMMR cohort with high densities all immune subtypes. Interestingly, the distribution of those subsets appears less organised than that the dMMR cohort and with a greater intra-tumoural variability. The appearances of the pMMR cohort were dramatically different with much sparser immune cell infiltrates throughout the cohort [Image 5.1].

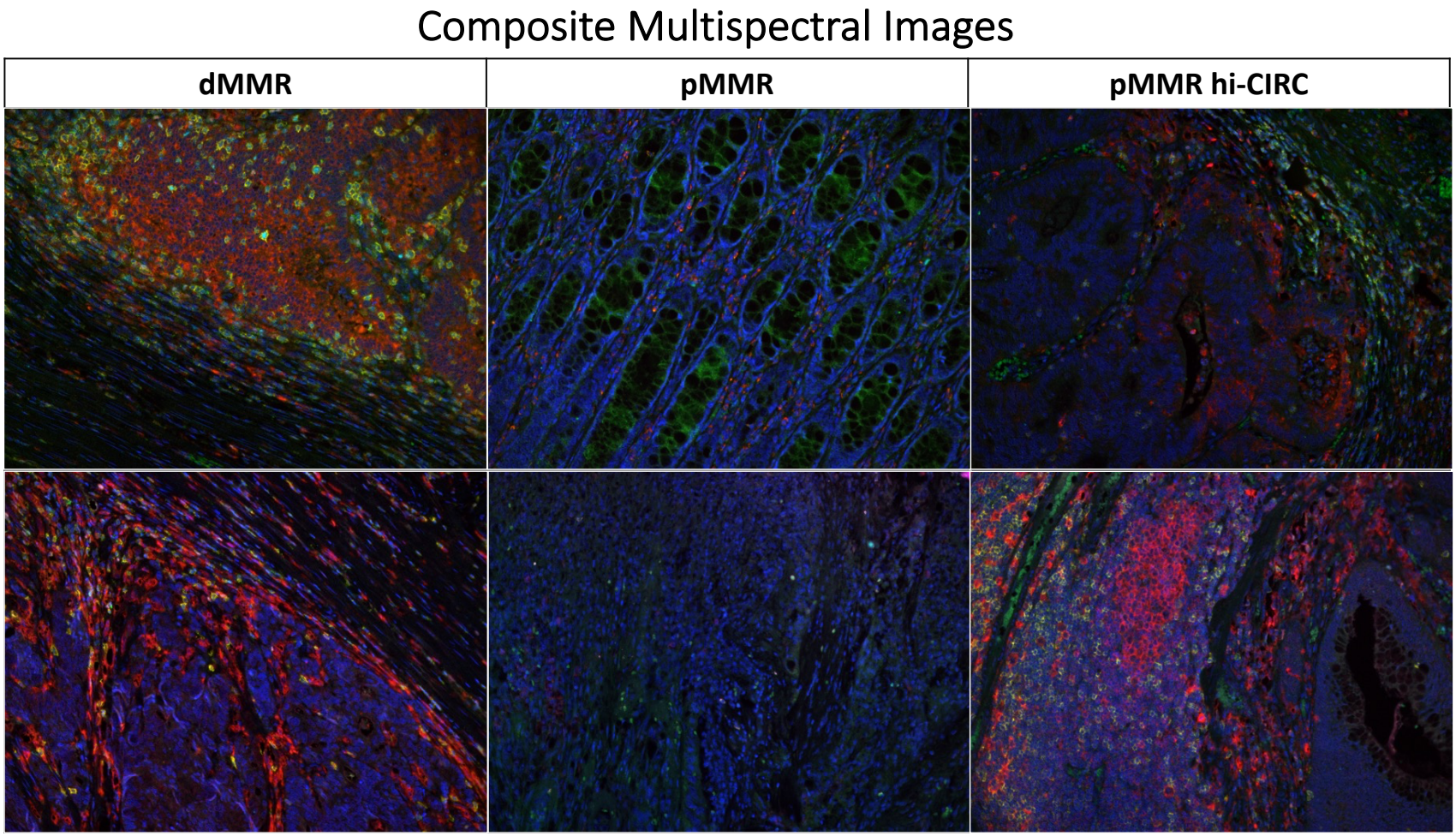

Figure 5.1 Captured high power field (400x) multispectral images of the three cohorts examined in this section. On the right, two dMMR tumour high power fields. In the middle, two pMMR tumour high power fields. On the right, two pMMR hi-CIRC tumour high power fields. The colours represent different markers as described in Table 4.1: Green: $CD4^+$, Yellow: $CD8^+$, Orange: FOXP3, Cyan: T-bet, Magenta: RORyt, Red: MHC Class II and Blue: Nuclei.

5.3.2. $CD4^+$ Representation analysis

5.3.2.1. $CD4^+$ in tumour stroma

The median proportion of $CD4^+$ lymphocytes in the stroma was highest in the dMMR cohort; 8.99% of all the cells in the stroma (IQR: 4.38% - 12.15%). This was followed by pMMR hi-CIRC with a median proportion of 6.24% of all the cells in the stroma (IQR: 4.28% - 9.07%). The lowest share was observed in the pMMR cohort where the density of $CD4^+$ lymphocytes was 2.97% of all the cells in the stroma (IQR: 1.54% - 6.16 %).

On statistical comparison, it was found that the there was a significant difference in density between pMMR and both dMMR and pMMR-hi-CIRC cohort (Mann-Whitney *U* $p = 0.0115$ and $p = 0.0355$ respectively). There was no statistically significant difference in the density of $CD4^+$ lymphocytes between the pMMR hi-CIRC and dMMR cohorts (Mann-Whitney *U* $p = 0.403$) [Figure 5.2A].

5.3.2.2. $CD4^+$ in tumour epithelium

The $CD4^+$ lymphocyte proportions in the epithelium of the tumours in the three cohorts were similar to that in the stroma. The highest median percentage was observed in the dMMR cohort at 1.51% of all the cells in the epithelium (IQR: 0.34% - 1.78%) followed by the pMMR hi-CIRC cohort with a median $CD4^+$ lymphocyte share of 0.82% of all the cells in the epithelium (IQR: 0.28% - 5.22%). The lowest density was observed in the pMMR cohort with a median proportion of 0.17% of all the cells in the epithelium (IQR: 0.09% - 0.54%).

Statistical analysis demonstrated a statistically significant difference in the density of $CD4^+$ lymphocytes in the epithelium of pMMR and both dMMR and pMMR hi-CIRC tumours (Mann-Whitney *U* $p = 0.027$ and $p = 0.02$ respectively). There was no

difference demonstrated between the density of $CD4^+$ lymphocytes between the dMMR and the pMMR hi-CIRC cohorts (Mann-Whitney *U p*= 1) [Figure 5.2B].

5.3.3. T_H1 Lymphocytes

5.3.3.1. T_H1 in tumour stoma

The median percentage of T_H1 lymphocytes was again highest in the stroma of dMMR cohort of tumours with a 0.6% of all the cells in the stroma (IQR: 0.25% - 1.66%) followed by pMMR hi-CIRC with a median share of 0.48% of all the cells in the stroma (IQR: 0.15% - 1.49%). The lowest proportion was that of the pMMR cohort with a median of 0.23% of all the cells in the stroma being positive for both CD4 and T-Bet (IQR: 0.16% - 0.51%).

Although there was a statistically significant difference in the density of T_H1 cells between pMMR and dMMR cohorts the difference did not reach statistical significance between pMMR and pMMR hi-CIRC (Mann-Whitney *U p*= 0.041 and *p*= 0.21 respectively). There was also no statistically significant difference between dMMR and pMMR hi-CIRC cohorts (Mann-Whitney *U p*= 0.52) [Figure 5.3A].

5.3.3.2. T_H1 in tumour epithelium

Analogously to the stroma, the proportions of T_H1 cells were highest in the epithelium of the dMMR cohort with a median of 0.21% of all the cells in the epithelium (IQR: 0.04% - 0.32%). This was followed by the pMMR hi-CIRC cohort with a median of 0.1% T_H1 cells of all the cells in the epithelium (IQR: 0.02% - 0.44%). The lowest was in the pMMR cohort where T_H1 representation was 0.025% of all the cells in the epithelium (IQR: 0% - 0.09%).

The density of T_H1 cells was significantly higher in the epithelium of the dMMR cohort than that of the pMMR cohort (unpaired t-test *p*= 0.015). Statistical significance was not reached when comparing the difference between pMMR and pMMR hi-CIRC (Mann-Whitney *U p*= 0.137) or when comparing pMMR hi-CIRC and dMMR cohorts (Mann-Whitney *U p*= 0.68) [Figure 5.3B].

5.3.4. Regulatory T-lymphocytes

5.3.4.1. T_{REG} in tumour stroma

The median fraction of T_{REG} cells in the stroma of the three cohorts was very similar. The highest being in the pMMR cohort at 0.35% of all the cells in the stroma (IQR: 0.05% - 1.42%). Followed closely by pMMR hi-CIRC with a median proportion of 0.33% of all the cells in the stroma (IQR: 0.06% - 0.83%). The dMMR cohort had the smallest proportion of T_{REG} lymphocytes with 0.31% of all the cells in the stroma (IQR: 0.05% - 1.45%).

There were no statistically significant differences between the three cohorts in terms of T_{REG} densities in the stroma: pMMR vs dMMR (Mann-Whitney *U p*=1), pMMR vs pMMR hi-CIRC (unpaired t-test *p*= 0.61) and dMMR vs pMMR hi-CIRC (Mann-Whitney *U p*= 0.87) [Figure 5.3C].

5.3.4.2. T_{REG} in tumour epithelium

The proportion of T_{REG} cells in the epithelium all three cohorts was very small with a higher median density in the pMMR hi-CIRC cohort of 0.07% of all the cells in the stroma (IQR: 0% - 0.31%). Followed by both dMMR and pMMR with a median proportion of T_{REG} cells of 0.025% of all the cells in the epithelium (IQR: 0.008% - 0.17% and 0.008 - 0.053% respectively).

Similar to the narrative in the stroma, there were no statistically significant differences between any of the three cohorts: pMMR vs. dMMR (Mann-Whitney *U p*= 0.59), pMMR hi-CIRC vs. pMMR (Mann-Whitney *U p*= 0.42) and pMMR hi-CIRC vs. dMMR (Mann-Whitney *U p*= 0.78) [Figure 5.3D].

5.3.5. T_H17

5.3.5.1. T_H17 in tumour stroma

The median proportion of T_H17 cells in the stroma of tumours was highest in the dMMR cohort where those cells formed 0.3% of all the cells in the stroma (IQR: 0.05% - 0.54%). Followed by pMMR hi-CIRC tumours where the proportion was 0.19% of all the cells in the stroma (IQR: 0.1% - 0.49%). Followed by the pMMR cohort with 0.13% of all the cells in the stroma being CD4 and RORγt positive (IQR: 0% - 0.53%).

There were no statistically significant differences in the proportion of T_H17 cells in the stroma between any two of the three cohorts: pMMR vs. dMMR (Mann-Whitney *U p*= 0.34), pMMR hi-CIRC vs. pMMR (Mann-Whitney *U p*= 0.43) and pMMR hi-CIRC vs. dMMR (Mann-Whitney *U p*= 0.97) [Figure 5.3E].

5.3.5.2. T_H17 in tumour epithelium

The proportion of T_H17 cells in the epithelium was the lowest across all cohorts with many high-power fields having virtually none. The cohort with the highest proportion was pMMR hi-CIRC with only 0.03% of all the cells in the epithelium being positive for CD4 and RORγt (IQR: 0% - 0.24%). This was followed by the pMMR cohort in which 0.015% of all the cells in the epithelium were positive (IQR: 0.0075% - 0.085%). The lowest cohort was the dMMR with only 0.005% of all the cells in the epithelium being T_H17 (IQR: 0% - 0.03%).

Probably owing to the very small number of T_H17 cells there were no statistically significant differences between any two of the three cohorts: pMMR vs. dMMR (Mann-Whitney *U* p= 0.17), pMMR hi-CIRC vs. pMMR (Mann-Whitney *U* p= 0.67) and pMMR hi-CIRC vs. dMMR (Mann-Whitney *U* p= 0.10) [Figure 5.3F].

CD4 Analysis

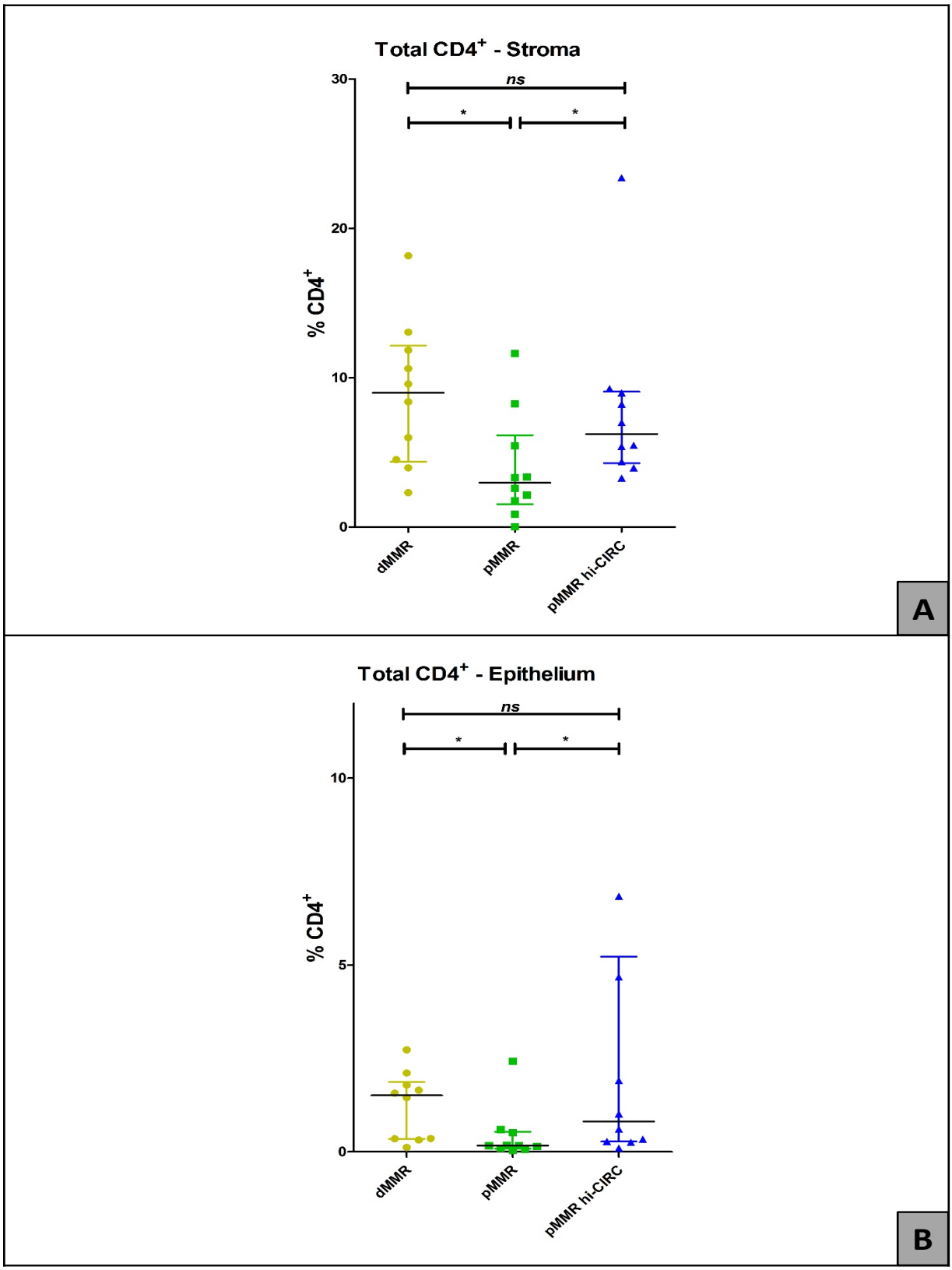

Figure 5.2. Graphic representation of the proportion of $CD4^+$ cells in the three different cohorts; in the stroma (A) and the epithelium (B). The bars represent medians and interquartile ranges (IQR). The asterisk (*) denotes a *p*-value of <0.05 and the double asterisk (**) denotes a *p*-value of <0.01. *ns*= not statistically significant (*p*-value ≥0.05).

CD4 subtype Analysis

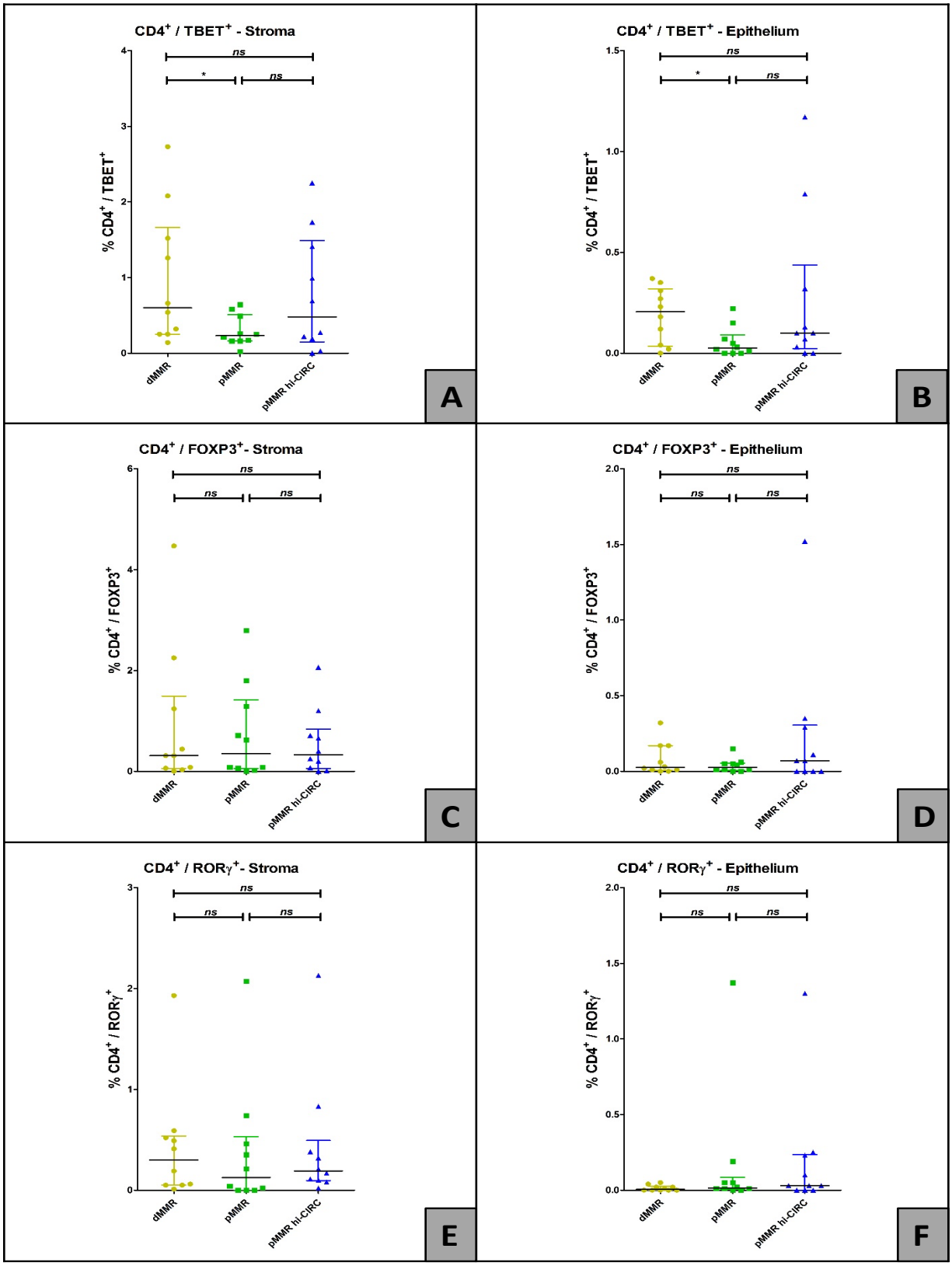

Figure 5.3. Graphic representation of the proportions of the different CD4 lymphocyte subtypes in both the stroma and the epithelium. T_H1 (A & B), T_{REG} (C & D) and T_H17 (E & F). The bars represent medians and interquartile ranges (IQR). The asterisk (*) denotes a *p*-value of <0.05 and the double asterisk (**) denotes a *p*-value of <0.01. *ns*= not statistically significant (*p*-value ≥0.05).

5.3.6. $CD8^+$ representation analysis

5.3.6.1. $CD8^+$ lymphocytes in the stroma

The proportion of cytotoxic $CD8^+$ T-lymphocytes was highest in the dMMR tumour cohort with a median proportion of 3.91% of all the cells in the stroma (IQR: 2.77% - 6.22%). This was followed by the pMMR hi-CIRC cohort where the proportion of $CD8^+$ cells was 3.05% of all the cells in the stroma (IQR: 1.51% - 7.28%). The lowest proportion was found in the pMMR cohort where only 1.25% of cells in the stroma were $CD8^+$ (IQR: 0.55% - 3.19%).

On statistical analysis, it was found that the difference between the dMMR and the pMMR was highly significant (unpaired t-test p= 0.0079). The difference between the pMMR and the pMMR hi-CIRC was found to be significant (unpaired t-test p= 0.045). The difference between pMMR hi-CIRC and d MMR cohorts was not statistically significant (unpaired t-test p= 0.91) [Figure 5.4A].

5.3.6.2. $CD8^+$ lymphocytes in the epithelium

The median proportion of $CD8^+$ T-lymphocytes was highest in the pMMR hi-CIRC cohort where the median proportion was 0.81% of all the cells in the epithelium (IQR: 0.23% - 8.43%). This was followed by the pMMR cohort in which the proportion of $CD8^+$ cells was 0.42% of all the cells in the epithelium (IQR: 0.07% - 0.96%) and the lowest proportion was found in the dMMR cohort with 0.31% of all the cells in the epithelium (IQR: 0.08% - 1.51%).

There were no statistically significant differences in the proportion of $CD8^+$ cells in the epithelium between any of the cohorts: dMMR vs. pMMR (Mann-Whitney U p= 0.53),

pMMR vs. pMMR hi-CIRC (Mann-Whitney *U p*= 0.12) and dMMR vs pMMR hi-CIRC (Mann-Whitney *U p*= 0.19) [Figure 5.4B].

5.3.7. T_C1

5.3.7.1. T_C1 lymphocytes in the stroma

The median proportion of T-bet positive cytotoxic lymphocytes was highest in the dMMR cohort of CRC with 1.34% of all the cells in the stroma testing positive for both CD8 and T-bet (IQR: 0.5% - 3.11%). This was followed by the pMMR hi-CIRC cohort with 0.28% of all the cells in the stroma testing positive for both markers (IQR: 0.07% - 2.1%). The cohort with the lowest proportion of Tc1 cells was the pMMR cohort with 0.07% of all the cells in the stroma being positive (IQR: 0.03% - 1.83%).

Statistical analysis did not show any statistical significance when the proportions were compared between the different cohorts: pMMR vs. dMMR (Mann-Whitney *U p*= 0.08), pMMR vs pMMR hi-CIRC (Mann-Whitney *U p*= 0.33) and dMMR vs. pMMR hi-CIRC (Mann-Whitney *U p*= 0.23) [Figure 5.4C].

5.3.7.2. T_C1 lymphocytes in the epithelium

On examining the proportion of T_C1 cells in the epithelium of the different cohorts there was very little difference seen. The median proportion of positive cells in the dMMR cohort was 0.07% of all the cells in the epithelium (IQR: 0.03% - 0.59%). The median proportion in the pMMR hi-CIRC cohort was 0.065% of all the cells in the epithelium (IQR: 0% - 1.07%). The lowest proportion was seen in the pMMR cohort with 0.06% of all the cells in the epithelium being T_C1 lymphocytes (IQR: 0.02% - 0.54%).

Statistical analysis did not reveal any significant differences in the proportion of T_C1 lymphocytes between the different cohorts: pMMR vs. dMMR (Mann-Whitney *U* p=

0.81), pMMR vs pMMR hi-CIRC (Mann-Whitney *U* p= 0.79) and dMMR vs. pMMR hi-CIRC (Mann-Whitney *U* p= 0.7) [Figure 5.4D].

CD8 and subtype Analysis

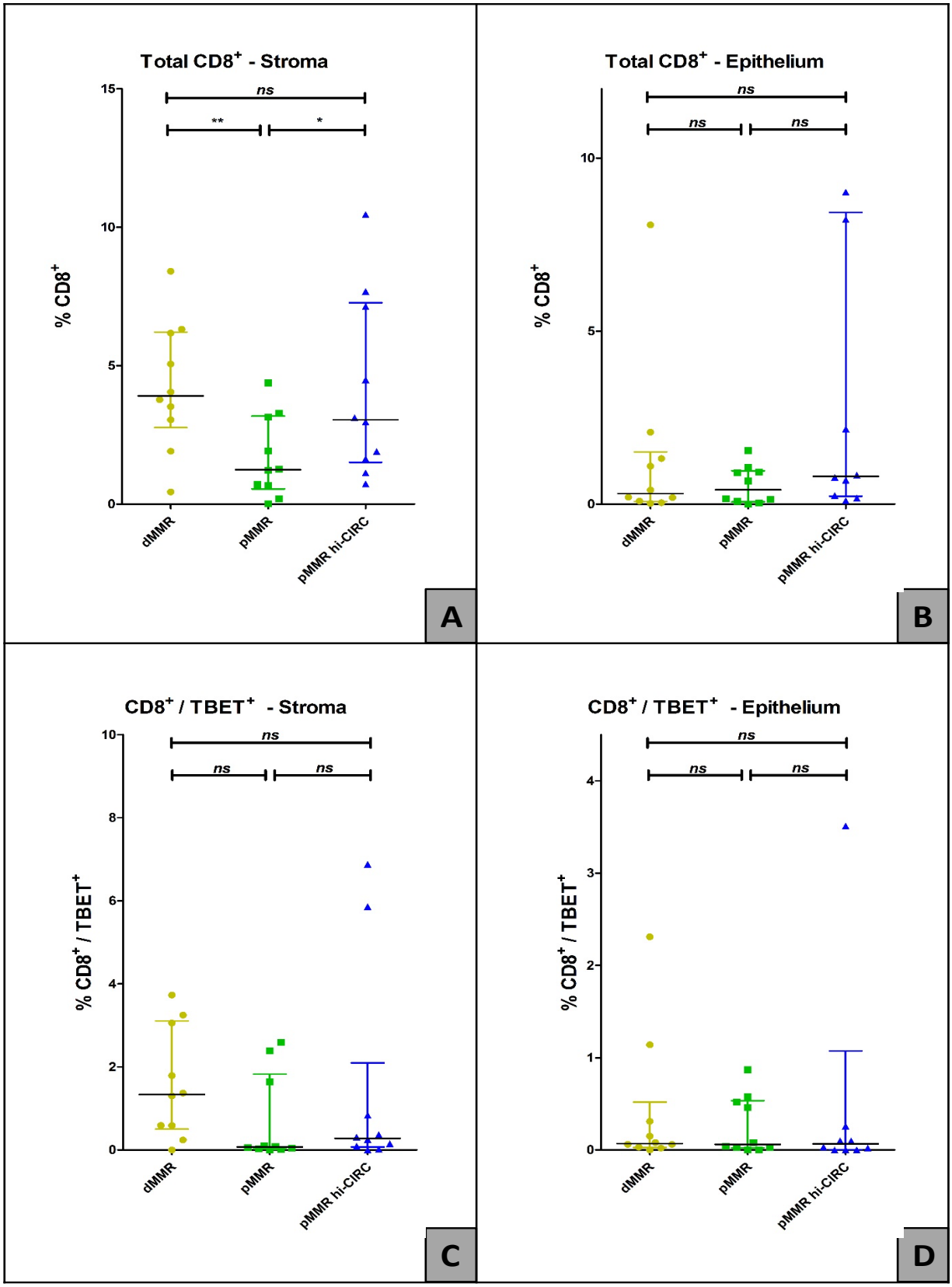

Figure 5.4. Graphic representation of the proportions of $CD8^+$ T lymphocytes and T_C1 lymphocyte in both the stroma and the epithelium. $CD8^+$ (A & B) and T_C1 (C & D). The bars represent medians and interquartile ranges (IQR). The asterisk (*) denotes a *p*-value of <0.05 and the double asterisk (**) denotes a *p*-value of <0.01. *ns*= not statistically significant (*p*-value ≥0.05).

5.3.8. MHC Class II

5.3.8.1. MHC Class II in the stroma

MHC Class II proportions were assessed in a similar manner to the previously described method and were found to follow a similar distribution to the $CD4^+$ and $CD8^+$ cells. The highest percentage was found in the dMMR cohort of tumours where the median proportion was 7.62% of all the cells in the stroma being positive for MHC Class II expression (IQR: 3.76% - 19.92%). This was followed by the pMMR hi-CIRC cohort where the share of MHC Class II positive cells was 6.74% of all the cells in the stroma (3.08% - 18.06%). The lowest proportion was in the pMMR cohort where there were only 1.99% of all the cells in the stroma positive for MHC Class 2 (IQR: 0.22% - 6.09%).

Upon statistical examination, there was a statistically significant difference between dMMR and pMMR (unpaired t-test p= 0.024). Also, there was a statistically significant difference between pMMR hi-CIRC and pMMR (unpaired t-test p= 0.038). There was no statistically significant difference between dMMR and pMMR hi-CIRC cohorts (unpaired t-test p= 0.62) [Figure 5.5A].

5.3.8.2. MHC Class II in the epithelium

The median proportion of MHC Class II positive cells in the epithelium was highest in the pMMR hi-CIRC cohort with the percentage of positive cells being 2.54% of all the cells in the tumour epithelium (IQR: 0.87% - 10.55%). This was followed by the dMMR cohort where the median share of MHC Class II positive cells was 1.22% of all the cells in the epithelium (IQR: 0.4% - 14.28%). The lowest proportion was in the pMMR cohort where the median percentage of positive cells was 0.075% of all the cells in the epithelium (IQR: 0.02% - 1.06%).

On performing statistical analysis on the differences between the three cohorts a highly statistically significant difference was demonstrated between the pMMR hi-CIRC and the pMMR cohorts (Mann-Whitney *U* p= 0.0028). There was a statistically significant difference between the dMMR and the pMMR cohorts (Mann-Whitney *U* p= 0.0197). No statistically significant difference was found between the pMMR hi-CIRC cohort and the dMMR cohort (Mann-Whitney *U* p= 0.542) [Figure 5.5B].

MHC Class II Analysis

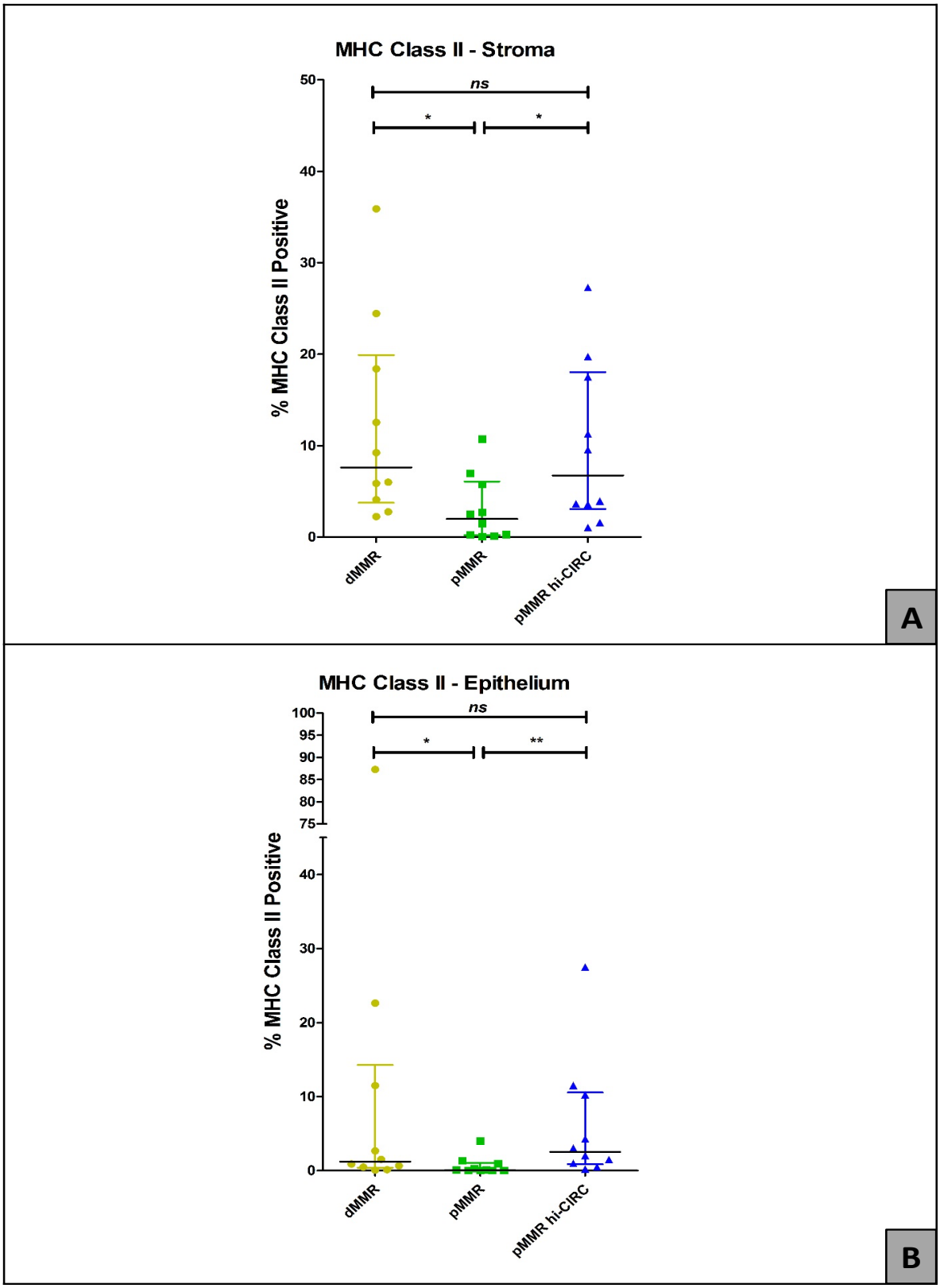

Figure 5.5. Graphic representation of the proportion of MHC Class II positive cells in the three different cohorts; in the stroma (A) and the epithelium (B). The bars represent medians and interquartile ranges (IQR). The asterisk (*) denotes a *p*-value of <0.05 and the double asterisk (**) denotes a *p*-value of <0.01. *ns*= not statistically significant (*p*-value ≥0.05).

5.4. Chapter Summary and Discussion

This study demonstrated that a subset of pMMR tumours evokes a strong immune response comparable to that of dMMR tumours. This subset is characterised by over expression of MHC Class II.

The objective of this chapter was to probe the immune microenvironment of a particular subset of microsatellite stable CRC which manifests with uncharacteristically high immune infiltrates (Lal et al., 2015). For comparison purposes, this subset was compared with two better defined subsets. The first subset is the common microsatellite stable type which constitutes around 85% of CRC cases. The second subset is the microsatellite unstable type which is normally characterised by high immune infiltrates probably owing to its high mutational burden. This subtype constitutes about 10-15% of CRCs and has a generally better stage-adjusted prognosis. To the best of my knowledge this is the first study of its kind to explore this comparison.

This chapter was conducted using a novel multiplex immunofluorescence staining technique. After comprehensive validation (see methods chapter) this technique allowed staining each section for 7 markers. The multispectral images were then digitally analysed using a custom-built algorithm to quantify stained markers in different tumour compartments. This new technology is unique in the sense that it allows the derivation of a large amount of information on different markers from a single slide without loss of information on tissue architecture and cellular geography (Pivetta et al., 2019). This vital information is usually lost with other multispectral quantification

techniques such as fluorescence-activated cell sorting (FACS) which require tissue digestion (Novelli et al., 2000).

The immune infiltrates in all three cohorts were more florid in the tumours' stromal compartment when compared to the epithelium (data not presented). This is in agreement with the findings in the previous workstream presented in chapter four.

The most interesting finding in this study is the fact that both $CD4^+$ and $CD8^+$ lymphocytes were significantly higher in the stroma of both the dMMR and pMMR hi-CIRC cohorts when compared to the pMMR cohort. Although the dMMR cohort had the highest density of infiltrates of both subsets of lymphocytes, it was striking to discover that the pMMR hi-CIRC cohort was almost as inflamed. In the epithelial compartment, only $CD4^+$ were found to be higher in both the pMMR hi-CIRC and the dMMR cohorts when compared to the pMMR cohort.

Upon exploring the functional orientation of $CD4^+$ lymphocytes by virtue of the co-expressed transcription factor, I determined that dMMR and pMMR hi-CIRC cohorts had equitable densities of cells co-expressing CD4 and TBET in both the stroma and the epithelium. Both cohorts had higher densities than in the pMMR cohort. Whilst not reaching statistical significance, the lowest density of cells co-expressing CD4 and FOXP3 was in the stroma of tumours in the dMMR cohort. Conversely, the density of $CD4^+$/ $ROR\gamma t^+$ lymphocytes was highest in the stroma of dMMR tumours. Taken together, these findings point to the fact that both the dMMR and pMMR hi-CIRC cohorts display a more type 1 pro-inflammatory response with less immune suppressive T_{REG} presence. Conclusions on T_{REG} and T_H17 cells in the epithelium were difficult to draw due to the extremely small numbers detected.

On exploration of the orientation of $CD8^+$ lymphocytes, there was a similar strong trend favouring a T_C1 type of immunity in the stroma in the dMMR and pMMR hi-CIRC cohorts when compared to the pMMR cohort. This comparison however did not reach statistical significance probably due to the small number of $CD8^+$ / $TBET^+$ cells and the small sample number.

High expression of MHC Class II in the pMMR hi-CIRC is entirely unsurprising, as the pMMR hi-CIRC samples were selected on the basis of a high expression of MHC class II as a central marker of type 1 immunity. Nevertheless, the robust expression of class II MHC detected is concordant with high levels of class II MHC gene expression at the transcriptional level in MSS-hi-CIRC samples (Lal et al., 2015), and lends credibility to the staining technique and the validity of the primary antibodies used in the staining process. The other interesting finding is the fact that the high expression of MHC class II was matched in the dMMR cohort and was significantly higher than the common pMMR cohort.

Collectively, these findings point strongly to the existence of a *bona fide* subset of microsatellite stable CRC with a high IFN-γ-centric type 1 immune response matching that of tumours with a deficient mismatch repair mechanism.

Those findings might have wide-ranging implications on the prognosis of patients harbouring this category of tumours as well as the treatment choices in the adjuvant setting. This calls for further research to better characterise the immune microenvironment of these tumours and link it to clinical outcomes. It would be of great interest to assess the expression of checkpoint blockade targets and explore immunotherapy in those patients. The latter is already being explored in the ANICCA-

Class II trial, which is a phase II clinical trial assessing the utility of Nivolumab, a PD-1 blocker in microsatellite stable CRC patients with high expression of MHC class II (NCT03981146).

The novelty of this study is perhaps its most obvious strength. Whilst MSS tumours with a high immune response have been previously described, to the best of my knowledge this is the first study to compare this group to a bona fide MSI-hi tumours. The other strength of this study is the validation of a high MHC Class II expression as a surrogate for a high CIRC response. The use of robustly validated antibodies and building of customised digital pathology algorithms to score the samples lends credibility to the derived results.

The main weakness of this study was the small sample size. This could have been the reason for the inability to obtain statistically significant results in the T-lymphocyte subtype analysis. This limitation was not avoidable to the limited availability of the study group (pMMR hi-CIRC). Due to exploratory nature of this study, it was not possible to obtain patient data or match the samples. As a result, it was not possible to compare the clinical outcomes or link the immune microenvironment to the pathological or oncological characteristics of those tumours. To reduce selection bias, consecutive samples were obtained for the control groups. It is plausible to assume that some of the MSS control samples might have had a high CIRC at random which may have biased the results.

The next steps for this project would be to expand the sample size based on a power calculation and collection patient and outcome date to aid matching the samples. It would also be interesting to explore the differential expression of CPB targets between

the subgroups. Comprehensive molecular profiling (genomic and transcriptomic analysis) of the different is likely to shed more light into the differences between those groups. Neo-antigen prediction would also be useful in exploring which antigens evoke the strongest immune responses and whether the frequency of those mutations is different in the different groups.

6. Chapter Six: Overall Discussion

The study of cancer immunobiology has been at the forefront of oncological research in the past few decades, catalysed by recognition that the tumour immune microenvironment and its composition can be both prognostic and predictive for response to treatment (Fridman et al., 2012, Angell and Galon, 2013). Interest has also been augmented by the discovery of novel immunotherapy targets and their successful exploitation in a variety of different cancers (Robert, 2020). In CRC, the role and importance of the tumour immune microenvironment has been elucidated in multiple studies and the prognostic value of tumour infiltrating lymphocytes (TILs) has been clinically validated in early-stage CRC (Galon et al., 2006, Galon et al., 2012, Pagès et al., 2018). Recently, compelling evidence has been evolving in support of a favourable impact of adaptive immune cell infiltrates in the context of metastatic CRC (Van den Eynde et al., 2018, Mlecnik et al., 2018, Mlecnik et al., 2020). There is also evidence that immune profile of the metastatic deposit has a positive predictive value for response to chemotherapy in the setting of colorectal liver metastases (Halama et al., 2011, Mlecnik et al., 2018). Mismatch repair deficient colorectal tumours with a high microsatellite instability (dMMR-MSI) were also recently shown to be responsive to treatment with checkpoint blockers and are now entering treatment algorithms in the metastatic setting (Overman et al., 2018a, Kreidieh et al., 2020, Almquist et al., 2020). Metastatic dMMR-MSI tumours however only account for 5% of all metastatic CRCs. Therefore, there is an impetus to study and characterise the immune microenvironment of the vastly more common mismatch repair proficient (pMMR) tumours in an attempt to define biomarkers for response to immunotherapies, and with a view to develop more optimised immunotherapeutic approaches for this challenging patient group.

In the first results chapter of this thesis, I explored the immune microenvironment in matched primary and lung metastatic colorectal tumours and established that the immune cell infiltrates and associated markers tend to be more focussed in the stroma of tumours. This is consistent with previous studies describing immune infiltrates in the invasive margin of the tumour which is essentially the stromal interface between the neoplastic epithelium and the underlying bowel wall layers. Those infiltrates in the invasive margin have been key in determining the clinically validated Immunoscore® in CRC (Galon et al., 2012, Pagès et al., 2018). Higher infiltrates were also observed in the invasive margin of colorectal metastases than in the tumour core which is consistent with my findings (Mlecnik et al., 2020, Mlecnik et al., 2018, Van den Eynde et al., 2018).

The abundance of $CD4^+$ cells in the stroma of the tumour is consistent with previously reported observations (Banner et al., 1993). This is likely to be important in regulating the anti-tumour immune response whether in a stimulatory (T_H1) or in an inhibitory (T_{REG}) manner. My results suggest a significant shift to a T_H1 orientation in lung metastases when compared to the primary tumours. This is manifested in proportionally higher expression of TBET transcription factor, which denotes a T_H1 response, when compared to FOXP3 expression. This is in keeping with an interferon gamma (IFN-γ) mediated response which indicates a more effective anti-tumour immunity and better prognosis in CRC (Ling et al., 2016). In support of this hypothesis, I found raised expression of MHC class I and II molecules as well as checkpoint blockade markers in the secondary site. All of those markers are part of a cluster of genes that is known to be co-expressed in the context of a type 1 immune response (Lal et al., 2015).

The proportionately higher density of $CD8^+$ cells in the tumour epithelium is also consistent with previously reported observations (Banner et al., 1993) and in a study from 2003, a low CD4+:CD8+ ratio coupled with raised HLA-DR expression was associated with a better prognosis in CRC (Diederichsen et al., 2003). This however was a flow cytometry analysis of enzymatically digested samples which sacrifices information about the localisation of those cells within tumour compartments. One possibility is that $CD8^+$ cells are activated and maintained in the stroma by professional antigen presenting cells (APCs) supported by $CD4^+$ cells before migrating into the epithelium to deliver their cytotoxic functions.

Departing from the conventional understanding of the role of $CD4^+$ cells, it is also possible that those cells in the stroma possess cytotoxic properties which may be key in controlling the tumour at the invasive margin. The cytotoxic properties of anti-tumour $CD4^+$ cells have been recently described in both mouse and human models (Quezada et al., 2010, Long et al., 2011, Tran et al., 2014, Tay et al., 2020).

The heightened type 1 immune response in lung metastases may, at least in part, explain the better prognosis in lung colorectal metastases when compared to liver metastases. The 5-year survival of untreated liver metastases is bleak and ranges between 1% and 11% at best (Stangl et al., 1994, Valderrama-Treviño et al., 2017). This contrasts sharply with the much better 5-year survival reported in untreated colorectal lung metastases in the PulMiCC trial of 29% (Treasure et al., 2019). In the latter randomised controlled trial, Treasure *et al*. postulate that colorectal lung metastases may not require surgical resection due to absence of a survival benefit (Treasure et al., 2009, Treasure et al., 2019). In a study of matched primary CRC and lung metastases, the immune patterns ($CD8^+$ lymphocytes and mature dendritic cells)

in the lung metastases were found to be more relevant to overall survival of patients than the immune patterns in the primary (Remark et al., 2013). Several recent reports highlighted the favourable impact of the adaptive immune system cells in the metastatic CRC microenvironment (Van den Eynde et al., 2018, Mlecnik et al., 2018, Angelova et al., 2018, Baldin et al., 2020). Although the vast majority of patients examined in those reports had liver metastases, it would stand to reason to assume that TIL infiltrates confer similar benefits in the context of lung metastases.

The expression of two clinically relevant checkpoint blockade targets, PD-1 and PD-L1 was found higher in the epithelium and stroma of the metastatic site respectively. This finding is in keeping with the notion of a higher T_H1 immune response in the lung (Lal et al., 2015). The prognostic value of both markers in primary CRC was explored by Lee *et al.* who found that neither PD-1 nor PD-L1 expression levels had any significant bearing on survival (Lee et al., 2016). The authors however found a positive survival benefit with a concomitantly raised PD-1 and lowered PD-L1 levels in the mismatch repair deficient (dMMR) subset of their cohort (Lee et al., 2016). Conversely, a more recent meta-analysis suggested that high expression of PD-L1 was associated with poor clinical outcomes and adverse pathological features (Shen et al., 2019). The contradicting results could be due to different assays used for quantification and differing definitions of positivity used in different studies (Topalian et al., 2016). In non-small cell lung cancer, a meta-analysis showed that high expression of PD-L1 was also associated with a poor outcome and adverse histological features (Wang et al., 2015).

In terms of the predictive value of CPB molecule expression, recent reports from clinical trials suggest that the expression levels of PD-L1 do not correlate with response to CPB immunotherapy (André et al., 2017, Overman et al., 2017). In advanced non-

small cell lung cancer however, higher expression of PD-L1 correlated with a better response to anti-PD-1 therapy (Garon et al., 2015). It has also been reported that expression levels of PD-L1 within the same tumour is variable due to heterogeneity (Topalian et al., 2016). This heterogeneity therefore renders histological analysis susceptible to selection and observer bias. Taken together, it appears that the prognostic and predictive value of CPB molecule expression varies according to the tumour site and it is likely that the benefits of CPB inhibitors is a multifactorial phenomenon that relates primarily to the presence of high T_H1-focused lymphocyte infiltrates that are exhausted by the high expression of PD-1/PD-L1 and other checkpoint molecules (Llosa et al., 2015, Zhang et al., 2017b). Encouragingly, a recent study of 24 patients with predominantly MSS metastatic CRC treated with regorafenib and nivolumab identified that patients with lung metastases had response rates of 50% (Fukuoka et al., 2020). The result of this study highlights the differential response in patients with lung metastases and opens the opportunity to explore the benefit of novel immunotherapies in this context.

The heightened TIL densities and type 1 orientation on the lung metastatic site could be due to a variety of factors. Those factors could be metastatic cell-autonomous or related to the difference in the microenvironment between the two sites and more likely due to a combination of both (Liu et al., 2017). In terms of cell autonomous factors, one explanation to the increased immunity at the metastatic site is the tumour mutational burden (TMB). The mutational burden of tumours which translates into an increased number of neoantigens has been found to correlate with the density of TILs in CRC (Giannakis et al., 2016). Of strong relevance, it has also recently been shown that the mutational load at metastatic sites is higher than that in matched primaries

with lung metastases tending to harbour a higher TMB than the liver in a pan-cancer analysis (Schnidrig et al., 2019). Also in keeping with a cell autonomous drive for a higher T_H1 immunity, Remark *et al.* demonstrated upregulation of acute T_H1-related genes in colorectal lung metastases whilst lung metastases from a renal cell carcinoma had upregulated T_H2-linked genes favouring chronic inflammation, angiogenesis and immunosuppression (Remark et al., 2013).

The host's microbiome undoubtedly plays a pivotal role in shaping the immune microenvironment of tumours, both primary and metastatic (Zitvogel et al., 2016). The influence of gastrointestinal microbes in modulating the effect of carcinogens in the colon and hence contributing to the pathogenesis of colon cancer was first demonstrated in the 70's (Reddy et al., 1975). Since then there have been several studies that attempted to probe the role of the microbiome in causing colon cancer (Jobin, 2013, Sears and Garrett, 2014). In spite of the plethora of research in the field of 'microbiomics', there remains a degree of obscurity on direct causality from human studies (Scott et al., 2019). There is however growing evidence on the application of faecal microbiota transplantation (FMT) as a treatment for inflammatory bowel disease (particularly ulcerative colitis), highlighting the clinical potential of this area (Paramsothy et al., 2017, Costello et al., 2017, Levy and Allegretti, 2019).

Given the enormous load of antigens that the gut is constantly exposed to either from its own commensal microbiota or from ingested antigens, the gastrointestinal immune response developed a unique ability to maintain immunological homeostasis and a degree of physiological tolerance to those antigens (Hooper et al., 2012, Mortha et al., 2014). It has recently been found that the cytokine secretory profile of $CD4^+$ T-lymphocytes can be modulated by bacterial metabolites such as butyrate. Stimulation

of $CD4^+$ cells in the presence of Butyrate resulted in increased secretion of IL-10, favouring a tolerogenic T_H2 phenotype as opposed to IL-17 which favours a more inflammatory T_H17 phenotype (Saito et al., 2015). The gut microbiome therefore influences the adjuvanticity of the tumour microenvironment, determining the local, and possibly distant, lymphocyte regulatory and effector functions (Zitvogel et al., 2016). It has also been found that certain gut pathogens, such as *Fusobacterium nucleatum* are directly implicated in deactivation of cytotoxic cells by secreting a protein called Fap2 which binds to TIGIT (T-cell immunoreceptor with Ig and ITIM), a checkpoint-like receptor, on T-lymphocytes and natural killer cells (Gur et al., 2015). Taken together, this argument could explain the lower immune response in the primary tumour when compared to the lung metastasis.

In the second results chapter of this thesis, I explored the composition of the microenvironment of a poorly defined subset of microsatellite CRC which involves a heightened intratumoural type 1 immune response. This cohort of cancers was identified transcriptomically on the basis of a high expression of MHC class II which is central to the coordinated immune response cluster (CIRC) (Lal et al., 2015). I examined the functional orientation of the TILs through multiplexed immunohistochemical fluorescent staining and digital quantification. I assessed three main T-helper lymphocyte lineages that were found to be relevant to the prognosis of CRC, namely T_H1, T_{REG} and T_H17 (Tosolini et al., 2011), based on expression of TBET, FoxP3, and RORgT transcription factors respectively. To understand where this cohort fits into the spectrum of CRC subtypes, I compared it against a mismatch repair deficient (dMMR) cohort as well as a mismatch repair proficient (pMMR) cohort.

The most striking finding was that the studied cohort (pMMR hi-CIRC) was significantly different from the common pMMR cohort and had an almost identically florid microenvironment as *bona fide* dMMR MSI-hi cancers. This was true in terms of the density of infiltrates and T_H1 orientation. The reasons for this are currently unclear but may be multifactorial and are likely related to cell autonomous as well as local environmental factors.

It is well-established that the tumour mutational burden (TMB) of dMMR MSI-hi colorectal tumours is multiple folds higher than that of its pMMR-MSS counterparts (Vogelstein et al., 2013). This is likely to be the reason for the vigorous immune microenvironment observed in these tumours and their susceptibility to checkpoint blockade inhibition therapies (Rizvi et al., 2015, Le et al., 2017, Yarchoan et al., 2017, Chan et al., 2019). It is however clear that microsatellite instability in not the only reason for an elevated TMB. In two focused next-generation sequencing (NGS) studies using an assay to determine the mutational burden, Chalmers *et al.* and Goodman *et al.* assessed this in 102,292 and 148,803 tumour samples respectively. They found that between 80 - 85% of samples with a high mutational burden were microsatellite stable (Chalmers et al., 2017, Goodman et al., 2019). Goodman *et al.* also found that although the majority of CRC samples with a high TMB were MSI-high, a small proportion was MSS (Goodman et al., 2019). Chalmers *et al.* found that TMB significantly increases with age (Chalmers et al., 2017). Defects in the replication of DNA is another way to induce an increased somatic mutational burden and some hyper-mutated tumour phenotypes have been shown to be a result of defective DNA polymerase functions (Briggs and Tomlinson, 2013). POLE and POLD mutations however are unlikely to offer a full explanation for the high CIRC signatures in this

cohort as they occur at a much lower frequency (2 – 7%) than the frequency of MSS hi-CIRC which is estimated to be around 30% (Lal et al., 2015).

It is widely accepted that the vast proportion of tumour cell neoantigens (tumour associated antigens – TAAs) are not greatly dissimilar to self-antigens, so the immune response to these antigens tends to be attenuated due to central immune system tolerance mechanisms. Therefore, the quality of the epitope presented in the context of an MHC complex is of crucial importance in determining the immunogenicity of the tumour and the vigour of the immune response it generates (Blankenstein et al., 2012). In an *in silico* neoantigen prediction model, the quality –rather than the quantity – of neoantigens was found to be of significant prognostic importance in patients with pancreatic ductal adenocarcinoma (Balachandran et al., 2017). The authors found that tumour neoantigens that mimicked infectious disease-derived epitopes independently predicted increased $CD8^+$ lymphocyte infiltrates and prolonged survival (Balachandran et al., 2017). Also, In a whole-exome sequencing (WES) study on 249 samples of tumour and matched normal tissue, Miao *et al.* found that certain mutations, especially in 'driver' genes, generate stronger immune responses (Miao et al., 2018). Therefore, the prediction of the immunogenicity of certain mutations is likely to become a biomarker in predicting a tumour's response to immunotherapy rather than just its TMB (Kim et al., 2020). Taken together, it is very likely that a tumour that develops a highly immunogenic neoantigen would generate a strong immune response. As hyper-mutated tumours develop mutations at a greater frequency than tumours with an average mutation rate, they perhaps have an exponentially greater chance of generating an immunogenic mutation. It is plausible however that some MSS tumours can develop such highly immunogenic mutations albeit at a lower frequency. I

speculate that this, at least in part, may explain the raised immunity in the MSS hi-CIRC cohort of my study.

It is possible that the heightened immune response in the pMMR hi-CIRC is due to factors beyond TMB and the immunogenicity of mutations. As discussed earlier in this section, the effect of the gut microbiome may play a significant role in shaping the immune microenvironment of those tumours. Therefore, tumours with high (or low) responses could be a result of the effect of the microbiome on the regulatory functions of mucosal lymphocytes.

The heighted type 1 immune response in this special subset of microsatellite stable tumours may confer a favourable prognosis. It has been robustly demonstrated that the value of tumour infiltrating lymphocytes in CRC (the Immunoscore®) and their functional orientation in predicting improved cancer-specific survival outperforms the microsatellite status of the tumour (Mlecnik et al., 2016a).

In terms of the therapeutic implications of the findings of this study, it would be reasonable to speculate that this subset of tumours would respond better to immunotherapies, namely checkpoint blockers in a similar fashion to their microsatellite instability-high counterparts. It is well-established that the success of immunotherapies is enhanced by the presence of an inflamed microenvironment (Overman et al., 2018a, Kreidieh et al., 2020, Almquist et al., 2020, Van den Eynde et al., 2020). It is however important to remember that checkpoint blockers are currently only indicated in metastatic (stage IV) CRC with an MSI-hi phenotype which accounts for only 5% of all mCRC (Malesci et al., 2007, Venderbosch et al., 2014). It is therefore clinically important to establish if there are subsets of MSS mCRC that would be

responsive to CPB. This avenue is currently being explored in an open-label phase II trial assessing the use of a PD-1 blocker (Nivolumab) in metastatic MSS CRCs stratified for high expression of MHC class II, ANICCA-Class II (NCT03981146). Despite the TCGA data suggesting that around 30% of MSS tumours have a high CIRC score, this data is derived from primary tumours and the prevalence of this subgroup in the metastatic setting is unknown (Lal et al., 2015). The established correlation between high intratumoural immunity and improved cancer-specific survival (Mlecnik et al., 2016b) would predict that those tumours would be less likely to progress to stage IV disease and would be less prevalent than anticipated from the TCGA data. The ANICCA-Class II trial estimates the prevalence to be around 10% (NCT03981146)

My results also validate the ability of MHC class II expression to predict a T_H1 response in pMMR-MSS colorectal tumours. Assessing its expression with immunohistochemistry makes it accessible in clinical settings as part of a staining panel on CRC specimens. This is a proof of concept that MHC class II is a potential prognostic and predictive biomarker for stratifying pMMR-MSS CRCs and predicting possible response to immunotherapies. Its utility as such a biomarker is currently being tested in the aforementioned ANICCA-Class II clinical trial (NCT03981146).

As discussed in individual previous chapters, the main limitation of both studies is the lack of relevant clinical data on patient outcomes to link the immunological findings. Given the exploratory nature of this work, the focus was on gleaning an understanding of the microenvironment. Both studies also suffer from a small cohort number and the inability to perform a power calculation. The reasons for this are multifactorial and have been discussed in previous chapters. This mainly pertains to the limited number of study samples that could be obtained within the timeframe of the research project.

One of the unacknowledged but key strengths of this research work is the meticulous antibody selection and painstaking validation process. This labour-intensive and time-consuming process was crucial to achieve credible and reliable outcomes. A testament to the robustness of the validation process, is the fact that one of those in-house-validated antibodies (MCH Class II) is currently being used in the ANICCA-Class II clinical trial. The other main strength is the use of digital pathology to automatically score markers. The use of custom-built IHC and IF scoring algorithms, played a key role in reducing observer bias and ensuring highly credible and reproducible scoring.

Bibliography

Ait Ouakrim, D., Dashti, S. G., Chau, R., Buchanan, D. D., Clendenning, M., Rosty, C., Winship, I. M., Young, J. P., Giles, G. G., Leggett, B., Macrae, F. A., Ahnen, D. J., Casey, G., Gallinger, S., Haile, R. W., Le Marchand, L., Thibodeau, S. N., Lindor, N. M., Newcomb, P. A., Potter, J. D., Baron, J. A., Hopper, J. L., Jenkins, M. A. & Win, A. K. 2015. Aspirin, Ibuprofen, and the Risk of Colorectal Cancer in Lynch Syndrome. *Journal of the National Cancer Institute,* 107**,** djv170.

Almquist, D. R., Ahn, D. H. & Bekaii-Saab, T. S. 2020. The Role of Immune Checkpoint Inhibitors in Colorectal Adenocarcinoma. *BioDrugs,* 34**,** 349-362.

André, T., Overman, M., Lonardi, S., Aglietta, M., Mcdermott, R., Wong, K. Y. M., Morse, M., Hendlisz, A., Moss, R. A., Ledeine, J., H. Tang, H., Cao, Z. A. & S., K. 2017. Analysis of tumor PD-L1 expression and biomarkers in relation to clinical activity in patients (pts) with deficient DNA mismatch repair (dMMR)/high microsatellite instability (MSI-H) metastatic colorectal cancer (mCRC) treated with nivolumab (NIVO) + ipilimumab (IPI): CheckMate 142. *ESMO 2017 Congress.* Madrid, Spain: Annals of Oncology.

André, T., Shiu, K.-K., Kim, T. W., Jensen, B. V., Jensen, L. H., Punt, C., Smith, D., Garcia-Carbonero, R., Benavides, M., Gibbs, P., De La Fouchardiere, C., Rivera, F., Elez, E., Bendell, J., Le, D. T., Yoshino, T., Van Cutsem, E., Yang, P., Farooqui, M. Z. H., Marinello, P. & Diaz, L. A. 2020. Pembrolizumab in Microsatellite-Instability–High Advanced Colorectal Cancer. *New England Journal of Medicine,* 383**,** 2207-2218.

Angell, H. & Galon, J. 2013. From the immune contexture to the Immunoscore: the role of prognostic and predictive immune markers in cancer. *Curr Opin Immunol,* 25**,** 261-7.

Angelova, M., Mlecnik, B., Vasaturo, A., Bindea, G., Fredriksen, T., Lafontaine, L., Buttard, B., Morgand, E., Bruni, D., Jouret-Mourin, A., Hubert, C., Kartheuser, A., Humblet, Y., Ceccarelli, M., Syed, N., Marincola, F. M., Bedognetti, D., Van Den Eynde, M. & Galon, J. 2018. Evolution of Metastases in Space and Time under Immune Selection. *Cell,* 175**,** 751-765.e16.

Argilés, G., Saro, J., Segal, N. H., Melero, I., Ros, W., Marabelle, A., Rodriguez, M. E., Albanell, J., Calvo, E., Moreno, V., Cleary, J. M., Eder, P., Paz-Ares, L., Hurwitz, H., Bacac, M., Perro, M., Bouseida, S., Sandoval, F., Sabanes Bove, D., Sreckovic, S., Jamois, C., Silva, A., Klein, C., Umana, P., Karanikas, V. & Tabernero, J. 2017. Novel carcinoembryonic antigen T-cell bispecific (CEA-TCB) antibody: Preliminary clinical data as a single agent and in combination with atezolizumab in patients with metastatic colorectal cancer (mCRC). *Annals of Oncology,* 28**,** iii151.

Bacac, M., Fauti, T., Sam, J., Colombetti, S., Weinzierl, T., Ouaret, D., Bodmer, W., Lehmann, S., Hofer, T., Hosse, R. J., Moessner, E., Ast, O., Bruenker, P., Grau-Richards, S., Schaller, T., Seidl, A., Gerdes, C., Perro, M., Nicolini, V., Steinhoff, N., Dudal, S., Neumann, S., Von Hirschheydt, T., Jaeger, C., Saro, J., Karanikas, V., Klein, C. & Umana, P. 2016a. A Novel Carcinoembryonic Antigen T-Cell Bispecific Antibody (CEA TCB) for the Treatment of Solid Tumors. *Clin Cancer Res,* 22**,** 3286-97.

Bacac, M., Klein, C. & Umana, P. 2016b. CEA TCB: A novel head-to-tail 2:1 T cell bispecific antibody for treatment of CEA-positive solid tumors. *Oncoimmunology,* 5**,** e1203498.

Baier, P. K., Wimmenauer, S., Hirsch, T., V. Specht, B. U., V. Kleist, S., Keller, H. & Farthmann, E. H. 1998. Analysis of the T Cell Receptor Variability of Tumor-Infiltrating Lymphocytes in Colorectal Carcinomas. *Tumor Biology,* 19**,** 205-212.

Balachandran, V. P., Łuksza, M., Zhao, J. N., Makarov, V., Moral, J. A., Remark, R., Herbst, B., Askan, G., Bhanot, U., Senbabaoglu, Y., Wells, D. K., Cary, C. I. O., Grbovic-Huezo, O., Attiyeh, M., Medina, B., Zhang, J., Loo, J., Saglimbeni, J., Abu-Akeel, M., Zappasodi, R., Riaz, N., Smoragiewicz, M., Kelley, Z. L., Basturk, O., Gönen, M., Levine, A. J., Allen, P. J., Fearon, D. T., Merad, M., Gnjatic, S., Iacobuzio-Donahue, C. A., Wolchok, J. D., Dematteo, R. P., Chan, T. A., Greenbaum, B. D., Merghoub, T. & Leach, S. D. 2017. Identification of unique neoantigen qualities in long-term survivors of pancreatic cancer. *Nature,* 551**,** 512-516.

Baldin, P., Van Den Eynde, M., Mlecnik, B., Bindea, G., Beniuga, G., Carrasco, J., Haicheur, N., Marliot, F., Lafontaine, L., Fredriksen, T., Lanthier, N., Hubert, C., Navez, B., Huyghe, N., Pagès, F., Jouret-Mourin, A., Galon, J. & Komuta, M. 2020. Prognostic assessment of resected colorectal liver metastases integrating pathological features, RAS mutation and Immunoscore. *The Journal of Pathology: Clinical Research*.

Banner, B. F., Savas, L., Baker, S. & Woda, B. A. 1993. Characterization of the inflammatory cell populations in normal colon and colonic carcinomas. *Virchows Archiv B Cell Pathology Including Molecular Pathology,* 64**,** 213-220.

Barretina, J., Caponigro, G., Stransky, N., Venkatesan, K., Margolin, A. A., Kim, S., Wilson, C. J., Lehar, J., Kryukov, G. V., Sonkin, D., Reddy, A., Liu, M., Murray, L., Berger, M. F., Monahan, J. E., Morais, P., Meltzer, J., Korejwa, A., Jane-Valbuena, J., Mapa, F. A., Thibault, J., Bric-Furlong, E., Raman, P., Shipway, A., Engels, I. H., Cheng, J., Yu, G. K., Yu, J., Aspesi, P., Jr., De Silva, M., Jagtap, K., Jones, M. D., Wang, L., Hatton, C., Palescandolo, E., Gupta, S., Mahan, S., Sougnez, C., Onofrio, R. C., Liefeld, T., Macconaill, L., Winckler, W., Reich, M., Li, N., Mesirov, J. P., Gabriel, S. B., Getz, G., Ardlie, K., Chan, V., Myer, V. E., Weber, B. L., Porter, J., Warmuth, M., Finan, P., Harris, J. L., Meyerson, M., Golub, T. R., Morrissey, M. P., Sellers, W. R., Schlegel, R. &

Garraway, L. A. 2012. The Cancer Cell Line Encyclopedia enables predictive modelling of anticancer drug sensitivity. *Nature,* 483**,** 603-7.

Beggs, A. D., Jones, A., El-Bahrawy, M., Abulafi, M., Hodgson, S. V. & Tomlinson, I. P. 2013. Whole-genome methylation analysis of benign and malignant colorectal tumours. *J Pathol,* 229**,** 697-704.

Bhattacharyya, N., Skandalis, A., Ganesh, A., Groden, J. & Meuth, M. 1994. Mutator Phenotypes in Human Colorectal Carcinoma Cell Lines. *Proceedings of the National Academy of Sciences of the United States of America,* 91**,** 6319-6323.

Bird, A. 2002. DNA methylation patterns and epigenetic memory. *Genes Dev,* 16**,** 6-21.

Blanchet, O., Bourge, J. F., Zinszner, H., Israel, A., Kourilsky, P., Dausset, J., Degos, L. & Paul, P. 1992. Altered binding of regulatory factors to HLA class I enhancer sequence in human tumor cell lines lacking class I antigen expression. *Proc Natl Acad Sci U S A,* 89**,** 3488-92.

Blankenstein, T., Coulie, P. G., Gilboa, E. & Jaffee, E. M. 2012. The determinants of tumour immunogenicity. *Nature Reviews Cancer,* 12**,** 307-313.

Boehm, U., Klamp, T., Groot, M. & Howard, J. C. 1997. Cellular Responses to Interferon-γ. *Annual Review of Immunology,* 15**,** 749-795.

Boland, C. R. & Goel, A. 2010. Microsatellite instability in colorectal cancer. *Gastroenterology,* 138**,** 2073-2087 e3.

Boland, C. R., Thibodeau, S. N., Hamilton, S. R., Sidransky, D., Eshleman, J. R., Burt, R. W., Meltzer, S. J., Rodriguez-Bigas, M. A., Fodde, R., Ranzani, G. N. & Srivastava, S. 1998. A National Cancer Institute Workshop on Microsatellite Instability for Cancer Detection and Familial Predisposition: Development of International Criteria for the Determination of Microsatellite Instability in Colorectal Cancer. *Cancer Research,* 58**,** 5248.

Boland, P. M., Yurgelun, M. B. & Boland, C. R. 2018. Recent progress in Lynch syndrome and other familial colorectal cancer syndromes. *CA Cancer J Clin,* 68**,** 217-231.

Bordeaux, J., Welsh, A., Agarwal, S., Killiam, E., Baquero, M., Hanna, J., Anagnostou, V. & Rimm, D. 2010. Antibody validation. *Biotechniques,* 48**,** 197-209.

Bos, J. L., Fearon, E. R., Hamilton, S. R., Verlaan-De Vries, M., Van Boom, J. H., Van Der Eb, A. J. & Vogelstein, B. 1987. Prevalence of ras gene mutations in human colorectal cancers. *Nature,* 327**,** 293-7.

Bosman, F. T., World Health Organization. & International Agency for Research on Cancer. 2010. *WHO classification of tumours of the digestive system,* Lyon, International Agency for Research on Cancer.

Bourdais, R., Rousseau, B., Pujals, A., Boussion, H., Joly, C., Guillemin, A., Baumgaertner, I., Neuzillet, C. & Tournigand, C. 2017. Polymerase proofreading domain mutations: New opportunities for immunotherapy in hypermutated colorectal cancer beyond MMR deficiency. *Critical Reviews in Oncology/Hematology,* 113**,** 242-248.

Brahmer, J. R., Tykodi, S. S., Chow, L. Q., Hwu, W. J., Topalian, S. L., Hwu, P., Drake, C. G., Camacho, L. H., Kauh, J., Odunsi, K., Pitot, H. C., Hamid, O., Bhatia, S., Martins, R., Eaton, K., Chen, S., Salay, T. M., Alaparthy, S., Grosso, J. F., Korman, A. J., Parker, S. M., Agrawal, S., Goldberg, S. M., Pardoll, D. M., Gupta, A. & Wigginton, J. M. 2012. Safety and activity of anti-PD-L1 antibody in patients with advanced cancer. *N Engl J Med,* 366**,** 2455-65.

Bray, F., Ferlay, J., Soerjomataram, I., Siegel, R. L., Torre, L. A. & Jemal, A. 2018. Global cancer statistics 2018: GLOBOCAN estimates of incidence and mortality worldwide for 36 cancers in 185 countries. *CA Cancer J Clin,* 68**,** 394-424.

Brierley, J. D., Gospodarowicz, M. K. & Wittekind, C. 2016. *TNM Classification of Malignant Tumours*, Wiley Blackwell.

Briggs, S. & Tomlinson, I. 2013. Germline and somatic polymerase epsilon and delta mutations define a new class of hypermutated colorectal and endometrial cancers. *J Pathol,* 230**,** 148-53.

Buchbinder, E. I. & Desai, A. 2016. CTLA-4 and PD-1 Pathways: Similarities, Differences, and Implications of Their Inhibition. *Am J Clin Oncol,* 39**,** 98-106.

Budinska, E., Popovici, V., Tejpar, S., D'ario, G., Lapique, N., Sikora, K. O., Di Narzo, A. F., Yan, P., Hodgson, J. G., Weinrich, S., Bosman, F., Roth, A. & Delorenzi, M. 2013. Gene expression patterns unveil a new level of molecular heterogeneity in colorectal cancer. *J Pathol,* 231**,** 63-76.

Buhard, O., Cattaneo, F., Wong, Y. F., Yim, S. F., Friedman, E., Flejou, J.-F., Duval, A. & Hamelin, R. 2006. Multipopulation Analysis of Polymorphisms in Five Mononucleotide Repeats Used to Determine the Microsatellite Instability Status of Human Tumors. *Journal of Clinical Oncology,* 24**,** 241-251.

Burn, J., Gerdes, A.-M., Macrae, F., Mecklin, J.-P., Moeslein, G., Olschwang, S., Eccles, D., Evans, D. G., Maher, E. R., Bertario, L., Bisgaard, M.-L., Dunlop, M. G., Ho, J. W. C., Hodgson, S. V., Lindblom, A., Lubinski, J., Morrison, P. J., Murday, V., Ramesar, R., Side, L., Scott, R. J., Thomas, H. J. W., Vasen, H. F.,

Barker, G., Crawford, G., Elliott, F., Movahedi, M., Pylvanainen, K., Wijnen, J. T., Fodde, R., Lynch, H. T., Mathers, J. C. & Bishop, D. T. 2011. Long-term effect of aspirin on cancer risk in carriers of hereditary colorectal cancer: an analysis from the CAPP2 randomised controlled trial. *The Lancet,* 378**,** 2081-2087.

Burnet, F. M. 1970. The concept of immunological surveillance. *Prog Exp Tumor Res,* 13**,** 1-27.

Caballero-Banos, M., Benitez-Ribas, D., Tabera, J., Varea, S., Vilana, R., Bianchi, L., Ayuso, J. R., Pages, M., Carrera, G., Cuatrecasas, M., Martin-Richard, M., Cid, J., Lozano, M., Castells, A., Garcia-Albeniz, X., Maurel, J. & Vilella, R. 2016. Phase II randomised trial of autologous tumour lysate dendritic cell plus best supportive care compared with best supportive care in pre-treated advanced colorectal cancer patients. *Eur J Cancer,* 64**,** 167-74.

Cancer Research Uk. *Bowel Cancer Statistics* [Online]. Available: http://www.cancerresearchuk.org/health-professional/cancer-statistics/statistics-by-cancer-type/bowel-cancer [Accessed 04/06/2020].

Chalabi, M., Fanchi, L. F., Dijkstra, K. K., Van Den Berg, J. G., Aalbers, A. G., Sikorska, K., Lopez-Yurda, M., Grootscholten, C., Beets, G. L., Snaebjornsson, P., Maas, M., Mertz, M., Veninga, V., Bounova, G., Broeks, A., Beets-Tan, R. G., De Wijkerslooth, T. R., Van Lent, A. U., Marsman, H. A., Nuijten, E., Kok, N. F., Kuiper, M., Verbeek, W. H., Kok, M., Van Leerdam, M. E., Schumacher, T. N., Voest, E. E. & Haanen, J. B. 2020. Neoadjuvant immunotherapy leads to pathological responses in MMR-proficient and MMR-deficient early-stage colon cancers. *Nature Medicine,* 26**,** 566-576.

Chalmers, Z. R., Connelly, C. F., Fabrizio, D., Gay, L., Ali, S. M., Ennis, R., Schrock, A., Campbell, B., Shlien, A., Chmielecki, J., Huang, F., He, Y., Sun, J., Tabori, U., Kennedy, M., Lieber, D. S., Roels, S., White, J., Otto, G. A., Ross, J. S., Garraway, L., Miller, V. A., Stephens, P. J. & Frampton, G. M. 2017. Analysis of 100,000 human cancer genomes reveals the landscape of tumor mutational burden. *Genome Med,* 9**,** 34.

Chan, T. A., Yarchoan, M., Jaffee, E., Swanton, C., Quezada, S. A., Stenzinger, A. & Peters, S. 2019. Development of tumor mutation burden as an immunotherapy biomarker: utility for the oncology clinic. *Ann Oncol,* 30**,** 44-56.

Chen, D. S. & Mellman, I. 2013. Oncology meets immunology: the cancer-immunity cycle. *Immunity,* 39**,** 1-10.

Chung, K. Y., Gore, I., Fong, L., Venook, A., Beck, S. B., Dorazio, P., Criscitiello, P. J., Healey, D. I., Huang, B., Gomez-Navarro, J. & Saltz, L. B. 2010. Phase II study of the anti-cytotoxic T-lymphocyte-associated antigen 4 monoclonal antibody,

tremelimumab, in patients with refractory metastatic colorectal cancer. *J Clin Oncol,* 28**,** 3485-90.

Ciampricotti, M., Hau, C.-S., Doornebal, C. W., Jonkers, J. & De Visser, K. E. 2012. Chemotherapy response of spontaneous mammary tumors is independent of the adaptive immune system. *Nat Med,* 18**,** 344-346.

Cohen, R., Rousseau, B., Vidal, J., Colle, R., Diaz, L. A. & André, T. 2019. Immune Checkpoint Inhibition in Colorectal Cancer: Microsatellite Instability and Beyond. *Targeted Oncology,* 15**,** 11-24.

Copija, A., Waniczek, D., Witkos, A., Walkiewicz, K. & Nowakowska-Zajdel, E. 2017. Clinical Significance and Prognostic Relevance of Microsatellite Instability in Sporadic Colorectal Cancer Patients. *Int J Mol Sci,* 18.

Costello, S. P., Soo, W., Bryant, R. V., Jairath, V., Hart, A. L. & Andrews, J. M. 2017. Systematic review with meta-analysis: faecal microbiota transplantation for the induction of remission for active ulcerative colitis. *Alimentary Pharmacology & Therapeutics,* 46**,** 213-224.

Coulie, P. G., Van Den Eynde, B. J., Van Der Bruggen, P. & Boon, T. 2014. Tumour antigens recognized by T lymphocytes: at the core of cancer immunotherapy. *Nature Reviews Cancer,* 14**,** 135-146.

Crispe, I. N. 2009. The liver as a lymphoid organ. *Annu Rev Immunol,* 27**,** 147-63.

De Simone, V., Pallone, F., Monteleone, G. & Stolfi, C. 2013. Role of TH17 cytokines in the control of colorectal cancer. *Oncoimmunology,* 2**,** e26617.

De Sousa, E. M. F., Wang, X., Jansen, M., Fessler, E., Trinh, A., De Rooij, L. P., De Jong, J. H., De Boer, O. J., Van Leersum, R., Bijlsma, M. F., Rodermond, H., Van Der Heijden, M., Van Noesel, C. J., Tuynman, J. B., Dekker, E., Markowetz, F., Medema, J. P. & Vermeulen, L. 2013. Poor-prognosis colon cancer is defined by a molecularly distinct subtype and develops from serrated precursor lesions. *Nat Med,* 19**,** 614-8.

Deaton, A. M. & Bird, A. 2011. CpG islands and the regulation of transcription. *Genes Dev,* 25**,** 1010-22.

Dejea, C. M., Wick, E. C., Hechenbleikner, E. M., White, J. R., Mark Welch, J. L., Rossetti, B. J., Peterson, S. N., Snesrud, E. C., Borisy, G. G., Lazarev, M., Stein, E., Vadivelu, J., Roslani, A. C., Malik, A. A., Wanyiri, J. W., Goh, K. L., Thevambiga, I., Fu, K., Wan, F., Llosa, N., Housseau, F., Romans, K., Wu, X., Mcallister, F. M., Wu, S., Vogelstein, B., Kinzler, K. W., Pardoll, D. M. & Sears,

C. L. 2014. Microbiota organization is a distinct feature of proximal colorectal cancers. *Proc Natl Acad Sci U S A,* 111**,** 18321-6.

Delgado-Canedo, A., Santos, D. G., Chies, J. A., Kvitko, K. & Nardi, N. B. 2006. Optimization of an electroporation protocol using the K562 cell line as a model: role of cell cycle phase and cytoplasmic DNAses. *Cytotechnology,* 51**,** 141-8.

Diederichsen, A. C. P., V. B. Hjelmborg, J., Christensen, P. B., Zeuthen, J. & Fenger, C. 2003. Prognostic value of the CD4+/CD8+ ratio of tumour infiltrating lymphocytes in colorectal cancer and HLA-DR expression on tumour cells. *Cancer Immunology, Immunotherapy,* 52**,** 423-428.

Drake, C. G., Lipson, E. J. & Brahmer, J. R. 2014. Breathing new life into immunotherapy: review of melanoma, lung and kidney cancer. *Nat Rev Clin Oncol,* 11**,** 24-37.

Drescher, K. M., Sharma, P. & Lynch, H. T. 2010. Current hypotheses on how microsatellite instability leads to enhanced survival of Lynch Syndrome patients. *Clin Dev Immunol,* 2010**,** 170432.

Dunn, G. P., Old, L. J. & Schreiber, R. D. 2004. The three Es of cancer immunoediting. *Annu Rev Immunol,* 22**,** 329-60.

Eshleman, J. R., Z., L. E., Bowerfind, G. K., Parsons, R., Vogelstein, B., Willson, J. K., Veigl, M. L., Sedwick, W. D. & Markowitz, S. D. 1995. Increased mutation rate at the hprt locus accompanies microsatellite instability in colon cancer. *Oncogene,* 10**,** 33-37.

Fearon, E. R., Cho, K. R., Nigro, J. M., Kern, S. E., Simons, J. W., Ruppert, J. M., Hamilton, S. R., Preisinger, A. C., Thomas, G., Kinzler, K. W. & Et Al. 1990. Identification of a chromosome 18q gene that is altered in colorectal cancers. *Science,* 247**,** 49-56.

Fearon, E. R. & Vogelstein, B. 1990. A genetic model for colorectal tumorigenesis. *Cell,* 61**,** 759-67.

Fossati, M., Buzzonetti, A., Monego, G., Catzola, V., Scambia, G., Fattorossi, A. & Battaglia, A. 2015. Immunological changes in the ascites of cancer patients after intraperitoneal administration of the bispecific antibody catumaxomab (anti-EpCAMxanti-CD3). *Gynecol Oncol,* 138**,** 343-51.

Freeman, G. J., Long, A. J., Iwai, Y., Bourque, K., Chernova, T., Nishimura, H., Fitz, L. J., Malenkovich, N., Okazaki, T., Byrne, M. C., Horton, H. F., Fouser, L., Carter, L., Ling, V., Bowman, M. R., Carreno, B. M., Collins, M., Wood, C. R. & Honjo, T. 2000. Engagement of the PD-1 immunoinhibitory receptor by a novel

B7 family member leads to negative regulation of lymphocyte activation. *J Exp Med,* 192**,** 1027-34.

Fridman, W. H., Pages, F., Sautes-Fridman, C. & Galon, J. 2012. The immune contexture in human tumours: impact on clinical outcome. *Nat Rev Cancer,* 12**,** 298-306.

Fukuoka, S., Hara, H., Takahashi, N., Kojima, T., Kawazoe, A., Asayama, M., Yoshii, T., Kotani, D., Tamura, H., Mikamoto, Y., Hirano, N., Wakabayashi, M., Nomura, S., Sato, A., Kuwata, T., Togashi, Y., Nishikawa, H. & Shitara, K. 2020. Regorafenib Plus Nivolumab in Patients With Advanced Gastric or Colorectal Cancer: An Open-Label, Dose-Escalation, and Dose-Expansion Phase Ib Trial (REGONIVO, EPOC1603). *Journal of Clinical Oncology,* 38**,** 2053-2061.

Galon, J., Costes, A., Sanchez-Cabo, F., Kirilovsky, A., Mlecnik, B., Lagorce-Pages, C., Tosolini, M., Camus, M., Berger, A., Wind, P., Zinzindohoue, F., Bruneval, P., Cugnenc, P. H., Trajanoski, Z., Fridman, W. H. & Pages, F. 2006. Type, density, and location of immune cells within human colorectal tumors predict clinical outcome. *Science,* 313**,** 1960-4.

Galon, J., Pages, F., Marincola, F. M., Angell, H. K., Thurin, M., Lugli, A., Zlobec, I., Berger, A., Bifulco, C., Botti, G., Tatangelo, F., Britten, C. M., Kreiter, S., Chouchane, L., Delrio, P., Arndt, H., Asslaber, M., Maio, M., Masucci, G. V., Mihm, M., Vidal-Vanaclocha, F., Allison, J. P., Gnjatic, S., Hakansson, L., Huber, C., Singh-Jasuja, H., Ottensmeier, C., Zwierzina, H., Laghi, L., Grizzi, F., Ohashi, P. S., Shaw, P. A., Clarke, B. A., Wouters, B. G., Kawakami, Y., Hazama, S., Okuno, K., Wang, E., O'donnell-Tormey, J., Lagorce, C., Pawelec, G., Nishimura, M. I., Hawkins, R., Lapointe, R., Lundqvist, A., Khleif, S. N., Ogino, S., Gibbs, P., Waring, P., Sato, N., Torigoe, T., Itoh, K., Patel, P. S., Shukla, S. N., Palmqvist, R., Nagtegaal, I. D., Wang, Y., D'arrigo, C., Kopetz, S., Sinicrope, F. A., Trinchieri, G., Gajewski, T. F., Ascierto, P. A. & Fox, B. A. 2012. Cancer classification using the Immunoscore: a worldwide task force. *J Transl Med,* 10**,** 205.

Garon, E. B., Rizvi, N. A., Hui, R., Leighl, N., Balmanoukian, A. S., Eder, J. P., Patnaik, A., Aggarwal, C., Gubens, M., Horn, L., Carcereny, E., Ahn, M.-J., Felip, E., Lee, J.-S., Hellmann, M. D., Hamid, O., Goldman, J. W., Soria, J.-C., Dolled-Filhart, M., Rutledge, R. Z., Zhang, J., Lunceford, J. K., Rangwala, R., Lubiniecki, G. M., Roach, C., Emancipator, K. & Gandhi, L. 2015. Pembrolizumab for the Treatment of Non–Small-Cell Lung Cancer. *New England Journal of Medicine,* 372**,** 2018-2028.

Giannakis, M., Mu, X. J., Shukla, S. A., Qian, Z. R., Cohen, O., Nishihara, R., Bahl, S., Cao, Y., Amin-Mansour, A., Yamauchi, M., Sukawa, Y., Stewart, C., Rosenberg, M., Mima, K., Inamura, K., Nosho, K., Nowak, J. A., Lawrence, M. S., Giovannucci, E. L., Chan, A. T., Ng, K., Meyerhardt, J. A., Van Allen, E. M.,

Getz, G., Gabriel, S. B., Lander, E. S., Wu, C. J., Fuchs, C. S., Ogino, S. & Garraway, L. A. 2016. Genomic Correlates of Immune-Cell Infiltrates in Colorectal Carcinoma. *Cell Rep,* 17**,** 1206.

Goere, D., Flament, C., Rusakiewicz, S., Poirier-Colame, V., Kepp, O., Martins, I., Pesquet, J., Eggermont, A., Elias, D., Chaput, N. & Zitvogel, L. 2013. Potent immunomodulatory effects of the trifunctional antibody catumaxomab. *Cancer Res,* 73**,** 4663-73.

Goldstein, J., Tran, B., Ensor, J., Gibbs, P., Wong, H. L., Wong, S. F., Vilar, E., Tie, J., Broaddus, R., Kopetz, S., Desai, J. & Overman, M. J. 2014. Multicenter retrospective analysis of metastatic colorectal cancer (CRC) with high-level microsatellite instability (MSI-H). *Ann Oncol,* 25**,** 1032-8.

Gong, J., Wang, C., Lee, P. P., Chu, P. & Fakih, M. 2017. Response to PD-1 Blockade in Microsatellite Stable Metastatic Colorectal Cancer Harboring a POLE Mutation. *J Natl Compr Canc Netw,* 15**,** 142-147.

Goodman, A. M., Sokol, E. S., Frampton, G. M., Lippman, S. M. & Kurzrock, R. 2019. Microsatellite-Stable Tumors with High Mutational Burden Benefit from Immunotherapy. *Cancer Immunology Research,* 7**,** 1570-1573.

Grinnell, R. S. & Lane, N. 1958. Benign and malignant adenomatous polyps and papillary adenomas of the colon and rectum; an analysis of 1,856 tumors in 1,335 patients. *Int Abstr Surg.,* 106**,** 519-538.

Gryfe, R., Kim, H., Hsieh, E. T., Aronson, M. D., Holowaty, E. J., Bull, S. B., Redston, M. & Gallinger, S. 2000. Tumor microsatellite instability and clinical outcome in young patients with colorectal cancer. *N Engl J Med,* 342**,** 69-77.

Guinney, J., Dienstmann, R., Wang, X., De Reynies, A., Schlicker, A., Soneson, C., Marisa, L., Roepman, P., Nyamundanda, G., Angelino, P., Bot, B. M., Morris, J. S., Simon, I. M., Gerster, S., Fessler, E., De Sousa, E. M. F., Missiaglia, E., Ramay, H., Barras, D., Homicsko, K., Maru, D., Manyam, G. C., Broom, B., Boige, V., Perez-Villamil, B., Laderas, T., Salazar, R., Gray, J. W., Hanahan, D., Tabernero, J., Bernards, R., Friend, S. H., Laurent-Puig, P., Medema, J. P., Sadanandam, A., Wessels, L., Delorenzi, M., Kopetz, S., Vermeulen, L. & Tejpar, S. 2015. The consensus molecular subtypes of colorectal cancer. *Nat Med,* 21**,** 1350-6.

Gur, C., Ibrahim, Y., Isaacson, B., Yamin, R., Abed, J., Gamliel, M., Enk, J., Bar-On, Y., Stanietsky-Kaynan, N., Coppenhagen-Glazer, S., Shussman, N., Almogy, G., Cuapio, A., Hofer, E., Mevorach, D., Tabib, A., Ortenberg, R., Markel, G., Miklić, K., Jonjic, S., Brennan, C. A., Garrett, W. S., Bachrach, G. & Mandelboim, O. 2015. Binding of the Fap2 Protein of Fusobacterium nucleatum

to Human Inhibitory Receptor TIGIT Protects Tumors from Immune Cell Attack. *Immunity,* 42**,** 344-355.

Halama, N., Michel, S., Kloor, M., Zoernig, I., Benner, A., Spille, A., Pommerencke, T., Von Knebel, D. M., Folprecht, G., Luber, B., Feyen, N., Martens, U. M., Beckhove, P., Gnjatic, S., Schirmacher, P., Herpel, E., Weitz, J., Grabe, N. & Jaeger, D. 2011. Localization and density of immune cells in the invasive margin of human colorectal cancer liver metastases are prognostic for response to chemotherapy. *Cancer Res,* 71**,** 5670-7.

Halama, N., Michel, S., Kloor, M., Zoernig, I., Pommerencke, T., Von Knebel Doeberitz, M., Schirmacher, P., Weitz, J., Grabe, N. & Jager, D. 2009. The localization and density of immune cells in primary tumors of human metastatic colorectal cancer shows an association with response to chemotherapy. *Cancer Immun,* 9**,** 1.

Haraldsdottir, S. 2017. Microsatellite Instability Testing Using Next-Generation Sequencing Data and Therapy Implications. *JCO Precision Oncology***,** 1-4.

Harris, J. E., Ryan, L., Hoover, H. C., Jr., Stuart, R. K., Oken, M. M., Benson, A. B., 3rd, Mansour, E., Haller, D. G., Manola, J. & Hanna, M. G., Jr. 2000. Adjuvant active specific immunotherapy for stage II and III colon cancer with an autologous tumor cell vaccine: Eastern Cooperative Oncology Group Study E5283. *J Clin Oncol,* 18**,** 148-57.

Hazama, S., Nakamura, Y., Tanaka, H., Hirakawa, K., Tahara, K., Shimizu, R., Ozasa, H., Etoh, R., Sugiura, F., Okuno, K., Furuya, T., Nishimura, T., Sakata, K., Yoshimatsu, K., Takenouchi, H., Tsunedomi, R., Inoue, Y., Kanekiyo, S., Shindo, Y., Suzuki, N., Yoshino, S., Shinozaki, H., Kamiya, A., Furukawa, H., Yamanaka, T., Fujita, T., Kawakami, Y. & Oka, M. 2014. A phase II study of five peptides combination with oxaliplatin-based chemotherapy as a first-line therapy for advanced colorectal cancer (FXV study). *J Transl Med,* 12**,** 108.

He, Y. W., Deftos, M. L., Ojala, E. W. & Bevan, M. J. 1998. RORgamma t, a novel isoform of an orphan receptor, negatively regulates Fas ligand expression and IL-2 production in T cells. *Immunity,* 9**,** 797-806.

Herrmann, I., Baeuerle, P. A., Friedrich, M., Murr, A., Filusch, S., Ruttinger, D., Majdoub, M. W., Sharma, S., Kufer, P., Raum, T. & Munz, M. 2010. Highly efficient elimination of colorectal tumor-initiating cells by an EpCAM/CD3-bispecific antibody engaging human T cells. *PLoS One,* 5**,** e13474.

Hollingsworth, R. E. & Jansen, K. 2019. Turning the corner on therapeutic cancer vaccines. *NPJ Vaccines,* 4**,** 7.

Hooper, L. V., Littman, D. R. & Macpherson, A. J. 2012. Interactions Between the Microbiota and the Immune System. *Science,* 336**,** 1268-1273.

Hoover Jr, H. C., Brandhorst, J. S., Peters, L. C., Surdyke, M. G., Takeshita, Y., Madariaga, J., Muenz, L. R. & Hanna Jr, M. G. 1993. Adjuvant active specific immunotherapy for human colorectal cancer: 6.5-year median follow-up of a phase III prospectively randomized trial. *Journal of Clinical Oncology,* 11**,** 390-399.

Hörig, H., Lee, D. S., Conkright, W., Divito, J., Hasson, H., Lamare, M., Rivera, A., Park, D., Tine, J., Guito, K., Tsang, K. W.-Y., Schlom, J. & Kaufman, H. L. 2000. Phase I clinical trial of a recombinant canarypoxvirus (ALVAC) vaccine expressing human carcinoembryonic antigen and the B7.1 co-stimulatory molecule. *Cancer Immunology, Immunotherapy,* 49**,** 504-514.

Illingworth, R. S., Gruenewald-Schneider, U., Webb, S., Kerr, A. R., James, K. D., Turner, D. J., Smith, C., Harrison, D. J., Andrews, R. & Bird, A. P. 2010. Orphan CpG islands identify numerous conserved promoters in the mammalian genome. *PLoS Genet,* 6**,** e1001134.

Ivanov, Ii, Mckenzie, B. S., Zhou, L., Tadokoro, C. E., Lepelley, A., Lafaille, J. J., Cua, D. J. & Littman, D. R. 2006. The orphan nuclear receptor RORgammat directs the differentiation program of proinflammatory IL-17+ T helper cells. *Cell,* 126**,** 1121-33.

Jansen, A. M., Van Wezel, T., Van Den Akker, B. E., Ventayol Garcia, M., Ruano, D., Tops, C. M., Wagner, A., Letteboer, T. G., Gomez-Garcia, E. B., Devilee, P., Wijnen, J. T., Hes, F. J. & Morreau, H. 2016. Combined mismatch repair and POLE/POLD1 defects explain unresolved suspected Lynch syndrome cancers. *Eur J Hum Genet,* 24**,** 1089-92.

Jass, J. R. 2003. Serrated adenoma of the colorectum: a lesion with teeth. *Am J Pathol,* 162**,** 705-8.

Jiang, S., Good, D. & Wei, M. Q. 2019. Vaccinations for Colorectal Cancer: Progress, Strategies, and Novel Adjuvants. *Int J Mol Sci,* 20.

Jobin, C. 2013. Colorectal Cancer: Looking for Answers in the Microbiota. *Cancer Discovery,* 3**,** 384-387.

Johnson, L. A. & June, C. H. 2017. Driving gene-engineered T cell immunotherapy of cancer. *Cell Res,* 27**,** 38-58.

Katz, S. C., Burga, R. A., Mccormack, E., Wang, L. J., Mooring, W., Point, G. R., Khare, P. D., Thorn, M., Ma, Q., Stainken, B. F., Assanah, E. O., Davies, R., Espat, N.

J. & Junghans, R. P. 2015. Phase I Hepatic Immunotherapy for Metastases Study of Intra-Arterial Chimeric Antigen Receptor-Modified T-cell Therapy for CEA+ Liver Metastases. *Clin Cancer Res,* 21**,** 3149-59.

Katz, S. C., Pillarisetty, V., Bamboat, Z. M., Shia, J., Hedvat, C., Gonen, M., Jarnagin, W., Fong, Y., Blumgart, L., D'angelica, M. & Dematteo, R. P. 2009. T cell infiltrate predicts long-term survival following resection of colorectal cancer liver metastases. *Ann Surg Oncol,* 16**,** 2524-30.

Katz, S. C., Pillarisetty, V. G., Bleier, J. I., Kingham, T. P., Chaudhry, U. I., Shah, A. B. & Dematteo, R. P. 2005. Conventional liver CD4 T cells are functionally distinct and suppressed by environmental factors. *Hepatology,* 42**,** 293-300.

Kaufman, H. L., Lenz, H. J., Marshall, J., Singh, D., Garett, C., Cripps, C., Moore, M., Von Mehren, M., Dalfen, R., Heim, W. J., Conry, R. M., Urba, W. J., Benson, A. B., 3rd, Yu, M., Caterini, J., Kim-Schulze, S., Debenedette, M., Salha, D., Vogel, T., Elias, I. & Berinstein, N. L. 2008. Combination chemotherapy and ALVAC-CEA/B7.1 vaccine in patients with metastatic colorectal cancer. *Clin Cancer Res,* 14**,** 4843-9.

Kautto, E. A., Bonneville, R., Miya, J., Yu, L., Krook, M. A., Reeser, J. W. & Roychowdhury, S. 2017. Performance evaluation for rapid detection of pan-cancer microsatellite instability with MANTIS. *Oncotarget,* 8**,** 7452-7463.

Kawakami, H., Zaanan, A. & Sinicrope, F. A. 2015. Microsatellite Instability Testing and Its Role in the Management of Colorectal Cancer. *Current Treatment Options in Oncology,* 16**,** 30.

Kim, B. K., Han, K. H. & Ahn, S. H. 2011. Prevention of hepatocellular carcinoma in patients with chronic hepatitis B virus infection. *Oncology,* 81 Suppl 1**,** 41-9.

Kim, K., Kim, H. S., Kim, J. Y., Jung, H., Sun, J.-M., Ahn, J. S., Ahn, M.-J., Park, K., Lee, S.-H. & Choi, J. K. 2020. Predicting clinical benefit of immunotherapy by antigenic or functional mutations affecting tumour immunogenicity. *Nature Communications,* 11.

Kim, R., Emi, M. & Tanabe, K. 2007. Cancer immunoediting from immune surveillance to immune escape. *Immunology,* 121**,** 1-14.

Knolle, P. A. & Gerken, G. 2000. Local control of the immune response in the liver. *Immunol Rev,* 174**,** 21-34.

Knudson, A. G., Jr. 1971. Mutation and cancer: statistical study of retinoblastoma. *Proc Natl Acad Sci U S A,* 68**,** 820-3.

Kreidieh, M., Mukherji, D., Temraz, S. & Shamseddine, A. 2020. Expanding the Scope of Immunotherapy in Colorectal Cancer: Current Clinical Approaches and Future Directions. *Biomed Res Int,* 2020**,** 9037217.

Krummel, M. F. & Allison, J. P. 1995. CD28 and CTLA-4 have opposing effects on the response of T cells to stimulation. *J Exp Med,* 182**,** 459-65.

Ladoire, S., Martin, F. & Ghiringhelli, F. 2011. Prognostic role of FOXP3+ regulatory T cells infiltrating human carcinomas: the paradox of colorectal cancer. *Cancer Immunol Immunother,* 60**,** 909-18.

Lal, N., Beggs, A. D., Willcox, B. E. & Middleton, G. W. 2015. An immunogenomic stratification of colorectal cancer: Implications for development of targeted immunotherapy. *Oncoimmunology,* 4**,** e976052.

Lao, V. V. & Grady, W. M. 2011. Epigenetics and colorectal cancer. *Nat Rev Gastroenterol Hepatol,* 8**,** 686-700.

Larocca, C. & Schlom, J. 2011. Viral vector-based therapeutic cancer vaccines. *Cancer J,* 17**,** 359-71.

Latchman, Y., Wood, C. R., Chernova, T., Chaudhary, D., Borde, M., Chernova, I., Iwai, Y., Long, A. J., Brown, J. A., Nunes, R., Greenfield, E. A., Bourque, K., Boussiotis, V. A., Carter, L. L., Carreno, B. M., Malenkovich, N., Nishimura, H., Okazaki, T., Honjo, T., Sharpe, A. H. & Freeman, G. J. 2001. PD-L2 is a second ligand for PD-1 and inhibits T cell activation. *Nat Immunol,* 2**,** 261-8.

Lazarevic, V., Glimcher, L. H. & Lord, G. M. 2013. T-bet: a bridge between innate and adaptive immunity. *Nature Reviews Immunology,* 13**,** 777-789.

Le, D. T., Durham, J. N., Smith, K. N., Wang, H., Bartlett, B. R., Aulakh, L. K., Lu, S., Kemberling, H., Wilt, C., Luber, B. S., Wong, F., Azad, N. S., Rucki, A. A., Laheru, D., Donehower, R., Zaheer, A., Fisher, G. A., Crocenzi, T. S., Lee, J. J., Greten, T. F., Duffy, A. G., Ciombor, K. K., Eyring, A. D., Lam, B. H., Joe, A., Kang, S. P., Holdhoff, M., Danilova, L., Cope, L., Meyer, C., Zhou, S., Goldberg, R. M., Armstrong, D. K., Bever, K. M., Fader, A. N., Taube, J., Housseau, F., Spetzler, D., Xiao, N., Pardoll, D. M., Papadopoulos, N., Kinzler, K. W., Eshleman, J. R., Vogelstein, B., Anders, R. A. & Diaz, L. A., Jr. 2017. Mismatch repair deficiency predicts response of solid tumors to PD-1 blockade. *Science,* 357**,** 409-413.

Le, D. T., Kim, T. W., Van Cutsem, E., Geva, R., Jager, D., Hara, H., Burge, M., O'neil, B., Kavan, P., Yoshino, T., Guimbaud, R., Taniguchi, H., Elez, E., Al-Batran, S. E., Boland, P. M., Crocenzi, T., Atreya, C. E., Cui, Y., Dai, T., Marinello, P., Diaz, L. A., Jr. & Andre, T. 2020. Phase II Open-Label Study of Pembrolizumab

in Treatment-Refractory, Microsatellite Instability-High/Mismatch Repair-Deficient Metastatic Colorectal Cancer: KEYNOTE-164. *J Clin Oncol,* 38**,** 11-19.

Le, D. T., Pardoll, D. M. & Jaffee, E. M. 2010. Cellular vaccine approaches. *Cancer J,* 16**,** 304-10.

Le, D. T., Uram, J. N., Wang, H., Bartlett, B. R., Kemberling, H., Eyring, A. D., Skora, A. D., Luber, B. S., Azad, N. S., Laheru, D., Biedrzycki, B., Donehower, R. C., Zaheer, A., Fisher, G. A., Crocenzi, T. S., Lee, J. J., Duffy, S. M., Goldberg, R. M., De La Chapelle, A., Koshiji, M., Bhaijee, F., Huebner, T., Hruban, R. H., Wood, L. D., Cuka, N., Pardoll, D. M., Papadopoulos, N., Kinzler, K. W., Zhou, S., Cornish, T. C., Taube, J. M., Anders, R. A., Eshleman, J. R., Vogelstein, B. & Diaz, L. A., Jr. 2015. PD-1 Blockade in Tumors with Mismatch-Repair Deficiency. *N Engl J Med,* 372**,** 2509-20.

Lee, H. E., Chae, S. W., Lee, Y. J., Kim, M. A., Lee, H. S., Lee, B. L. & Kim, W. H. 2008. Prognostic implications of type and density of tumour-infiltrating lymphocytes in gastric cancer. *Br J Cancer,* 99**,** 1704-11.

Lee, L. H., Cavalcanti, M. S., Segal, N. H., Hechtman, J. F., Weiser, M. R., Smith, J. J., Garcia-Aguilar, J., Sadot, E., Ntiamoah, P., Markowitz, A. J., Shike, M., Stadler, Z. K., Vakiani, E., Klimstra, D. S. & Shia, J. 2016. Patterns and prognostic relevance of PD-1 and PD-L1 expression in colorectal carcinoma. *Modern Pathology,* 29**,** 1433-1442.

Levy, A. N. & Allegretti, J. R. 2019. Insights into the role of fecal microbiota transplantation for the treatment of inflammatory bowel disease. *Therapeutic Advances in Gastroenterology,* 12**,** 175628481983689.

Lindor, N. M., Burgart, L. J., Leontovich, O., Goldberg, R. M., Cunningham, J. M., Sargent, D. J., Walsh-Vockley, C., Petersen, G. M., Walsh, M. D., Leggett, B. A., Young, J. P., Barker, M. A., Jass, J. R., Hopper, J., Gallinger, S., Bapat, B., Redston, M. & Thibodeau, S. N. 2002. Immunohistochemistry Versus Microsatellite Instability Testing in Phenotyping Colorectal Tumors. *Journal of Clinical Oncology,* 20**,** 1043-1048.

Ling, A., Lundberg, I. V., Eklof, V., Wikberg, M. L., Oberg, A., Edin, S. & Palmqvist, R. 2016. The infiltration, and prognostic importance, of Th1 lymphocytes vary in molecular subgroups of colorectal cancer. *J Pathol Clin Res,* 2**,** 21-31.

Linnemann, C., Van Buuren, M. M., Bies, L., Verdegaal, E. M., Schotte, R., Calis, J. J., Behjati, S., Velds, A., Hilkmann, H., Atmioui, D. E., Visser, M., Stratton, M. R., Haanen, J. B., Spits, H., Van Der Burg, S. H. & Schumacher, T. N. 2015. High-throughput epitope discovery reveals frequent recognition of neo-antigens by CD4+ T cells in human melanoma. *Nat Med,* 21**,** 81-5.

Liu, Q., Zhang, H., Jiang, X., Qian, C., Liu, Z. & Luo, D. 2017. Factors involved in cancer metastasis: a better understanding to "seed and soil" hypothesis. *Mol Cancer,* 16**,** 176.

Llosa, N. J., Cruise, M., Tam, A., Wicks, E. C., Hechenbleikner, E. M., Taube, J. M., Blosser, R. L., Fan, H., Wang, H., Luber, B. S., Zhang, M., Papadopoulos, N., Kinzler, K. W., Vogelstein, B., Sears, C. L., Anders, R. A., Pardoll, D. M. & Housseau, F. 2015. The vigorous immune microenvironment of microsatellite instable colon cancer is balanced by multiple counter-inhibitory checkpoints. *Cancer Discov,* 5**,** 43-51.

Loeb, L. A., Loeb, K. R. & Anderson, J. P. 2003. Multiple mutations and cancer. *Proc Natl Acad Sci U S A,* 100**,** 776-81.

Long, H. M., Leese, A. M., Chagoury, O. L., Connerty, S. R., Quarcoopome, J., Quinn, L. L., Shannon-Lowe, C. & Rickinson, A. B. 2011. Cytotoxic CD4+T Cell Responses to EBV Contrast with CD8 Responses in Breadth of Lytic Cycle Antigen Choice and in Lytic Cycle Recognition. *The Journal of Immunology,* 187**,** 92-101.

Lu, L., Barbi, J. & Pan, F. 2017. The regulation of immune tolerance by FOXP3. *Nature Reviews Immunology,* 17**,** 703-717.

Lutterbuese, R., Raum, T., Kischel, R., Hoffmann, P., Mangold, S., Rattel, B., Friedrich, M., Thomas, O., Lorenczewski, G., Rau, D., Schaller, E., Herrmann, I., Wolf, A., Urbig, T., Baeuerle, P. A. & Kufer, P. 2010. T cell-engaging BiTE antibodies specific for EGFR potently eliminate KRAS- and BRAF-mutated colorectal cancer cells. *Proc Natl Acad Sci U S A,* 107**,** 12605-10.

Lutterbuese, R., Raum, T., Kischel, R., Lutterbuese, P., Schlereth, B., Schaller, E., Mangold, S., Rau, D., Meier, P., Kiener, P. A., Mulgrew, K., Oberst, M. D., Hammond, S. A., Baeuerle, P. A. & Kufer, P. 2009. Potent control of tumor growth by CEA/CD3-bispecific single-chain antibody constructs that are not competitively inhibited by soluble CEA. *J Immunother,* 32**,** 341-52.

Madabhushi, A. & Lee, G. 2016. Image analysis and machine learning in digital pathology: Challenges and opportunities. *Medical Image Analysis,* 33**,** 170-175.

Magee, M. S., Abraham, T. S., Baybutt, T. R., Flickinger, J. C., Jr., Ridge, N. A., Marszalowicz, G. P., Prajapati, P., Hersperger, A. R., Waldman, S. A. & Snook, A. E. 2018. Human GUCY2C-Targeted Chimeric Antigen Receptor (CAR)-Expressing T Cells Eliminate Colorectal Cancer Metastases. *Cancer Immunol Res,* 6**,** 509-516.

Mäkinen, M. J. 2007. Colorectal serrated adenocarcinoma. *Histopathology,* 50**,** 131-150.

Malesci, A., Laghi, L., Bianchi, P., Delconte, G., Randolph, A., Torri, V., Carnaghi, C., Doci, R., Rosati, R., Montorsi, M., Roncalli, M., Gennari, L. & Santoro, A. 2007. Reduced likelihood of metastases in patients with microsatellite-unstable colorectal cancer. *Clin Cancer Res,* 13**,** 3831-9.

Marisa, L., De Reynies, A., Duval, A., Selves, J., Gaub, M. P., Vescovo, L., Etienne-Grimaldi, M. C., Schiappa, R., Guenot, D., Ayadi, M., Kirzin, S., Chazal, M., Flejou, J. F., Benchimol, D., Berger, A., Lagarde, A., Pencreach, E., Piard, F., Elias, D., Parc, Y., Olschwang, S., Milano, G., Laurent-Puig, P. & Boige, V. 2013. Gene expression classification of colon cancer into molecular subtypes: characterization, validation, and prognostic value. *PLoS Med,* 10**,** e1001453.

Mau-Sorensen, M., Dittrich, C., Dienstmann, R., Lassen, U., Buchler, W., Martinius, H. & Tabernero, J. 2015. A phase I trial of intravenous catumaxomab: a bispecific monoclonal antibody targeting EpCAM and the T cell coreceptor CD3. *Cancer Chemother Pharmacol,* 75**,** 1065-73.

Merika, E., Saif, M. W., Katz, A., Syrigos, K. & Morse, M. 2010. Review. Colon cancer vaccines: an update. *In Vivo,* 24**,** 607 - 628.

Miao, D., Margolis, C. A., Vokes, N. I., Liu, D., Taylor-Weiner, A., Wankowicz, S. M., Adeegbe, D., Keliher, D., Schilling, B., Tracy, A., Manos, M., Chau, N. G., Hanna, G. J., Polak, P., Rodig, S. J., Signoretti, S., Sholl, L. M., Engelman, J. A., Getz, G., Jänne, P. A., Haddad, R. I., Choueiri, T. K., Barbie, D. A., Haq, R., Awad, M. M., Schadendorf, D., Hodi, F. S., Bellmunt, J., Wong, K.-K., Hammerman, P. & Van Allen, E. M. 2018. Genomic correlates of response to immune checkpoint blockade in microsatellite-stable solid tumors. *Nature Genetics,* 50**,** 1271-1281.

Middha, S., Zhang, L., Nafa, K., Jayakumaran, G., Wong, D., Kim, H. R., Sadowska, J., Berger, M. F., Delair, D. F., Shia, J., Stadler, Z., Klimstra, D. S., Ladanyi, M., Zehir, A. & Hechtman, J. F. 2017. Reliable Pan-Cancer Microsatellite Instability Assessment by Using Targeted Next-Generation Sequencing Data. *JCO Precis Oncol,* 2017.

Minde, D. P., Anvarian, Z., Rudiger, S. G. & Maurice, M. M. 2011. Messing up disorder: how do missense mutations in the tumor suppressor protein APC lead to cancer? *Mol Cancer,* 10**,** 101.

Mitry, E., Guiu, B., Cosconea, S., Jooste, V., Faivre, J. & Bouvier, A. M. 2010. Epidemiology, management and prognosis of colorectal cancer with lung metastases: a 30-year population-based study. *Gut,* 59**,** 1383-8.

Mlecnik, B., Bindea, G., Angell, H. K., Maby, P., Angelova, M., Tougeron, D., Church, S. E., Lafontaine, L., Fischer, M., Fredriksen, T., Sasso, M., Bilocq, A. M., Kirilovsky, A., Obenauf, A. C., Hamieh, M., Berger, A., Bruneval, P., Tuech, J. J., Sabourin, J. C., Le Pessot, F., Mauillon, J., Rafii, A., Laurent-Puig, P., Speicher, M. R., Trajanoski, Z., Michel, P., Sesboue, R., Frebourg, T., Pages, F., Valge-Archer, V., Latouche, J. B. & Galon, J. 2016a. Integrative Analyses of Colorectal Cancer Show Immunoscore Is a Stronger Predictor of Patient Survival Than Microsatellite Instability. *Immunity,* 44**,** 698-711.

Mlecnik, B., Bindea, G., Kirilovsky, A., Angell, H. K., Obenauf, A. C., Tosolini, M., Church, S. E., Maby, P., Vasaturo, A., Angelova, M., Fredriksen, T., Mauger, S., Waldner, M., Berger, A., Speicher, M. R., Pages, F., Valge-Archer, V. & Galon, J. 2016b. The tumor microenvironment and Immunoscore are critical determinants of dissemination to distant metastasis. *Sci Transl Med,* 8**,** 327ra26.

Mlecnik, B., Bindea, G., Van Den Eynde, M. & Galon, J. 2020. Metastasis immune-based scores predict patient survival. *OncoImmunology,* 9**,** 1806000.

Mlecnik, B., Van Den Eynde, M., Bindea, G., Church, S. E., Vasaturo, A., Fredriksen, T., Lafontaine, L., Haicheur, N., Marliot, F., Debetancourt, D., Pairet, G., Jouret-Mourin, A., Gigot, J.-F., Hubert, C., Danse, E., Dragean, C., Carrasco, J., Humblet, Y., Valge-Archer, V., Berger, A., Pagès, F., Machiels, J.-P. & Galon, J. 2018. Comprehensive Intrametastatic Immune Quantification and Major Impact of Immunoscore on Survival. *JNCI: Journal of the National Cancer Institute,* 110**,** 97-108.

Morse, M. A., Deng, Y., Coleman, D., Hull, S., Kitrell-Fisher, E., Nair, S., Schlom, J., Ryback, M.-E. & Lyerly, H. K. 1999. A Phase I Study of Active Immunotherapy with Carcinoembryonic Antigen Peptide (CAP-1)-pulsed, Autologous Human Cultured Dendritic Cells in Patients with Metastatic Malignancies Expressing Carcinoembryonic Antigen. *Clinical Cancer Research,* 5**,** 1331-1338.

Morse, M. A., Hochster, H. & Benson, A. 2019a. Perspectives on Treatment of Metastatic Colorectal Cancer with Immune Checkpoint Inhibitor Therapy. *The Oncologist,* 25**,** 33-45.

Morse, M. A., Overman, M. J., Hartman, L., Khoukaz, T., Brutcher, E., Lenz, H. J., Atasoy, A., Shangguan, T., Zhao, H. & El-Rayes, B. 2019b. Safety of Nivolumab plus Low-Dose Ipilimumab in Previously Treated Microsatellite Instability-High/Mismatch Repair-Deficient Metastatic Colorectal Cancer. *Oncologist,* 24**,** 1453-1461.

Morson, B. 1974. The Polyp-cancer Sequence in the Large Bowel. *Proceedings of the Royal Society of Medicine,* 67**,** 451-457.

Mortha, A., Chudnovskiy, A., Hashimoto, D., Bogunovic, M., Spencer, S. P., Belkaid, Y. & Merad, M. 2014. Microbiota-Dependent Crosstalk Between Macrophages and ILC3 Promotes Intestinal Homeostasis. *Science,* 343**,** 1249288-1249288.

Movahedi, M., Bishop, D. T., Macrae, F., Mecklin, J.-P., Moeslein, G., Olschwang, S., Eccles, D., Evans, D. G., Maher, E. R., Bertario, L., Bisgaard, M.-L., Dunlop, M. G., Ho, J. W. C., Hodgson, S. V., Lindblom, A., Lubinski, J., Morrison, P. J., Murday, V., Ramesar, R. S., Side, L., Scott, R. J., Thomas, H. J. W., Vasen, H. F., Burn, J. & Mathers, J. C. 2015. Obesity, Aspirin, and Risk of Colorectal Cancer in Carriers of Hereditary Colorectal Cancer: A Prospective Investigation in the CAPP2 Study. *Journal of Clinical Oncology,* 33**,** 3591-3597.

Mur, P., García-Mulero, S., Del Valle, J., Magraner-Pardo, L., Vidal, A., Pineda, M., Cinnirella, G., Martín-Ramos, E., Pons, T., López-Doriga, A., Belhadj, S., Feliubadaló, L., Munoz-Torres, P. M., Navarro, M., Grau, E., Darder, E., Llort, G., Sanz, J., Ramón Y Cajal, T., Balmana, J., Brunet, J., Moreno, V., Piulats, J. M., Matías-Guiu, X., Sanz-Pamplona, R., Aligué, R., Capellá, G., Lázaro, C. & Valle, L. 2020. Role of POLE and POLD1 in familial cancer. *Genetics in Medicine,* 22**,** 2089-2100.

Naito, Y., Saito, K., Shiiba, K., Ohuchi, A., Saigenji, K., Nagura, H. & Ohtani, H. 1998. CD8+ T cells infiltrated within cancer cell nests as a prognostic factor in human colorectal cancer. *Cancer Research,* 58**,** 3491.

Nct02324257. *An Open-Label, Multicenter, Dose-Escalation Phase I Study to Evaluate the Safety, Pharmacokinetics, and Therapeutic Activity of RO6958688, A Novel T-cell Bispecific Antibody That Targets the Human Carcinoembryonic Antigen (CEA) on Tumor Cells and CD3 on T Cells, Administered Intravenously in Patients With Locally Advanced and/or Metastatic CEA(+) Solid Tumors* [Online]. NIH. Available: https://clinicaltrials.gov/ct2/show/NCT02324257 [Accessed 09/07/2020].

Nct02563002. *A Phase III Study of Pembrolizumab (MK-3475) vs. Chemotherapy in Microsatellite Instability-High (MSI-H) or Mismatch Repair Deficient (dMMR) Stage IV Colorectal Carcinoma (KEYNOTE-177)* [Online]. NIH. Available: https://clinicaltrials.gov/ct2/show/NCT02563002 [Accessed 01/07/2020].

Nct02650713. *An Open-Label, Multicenter, Dose Escalation and Expansion Phase Ib Study to Evaluate the Safety, Pharmacokinetics, and Therapeutic Activity of RO6958688 in Combination With Atezolizumab in Patients With Locally Advanced and/or Metastatic CEA-Positive Solid Tumors* [Online]. NIH. Available: https://clinicaltrials.gov/ct2/show/NCT02650713 [Accessed 09/07/2020].

Nct02912559. *Randomized Trial of Standard Chemotherapy Alone or Combined With Atezolizumab as Adjuvant Therapy for Patients With Stage III Colon Cancer and*

Deficient DNA Mismatch Repair [Online]. NIH. Available: https://clinicaltrials.gov/ct2/show/study/NCT02912559 [Accessed 01/07/2020].

Nct03026140. *Nivolumab, Ipilimumab and COX2-inhibition in Early Stage Colon Cancer: an Unbiased Approach for Signals of Sensitivity: The NICHE TRIAL* [Online]. NIH. Available: https://clinicaltrials.gov/ct2/show/NCT03026140 [Accessed 01/07/2020].

Nct03981146. *A Phase II Trial Assessing Nivolumab in Class II Expressing Microsatellite Stable Colorectal Cancer ANICCA-Class II* [Online]. NIH. Available: https://clinicaltrials.gov/ct2/show/NCT03981146 [Accessed 18/09/2020].

Nct04017455. *Neoadjuvant Treatment in Rectal Cancer With Radiotherapy Followed by Atezolizumab and Bevacizumab (TARZAN)* [Online]. NIH. Available: https://clinicaltrials.gov/ct2/show/NCT04017455 [Accessed].

Nguyen, H. T. & Duong, H. Q. 2018. The molecular characteristics of colorectal cancer: Implications for diagnosis and therapy. *Oncol Lett,* 16**,** 9-18.

Nieuwenhuis, M. H. & Vasen, H. F. 2007. Correlations between mutation site in APC and phenotype of familial adenomatous polyposis (FAP): a review of the literature. *Crit Rev Oncol Hematol,* 61**,** 153-61.

Nosho, K., Irahara, N., Shima, K., Kure, S., Kirkner, G. J., Schernhammer, E. S., Hazra, A., Hunter, D. J., Quackenbush, J., Spiegelman, D., Giovannucci, E. L., Fuchs, C. S. & Ogino, S. 2008. Comprehensive biostatistical analysis of CpG island methylator phenotype in colorectal cancer using a large population-based sample. *PLoS One,* 3**,** e3698.

Novelli, M., Savoia, P., Cambieri, I., Ponti, R., Comessatti, A., Lisa, F. & Bernengo, M. G. 2000. Collagenase digestion and mechanical disaggregation as a method to extract and immunophenotype tumour lymphocytes in cutaneous T-cell lymphomas. Experimental dermatology . Original article. *Clinical and Experimental Dermatology,* 25**,** 423-431.

Ogino, S., Kawasaki, T., Kirkner, G. J., Loda, M. & Fuchs, C. S. 2006. CpG island methylator phenotype-low (CIMP-low) in colorectal cancer: possible associations with male sex and KRAS mutations. *J Mol Diagn,* 8**,** 582-8.

Ogino, S., Kawasaki, T., Kirkner, G. J., Ohnishi, M. & Fuchs, C. S. 2007. 18q loss of heterozygosity in microsatellite stable colorectal cancer is correlated with CpG island methylator phenotype-negative (CIMP-0) and inversely with CIMP-low and CIMP-high. *BMC Cancer,* 7**,** 72.

Osada, T., Patel, S. P., Hammond, S. A., Osada, K., Morse, M. A. & Lyerly, H. K. 2015. CEA/CD3-bispecific T cell-engaging (BiTE) antibody-mediated T lymphocyte cytotoxicity maximized by inhibition of both PD1 and PD-L1. *Cancer Immunol Immunother,* 64**,** 677-88.

Overman, M. J., Ernstoff, M. S. & Morse, M. A. 2018a. Where We Stand With Immunotherapy in Colorectal Cancer: Deficient Mismatch Repair, Proficient Mismatch Repair, and Toxicity Management. *American Society of Clinical Oncology Educational Book***,** 239-247.

Overman, M. J., Lonardi, S., Wong, K. Y. M., Lenz, H. J., Gelsomino, F., Aglietta, M., Morse, M. A., Van Cutsem, E., Mcdermott, R., Hill, A., Sawyer, M. B., Hendlisz, A., Neyns, B., Svrcek, M., Moss, R. A., Ledeine, J. M., Cao, Z. A., Kamble, S., Kopetz, S. & Andre, T. 2018b. Durable Clinical Benefit With Nivolumab Plus Ipilimumab in DNA Mismatch Repair-Deficient/Microsatellite Instability-High Metastatic Colorectal Cancer. *J Clin Oncol,* 36**,** 773-779.

Overman, M. J., Mcdermott, R., Leach, J. L., Lonardi, S., Lenz, H.-J., Morse, M. A., Desai, J., Hill, A., Axelson, M., Moss, R. A., Goldberg, M. V., Cao, Z. A., Ledeine, J.-M., Maglinte, G. A., Kopetz, S. & André, T. 2017. Nivolumab in patients with metastatic DNA mismatch repair-deficient or microsatellite instability-high colorectal cancer (CheckMate 142): an open-label, multicentre, phase 2 study. *The Lancet Oncology,* 18**,** 1182-1191.

Pagès, F., Mlecnik, B., Marliot, F., Bindea, G., Ou, F.-S., Bifulco, C., Lugli, A., Zlobec, I., Rau, T. T., Berger, M. D., Nagtegaal, I. D., Vink-Börger, E., Hartmann, A., Geppert, C., Kolwelter, J., Merkel, S., Grützmann, R., Van Den Eynde, M., Jouret-Mourin, A., Kartheuser, A., Léonard, D., Remue, C., Wang, J. Y., Bavi, P., Roehrl, M. H. A., Ohashi, P. S., Nguyen, L. T., Han, S., Macgregor, H. L., Hafezi-Bakhtiari, S., Wouters, B. G., Masucci, G. V., Andersson, E. K., Zavadova, E., Vocka, M., Spacek, J., Petruzelka, L., Konopasek, B., Dundr, P., Skalova, H., Nemejcova, K., Botti, G., Tatangelo, F., Delrio, P., Ciliberto, G., Maio, M., Laghi, L., Grizzi, F., Fredriksen, T., Buttard, B., Angelova, M., Vasaturo, A., Maby, P., Church, S. E., Angell, H. K., Lafontaine, L., Bruni, D., El Sissy, C., Haicheur, N., Kirilovsky, A., Berger, A., Lagorce, C., Meyers, J. P., Paustian, C., Feng, Z., Ballesteros-Merino, C., Dijkstra, J., Van De Water, C., Van Lent-Van Vliet, S., Knijn, N., Mușină, A.-M., Scripcariu, D.-V., Popivanova, B., Xu, M., Fujita, T., Hazama, S., Suzuki, N., Nagano, H., Okuno, K., Torigoe, T., Sato, N., Furuhata, T., Takemasa, I., Itoh, K., Patel, P. S., Vora, H. H., Shah, B., Patel, J. B., Rajvik, K. N., Pandya, S. J., Shukla, S. N., Wang, Y., Zhang, G., Kawakami, Y., Marincola, F. M., Ascierto, P. A., Sargent, D. J., Fox, B. A. & Galon, J. 2018. International validation of the consensus Immunoscore for the classification of colon cancer: a prognostic and accuracy study. *The Lancet,* 391**,** 2128-2139.

Pagès, F., Taieb, J., Laurent-Puig, P. & Galon, J. 2020. The consensus Immunoscore in phase 3 clinical trials; potential impact on patient management decisions. *OncoImmunology,* 9.

Palles, C., Cazier, J. B., Howarth, K. M., Domingo, E., Jones, A. M., Broderick, P., Kemp, Z., Spain, S. L., Guarino, E., Salguero, I., Sherborne, A., Chubb, D., Carvajal-Carmona, L. G., Ma, Y., Kaur, K., Dobbins, S., Barclay, E., Gorman, M., Martin, L., Kovac, M. B., Humphray, S., Consortium, C., Consortium, W. G. S., Lucassen, A., Holmes, C. C., Bentley, D., Donnelly, P., Taylor, J., Petridis, C., Roylance, R., Sawyer, E. J., Kerr, D. J., Clark, S., Grimes, J., Kearsey, S. E., Thomas, H. J., Mcvean, G., Houlston, R. S. & Tomlinson, I. 2013. Germline mutations affecting the proofreading domains of POLE and POLD1 predispose to colorectal adenomas and carcinomas. *Nat Genet,* 45**,** 136-44.

Palucka, K. & Banchereau, J. 2012. Cancer immunotherapy via dendritic cells. *Nat Rev Cancer,* 12**,** 265-77.

Paramsothy, S., Kamm, M. A., Kaakoush, N. O., Walsh, A. J., Van Den Bogaerde, J., Samuel, D., Leong, R. W. L., Connor, S., Ng, W., Paramsothy, R., Xuan, W., Lin, E., Mitchell, H. M. & Borody, T. J. 2017. Multidonor intensive faecal microbiota transplantation for active ulcerative colitis: a randomised placebo-controlled trial. *The Lancet,* 389**,** 1218-1228.

Parkhurst, M. R., Yang, J. C., Langan, R. C., Dudley, M. E., Nathan, D. A., Feldman, S. A., Davis, J. L., Morgan, R. A., Merino, M. J., Sherry, R. M., Hughes, M. S., Kammula, U. S., Phan, G. Q., Lim, R. M., Wank, S. A., Restifo, N. P., Robbins, P. F., Laurencot, C. M. & Rosenberg, S. A. 2011. T cells targeting carcinoembryonic antigen can mediate regression of metastatic colorectal cancer but induce severe transient colitis. *Mol Ther,* 19**,** 620-6.

Parra, E. R., Uraoka, N., Jiang, M., Cook, P., Gibbons, D., Forget, M.-A., Bernatchez, C., Haymaker, C., Wistuba, I. I. & Rodriguez-Canales, J. 2017. Validation of multiplex immunofluorescence panels using multispectral microscopy for immune-profiling of formalin-fixed and paraffin-embedded human tumor tissues. *Scientific Reports,* 7**,** 13380.

Pino, M. S. & Chung, D. C. 2010. The Chromosomal Instability Pathway in Colon Cancer. *Gastroenterology,* 138**,** 2059-2072.

Pishvaian, M., Morse, M. A., Mcdevitt, J., Norton, J. D., Ren, S., Robbie, G. J., Ryan, P. C., Soukharev, S., Bao, H. & Denlinger, C. S. 2016. Phase 1 Dose Escalation Study of MEDI-565, a Bispecific T-Cell Engager that Targets Human Carcinoembryonic Antigen, in Patients With Advanced Gastrointestinal Adenocarcinomas. *Clin Colorectal Cancer,* 15**,** 345-351.

Pivetta, E., Capuano, A., Scanziani, E., Minoli, L., Andreuzzi, E., Mongiat, M., Baldassarre, G., Doliana, R. & Spessotto, P. 2019. Multiplex staining depicts the immune infiltrate in colitis-induced colon cancer model. *Scientific Reports,* 9.

Polakis, P. 1997. The adenomatous polyposis coli (APC) tumor suppressor. *Biochimica et Biophysica Acta (BBA) - Reviews on Cancer,* 1332**,** F127-F147.

Popat, S., Hubner, R. & Houlston, R. S. 2005. Systematic review of microsatellite instability and colorectal cancer prognosis. *J Clin Oncol,* 23**,** 609-18.

Powell, S. M., Zilz, N., Beazer-Barclay, Y., Bryan, T. M., Hamilton, S. R., Thibodeau, S. N., Vogelstein, B. & Kinzler, K. W. 1992. APC mutations occur early during colorectal tumorigenesis. *Nature,* 359**,** 235-7.

Quezada, S. A., Simpson, T. R., Peggs, K. S., Merghoub, T., Vider, J., Fan, X., Blasberg, R., Yagita, H., Muranski, P., Antony, P. A., Restifo, N. P. & Allison, J. P. 2010. Tumor-reactive CD4+ T cells develop cytotoxic activity and eradicate large established melanoma after transfer into lymphopenic hosts. *The Journal of Experimental Medicine,* 207**,** 637-650.

Reddy, B. S., Narisawa, T., Wright, P., Vukusich, D., Weisburger, J. H. & Wynder, E. L. 1975. Colon Carcinogenesis with Azoxymethane and Dimethylhydrazine in Germ-free Rats. *Cancer Res,* 35**,** 287 - 290.

Remark, R., Alifano, M., Cremer, I., Lupo, A., Dieu-Nosjean, M. C., Riquet, M., Crozet, L., Ouakrim, H., Goc, J., Cazes, A., Flejou, J. F., Gibault, L., Verkarre, V., Regnard, J. F., Pages, O. N., Oudard, S., Mlecnik, B., Sautes-Fridman, C., Fridman, W. H. & Damotte, D. 2013. Characteristics and clinical impacts of the immune environments in colorectal and renal cell carcinoma lung metastases: influence of tumor origin. *Clin Cancer Res,* 19**,** 4079-91.

Rizvi, N. A., Hellmann, M. D., Snyder, A., Kvistborg, P., Makarov, V., Havel, J. J., Lee, W., Yuan, J., Wong, P., Ho, T. S., Miller, M. L., Rekhtman, N., Moreira, A. L., Ibrahim, F., Bruggeman, C., Gasmi, B., Zappasodi, R., Maeda, Y., Sander, C., Garon, E. B., Merghoub, T., Wolchok, J. D., Schumacher, T. N. & Chan, T. A. 2015. Cancer immunology. Mutational landscape determines sensitivity to PD-1 blockade in non-small cell lung cancer. *Science,* 348**,** 124-8.

Robert, C. 2020. A decade of immune-checkpoint inhibitors in cancer therapy. *Nature Communications,* 11.

Roden, R. B. S. & Stern, P. L. 2018. Opportunities and challenges for human papillomavirus vaccination in cancer. *Nat Rev Cancer,* 18**,** 240-254.

Roepman, P., Schlicker, A., Tabernero, J., Majewski, I., Tian, S., Moreno, V., Snel, M. H., Chresta, C. M., Rosenberg, R., Nitsche, U., Macarulla, T., Capella, G., Salazar, R., Orphanides, G., Wessels, L. F., Bernards, R. & Simon, I. M. 2014. Colorectal cancer intrinsic subtypes predict chemotherapy benefit, deficient mismatch repair and epithelial-to-mesenchymal transition. *Int J Cancer,* 134**,** 552-62.

Ropponen, K. M., Eskelinen, M. J., Lipponen, P. K., Alhava, E. & Kosma, V.-M. 1997. Prognostic value of tumour-infiltrating lymphocytes (TILs) in colorectal cancer. *The Journal of Pathology,* 182**,** 318-324.

Rosenberg, D. W., Yang, S., Pleau, D. C., Greenspan, E. J., Stevens, R. G., Rajan, T. V., Heinen, C. D., Levine, J., Zhou, Y. & O'brien, M. J. 2007. Mutations in BRAF and KRAS differentially distinguish serrated versus non-serrated hyperplastic aberrant crypt foci in humans. *Cancer Res,* 67**,** 3551-4.

Rosenberg, S. A. & Restifo, N. P. 2015. Adoptive cell transfer as personalized immunotherapy for human cancer. *Science,* 348**,** 62-68.

Ruella, M. & Kalos, M. 2014. Adoptive immunotherapy for cancer. *Immunol Rev,* 257**,** 14-38.

Sadanandam, A., Lyssiotis, C. A., Homicsko, K., Collisson, E. A., Gibb, W. J., Wullschleger, S., Ostos, L. C., Lannon, W. A., Grotzinger, C., Del Rio, M., Lhermitte, B., Olshen, A. B., Wiedenmann, B., Cantley, L. C., Gray, J. W. & Hanahan, D. 2013. A colorectal cancer classification system that associates cellular phenotype and responses to therapy. *Nat Med,* 19**,** 619-25.

Saito, K., Pignon, P., Ayyoub, M. & Valmori, D. 2015. Modulation of Cytokine Secretion Allows CD4 T Cells Secreting IL-10 and IL-17 to Simultaneously Participate in Maintaining Tolerance and Immunity. *Plos One,* 10**,** e0145788.

Samowitz, W. S., Curtin, K., Ma, K.-N., Schaffer, D., Coleman, L. W., Leppert, M. & Slattery, M. L. 2001. Microsatellite Instability in Sporadic Colon Cancer Is Associated with an Improved Prognosis at the Population Level. *Cancer Epidemiology Biomarkers & Prevention,* 10**,** 917-923.

Samstein, R. M., Lee, C. H., Shoushtari, A. N., Hellmann, M. D., Shen, R., Janjigian, Y. Y., Barron, D. A., Zehir, A., Jordan, E. J., Omuro, A., Kaley, T. J., Kendall, S. M., Motzer, R. J., Hakimi, A. A., Voss, M. H., Russo, P., Rosenberg, J., Iyer, G., Bochner, B. H., Bajorin, D. F., Al-Ahmadie, H. A., Chaft, J. E., Rudin, C. M., Riely, G. J., Baxi, S., Ho, A. L., Wong, R. J., Pfister, D. G., Wolchok, J. D., Barker, C. A., Gutin, P. H., Brennan, C. W., Tabar, V., Mellinghoff, I. K., Deangelis, L. M., Ariyan, C. E., Lee, N., Tap, W. D., Gounder, M. M., D'angelo, S. P., Saltz, L., Stadler, Z. K., Scher, H. I., Baselga, J., Razavi, P., Klebanoff, C. A., Yaeger, R., Segal, N. H., Ku, G. Y., Dematteo, R. P., Ladanyi, M., Rizvi,

N. A., Berger, M. F., Riaz, N., Solit, D. B., Chan, T. A. & Morris, L. G. T. 2019. Tumor mutational load predicts survival after immunotherapy across multiple cancer types. *Nat Genet,* 51**,** 202-206.

Sato, E., Olson, S. H., Ahn, J., Bundy, B., Nishikawa, H., Qian, F., Jungbluth, A. A., Frosina, D., Gnjatic, S., Ambrosone, C., Kepner, J., Odunsi, T., Ritter, G., Lele, S., Chen, Y. T., Ohtani, H., Old, L. J. & Odunsi, K. 2005. Intraepithelial CD8+ tumor-infiltrating lymphocytes and a high CD8+/regulatory T cell ratio are associated with favorable prognosis in ovarian cancer. *Proc Natl Acad Sci U S A,* 102**,** 18538-43.

Schlicker, A., Beran, G., Chresta, C. M., Mcwalter, G., Pritchard, A., Weston, S., Runswick, S., Davenport, S., Heathcote, K., Castro, D. A., Orphanides, G., French, T. & Wessels, L. F. 2012. Subtypes of primary colorectal tumors correlate with response to targeted treatment in colorectal cell lines. *BMC Med Genomics,* 5**,** 66.

Schnidrig, D., Turajlic, S. & Litchfield, K. 2019. Tumour mutational burden: primary versus metastatic tissue creates systematic bias. *Immuno-Oncology Technology,* 4**,** 8-14.

Schreiber, R. D., Old, L. J. & Smyth, M. J. 2011. Cancer immunoediting: integrating immunity's roles in cancer suppression and promotion. *Science,* 331**,** 1565-70.

Schulze, T., Kemmner, W., Weitz, J., Wernecke, K. D., Schirrmacher, V. & Schlag, P. M. 2009. Efficiency of adjuvant active specific immunization with Newcastle disease virus modified tumor cells in colorectal cancer patients following resection of liver metastases: results of a prospective randomized trial. *Cancer Immunol Immunother,* 58**,** 61-9.

Schumacher, T. N. & Schreiber, R. D. 2015. Neoantigens in cancer immunotherapy. *Science,* 348**,** 69-74.

Scott, A. J., Alexander, J. L., Merrifield, C. A., Cunningham, D., Jobin, C., Brown, R., Alverdy, J., O'keefe, S. J., Gaskins, H. R., Teare, J., Yu, J., Hughes, D. J., Verstraelen, H., Burton, J., O'toole, P. W., Rosenberg, D. W., Marchesi, J. R. & Kinross, J. M. 2019. International Cancer Microbiome Consortium consensus statement on the role of the human microbiome in carcinogenesis. *Gut,* 68**,** 1624-1632.

Sears, Cynthia l. & Garrett, Wendy s. 2014. Microbes, Microbiota, and Colon Cancer. *Cell Host & Microbe,* 15**,** 317-328.

Shankaran, V., Ikeda, H., Bruce, A. T., White, J. M., Swanson, P. E., Old, L. J. & Schreiber, R. D. 2001. IFNgamma and lymphocytes prevent primary tumour development and shape tumour immunogenicity. *Nature,* 410**,** 1107-11.

Shen, Z., Gu, L., Mao, D., Chen, M. & Jin, R. 2019. Clinicopathological and prognostic significance of PD-L1 expression in colorectal cancer: a systematic review and meta-analysis. *World Journal of Surgical Oncology,* 17.

Shih, I. M., Zhou, W., Goodman, S. N., Lengauer, C., Kinzler, K. W. & Vogelstein, B. 2001. Evidence That Genetic Instability Occurs at an Early Stage of Colorectal Tumorigenesis. *Cancer Res,* 61**,** 818-22.

Shimizu, Y. & Demars, R. 1989. Production of human cells expressing individual transferred HLA-A,-B,-C genes using an HLA-A,-B,-C null human cell line. *J Immunol,* 142**,** 3320-8.

Siegel, R. L., Miller, K. D. & Jemal, A. 2018. Cancer statistics, 2018. *CA Cancer J Clin,* 68**,** 7-30.

Sinicrope, F. A. 2010. DNA mismatch repair and adjuvant chemotherapy in sporadic colon cancer. *Nat Rev Clin Oncol,* 7**,** 174-7.

Snook, A. E., Baybutt, T. R., Xiang, B., Abraham, T. S., Flickinger, J. C., Jr., Hyslop, T., Zhan, T., Kraft, W. K., Sato, T. & Waldman, S. A. 2019. Split tolerance permits safe Ad5-GUCY2C-PADRE vaccine-induced T-cell responses in colon cancer patients. *J Immunother Cancer,* 7**,** 104.

Stangl, R., Altendorf-Hofmann, A., Charnley, R. M. & Scheele, J. 1994. Factors influencing the natural history of colorectal liver metastases. *The Lancet,* 343**,** 1405-1410.

Steimle, V., Siegrist, C., Mottet, A., Lisowska-Grospierre, B. & Mach, B. 1994. Regulation of MHC class II expression by interferon-gamma mediated by the transactivator gene CIITA. *Science,* 265**,** 106-109.

Syn, N. L., Teng, M. W. L., Mok, T. S. K. & Soo, R. A. 2017. De-novo and acquired resistance to immune checkpoint targeting. *The Lancet Oncology,* 18**,** e731-e741.

Tabassum, D. P. & Polyak, K. 2015. Tumorigenesis: it takes a village. *Nat Rev Cancer,* 15**,** 473-483.

Tabernero, J., Melero, I., Ros, W., Argiles, G., Marabelle, A., Rodriguez-Ruiz, M. E., Albanell, J., Calvo, E., Moreno, V., Cleary, J. M., Eder, J. P., Karanikas, V., Bouseida, S., Sandoval, F., Sabanes, D., Sreckovic, S., Hurwitz, H. I., Paz-Ares,

L. G., Suarez, J. M. S. & Segal, N. H. 2017. Phase Ia and Ib studies of the novel carcinoembryonic antigen (CEA) T-cell bispecific (CEA CD3 TCB) antibody as a single agent and in combination with atezolizumab: Preliminary efficacy and safety in patients with metastatic colorectal cancer (mCRC). *Journal of Clinical Oncology,* 35**,** 3002-3002.

Tay, R. E., Richardson, E. K. & Toh, H. C. 2020. Revisiting the role of CD4+ T cells in cancer immunotherapy—new insights into old paradigms. *Cancer Gene Therapy*.

The Cancer Genome Atlas, N. 2012. Comprehensive molecular characterization of human colon and rectal cancer. *Nature,* 487**,** 330.

The Office of National Statistics. 2019. *Cancer survival in England* [Online]. ONS. Available: https://www.ons.gov.uk/peoplepopulationandcommunity/healthandsocialcare/conditionsanddiseases/datasets/cancersurvivalratescancersurvivalinenglandadultsdiagnosed [Accessed 04/06/2020].

Thomas, L. 1982. On immunosurveillance in human cancer. *Yale J Biol Med,* 55**,** 329-33.

Topalian, S. L., Hodi, F. S., Brahmer, J. R., Gettinger, S. N., Smith, D. C., Mcdermott, D. F., Powderly, J. D., Carvajal, R. D., Sosman, J. A., Atkins, M. B., Leming, P. D., Spigel, D. R., Antonia, S. J., Horn, L., Drake, C. G., Pardoll, D. M., Chen, L., Sharfman, W. H., Anders, R. A., Taube, J. M., Mcmiller, T. L., Xu, H., Korman, A. J., Jure-Kunkel, M., Agrawal, S., Mcdonald, D., Kollia, G. D., Gupta, A., Wigginton, J. M. & Sznol, M. 2012. Safety, activity, and immune correlates of anti-PD-1 antibody in cancer. *N Engl J Med,* 366**,** 2443-54.

Topalian, S. L., Taube, J. M., Anders, R. A. & Pardoll, D. M. 2016. Mechanism-driven biomarkers to guide immune checkpoint blockade in cancer therapy. *Nature Reviews Cancer,* 16**,** 275-287.

Tosolini, M., Kirilovsky, A., Mlecnik, B., Fredriksen, T., Mauger, S., Bindea, G., Berger, A., Bruneval, P., Fridman, W. H., Pages, F. & Galon, J. 2011. Clinical impact of different classes of infiltrating T cytotoxic and helper cells (Th1, th2, treg, th17) in patients with colorectal cancer. *Cancer Res,* 71**,** 1263-71.

Toyota, M., Ahuja, N., Ohe-Toyota, M., Herman, J. G., Baylin, S. B. & Issa, J. P. 1999. CpG island methylator phenotype in colorectal cancer. *Proc Natl Acad Sci U S A,* 96**,** 8681-6.

Tran, E., Turcotte, S., Gros, A., Robbins, P. F., Lu, Y. C., Dudley, M. E., Wunderlich, J. R., Somerville, R. P., Hogan, K., Hinrichs, C. S., Parkhurst, M. R., Yang, J.

C. & Rosenberg, S. A. 2014. Cancer immunotherapy based on mutation-specific CD4+ T cells in a patient with epithelial cancer. *Science,* 344**,** 641-5.

Treasure, T., Fallowfield, L., Farewell, V., Ferry, D., Lees, B., Leonard, P., Macbeth, F., Utley, M. & Pulmonary Metastasectomy in Colorectal Cancer Trial Development, G. 2009. Pulmonary metastasectomy in colorectal cancer: time for a trial. *Eur J Surg Oncol,* 35**,** 686-9.

Treasure, T., Farewell, V., Macbeth, F., Monson, K., Williams, N. R., Brew-Graves, C., Lees, B., Grigg, O. & Fallowfield, L. 2019. Pulmonary Metastasectomy versus Continued Active Monitoring in Colorectal Cancer (PulMiCC): a multicentre randomised clinical trial. *Trials,* 20.

Tumeh, P. C., Harview, C. L., Yearley, J. H., Shintaku, I. P., Taylor, E. J. M., Robert, L., Chmielowski, B., Spasic, M., Henry, G., Ciobanu, V., West, A. N., Carmona, M., Kivork, C., Seja, E., Cherry, G., Gutierrez, A. J., Grogan, T. R., Mateus, C., Tomasic, G., Glaspy, J. A., Emerson, R. O., Robins, H., Pierce, R. H., Elashoff, D. A., Robert, C. & Ribas, A. 2014. PD-1 blockade induces responses by inhibiting adaptive immune resistance. *Nature,* 515**,** 568-571.

Turin, I., Delfanti, S., Ferulli, F., Brugnatelli, S., Tanzi, M., Maestri, M., Cobianchi, L., Lisini, D., Luinetti, O., Paulli, M., Perotti, C., Todisco, E., Pedrazzoli, P. & Montagna, D. 2018. In Vitro Killing of Colorectal Carcinoma Cells by Autologous Activated NK Cells is Boosted by Anti-Epidermal Growth Factor Receptor-induced ADCC Regardless of RAS Mutation Status. *J Immunother,* 41**,** 190-200.

Valderrama-Treviño, A. I., Barrera-Mera, B., Ceballos-Villalva, J. C. & Montalvo-Javé, E. E. 2017. Hepatic Metastasis from Colorectal Cancer. *Euroasian Journal of Hepato-Gastroenterology,* 7**,** 166-175.

Valle, L., Hernandez-Illan, E., Bellido, F., Aiza, G., Castillejo, A., Castillejo, M. I., Navarro, M., Segui, N., Vargas, G., Guarinos, C., Juarez, M., Sanjuan, X., Iglesias, S., Alenda, C., Egoavil, C., Segura, A., Juan, M. J., Rodriguez-Soler, M., Brunet, J., Gonzalez, S., Jover, R., Lazaro, C., Capella, G., Pineda, M., Soto, J. L. & Blanco, I. 2014. New insights into POLE and POLD1 germline mutations in familial colorectal cancer and polyposis. *Hum Mol Genet,* 23**,** 3506-12.

Van Cutsem, E., Cervantes, A., Adam, R., Sobrero, A., Van Krieken, J. H., Aderka, D., Aranda Aguilar, E., Bardelli, A., Benson, A., Bodoky, G., Ciardiello, F., D'hoore, A., Diaz-Rubio, E., Douillard, J. Y., Ducreux, M., Falcone, A., Grothey, A., Gruenberger, T., Haustermans, K., Heinemann, V., Hoff, P., Kohne, C. H., Labianca, R., Laurent-Puig, P., Ma, B., Maughan, T., Muro, K., Normanno, N., Osterlund, P., Oyen, W. J., Papamichael, D., Pentheroudakis, G., Pfeiffer, P., Price, T. J., Punt, C., Ricke, J., Roth, A., Salazar, R., Scheithauer, W., Schmoll,

H. J., Tabernero, J., Taieb, J., Tejpar, S., Wasan, H., Yoshino, T., Zaanan, A. & Arnold, D. 2016. ESMO consensus guidelines for the management of patients with metastatic colorectal cancer. *Ann Oncol,* 27**,** 1386-422.

Van Den Eynde, M., Baldin, P. & Huyghe, N. 2020. Immunotherapy with immune checkpoint inhibitors in colorectal cancer: what is the future beyond deficient mismatch-repair tumours? *Gastroenterology Report,* 8**,** 11-24.

Van Den Eynde, M., Mlecnik, B., Bindea, G., Fredriksen, T., Church, S. E., Lafontaine, L., Haicheur, N., Marliot, F., Angelova, M., Vasaturo, A., Bruni, D., Jouret-Mourin, A., Baldin, P., Huyghe, N., Haustermans, K., Debucquoy, A., Van Cutsem, E., Gigot, J.-F., Hubert, C., Kartheuser, A., Remue, C., Léonard, D., Valge-Archer, V., Pagès, F., Machiels, J.-P. & Galon, J. 2018. The Link between the Multiverse of Immune Microenvironments in Metastases and the Survival of Colorectal Cancer Patients. *Cancer Cell,* 34**,** 1012-1026.e3.

Veluchamy, J. P., Lopez-Lastra, S., Spanholtz, J., Bohme, F., Kok, N., Heideman, D. A., Verheul, H. M., Di Santo, J. P., De Gruijl, T. D. & Van Der Vliet, H. J. 2017. In Vivo Efficacy of Umbilical Cord Blood Stem Cell-Derived NK Cells in the Treatment of Metastatic Colorectal Cancer. *Front Immunol,* 8**,** 87.

Veluchamy, J. P., Spanholtz, J., Tordoir, M., Thijssen, V. L., Heideman, D. A., Verheul, H. M., De Gruijl, T. D. & Van Der Vliet, H. J. 2016. Combination of NK Cells and Cetuximab to Enhance Anti-Tumor Responses in RAS Mutant Metastatic Colorectal Cancer. *PLoS One,* 11**,** e0157830.

Venderbosch, S., Nagtegaal, I. D., Maughan, T. S., Smith, C. G., Cheadle, J. P., Fisher, D., Kaplan, R., Quirke, P., Seymour, M. T., Richman, S. D., Meijer, G. A., Ylstra, B., Heideman, D. a. M., De Haan, A. F. J., Punt, C. J. A. & Koopman, M. 2014. Mismatch Repair Status and BRAF Mutation Status in Metastatic Colorectal Cancer Patients: A Pooled Analysis of the CAIRO, CAIRO2, COIN, and FOCUS Studies. *Clinical Cancer Research,* 20**,** 5322-5330.

Vermorken, J. B., Claessen, A. M. E., Van Tinteren, H., Gall, H. E., Ezinga, R., Meijer, S., Scheper, R. J., Meijer, C. J. L. M., Bloemena, E., Ransom, J. H., Hanna, M. G. & Pinedo, H. M. 1999. Active specific immunotherapy for stage II and stage III human colon cancer: a randomised trial. *The Lancet,* 353**,** 345-350.

Vigneron, N. 2015. Human Tumor Antigens and Cancer Immunotherapy. *BioMed Research International,* 2015**,** 1-17.

Vogelstein, B., Fearon, E. R., Hamilton, S. R., Kern, S. E., Preisinger, A. C., Leppert, M., Nakamura, Y., White, R., Smits, A. M. & Bos, J. L. 1988. Genetic alterations during colorectal-tumor development. *N Engl J Med,* 319**,** 525-32.

Vogelstein, B., Papadopoulos, N., Velculescu, V. E., Zhou, S., Diaz, L. A., Jr. & Kinzler, K. W. 2013. Cancer genome landscapes. *Science,* 339**,** 1546-58.

Von Mehren, M., Arlen, P., Tsang, K. Y., Rogatko, A., Meropol, N., Cooper, H. S., Davey, M., Mclaughlin, S., Schlom, J. & Weiner, L. M. 2000. Pilot Study of a Dual Gene Recombinant Avipox Vaccine Containing Both Carcinoembryonic Antigen (CEA) and B7.1 Transgenes in Patients with Recurrent CEA-expressing Adenocarcinomas. *Clinical Cancer Research,* 6**,** 2219-2228.

Wagner, P., Koch, M., Nummer, D., Palm, S., Galindo, L., Autenrieth, D., Rahbari, N., Schmitz-Winnenthal, F. H., Schirrmacher, V., Buchler, M. W., Beckhove, P. & Weitz, J. 2008. Detection and functional analysis of tumor infiltrating T-lymphocytes (TIL) in liver metastases from colorectal cancer. *Ann Surg Oncol,* 15**,** 2310-7.

Walther, A., Johnstone, E., Swanton, C., Midgley, R., Tomlinson, I. & Kerr, D. 2009. Genetic prognostic and predictive markers in colorectal cancer. *Nat Rev Cancer,* 9**,** 489-99.

Wang, A., Wang, H. Y., Liu, Y., Zhao, M. C., Zhang, H. J., Lu, Z. Y., Fang, Y. C., Chen, X. F. & Liu, G. T. 2015. The prognostic value of PD-L1 expression for non-small cell lung cancer patients: A meta-analysis. *European Journal of Surgical Oncology (EJSO),* 41**,** 450-456.

Weinberg, R. A. 1989. Oncogenes, antioncogenes, and the molecular bases of multistep carcinogenesis. *Cancer Res. ,* 49**,** 3713-3721.

Weisenberger, D. J., Siegmund, K. D., Campan, M., Young, J., Long, T. I., Faasse, M. A., Kang, G. H., Widschwendter, M., Weener, D., Buchanan, D., Koh, H., Simms, L., Barker, M., Leggett, B., Levine, J., Kim, M., French, A. J., Thibodeau, S. N., Jass, J., Haile, R. & Laird, P. W. 2006. CpG island methylator phenotype underlies sporadic microsatellite instability and is tightly associated with BRAF mutation in colorectal cancer. *Nat Genet,* 38**,** 787-93.

Weiser, M. R., Jarnagin, W. R. & Saltz, L. B. 2013. Colorectal Cancer Patients With Oligometastatic Liver Disease: What Is the Optimal Approach? *Oncology (Williston Park),* 27**,** 1074 - 1078.

Wherry, E. J. 2011. T cell exhaustion. *Nat Immunol,* 12**,** 492-9.

Wrona, E. & Potemski, P. 2019. A novel immunotherapy — the history of CAR T-cell therapy. *Oncology in Clinical Practice,* 15**,** 202-207.

Wu, J., Fu, J., Zhang, M. & Liu, D. 2015. Blinatumomab: a bispecific T cell engager (BiTE) antibody against CD19/CD3 for refractory acute lymphoid leukemia. *J Hematol Oncol,* 8**,** 104.

Yamane, L., Scapulatempo-Neto, C., Reis, R. M. & Guimarães, D. P. 2014. Serrated pathway in colorectal carcinogenesis. *World Journal of Gastroenterology : WJG,* 20**,** 2634-2640.

Yarchoan, M., Hopkins, A. & Jaffee, E. M. 2017. Tumor Mutational Burden and Response Rate to PD-1 Inhibition. *New England Journal of Medicine,* 377**,** 2500-2501.

Yu, S., Li, A., Liu, Q., Yuan, X., Xu, H., Jiao, D., Pestell, R. G., Han, X. & Wu, K. 2017. Recent advances of bispecific antibodies in solid tumors. *J Hematol Oncol,* 10**,** 155.

Zhang, C., Wang, Z., Yang, Z., Wang, M., Li, S., Li, Y., Zhang, R., Xiong, Z., Wei, Z., Shen, J., Luo, Y., Zhang, Q., Liu, L., Qin, H., Liu, W., Wu, F., Chen, W., Pan, F., Zhang, X., Bie, P., Liang, H., Pecher, G. & Qian, C. 2017a. Phase I Escalating-Dose Trial of CAR-T Therapy Targeting CEA(+) Metastatic Colorectal Cancers. *Mol Ther,* 25**,** 1248-1258.

Zhang, H., Hong, H., Li, D., Ma, S., Di, Y., Stoten, A., Haig, N., Di Gleria, K., Yu, Z., Xu, X. N., Mcmichael, A. & Jiang, S. 2009. Comparing pooled peptides with intact protein for accessing cross-presentation pathways for protective CD8+ and CD4+ T cells. *J Biol Chem,* 284**,** 9184-91.

Zhang, Y., Sun, Z., Mao, X., Wu, H., Luo, F., Wu, X., Zhou, L., Qin, J., Zhao, L. & Bai, C. 2017b. Impact of mismatch-repair deficiency on the colorectal cancer immune microenvironment. *Oncotarget,* 8**,** 85526-85536.

Zhou, F. 2009. Molecular Mechanisms of IFN-γ to Up-Regulate MHC Class I Antigen Processing and Presentation. *International Reviews of Immunology,* 28**,** 239-260.

Zitvogel, L., Ayyoub, M., Routy, B. & Kroemer, G. 2016. Microbiome and Anticancer Immunosurveillance. *Cell,* 165**,** 276-287.

Zitvogel, L., Galluzzi, L., Smyth, M. J. & Kroemer, G. 2013. Mechanism of action of conventional and targeted anticancer therapies: reinstating immunosurveillance. *Immunity,* 39**,** 74-88.

Appendix – Presentations and Relevant Publications

Presentations

Comparing the immune signatures of primary colorectal cancer and pulmonary metastasis.

Goussous G, Lal N, Bagnall CJ, Bancroft H, Langman G, Naidu N, Ismail T, Willcox BE, Middleton GW.

Oral presentation at: The West Midlands Surgical Society Spring meeting, May 2017

Comparing the immune signatures of primary colorectal cancer and pulmonary metastasis.

Goussous G, Lal N, Bagnall CJ, Bancroft H, Langman G, Naidu N, Ismail T, Willcox BE, Middleton GW.

Poster presentation at: The Association of Coloproctology of Great Britain and Ireland, Bournemouth, July 2017

Published papers

This is a collaborative paper where I contributed to the validation of MHC Class II:

Lal N, White BS, Goussous G, Pickles O, Mason M, Beggs A, Taniere P, Willcox BE, Guinney J, Middleton GW. **KRAS mutation and Consensus Molecular Subtypes 2 and 3 independently suppress microenvironmental immunity in colorectal cancer**. Clin Cancer Res. 2018 Jan 1;24(1):224-233. doi: 10.1158/1078-0432.CCR-17-1090.

Manuscripts in preparation:

I am joint first author on this manuscript:

Immune contexture of liver and lung metastases of colorectal cancer and identification of pre-initiated dendritic cells as a mechanism of immune initiation in lung metastases.

Authors: Lennard YW Lee, Thomas Starkey, Ghaleb Goussous, Neeraj Lal, Rebecca Davies, Connor Woolley, Lai Mun Wang, Robert Jones, Prof Andrew Beggs, Prof Gary Middleton

Comparing the Immune Signatures of Primary Colorectal Cancer and Pulmonary Metastases

G Goussous[1,2], N Lal[1], CJ Bagnall[1], H Bancroft[3], G Langman[3], B Naidu[1,3], T Ismail[2], BE Willcox[1] and GW Middleton[1,2]

(1) Institute of Immunology and Immunotherapy, University of Birmingham, Birmingham, UK
(2) University Hospitals Birmingham NHS Foundation Trust, Birmingham, UK
(3) Heart of England NHS Foundation Trust, Birmingham, UK

Introduction

- The positive impact of Tumour Infiltrating Lymphocytes (TILs) on prognosis has been established in colorectal cancer (CRC).
- Emerging targeted immunotherapies such as Checkpoint Blockade (CPB) have been shown to be effective in a small subset of CRC.
- Metastases continue to be the main cause of mortality in CRC and despite population screening about 25% of new cases are diagnosed at Stage IV.
- There is a dearth of literature examining the immune micro-environment at metastatic sites.
- After the liver, the lung is the commonest site of metastatic spread and account for 10% of metastatic CRC.
- Unlike the liver, the lung circulation is not affected by antigen-rich portal blood.

Methods

- Thirty four paired formalin fixed paraffin embedded samples of primary CRC and resected pulmonary metastasis.
- Immunohistochemistry (IHC) for key immunological markers using validated antibodies.
- Digital whole slide quantification using DEFINIENS® software.

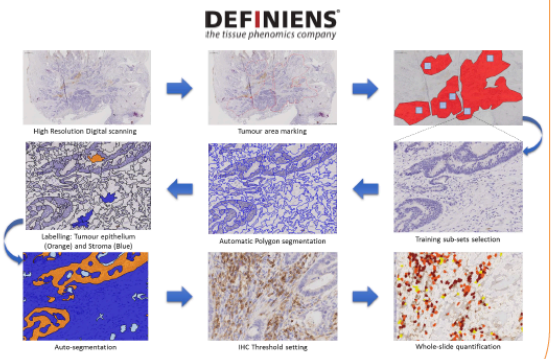

Figure 1| Digital pathology workflow demonstrating the steps involved in digital scoring.

Results

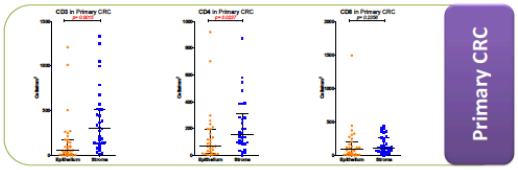

Figure 2| Mapping the distribution of TILs within the primary tumour compartments: Epithelium (Orange) and Stroma (Blue).

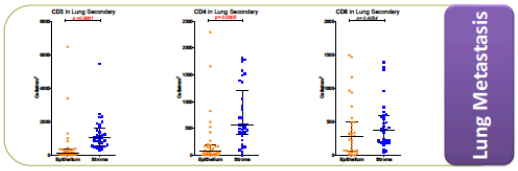

Figure 3| Mapping the distribution of TILs within the lung metastasis: Epithelium (Orange) and Stroma (Blue).

Results cont.

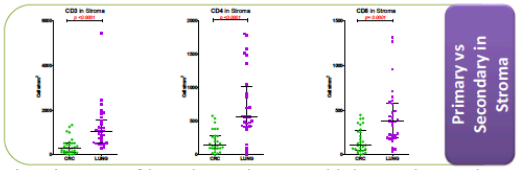

Figure 4| Comparison of the TILs density in the primary and the lung secondary site within the tumour stroma. Primary CRC (Green) and lung metastasis (Purple)

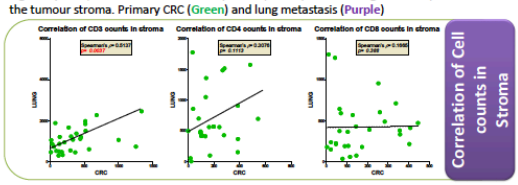

Figure 5| Correlation of cell counts (cell/mm²) between primary CRC and paired lung metastasis

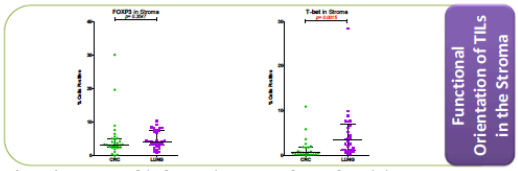

Figure 6| Assessment of the functional orientation of TILs. Left graph demonstrates Regulatory T lymphocytes (T_{Reg}) and right graph demonstrates T-helper 1 lymphocytes (T_H1)

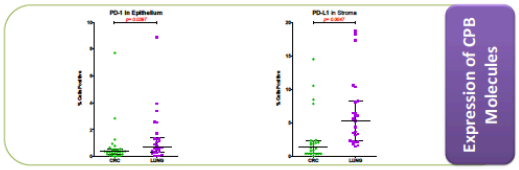

Figure 7| Assessment of the expression of two checkpoint blockade (CPB) therapeutic targets: Programmed Death protein 1 PD-1 and its ligand PD-L1

Conclusions

- We quantitatively demonstrated that TILs appear to be trapped in the stromal compartment of the tumour.
- Pulmonary metastasis are more immunologically active than the primary tumour. We hypothesise that this might be due to the immunosuppressive influence of the colonic microbiome.
- There is a statistically significant positive correlation between the total TIL count in the stroma of the primary tumour and the corresponding pulmonary metastasis.
- Our results suggest that the lymphocytes in the metastatic site are functionally skewed towards an anti-tumour orientation but appear to be suppressed by upregulation of checkpoint blockade molecules.
- These results open promising avenues to explore anti-CPB therapies in the treatment of metastatic colorectal cancer.

References

Shankaran V, Ikeda H, Bruce AT, White JM, Swanson PE, Old LJ, et al. IFNgamma and lymphocytes prevent primary tumour development and shape tumour immunogenicity. Nature. 2001;410(6832):1107-11.

Galon J, Costes A, Sanchez-Cabo F, Kirilovsky A, Mlecnik B, Lagorce-Pages C, et al. Type, density, and location of immune cells within human colorectal tumors predict clinical outcome. Science. 2006;313(5795):1960-4.

Lal N, Beggs AD, Willcox BE, Middleton GW. An immunogenomic stratification of colorectal cancer: implications for development of targeted immunotherapy. Oncoimmunology. 2015;4(1):e976052.

Le DT, Uram JN, Wang H, Bartlett BR, Kemberling H, Eyring AD, et al. PD-1 Blockade in Tumors with Mismatch-Repair Deficiency. N Engl J Med. 2015;372(26):2509-20

Tosolini M, Kirilovsky A, Mlecnik B, Fredriksen T, Mauger S, Bindea G, et al. Clinical impact of different classes of infiltrating T cytotoxic and helper cells (Th1, th2, treg, th17) in patients with colorectal cancer. Cancer Res. 2011;71(4):1263-71.

Mitry E, Guiu B, Cosconea S, Jooste V, Faivre J, Bouvier AM. Epidemiology, management and prognosis of colorectal cancer with lung metastases: a 30-year population-based study. Gut. 2010;59(10):1383-8.

Ladoire S, Martin F, Ghiringhelli F. Prognostic role of FOXP3+ regulatory T cells infiltrating human carcinomas: the paradox of colorectal cancer. Cancer Immunol Immunother. 2011;60(7):909-18.

Ling A, Lundberg IV, Eklof V, Wikberg ML, Oberg A, Edin S, et al. The infiltration, and prognostic importance, of Th1 lymphocytes vary in molecular subgroups of colorectal cancer. J Pathol Clin Res. 2016;2(1):21-31.

Published OnlineFirst October 23, 2017; DOI: 10.1158/1078-0432.CCR-17-1090

Biology of Human Tumors

Clinical Cancer Research

KRAS Mutation and Consensus Molecular Subtypes 2 and 3 Are Independently Associated with Reduced Immune Infiltration and Reactivity in Colorectal Cancer

Neeraj Lal[1], Brian S. White[2], Ghaleb Goussous[1], Oliver Pickles[1], Mike J. Mason[2], Andrew D. Beggs[3], Philippe Taniere[4], Benjamin E. Willcox[1], Justin Guinney[2], and Gary W. Middleton[1,4]

Abstract

Purpose: *KRAS* mutation is a common canonical mutation in colorectal cancer, found at differing frequencies in all consensus molecular subtypes (CMS). The independent immunobiological impacts of RAS mutation and CMS are unknown. Thus, we explored the immunobiological effects of *KRAS* mutation across the CMS spectrum.

Experimental Design: Expression analysis of immune genes/signatures was performed using The Cancer Genome Atlas (TCGA) RNA-seq and the KFSYSCC microarray datasets. Multivariate analysis included *KRAS* status, CMS, tumor location, MSI status, and neoantigen load. Protein expression of STAT1, HLA-class II, and CXCL10 was analyzed by digital IHC.

Results: The Th1-centric co-ordinate immune response cluster (CIRC) was significantly, albeit modestly, reduced in *KRAS*-mutant colorectal cancer in both datasets. Cytotoxic T cells, neutrophils, and the IFNγ pathway were suppressed in *KRAS*-mutant samples. The expressions of STAT1 and CXCL10 were reduced at the mRNA and protein levels. In multivariate analysis, *KRAS* mutation, CMS2, and CMS3 were independently predictive of reduced CIRC expression. Immune response was heterogeneous across *KRAS*-mutant colorectal cancer: *KRAS*-mutant CMS2 samples have the lowest CIRC expression, reduced expression of the IFNγ pathway, *STAT1* and *CXCL10*, and reduced infiltration of cytotoxic cells and neutrophils relative to CMS1 and CMS4 and to *KRAS* wild-type CMS2 samples in the TCGA. These trends held in the KFSYSCC dataset.

Conclusions: *KRAS* mutation is associated with suppressed Th1/cytotoxic immunity in colorectal cancer, the extent of the effect being modulated by CMS subtype. These results add a novel immunobiological dimension to the biological heterogeneity of colorectal cancer. *Clin Cancer Res; 24(1); 224–33. ©2017 AACR.*

Introduction

Galon and colleagues first demonstrated the positive prognostic impact of tumor-infiltrating lymphocytes (TIL) in colorectal cancer (1). The strength of Th type 1 (Th1) adaptive immunity was shown to be a strong prognostic factor. Th1 cells have an essential role in initiating and maintaining an effective $CD8^+$ cytotoxic T-cell response (2–4), in the recruitment of $CD8^+$ cells to the tumor bed (5) and in directly mediating immunologic tumor cell death (6). Th1 cells recognize antigen in association with MHC-II molecules. They secrete the inflammatory cytokine IFNγ, which provokes class II upregulation on tumor cells. The majority of immunogenic neoepitopes are class II restricted (7). Tumor cells evade cytotoxic immune responses by expressing the programmed death-ligand 1 (PD-L1) that activates the PD-1 negative feedback pathway (8). This checkpoint may be inhibited using anti–PD-1 or anti–PD-L1 antibodies that block interactions between the PD-1 receptor and its ligand PD-L1. However, the strategy has only been efficacious in microsatellite unstable (MSI-high) colorectal cancer (9), that is, those having a high neoantigen burden that can stimulate microenvironmental immunological reactivity (10). Class II expression on cancer cells is clearly important in the efficacy of checkpoint blockage. Indeed, cancer cell MHC-II–negative melanoma patients have lower response rates, PFS, and OS when treated with PD-1/PD-L1 blockade relative to class II-positive patients (11). Furthermore, *in vitro* PD-L1 blockade enhances Th1-mediated cytotoxicity only against cells that express high class II (12). Hence, an effective immune response is critically dependent on neoantigen presentation by MHC-II molecules.

The upregulation of MHC-II molecules via the IFNγ pathway is dependent on the STAT1 and CIITA proteins: extracellular IFNγ induces and activates STAT1, which activates transcription of CIITA. CIITA is the master transcriptional activator of MHC-II

[1]Institute of Immunology and Immunotherapy, University of Birmingham, Birmingham, United Kingdom. [2]Computational Oncology, Sage Bionetworks, Seattle, USA. [3]Institute of Cancer and Genomic Sciences, University of Birmingham, Birmingham, United Kingdom. [4]University Hospitals Birmingham NHS Foundation Trust, Birmingham, United Kingdom.

Note: Supplementary data for this article are available at Clinical Cancer Research Online (http://clincancerres.aacrjournals.org/).

N. Lal and B.S. White contributed equally to this article.

J. Guinney and G.W. Middleton are co-senior authors of this article.

Corresponding Author: Gary W. Middleton, University of Birmingham, Vincent Drive, Birmingham B15 2TT, United Kingdom. Phone: 121-415-8237; Fax: 121-371-3590; E-mail: g.middleton@bham.ac.uk

doi: 10.1158/1078-0432.CCR-17-1090

Published OnlineFirst October 23, 2017; DOI: 10.1158/1078-0432.CCR-17-1090

Translational Relevance

Understanding how mutational and transcriptional differences mold the immune contexture in cancer is key to accurate immunobiological stratification. We analyze how KRAS mutation shapes the immune microenvironment of colorectal cancer in the context of the consensus molecular subtypes (CMS). We show that KRAS mutation is associated with modest suppression of Th1 cell and cytotoxic cell immunity independently of mismatch repair status, tumor location, neoantigen load, and transcriptional subtype, but also show that the cumulative effect is dependent upon the CMS in which the mutation is found. Immunity in KRAS-mutant CMS2 is more suppressed than CMS1 and CMS4 as well as in comparison with KRAS wild-type CMS2. Our findings refine stratification factors for immunotherapy trial entry in colorectal cancer and suggest potential immunotherapeutic strategies to test in KRAS-mutant patients. Variation in the immune status of RAS-mutant colorectal cancer according to its transcriptional context might underlie part of the heterogeneity of response to molecularly stratified medicines.

molecules. STAT1-deficient cells show no induction of *CIITA* mRNA despite IFNγ stimulation (13) and STAT1-deficient cancer cells progress rapidly due to the evasion of adaptive immunity (14). Class I–positive but class II–negative mammary adenocarcinoma cells grew rapidly in immunocompetent mice, but were rejected when these cells were transfected with CIITA. Rejection correlated with induction of class II expression and was mediated by both $CD4^+$ and $CD8^+$ cells. STAT1 deficiency also severely impairs the induction of CXCL10, another STAT1 target gene. CXCL10 maintains the Th1 phenotype (15), and the decreased accumulation of Th1 cells in STAT1-deficient mice is related to reduced levels of CXCL10 (16).

KRAS mutation is the commonest canonical gain-of-function mutation in colorectal cancer, and earlier functional studies clearly demonstrated that mutant RAS reduces both STAT1 and class II expression. Using different cell line models (including HCT116 and clones thereof with deleted mutant KRAS, and intestinal epithelial cells with inducible mutant RAS), Klampfer and colleagues demonstrated that mutant RAS downregulates both constitutive and IFNγ-inducible STAT1 mRNA and protein and reduces STAT1 transcriptional activity and the expression of many IFNγ target genes, including class II (17, 18). Maudsley and colleagues showed that mutant KRAS resulted in loss of class II inducibility upon IFNγ treatment (without inhibiting class I expression), significantly reduced the ability of these cells to stimulate allogeneic T cells, and reduced the IFNγ secretion of the costimulated cells (19). They suggested that this RAS-mediated class II downregulation interrupted an amplification loop whereby Th1 cells are stimulated to produce IFNγ that would then stimulate further cancer cell class II expression.

These isolated cell line experiments suggest a role for STAT1 and its target genes in RAS-mutant colorectal cancer, but fail to replicate the complexities of the intact tumoral microenvironment. Hence, guided by these preclinical studies, we asked whether RAS-mutant colorectal cancer was associated with reduced expression of STAT1, CIITA, and CXCL10, as well as that of a number of associated signatures of immune reactivity, in human colorectal cancer tumor tissues. We have previously demonstrated using transcriptional analysis of bulk tumors that RAS-mutant colorectal cancer is associated with lower expression of a Th1-centric immune metagene that we termed the Co-ordinate Immune Response Cluster (CIRC; ref. 20). This metagene includes *STAT1*, *CXCL10*, nine separate class II genes, and the Th1 transcription factor T-bet (*TBX21*). We have also previously described a second immunological stratifier, the colorectal cancer "consensus molecular subtypes" (CMS; ref. 21). These subtypes include a "mesenchymal" group (CMS4) that is enriched for MSS tumors and yet is characterized by appreciable immune infiltration, intermediate between that of the MSI-enriched subtype (CMS1) and of the "canonical" (CMS2) and "metabolic" (CMS3) subtypes. RAS mutations occur in all of these CMS subtypes (albeit with differing proportions), and thus, RAS mutations in colorectal cancer occur in different transcriptional contexts with heterogeneous biology. In particular, RAS mutations are present in both mismatch repair–deficient and proficient cancers. To determine whether these two stratifiers are independent, we dissected the various innate and adaptive immune components of the CIRC in the context of CMS and KRAS mutation status using transcriptional analysis of two large independent datasets and digital IHC analysis of compartment-specific protein expression.

We demonstrate that CMS is more strongly associated with reduced anticancer immunity in colorectal cancer than RAS mutation, with both CMS2 and CMS3 being immunosuppressed relative to CMS1 and CMS4. Nevertheless, we find that the modest RAS mutation association is significant and independent of expression subtype. The cumulative effect on immunity is dependent upon the CMS context of RAS mutation, with RAS-mutant CMS2 being particularly immunosuppressed.

Materials and Methods

CMS analysis

Statistical analyses of The Cancer Genome Atlas (TCGA) and KFSYSCC expression data were performed in R (https://www.r-project.org/). To summarize the expression of a gene set [i.e., CIRC, immune subpopulations (22), and Hallmark gene sets (23)], we condensed the expression of the multiple genes in the set into a single gene set enrichment value using gene set variation analysis (24). Two-tailed nonparametric Wilcoxon rank sum tests, two-tailed *t* tests, two-tailed Fisher tests, and one-tailed *F* tests were applied, as indicated. Relative enrichments or expression between two populations are summarized by the Hodges–Lehmann estimator of the difference between those populations, for example, the median of all pairwise differences between CIRC enrichment in a *KRAS* WT sample and a *KRAS* MT sample. Ninety-five percent confidence intervals in this estimator were calculated using the method of Bauer (25). Multivariate analyses were performed using the forestmodel R package, with linear model CIRC ~ KRAS + CMS + site + status + neoantigens and where CIRC is the gene set enrichment for the immune signature, site indicates tumor location as left, right, or rectum, KRAS indicates mutation status WT or MT, CMS indicates subtype, status indicates MSI or MSS, and neoantigens is a continuous value indicating the (log-transformed) number of neoantigens. To assess potential synergy between the main effects corresponding to CMS subtype (CMS) and *KRAS* mutation status (KRAS), we used ANOVA to compare

Published OnlineFirst October 23, 2017; DOI: 10.1158/1078-0432.CCR-17-1090

linear models with and without the interaction effect (CMS: KRAS), i.e., CIRC ~ CMS + KRAS versus CIRC ~ CMS + KRAS + CMS:KRAS. Samples that did not correspond to one of the four CMS groups (i.e., "unlabeled") were excluded from any analysis that include CMS. Expression datasets, as well as clinical annotations, CMS labels, neoantigen predictions (obtained from The Cancer Immune Atlas; ref. 26), and gene set definitions, are available on the Synapse data commons platform (ref. 27 and https://www.synapse.org) under Synapse ID syn8533552. Source code to perform all genomic analyses and to generate the respective figures is available at https://github.com/Sage-Bionetworks/crc-cms-kras. Additional detail is provided in Supplementary Methods.

IHC analysis

Samples for IHC from patients undergoing resection of primary colorectal cancer were obtained from the completed CRUK Stratified Medicine Programme One pilot study and colorectal cancer patients from the Queen Elizabeth Hospital (Birmingham, United Kingdom). Samples were collected under ethical approval HBRC 14-205 (Sponsor: University of Birmingham). All patients had provided informed written consent for the use of their tissue, and studies were conducted in accordance with the Declaration of Helsinki. The cohort comprised 28 RAS G12D/G13D mutants (24.3%), 38 RAS non-G12D/G13D mutants (33.0%), and 49 RAS wild types (42.65%) for a total of 115. Suitable formalin-fixed, paraffin-embedded (FFPE) blocks were retrieved and processed at the HBRC biobank, University of Birmingham. Microsatellite status was assessed by extracting total DNA from FFPE tumor scrolls by fragment analysis (Supplementary Methods). Seven tumors (6.09%) were MSI-high, of which 3 were RAS mutant.

IHC was performed using a Leica BOND-MAX autostainer. For STAT1, an antibody that had undergone robust validation was selected (Cell Signaling Technology clone D1K9Y). For class II HLA (Abcam clone CR3/43) and CXCL10 (Novus Biologicals clone 6D4), in-house validation was performed as described in Supplementary Methods.

Staining conditions and concentrations were iteratively optimized in conjunction with a histopathologist (P. Taniere): STAT1: 1:500, 20-minute incubation, class II HLA: 1:100, 20 minutes, CXCL10: 1:50, 20 minutes. Slides were scanned at ×40 magnification using a Leica SCN400 slide scanner and digitally analyzed using Definiens Tissue Studio software. Analysis algorithms were created and optimized for each marker. Regions of interest were created in the tumor regions of each slide. All tumors were digitally segmented into tumor epithelium and stroma regions using trained segmentation algorithms (Supplementary Fig. S1A and S1B). Depending on the marker, staining was quantified on a per cell basis or on an area basis (Supplementary Fig. S1C and S1D). Percentages of cells or pixels with high, medium, low, or no immunoreactivity were quantified in each region. This produced either histologic scores for cell-based scoring, or percentile scores for pixel-based scoring, which are functions of the number and intensity of immunoreactive cells or pixels in the scanned specimens respectively [1 × (% cells/pixels with low staining) + 2 × (% cells/pixels with medium staining) + 3 × (% cells/pixels with high staining) = score out of 300]. Thresholds for negative/low, low/medium, and medium/high were set for each antibody in conjunction with a pathologist to maximize the dynamic range of results between samples and to reduce false-positive results. Hematoxylin thresholds (the staining intensities at which hematoxylin was recognized) were set individually and differed for each antibody due to differences in DAB staining. Hematoxylin thresholds were set to ensure accurate identification of individual cells. After analysis, segmentation was manually validated for each slide.

IHC results were analyzed using Excel (Microsoft Corp.) and Minitab (Minitab, Inc.). The normality of the distribution of histologic scores in each group (*RAS* mutant or *RAS* wild type) was determined by performing the Anderson–Darling test. All data were nonparametrically distributed. Therefore, for one-by-one comparisons, Mann–Whitney *U* tests were performed for significance testing. In addition, for STAT1 and CXCL10, staining for each case was grouped into low and high using H-score thresholds of both 100 and 200. For class II HLA, cases were grouped into negative (0%–5% staining), low (5%–50% staining), and high (>50% staining) as described by Lovig and colleagues (Supplementary Fig. S2F–S2H; ref. 28). χ^2 tests were performed to investigate significance between the RAS-mutant and wild-type groups. $P < 0.05$ was considered statistically significant.

Results

Immune subpopulations are suppressed in *KRAS* MT colorectal cancer

In our previous work, we demonstrated that RAS-mutant colorectal cancer had lower expression of the CIRC, a metagene that integrates 28 genes involved in innate and adaptive immunity (20). The CIRC was defined using 195 microarray colorectal cancer samples, of which 190 have also been subjected to RNA sequencing (RNA-seq) as part of an extended TCGA study. We analyzed this full dataset ($n = 344$) to validate our original findings on the orthogonal RNA-seq platform: consistent with those previous results, the analysis showed a significant reduction in the expression of the CIRC metagene in *KRAS* mutant (MT) relative to wild type (WT) samples (Supplementary Fig. S3A; two-tailed Wilcoxon rank sum $P = 2.4 \times 10^{-3}$). We additionally validated these results in the independent KFSYSCC (29) dataset ($n = 290$) of fresh-frozen colorectal cancer samples (Supplementary Fig. S3B; two-tailed Wilcoxon rank sum $P = 4.4 \times 10^{-3}$).

The CIRC signature was previously defined by performing an unsupervised hierarchical clustering of TCGA patients based on 61 highly curated, immune response–related genes. The genes comprising the signature were selected on the basis of their strong coordinated regulation across patient subgroups (20). The CIRC is enriched for Th1-associated genes, as well as genes encoding chemokines, adhesion molecules, MHC class II molecules, and immune checkpoints. Therefore, to dissect the specific immune subpopulations differentially recruited to *KRAS* MT tumors, we examined the effect of *KRAS* mutation on expression of each of seven immune cell types [neutrophils, and immature dendritic (iDC), B, T, Th1, Th2, and cytotoxic cells (22)]. Despite having few genes in common (Supplementary Fig. S4), all immune subpopulations except Th2 cells were highly correlated with the CIRC in both datasets (Pearson correlation $r \geq 0.42$; $P \leq 6.4 \times 10^{-14}$; Supplementary Fig. S5). Cytotoxic ($r \geq 0.85$; $P \leq 4.3 \times 10^{-82}$), T ($r \geq 0.73$; $P \leq 2.7 \times 10^{-50}$), and, as expected, Th1 ($r \geq 0.71$; $P \leq 3.2 \times 10^{-45}$) cells were most highly correlated with the CIRC in both datasets. *KRAS* mutation is associated with reduced cytotoxic cell (Fig. 1A; TCGA: two-tailed Wilcoxon rank sum $P = 0.04$; KFSYSCC: $P = 0.02$) and neutrophil (TCGA: $P = 9.7 \times 10^{-3}$; KFSYSCC: $P = 5.3 \times 10^{-3}$) infiltration. Th1 cells themselves

Published OnlineFirst October 23, 2017; DOI: 10.1158/1078-0432.CCR-17-1090

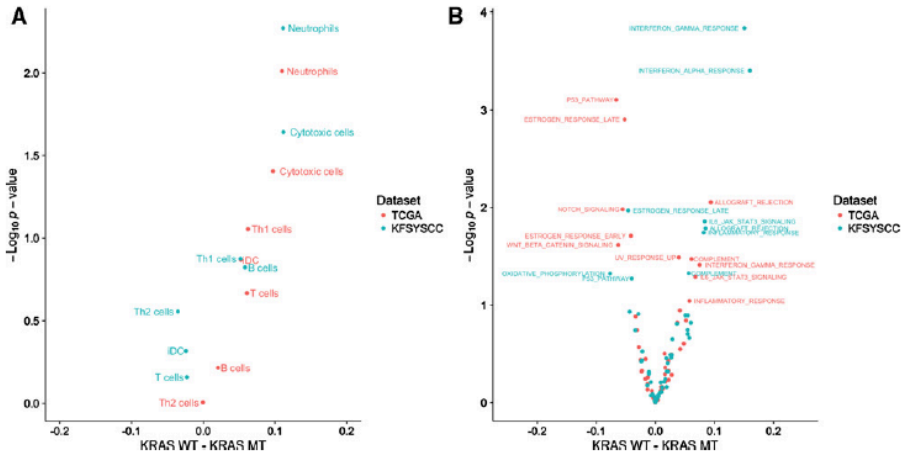

Figure 1.

KRAS mutation is associated with reduced immune infiltration and downregulation of immune pathways. **A,** Volcano plot showing enrichment (*x*-axis) of immune cell subpopulations in *KRAS* WT relative to *KRAS* MT tumors, with associated *P* values (*y*-axis) across TCGA (red) and KFSYSCC (blue) datasets. Relative enrichment is the Hodges–Lehmann estimator of the difference between the *KRAS* WT and *KRAS* MT populations, that is, the median of all pairwise differences between the enrichment in an indicated immune subpopulation in a *KRAS* WT sample and a *KRAS* MT sample. **B,** Volcano plot as in **A**, but showing effect of *KRAS* mutation on Hallmark gene sets. The subset of the full set of 50 Hallmark gene sets with $P < 0.1$ is labeled.

consistently trend toward reduced infiltration in *KRAS* MT colorectal cancer (TCGA: $P = 0.09$; KFSYSCC: $P = 0.13$). To further characterize biological differences between *KRAS* MT and WT colorectal cancer, we compared the differences in expression of all 50 Hallmark gene sets (23). This revealed downregulation of multiple immune-related pathways within *KRAS* MT tumors across both datasets (Fig. 1B). In particular, we observed suppression of the IFNγ pathway in *KRAS* MT colorectal cancer in both datasets.

STAT1 and CXCL10 are downregulated in *KRAS* MT colorectal cancer

Given the disruption of the IFNγ pathway in *KRAS* MT colorectal cancer, we hypothesized that downstream genes would also be affected in these tumors. To test this, we examined the expression of the key IFNγ response gene, STAT1, at the mRNA level and at the protein level using digital IHC (Supplementary Fig. S2A–S2E). We found that *STAT1* mRNA expression was downregulated in *KRAS* MT colorectal cancer in both datasets (Supplementary Fig. S6). By performing IHC and then digitally segmenting tumors into epithelium, stromal, and background regions (Supplementary Fig. S1A and S1B), we found that the STAT1 protein was also downregulated in the epithelial compartment across a series of whole mount sections taken from 115 patients with primary colorectal cancer (RAS G12D/G13D MT $n = 28$, RAS non-G12D/G13D MT $n = 38$, RAS WT $n = 49$): STAT1 expression was reduced by RAS mutation whether samples were analyzed by H-scores ($P = 0.016$) or according to percentage of positive staining for STAT1 ($\chi^2 P = 0.033$; Table 1).

Table 1. IHC analysis

		Epithelium			Stroma		
		RAS MT	RAS WT	*P*	RAS MT	RAS WT	*P*
STAT1	Median H-score	180	238	0.016	88	122	0.086
	% H-score < 100	32.2	10.5	0.014	54.2	47.4	0.508
	% H-score > 200	40.7	60.5	0.056	13.6	23.7	0.200
CXCL10	Median H-score	93.5	108	0.080	24	24	0.858
	% H-score < 100	58.1	38.3	0.041	85.5	85.1	0.956
	% H-score > 200	8	23.4	0.025	4.8	2.1	0.558
Class II HLA	Median percentile score	125.2	136.8	0.260	143.9	135.8	0.051
	% Negative (0%–5%)	50.8	51.2	0.590	11.3	20.9	0.300
	% Positive (5%–50%)	42.9	37.2		87.1	79.1	
	% Strong (>50%)	6.4	11.6		1.6	0	

NOTE: Median histologic scores or percentile scores in epithelial and stromal regions. STAT1 and PD-L1 reactivity are represented by histologic scores. Class II HLA reactivity is represented by percentile scores. For median H and percentile scores, *P* values are derived with Mann–Whitney *U* test. For all other comparisons, *P* values are derived with χ^2 test.

Published OnlineFirst October 23, 2017; DOI: 10.1158/1078-0432.CCR-17-1090

We next asked whether STAT1 target molecules, CXCL10 and CIITA, were also dysregulated in *KRAS* MT tumors. We found that *CXCL10* was strongly downregulated in both datasets (Supplementary Fig. S6). This downregulation was confirmed at the protein level, with significantly more MT samples having H-scores <100 ($\chi^2 P = 0.04$) and significantly more WT samples having H-scores >200 ($\chi^2 P = 0.03$; Table 1). We also found that *CIITA* was downregulated in *KRAS* MT samples in the TCGA dataset (Supplementary Fig. S6). Although there was no such evidence for dysregulation of the mRNA in the KFSYSCC dataset (Supplementary Fig. S6), *CIITA* expression was generally low in this dataset (median *CIITA* expression below the fifth percentile). At the protein level, around 50% of both RAS MT and RAS WT colorectal cancer samples were completely negative for class II expression by IHC and only 6.4% RAS MT tumors had >50% class II–positive cells (Supplementary Figs. S1C and S1D and S2F–S2H; Table 1). When class II protein expression was analyzed in the cancer samples that had detectable expression of class II (i.e., excluding the class II negative cases in which transcriptional silencing of CIITA would prevent IFNγ inducibility via STAT1; refs. 30, 31), we found that RAS mutation was associated with reduced class II expression on the cancer cells (RAS MT class II–expressing colorectal cancer median epithelial class II H-score = 136.14, RAS WT median = 168.33, Mann–Whitney U $P = 0.01$) with no differences in stromal class II expression (RAS MT colorectal cancer stromal median = 146.96, RAS WT median = 141.56, Mann–Whitney U $P = 0.16$).

Reduced immune infiltration is independently associated with *KRAS* mutation and CMS subtype

Immune response in colorectal cancer has been reported to be suppressed in CMS2 (21). Hence, we hypothesized that the CIRC and other measures of immunity would be lowest in *KRAS* MT CMS2 tumors. We first confirmed that the CIRC was strongly suppressed in CMS2 relative to CMS1 and CMS4 in both the TCGA (Supplementary Fig. S7A; CMS2 vs. CMS1: two-tailed Wilcoxon rank sum $P = 1.2 \times 10^{-18}$; CMS2 vs. CMS4: $P = 5.5 \times 10^{-15}$) and KFSYSCC (Supplementary Fig. S7B; CMS2 vs. CMS1: $P = 1.1 \times 10^{-4}$; CMS2 vs. CMS4: $P = 9.0 \times 10^{-8}$) datasets. As expected, *KRAS* MT CMS2 samples had the lowest CIRC expression among all genotype × CMS subtype combinations in the TCGA dataset (Fig. 2A). These results were independently validated in the KFSYSCC dataset (Fig. 2B), although the consistent trends in relation to CMS3 did not reach significance. To determine whether *KRAS* mutation status and CMS classification are significantly and independently associated with immune infiltration, we performed a multivariate analysis of CIRC expression that included as parameters *KRAS* mutation status, CMS classification, primary tumor location, and, in the TCGA dataset where they were available, MSI status and neoantigen load. The analysis showed that *KRAS* MT and CMS2 (relative to CMS1 and CMS4) were independently predictive of reduced CIRC expression in the TCGA (Fig. 3A) and KFSYSCC (Fig. 3B) datasets. We next assessed whether *KRAS* mutation might have a CMS subtype-dependent effect. However, there was no evidence for a *KRAS* × CMS interaction in either dataset (TCGA: F test $P = 0.15$; KFSYSCC: $P = 0.67$). Finally, to delineate potential differential infiltration of specific subpopulations associated with *KRAS* MT CMS2 tumors, we examined the immune subpopulations most strongly associated with *KRAS* status (Fig. 1A) in the additional context of molecular subtype. We found that *KRAS* MT CMS2 tumors had reduced infiltration of cytotoxic cells relative to all other patient groups in the TCGA dataset (Fig. 4A), with a similar trend in the KFSYSCC dataset (Fig. 4B). *KRAS* MT CMS2 tumors also showed reduced infiltration of neutrophils and Th1 cells in both datasets relative to CMS1 and CMS4 patients, but not necessarily to *KRAS* WT CMS2 or (*KRAS* MT or WT) CMS3 patients.

Taken together, our results indicate that there is considerable heterogeneity within CMS subtypes, even when controlling for MSI status, and that this may be further dissected using *KRAS*

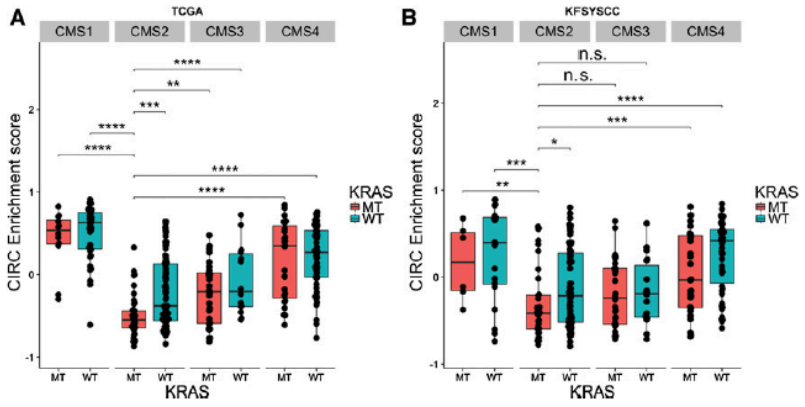

Figure 2.

CIRC expression is reduced in *KRAS*-mutant CMS2 tumors. Expression of CIRC versus CMS subtype and *KRAS* mutation status in TCGA (**A**; $n = 316$) or KFSYSCC (**B**; $n = 258$) datasets. n.s., not significant; *, $P < 0.05$; **, $P < 0.01$; ***, $P < 0.001$; ****, $P < 0.0001$; MT, mutation; WT, wild type.

Published OnlineFirst October 23, 2017; DOI: 10.1158/1078-0432.CCR-17-1090

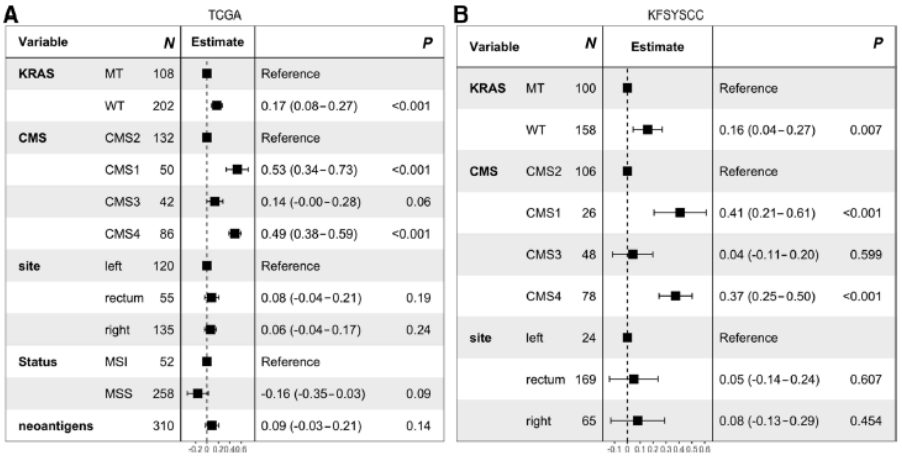

A TCGA				
Variable		N	Estimate	P
KRAS	MT	108	Reference	
	WT	202	0.17 (0.08–0.27)	<0.001
CMS	CMS2	132	Reference	
	CMS1	50	0.53 (0.34–0.73)	<0.001
	CMS3	42	0.14 (-0.00–0.28)	0.06
	CMS4	86	0.49 (0.38–0.59)	<0.001
site	left	120	Reference	
	rectum	55	0.08 (-0.04–0.21)	0.19
	right	135	0.06 (-0.04–0.17)	0.24
Status	MSI	52	Reference	
	MSS	258	-0.16 (-0.35–0.03)	0.09
neoantigens		310	0.09 (-0.03–0.21)	0.14

B KFSYSCC				
Variable		N	Estimate	P
KRAS	MT	100	Reference	
	WT	158	0.16 (0.04–0.27)	0.007
CMS	CMS2	106	Reference	
	CMS1	26	0.41 (0.21–0.61)	<0.001
	CMS3	48	0.04 (-0.11–0.20)	0.599
	CMS4	78	0.37 (0.25–0.50)	<0.001
site	left	24	Reference	
	rectum	169	0.05 (-0.14–0.24)	0.607
	right	65	0.08 (-0.13–0.29)	0.454

Figure 3.
CMS subtype and *KRAS* mutation are independently predictive of CIRC expression. Multivariate analysis performed across TCGA (**A**; $n = 310$) or KFSYSCC (**B**; $n = 258$) datasets.

mutation status. Although the data could not unambiguously resolve whether *KRAS* mutation has an effect specific to CMS2, the two factors are independently significant, that is, the level of immune infiltration and its characterization across immune cell subpopulations cannot be inferred without knowledge of both factors. The cumulative effect is such that *KRAS* MT CMS2 samples have reduced immune infiltration (of cytotoxic cells, neutrophils, and Th1 cells, as well as measured by the CIRC) relative to CMS1 or CMS4 samples harboring either MT or WT *KRAS*.

IFNγ pathway suppression is associated with both *KRAS* mutation and CMS subtype

To determine whether immune pathways downregulated in *KRAS* MT tumors (Fig. 1B) were additionally suppressed in CMS2 colorectal cancer, we evaluated the expression of these signatures in the context of *KRAS* mutation status and molecular classification. In the TCGA dataset, we found that *KRAS* MT CMS2 tumors exhibited reduced expression of all examined immune signatures (IFNγ, inflammatory response, IL6/JAK/STAT3 signaling, complement, and IFNα) relative to all patient groups (although the trend did not reach significance in relation to *KRAS* WT CMS2 when examining the IFNα pathway; Fig. 4C). These trends held in the KFSYSCC data set (Fig. 4D). In particular, *KRAS* MT CMS2 tumors showed significantly reduced expression of the IFNγ pathway relative to all other patient groups in both datasets, except relative to *KRAS* WT CMS2 in the KFSYSCC dataset, which nevertheless exhibited the same trend ($P = 0.05$).

Finally, we examined the IFNγ target gene STAT1, as well as its downstream targets, *CXCL10* and *CIITA*, to determine whether the previously observed association between the reduced expression of these three genes and *KRAS* mutation was independent of molecular subtype. First, we observed that, within CMS2, *KRAS* MT samples had lower expression of each of the genes relative to WT samples in both the TCGA ($P < 0.02$) and KFSYSCC ($P < 5.8 \times 10^{-3}$) datasets, with the exception of *CIITA* in the KFSYSCC dataset, as expected from its low expression in this dataset (Supplementary Fig. S8). Second, we performed multivariate analyses for all three genes in both datasets, excluding *CIITA* in the KFSYSCC dataset, which generally indicated that both *KRAS* mutation and CMS2 (relative to CMS1 and CMS4) were significantly and independently associated with reduced expression of the three genes. Specifically, *KRAS* mutation was significantly ($P < 1.1 \times 10^{-2}$) or marginally ($P = 0.05$ for *STAT1* in the TCGA dataset) associated with reduced gene expression, while CMS2 was associated with reduced gene expression relative to CMS1 ($P < 3.1 \times 10^{-3}$) and to CMS4 ($P < 1.2 \times 10^{-3}$, except for *STAT1* in the KFSYSCC dataset, where $P = 0.17$).

Discussion

We have previously shown that *KRAS* mutation is associated with reduced expression of the CIRC metagene, which summarizes 28 genes associated with innate and adaptive immunity. Here, we extend those earlier findings to: (i) explicitly characterize the nature of the suppressed immune infiltration, showing that *KRAS* MT tumors have reduced infiltration of cytotoxic cells and neutrophils (Fig. 1A); (ii) demonstrate that the IFNγ pathway is suppressed in *KRAS* MT tumors (Fig. 1B); (iii) demonstrate that KRAS mutation is associated with downregulation of STAT1 and CXCL10 at the mRNA (Supplementary Fig. S6) and protein (Table 1) levels; (iv) show that *KRAS* MT–associated immunosuppression is independent of CMS classification (Fig. 3; Supplementary Fig. S8); and (v) show that *KRAS* MT CMS2 colorectal cancer is significantly immunosuppressed relative to (*KRAS* MT or WT) CMS1 and CMS4 cancers and, based on several signatures in

Published OnlineFirst October 23, 2017; DOI: 10.1158/1078-0432.CCR-17-1090

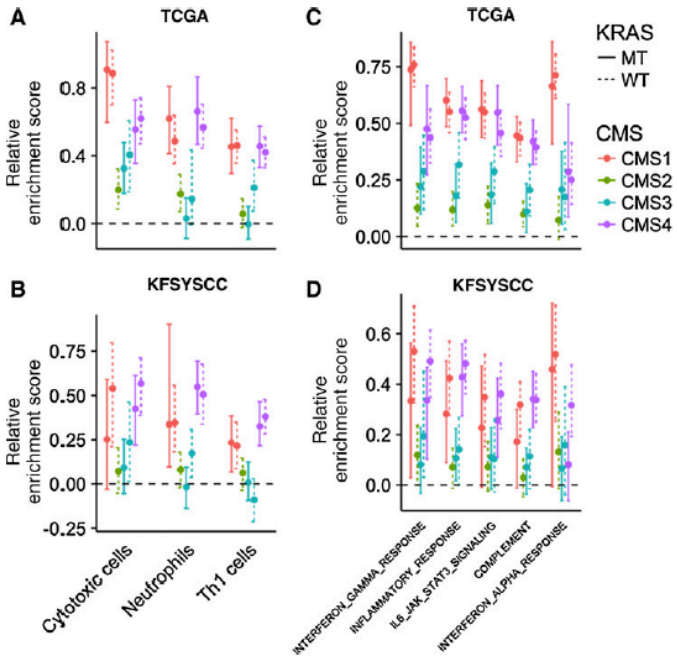

Figure 4.
KRAS MT CMS2 tumors are associated with reduced immune infiltration and downregulation of immune pathways. Enrichment score (*y*-axis) of immune populations (*x*-axis) of indicated *KRAS* x CMS subgroup relative to *KRAS* MT CMS2 subgroup in TCGA (**A**) and KFSYSCC (**B**) datasets. Relative enrichment is the Hodges–Lehmann estimator of the difference between the indicated subgroup and the *KRAS* MT CMS2 subgroup. Error bars represent 95% confidence intervals in estimator calculated using the method of Bauer (25). Enrichment relative to *KRAS* MT CMS2 subgroup of Hallmark immune pathways in TCGA (**C**) and KFSYSCC (**D**) datasets.

at least one of the two datasets, relative to *KRAS* WT CMS2 colorectal cancer as well (Figs. 2 and 4).

The *KRAS* MT–associated downregulation of the IFNγ pathway and reduced infiltration of cytotoxic T cells [i.e., those with properties common to $CD8^+$ T, Tγδ, and natural killer (NK) cells] and neutrophils indicate that the immunosuppressive impact of KRAS mutation that we previously observed is robust, if modest. Recent data demonstrate the interconnectedness of $CD8^+$ T cells and neutrophils with the IFNγ pathway in CRC (32): addition of neutrophils to $CD8^+$ T cells (activated via suboptimal concentrations of anti-CD3 and anti-CD28 antibodies) led to increased IFNγ release and T-cell proliferation. In turn, activated $CD8^+$ cells enhanced neutrophil viability. Furthermore, activated neutrophils colocalize with immature DCs, leading to their maturation (33). The resulting DCs drive T-cell proliferation and Th1 skewing.

Preclinically, RAS mutation has been shown to reduce the levels of STAT1 (17, 18). Consistent with these findings, we demonstrated that RAS MT cancers are associated with significantly lower STAT1 within the context of the tumor microenvironment. The preclinical data also showed that RAS mutation reduced STAT1-dependent transcriptional activity (17); indeed, we detected reduced expression of the STAT1 target CXCL10 at the RNA and protein levels in *KRAS* MT relative to WT samples. *KRAS* mutation may additionally downregulate CXCL10 via its activation of MEK–ERK signaling, which we observed in both datasets using a previously published (34) five-gene MEK signature (data not shown). We observed that *KRAS* MT reduced expression of a second STAT1 target, *CIITA*, in the TCGA dataset. No such trend was detected in the KFSYSCC dataset. However, *CIITA* expression was suppressed in this dataset, which would likely mask any *KRAS* MT–mediated STAT1 impact. Transcriptional repression of CIITA is seen in a proportion of colorectal cancer samples (30) as is the complete failure of IFNγ to induce class II expression in half of primary colorectal cancer cells (31). Both of these effects are RAS independent. To control for *CIITA* silencing (and thus lack of class II inducibilty), we analyzed the 50% of colorectal cancer samples that detectably expressed class II molecules (and in which *CIITA* must be transcribed and hence under the influence of STAT1). In these samples, we demonstrated that RAS MT cancers had significantly lower expression of class II surface makers compared with RAS WT cases. Significantly, we demonstrated that both CMS classification and *KRAS* mutation status are independently and significantly associated with dysregulation of *STAT1*, *CXCL10*, and *CIITA*. The CMS-associated effect presumably reflects previously reported reduced IFNγ signaling in CMS2 tumors (21), which leads to correspondingly reduced transcription of STAT1 target genes (17). Our findings and the cited literature are consistent with a cell-autonomous role for *KRAS* in modulating STAT1 and its downstream targets *CXCL10* and *CIITA*. Nevertheless, we cannot formally exclude the possibility that this *KRAS* effect is attributable, in whole or in part, to the reduced immune infiltration of CMS2 colorectal cancer with corresponding reduced environmental IFNγ. However these two factors are clearly intimately related.

Published OnlineFirst October 23, 2017; DOI: 10.1158/1078-0432.CCR-17-1090

Suppression of the CIRC was greatest in *KRAS* MT CMS2 samples. There may be a straightforward explanation for this phenomenon. CMS2 is the most Th1 immunosuppressed of the molecular subtypes with the lowest level of IFNγ signaling and thus lower levels of STAT1 and STAT1 target gene transcription. KRAS mutation shifts the IFNγ/STAT1 dose–response curve (17), such that for any level of IFNγ, there is less STAT1 transcription in a KRAS-mutated context. This effect is likely to be most biologically relevant where IFNγ levels are already limiting. The cumulative impact of low IFNγ (CMS2) and blunting of the IFNγ response (via mutant KRAS) may result in a level of STAT1-dependent promoter transcription that is insufficient to support robust and consistent expression of the critical downstream molecules. We considered the alternative explanation that the effect of KRAS mutation in CMS2 was due to it impacting the particular biology of CMS2. This subtype is characterized by high levels of Wnt and Myc signaling (21). Activation of Wnt/β-catenin signaling in melanoma reduces $CD8^+$ and IFNγ-producing $CD4^+$ cells, findings that have been generalized across other cancer types, including colorectal cancer (35), while MYC upregulation has been associated with reduced $CD4^+$ T-cell tumoral accumulation (36). *In vitro*, mutant RAS significantly enhances Wnt/β-catenin signaling in a mutant APC background and enhances downstream *MYC* transcription (37). Thus, we investigated whether KRAS mutation was deepening the Wnt and Myc drive in CMS2, and thus deepening immunosuppression via this mechanism. We found no robust, consistent evidence that *KRAS* mutation dysregulated the expression of the Wnt or Myc signatures within the context of CMS2 ($P > 0.07$ for comparisons of KRAS MT CMS2 vs. KRAS WT CMS2 for Wnt/β-catenin and Myc target gene sets).

As is the case for the majority of transcriptional and IHC analyses in colorectal cancer, our analysis was performed using primary resection samples. It is important to stress that the strength of Th1 immunity and class II expression in primary tissue are highly prognostic factors and are predictive of the presence of both synchronous metastatic disease and the development of subsequent metastases (38). Thus, understanding the independent impacts on the strength of Th1 immunity in primary tissue is of value in its own right. These results pose important questions for the larger body of immunotherapy trials that are instead directed at established metastatic or, in an adjuvant context, micrometastatic disease. Longitudinal expression studies following the evolution of disease progression should be undertaken to ascertain the concordance of CMS classification between primary and metastatic disease. However, existing data already suggest that immune cell densities ($CD8^+$, dendritic, and NK cells) are highly correlated between primary and metastatic colorectal cancer and between separate metastatic sites (39). Although it has been suggested that there is significant intratumoral heterogeneity of CMS, this analysis used separately macrodissected tissue from the center of the tumor and from the invasive front rather than bulk tumor (40). As was pointed out in the accompanying editorial, biopsy from the invasive margin will result in a large admixture of stromal cells not found in the center of the tumor, thus giving a CMS4-like signature and artificially introducing heterogeneity through selective sampling (41). Regardless of whether CMS or some other molecular subtypes prove to be pertinent to metastatic colorectal cancer, our results suggest that *KRAS* mutation is likely to modulate immune response within these subtypes: these data provide proof of principle that the immune status of RAS-mutant colorectal cancer is not homogenous across all colorectal cancer and that RAS mutation influences the immunobiology of molecularly defined colorectal cancer subtypes.

In summary, our results add a novel immunologic dimension to the growing appreciation of the biological heterogeneity of tumors harboring canonical mutations in colorectal cancer. The immunobiological status of RAS-mutant colorectal cancer varies according to transcriptional context, and the immunobiological status of CMS2 is dependent on RAS status. *KRAS* MT CMS2 appears to be a particularly immune-neglected group that will require therapy to initially activate a microenvironmental immune response if checkpoint blockade is considered in a combinatorial approach. RAS mutation itself may be a useful immunologic target in this group. Adoptive T-cell transfer of RAS MT-specific T cells has recently been shown to have therapeutic efficacy in colorectal cancer (42), and the use of T cells transduced with T-cell receptors recognizing RAS MT epitopes is also a potential therapy option (43). Our demonstration that a canonical mutation can be associated with widely differing expression of immune-related genes based on its transcriptional subtype may underlie some of the heterogeneity of responses seen with targeted therapies, although it is important to qualify this by acknowledging that our understanding of the transcriptional biology of metastatic disease is limited. In animal models, the activity of BRAF inhibitors is dependent on Th1 cell–mediated provision of CD40L and IFNγ (44). Similarly, the therapeutic effect of inactivation of oncogenic MYC is dependent upon $CD4^+$ cells (45). This suggests that the use of individual mutations as predictive biomarkers in colorectal cancer may be insufficient to predict the efficacy of targeted therapies without knowledge of the associated CMS subtype and its immune contexture. This hypothesis should be readily testable in the clinic.

Disclosure of Potential Conflicts of Interest

A.D. Beggs reports receiving other commercial research support from Illumina Inc. No potential conflicts of interest were disclosed by the other authors.

Authors' Contributions

Conception and design: N. Lal, O. Pickles, A.D. Beggs, B.E. Willcox, J. Guinney, G.W. Middleton

Development of methodology: N. Lal, G. Goussous, O. Pickles, A.D. Beggs, B.E. Willcox, J. Guinney

Acquisition of data (provided animals, acquired and managed patients, provided facilities, etc.): N. Lal, G. Goussous, O. Pickles, P. Taniere

Analysis and interpretation of data (e.g., statistical analysis, biostatistics, computational analysis): N. Lal, B.S. White, G. Goussous, M.J. Mason, B.E. Willcox, J. Guinney, G.W. Middleton

Writing, review, and/or revision of the manuscript: N. Lal, B.S. White, G. Goussous, O. Pickles, M.J. Mason, B.E. Willcox, J. Guinney, G.W. Middleton

Administrative, technical, or material support (i.e., reporting or organizing data, constructing databases): A.D. Beggs, J. Guinney

Study supervision: B.E. Willcox, J. Guinney, G.W. Middleton

Acknowledgments

B.S. White, M.J. Mason, and J. Guinney are grateful for the fruitful conversations with Drs. Benjamin Logsdon, Solveig Sieberts, and Rodrigo Dienstmann. N. Lal, G.W. Middleton, and B.E. Willcox gratefully acknowledge the contribution to this study made by Christopher Bagnall, the University of Birmingham's Digital Pathology Unit, and the Human Biomaterials Resource Centre, which has been supported through Birmingham Science City - Experimental Medicine Network of Excellence project. We would like to thank University of Birmingham Alumni for funding the automated staining platform. N. Lal and O. Pickles

Published OnlineFirst October 23, 2017; DOI: 10.1158/1078-0432.CCR-17-1090

were supported by Cancer Research UK clinical PhD studentships. B.E. Willcox was supported by a Wellcome Trust investigator award. IHC costs and software were supported by a Birmingham Experimental Cancer Medicine Centre (ECMC) research programme (principal investigators: G.W. Middleton and B.E. Willcox).

A.D. Beggs acknowledges funding from the Wellcome Trust (102732/Z/13/Z), Cancer Research UK (C31641/A23923), and the Medical Research Council (MR/M016587/1).

The costs of publication of this article were defrayed in part by the payment of page charges. This article must therefore be hereby marked *advertisement* in accordance with 18 U.S.C. Section 1734 solely to indicate this fact.

Received April 20, 2017; revised August 22, 2017; accepted October 17, 2017; published OnlineFirst October 23, 2017.

References

1. Galon J. Type, density, and location of immune cells within human colorectal tumors predict clinical outcome. Science 2006;313:1960–4.
2. Ossendorp F, Mengede E, Camps M, Filius R, Melief CJ. Specific T helper cell requirement for optimal induction of cytotoxic T lymphocytes against major histocompatibility complex class II negative tumors. J Exp Med 1998;187:693–702.
3. Becht E, Giraldo NA, Dieu-Nosjean MC, Sautes-Fridman C, Fridman WH. Cancer immune contexture and immunotherapy. Curr Opin Immunol 2016;39:7–13.
4. Ridge JP, Di Rosa F, Matzinger P. A conditioned dendritic cell can be a temporal bridge between a CD4+ T-helper and a T-killer cell. Nature 1998;393:474–8.
5. Bos R, Sherman LA. CD4+ T-cell help in the tumor milieu is required for recruitment and cytolytic function of CD8+ T lymphocytes. Cancer Res 2010;70:8368–77.
6. Quezada SA, Simpson TR, Peggs KS, Merghoub T, Vider J, Fan X, et al. Tumor-reactive CD4(+) T cells develop cytotoxic activity and eradicate large established melanoma after transfer into lymphopenic hosts. J Exp Med 2010;207:637–50.
7. Kreiter S, Vormehr M, van de Roemer N, Diken M, Löwer M, Diekmann J, et al. Mutant MHC class II epitopes drive therapeutic immune responses to cancer. Nature 2015;520:692–6.
8. Topalian SL, Drake CG, Pardoll DM. Immune checkpoint blockade: a common denominator approach to cancer therapy. Cancer Cell 2015;27:450–61.
9. Le DT, Uram JN, Wang H, Bartlett BR, Kemberling H, Eyring AD, et al. PD-1 blockade in tumors with mismatch-repair deficiency. N Engl J Med 2015;372:2509–20.
10. Giannakis M, Mu XJ, Shukla SA, Qian ZR, Cohen O, Nishihara R, et al. Genomic correlates of immune-cell infiltrates in colorectal carcinoma. Cell Rep 2016 Apr 14. [Epub ahead of print].
11. Johnson DB, Estrada MV, Salgado R, Sanchez V, Doxie DB, Opalenik SR, et al. Melanoma-specific MHC-II expression represents a tumour-autonomous phenotype and predicts response to anti-PD-1/PD-L1 therapy. Nat Commun 2016;7:10582.
12. Yan H, Hou X, Li T, Zhao L, Yuan X, Fu H, et al. CD4+ T cell-mediated cytotoxicity eliminates primary tumor cells in metastatic melanoma through high MHC class II expression and can be enhanced by inhibitory receptor blockade. Tumour Biol 2016 Oct 5. [Epub ahead of print].
13. Muhlethaler-Mottet A, Di Berardino W, Otten LA, Mach B. Activation of the MHC class II transactivator CIITA by interferon-gamma requires cooperative interaction between Stat1 and USF-1. Immunity 1998;8:157–66.
14. Kaplan DH, Shankaran V, Dighe AS, Stockert E, Aguet M, Old LJ, et al. Demonstration of an interferon gamma-dependent tumor surveillance system in immunocompetent mice. Proc Natl Acad Sci U S A 1998;95:7556–61.
15. Gangur V, Simons FE, Hayglass KT. Human IP-10 selectively promotes dominance of polyclonally activated and environmental antigen-driven IFN-gamma over IL-4 responses. FASEB J 1998;12:705–13.
16. Mikhak Z, Fleming CM, Medoff BD, Thomas SY, Tager AM, Campanella GS, et al. STAT1 in peripheral tissue differentially regulates homing of antigen-specific Th1 and Th2 cells. J Immunol 2006;176:4959–67.
17. Klampfer L, Huang J, Corner G, Mariadason J, Arango D, Sasazuki T, et al. Oncogenic Ki-ras inhibits the expression of interferon-responsive genes through inhibition of STAT1 and STAT2 expression. J Biol Chem 2003;278:46278–87.
18. Klampfer L, Huang J, Shirasawa S, Sasazuki T, Augenlicht L. Histone deacetylase inhibitors induce cell death selectively in cells that harbor activated kRasV12: The role of signal transducers and activators of transcription 1 and p21. Cancer Res 2007;67:8477–85.
19. Maudsley DJ, Bateman WJ, Morris AG. Reduced stimulation of helper T cells by Ki-ras transformed cells. Immunology 1991;72:277–81.
20. Lal N, Beggs AD, Willcox BE, Middleton GW. An immunogenomic stratification of colorectal cancer: Implications for development of targeted immunotherapy. OncoImmunology 2015;4:e976052.
21. Guinney J, Dienstmann R, Wang X, de Reynies A, Schlicker A, Soneson C, et al. The consensus molecular subtypes of colorectal cancer. Nat Med 2015;21:1350–6.
22. Bindea G, Mlecnik B, Tosolini M, Kirilovsky A, Waldner M, Obenauf Anna C, et al. Spatiotemporal dynamics of intratumoral immune cells reveal the immune landscape in human cancer. Immunity 2013;39:782–95.
23. Liberzon A, Birger C, Thorvaldsdottir H, Ghandi M, Mesirov JP, Tamayo P. The Molecular Signatures Database (MSigDB) hallmark gene set collection. Cell Syst 2015;1:417–25.
24. Hanzelmann S, Castelo R, Guinney J. GSVA: gene set variation analysis for microarray and RNA-seq data. BMC Bioinformatics 2013;14:7.
25. Bauer DF. Constructing confidence sets using rank statistics. J Am Stat Assoc 1972;67:687–90.
26. Charoentong P, Finotello F, Angelova M, Mayer C, Efremova M, Rieder D, et al. Pan-cancer immunogenomic analyses reveal genotype-immunophenotype relationships and predictors of response to checkpoint blockade. Cell Rep 2017;18:248–62.
27. Derry JM, Mangravite LM, Suver C, Furia MD, Henderson D, Schildwachter X, et al. Developing predictive molecular maps of human disease through community-based modeling. Nat Genet 2012;44:127–30.
28. Løvig T, Andersen SN, Thorstensen L, Diep CB, Meling GI, Lothe RA, et al. Strong HLA-DR expression in microsatellite stable carcinomas of the large bowel is associated with good prognosis. Br J Cancer 2002;87:756–62.
29. Guinney J, Ferte C, Dry J, McEwen R, Manceau G, Kao KJ, et al. Modeling RAS phenotype in colorectal cancer uncovers novel molecular traits of RAS dependency and improves prediction of response to targeted agents in patients. Clin Cancer Res 2014;20:265–72.
30. Satoh A, Toyota M, Ikeda H, Morimoto Y, Akino K, Mita H, et al. Epigenetic inactivation of class II transactivator (CIITA) is associated with the absence of interferon-gamma-induced HLA-DR expression in colorectal and gastric cancer cells. Oncogene 2004;23:8876–86.
31. Stoneman V, Morris A. Induction of intercellular adhesion molecule 1 and class II histocompatibility antigens in colorectal tumour cells expressing activated ras oncogene. Clin Mol Pathol 1995;48:M326–32.
32. Govema V, Trella E, Mele V, Tornillo L, Amicarella F, Cremonesi E, et al. The interplay between neutrophils and CD8+ T cells improves survival in human colorectal cancer. Clin Cancer Res 2017;23:3847–58.
33. van Gisbergen KP, Sanchez-Hernandez M, Geijtenbeek TB, van Kooyk Y. Neutrophils mediate immune modulation of dendritic cells through glycosylation-dependent interactions between Mac-1 and DC-SIGN. J Exp Med 2005;201:1281–92.
34. Dry JR, Pavey S, Pratilas CA, Harbron C, Runswick S, Hodgson D, et al. Transcriptional pathway signatures predict MEK addiction and response to selumetinib (AZD6244). Cancer Res 2010;70:2264–73.
35. Luke JJ, Bao R, Spranger S, Sweis RF, Gajewski TF. Correlation of WNT/β-catenin pathway activation with immune exclusion across most human cancers. J Clin Oncol 34:15s, 2016(suppl; abstr 3004).

Published OnlineFirst October 23, 2017; DOI: 10.1158/1078-0432.CCR-17-1090

36. Casey SC, Tong L, Li Y, Do R, Walz S, Fitzgerald KN, et al. MYC regulates the antitumor immune response through CD47 and PD-L1. Science 2016; 352:227–31.
37. Janssen KP, Alberici P, Fsihi H, Gaspar C, Breukel C, Franken P, et al. APC and oncogenic KRAS are synergistic in enhancing Wnt signaling in intestinal tumor formation and progression. Gastroenterology 2006;131: 1096–109.
38. Mlecnik B, Bindea G, Kirilovsky A, Angell HK, Obenauf AC, Tosolini M, et al. The tumor microenvironment and Immunoscore are critical determinants of dissemination to distant metastasis. Sci Transl Med 2016; 8:327ra26.
39. Remark R, Alifano M, Cremer I, Lupo A, Dieu-Nosjean MC, Riquet M, et al. Characteristics and clinical impacts of the immune environments in colorectal and renal cell carcinoma lung metastases: influence of tumor origin. Clin Cancer Res 2013;19:4079–91.
40. Dunne PD, McArt DG, Bradley CA, O'Reilly PG, Barrett HL, Cummins R, et al. Challenging the cancer molecular stratification dogma: intratumoral heterogeneity undermines consensus molecular subtypes and potential diagnostic value in colorectal cancer. Clin Cancer Res 2016; 22:4095–104.
41. Morris JS, Kopetz S. Tumor microenvironment in gene signatures: critical biology or confounding noise? Clin Cancer Res 2016;22:3989–91.
42. Tran E, Robbins PF, Lu YC, Prickett TD, Gartner JJ, Jia L, et al. T-cell transfer therapy targeting mutant KRAS in cancer. N Engl J Med 2016;375:2255–62.
43. Wang QJ, Yu Z, Griffith K, Hanada K, Restifo NP, Yang JC. Identification of T-cell receptors targeting KRAS-mutated human tumors. Cancer Immunol Res 2016;4:204–14.
44. Ho PC, Meeth KM, Tsui YC, Srivastava B, Bosenberg MW, Kaech SM. Immune-based antitumor effects of BRAF inhibitors rely on signaling by CD40L and IFNgamma. Cancer Res 2014;74:3205–17.
45. Rakhra K, Bachireddy P, Zabuawala T, Zeiser R, Xu L, Kopelman A, et al. CD4(+) T cells contribute to the remodeling of the microenvironment required for sustained tumor regression upon oncogene inactivation. Cancer Cell 2010;18:485–98.